University of Alberta

IN-SITU MOLDING OF GLASS FIBRE/NYLON 6 COMPOSITES : STUDIES IN THE DEVELOPMENT OF COMPOSITE PROPERTIES BY SURFACE - MODIFICATION OF GLASS FIBRE

by

DEEPIKA SHAH ©

A thesis submitted to the Faculty of Graduate Studies and Research in partial fulfillment of the requirements for the degree of **MASTER OF SCIENCE.**

Department of Chemical Engineering

Edmonton, Alberta
Fall, 1996

National Library
of Canada

Acquisitions and
Bibliographic Services Branch

395 Wellington Street
Ottawa, Ontario
K1A 0N4

Bibliothèque nationale
du Canada

Direction des acquisitions et
des services bibliographiques

395, rue Wellington
Ottawa (Ontario)
K1A 0N4

Your file Votre référence

Our file Notre référence

The author has granted an irrevocable non-exclusive licence allowing the National Library of Canada to reproduce, loan, distribute or sell copies of his/her thesis by any means and in any form or format, making this thesis available to interested persons.

L'auteur a accordé une licence irrévocable et non exclusive permettant à la Bibliothèque nationale du Canada de reproduire, prêter, distribuer ou vendre des copies de sa thèse de quelque manière et sous quelque forme que ce soit pour mettre des exemplaires de cette thèse à la disposition des personnes intéressées.

The author retains ownership of the copyright in his/her thesis. Neither the thesis nor substantial extracts from it may be printed or otherwise reproduced without his/her permission.

L'auteur conserve la propriété du droit d'auteur qui protège sa thèse. Ni la thèse ni des extraits substantiels de celle-ci ne doivent être imprimés ou autrement reproduits sans son autorisation.

ISBN 0-612-18323-8

Canada

University of Alberta

Release Form

Name of Author : Deepika Shah

Title of Thesis : In-Situ Molding of Glass Fibre/Nylon 6 Composites: Studies in the Development of Composite Properties by Surface - Modification of Glass fibre

Degree : Master of Science

Year this Degree Granted : Fall 1996

Permission is hereby granted to the University of Alberta Library to reproduce single copies of this thesis and to lend or sell such copies for private, scholarly, or scientific research purposes only.

The author reserves all other publication and other rights in association with the copyright in the thesis, and except as hereinbefore provided, neither the thesis nor any substantial thereof may be printed or otherwise reproduced in any material form whatever without the author's prior written permission.

505, Nandadevi, Neelkanth-valley
Rajawadi, Ghatkopar (East)
Bombay - 400 077
India

May 06, 1996

UNIVERSITY OF ALBERTA

FACULTY OF GRADUATE STUDIES AND RESEARCH

The undersigned certify that they have read, and recommended to the Faculty of Graduate Studies and Research for acceptance, a thesis entitled **IN-SITU MOLDING OF GLASS FIBRE/NYLON 6 COMPOSITES : STUDIES IN THE DEVELOPMENT OF COMPOSITE PROPERTIES BY SURFACE-MODIFICATION OF GLASS FIBRE** submitted by **DEEPIKA C. SHAH** in partial fulfillment of the requirements for the degree of **MASTER OF SCIENCE**.

M. C. Williams

Dr. M. C. Williams (Supervisor)

Dr. Uttandaraman Sundararaj

Nancy Kerr

Dr. Nancy Kerr

Date : May 3, 1996

Abstract

ε-Caprolactam has been anionically polymerized at a temperature of 150°C (using sodium hydride and phenyl isocyanate as initiator and activator, respectively,) within a random continuous glass fibre mat reinforcement to obtain composites of nylon 6 (N6) with about 28% volume fraction of glass fibre (V_f). Attempts were made to improve interfacial adhesion between fibre and nylon 6, by carrying out several fibre surface treatments: **(a)** Several techniques for cleaning and removing the organic sizing from the as-received fibre surfaces, including furnace-cleaning, exposure to buffered solution of HF as a cleanser, and to piranha solution (sulfuric acid/hydrogen peroxide mixture); **(b)** adsorption from solutions of various silane coupling agents, designated as Silane I, Silane III, Silane IV and Silane V. Solution concentrations of Silane III, IV and V in toluene were varied, and solvent effects were probed by replacing toluene with aqueous ethanol to deposit Silane-IV. A blend of crosslinking additive [1,2-bis-(trimethoxysilyl)ethane] with Silane-IV was also studied; **(c)** Etching, with either a buffered solution of HF or a gaseous plasma, to provide rough surfaces. The polymerization temperature was also varied, to discover whether this affected either the quality of N6 or its bonding to glass. Composites and pure nylon were characterized in terms of tensile properties (breaking stress σ_b and strain ε_b, modulus E, toughness τ), impact strength (E_s), and structural properties (density, V_f, voids volume fraction V_v).

Untreated-fibre composites possessed a lower σ_b (53.8 MPa) than the nylon alone (62.5MPa), indicating poor adhesion between glass fibre and matrix. Surface treatment with Silanes IV and V improved σ_b by ~104%, E by ~30%, τ by 30% over the untreated composite. The ε_b remained the same for all composites. Concentration effects were observed with Silane IV and

V toluene solutions with a maximum in strength obtained at 1.25%. Silane III gave slightly lesser improvement in tensile properties compared to the above two silanes. Even with a very low $\overline{V_f}$ (18%), the HF-treated composites gave a significant improvement (49%) in σ_b over the untreated, while composites with piranha-cleaned fibres showed no improvement in properties compared to the furnace-cleaned but untreated fibre composite. However, piranha cleaning as an alternative cleaning method was shown to be effective and convenient. Lowering the polymerization temperature from 150°C to 120°C gave composites with improved σ_b (53%), using cleaned but untreated fibres.

Property differences may be due to N6 crystallinity, which varied with different surface treatment techniques. Crystallinity of matrix N6 was 14% higher in untreated-fibre composite polymerized at 120°C than in pure N6. Most treated-fibre composites gave crystallinity higher than pure N6 by ~30%, although piranha-cleaned fibres led to a drop of 17%.

Acknowledgments

I would like to express my heartfelt gratitude and appreciation to Professor M. C. Williams for his support, encouragement and personal and academic guidance through the course of my program.

The help provided by the Alberta Microelectronic Centre and particularly by Dr. Graham McKinnon, regarding the plasma and chemical treatment of glass fibres is appreciated. Access provided by NAIT to their Lloyds L6000R Universal Testing Machine for tensile tests, and to the Tinius Olsen Izod Testing Machine for impact tests is acknowledged. I would also like to thank the Mechanical Engineering Machine Shop at the University of Alberta for allowing me the use of their MTS tester for carrying out my tensile tests. Without the help of the above, this work could not have been successfully completed.

Special thanks are due to my colleagues, in the Polymer and Rheology Group for their support and help during my experiments and especially to Moin Mohammad for help with carrying out the mechanical tests at NAIT and providing transportation. I am also grateful to Yatin Sankholkar for the many fruitful discussions which helped me in the understanding of this vast and complex area of research. I would also like to thank Parag Ghodgaonkar for helping me with the calculation of the mechanical properties using image analysis and Manav Lahoti for scanning the SEM pictures for my thesis and providing emotional support and encouragement during the course of this work.

In addition, I wish to acknowledge the help provided by Walter Boddez and Richard Cooper of the Chemical Engineering Instrument Shop, and the assistance by the Chemical Engineering Machine Shop for specimen preparation and for being around whenever I needed help.

My earnest appreciation is to the professors and staff of the Department of Chemical Engineering and my friends who stood by me in times of need and contributed to making my stay here an enjoyable experience.

I acknowledge with gratitude my thesis committee members : Dr. Uttandaraman Sundararaj and Dr. Nancy Kerr for their criticism, advice and for their time spent in reviewing my thesis.

I gratefully acknowledge the Natural Sciences and Engineering Council of Canada strategic grant which supported the major part of my research and their operating grant which saw me through the last year of my work.

Finally, I would like to thank my parents for their unconditional love and support throughout my life.

Table of Contents

Chapter 1. Introduction **1**

1.1 Definition and classification of composite materials 1

1.2 History and development of composite materials 2

1.3 Composite materials versus conventional materials 3

1.4 General features of thermoset and thermoplastic matrices 3

1.5 Goals of this work 4

1.6 Adhesion at the interface 5

Chapter 2. Materials Used in Composites **8**

2.1 Glass fibres 8

2.2 Nylon 6 12

Chapter 3. Fibre - Matrix Interface **22**

3.1 Adsorption and wetting 22

3.2 Electrostatic attraction 26

3.3 Chemical bonding 26

3.4 Interdiffusion 30

3.5 Mechanical adhesion (roughening or surface interlocking) 31

3.6 Chemical acid etching 32

3.7 Plasma treatment 33

Chapter 4. Fabrication of Glassfibre/Nylon 6 composites **35**

4.1 Equipment 35

4.1.1 Mold 35

Temperature inside mold 38

4.1.2 Chemical feed vessel 42

4.2 Procedures for producing continuous-fibre composite 43

sheet
4.2.1 Previous work 43
4.2.2 Procedures used in this work to make continuous-fibre composite sheet 44
4.3 Fibre surface treatment 54
4.3.1 Review of Duangchan's work 54
4.3.2 Fibre surface treatments employed in this work 59

Chapter 5. Structure and composition of composite disks **69**
5.1 Density (ρ) 69
5.2 Volume fraction of fibre (V_f) 74
5.2.1 Reproducibility and homogeneity of disks 74
5.2.2 Masking fibre pretreatment effects with variations in V_f 76
5.3 Void volume fraction (V_v) 78
5.3.1 Voidage and ρ_a uncertainty 80
5.3.2 Distribution of local voidage within disks 82
5.4 Scanning electron microscope (SEM) micrographs of composites 89

Chapter 6. Mechanical properties of composite specimens **92**
6.1 Tensile properties 92
6.1.1 Tensile properties of unreinforced nylon 6 97
6.1.2 Reproducibility of composite disks 101
6.1.3 Tensile properties of the composite 102
Comparison of different types of surface treatment 106
6.1.4 Role of nylon and surface treatment in glass fibre reinforcement 122
6.1.5 Role of silane coupling agents 126
6.1.6 Failure mechanism of glass fibre/nylon 6 composites 132
6.2 Impact properties 134

6.2.1 Improvement of E_s by glass fibre reinforcement 136
6.2.2 Effect of different surface treatments on E_s 137
6.2.3 Dependence of on the concentration of Silane-IV solutions used for treatment of fibres in composites 140
6.2.4 Qualitative results from other composite specimens 142
6.3 Thermal behavior of nylon 6 and its composites 143
6.3.1 Effect of surface treatment on the thermal properties of nylon matrix in composite 156

Chapter 7. Conclusions and Recommendations **160**
7.1 Conclusions 160
7.2 Recommendations 165
7.2.1 Mold Improvements 165
7.2.2 New Experiments 167

References **170**

Appendix A SEM micrographs of glass-fibres subjected to different cleaning techniques **176**
Appendix B Sample calculation **180**
Appendix C Structural and mechanical properties **188**
Appendix D Load-strain curves of nylon 6/glass fibre composites **211**
Appendix E Molecular weight determination of nylon 6 using Dilute solution viscometry **222**
Appendix F DSC scans of various composites **235**

List of Figures

Figure 1.1	Comparison between conventional monolithic materials and composite materials.	3
Figure 2.1	Amorphous structure of glass (a) a two-dimensional representation of silica glass network and (b) a modified network that results when Na_2O is added to (a).	10
Figure 3.1	A liquid drop on a solid surface making a contact angle (θ) between the solid and the liquid.	23
Figure 3.2	(a) Bond formed by electrostatic attraction. (b) Chemical bond formed between groups A on one surface and groups B on the other surface. (c) Bond formed by molecular entanglement following interdiffusion. (d) Mechanical bond formed when a liquid polymer wets a rough solid surface.	25
Figure 3.3	Function of coupling agent (a) Hydrolysis of organo-silane to corresponding silanol, (b) Hydrogen bonding between hydroxyl groups of silanol and glass surface, (c) polysiloxane bonded to glass surface and laterally to neighboring coupling molecules to form a network structure surrounding the fibre, (d) organo-functional R group reacted with polymer matrix.	28
Figure 3.4	Function of coupling agent, (a) Reaction between silane and hydroxyl group at glassfibre surface in toluene solution (non-aqueous), (b) organo-functional R group reacted with polymer matrix.	29
Figure 3.5	(a) Mechanism of reversible bond formation associated with hydrolysis, (b) shear displacements without permanent damage to interface bond.	30
Figure 4.1	Diagram of experimental equipment.	36
Figure 4.2	Mold diagram.	37
Figure 4.3	Locations of thermocouples on the (a) upper and (b) lower surfaces of the mold cavity .	41
Figure 4.4	Temperature distributions on mold surfaces when nominal set point is at 100°C.	42
Figure 4.5	Temperature distributions on mold surfaces when nominal set point is at 150°C.	42
Figure 4.6	Procedure to make nylon 6/glass fibre composite.	45
Figure 4.7	Diagram of insert which fits into the female part, (a) top view, (b) front view.	51
Figure 4.8	Mechanical properties from tensile test of Silane III at different concentrations (5, 10, 15%).	58
Figure 4.9	Tensile strengths of tapes as affected by heating for 1 hr at various temperatures (a) fibrous glass tape 1/0.015 in. (b) fibrous glass tape 1/0.007 in.	60
Figure 5.1	Locations of regions from which specimens were taken for obtaining data on composition, impact strength and tensile behavior.	71
Figure 5.2	Fibre volume fraction of composite disks having different glass fibre treatment and molded on different days.	75

Figure 5.3 Fibre volume fraction at different positions in composite disks. 77

Figure 5.4 Comparing void volume fraction of composites with treated and untreated glass fibres. 81

Figure 5.5 Void volume fraction at different positions in composite disks. 83

Figure 5.6 Void volume fraction at different positions in composite disks. V_v ranking, as a scale of 6-1, with 6 highest. 85

Figure 5.7 Fibre volume fraction (V_f) vs. void volume fraction (V_v) of composite disks (a) local V_v vs local V_f for all specimens of all disks (b) V_v vs. V_f for all disks (c), (d), (e) local V_v vs. local V_f. 86

Figure 5.8 Top surfaces of (a) untreated glass fibre composites (b) piranha-cleaned glassfibre composite (c) HF treated glass fibre composite 90

(d) Silane III (0.2%) treated glass fibre composite (e) ^{2}Silane IV (1.25%) treated glass fibre composite (f) Silane V (0.2%) treated glass fibre composite. 91

Figure 6.1 SEM of fracture surface of nylon from disks with (a) rectangular configuration (600 μm) (b) circular configuration (600 μm) (c) rectangular configuration (150 μm) (d) circular configuration (150 μm). 98

Figure 6.2 (a) Tensile strengths and volume fractions of pure nylon, furnace cleaned untreated, piranha cleaned untreated and furnace cleaned HF treated disks at RH 66%. 103

(b) Silane III disks (c) Silane V disks. Toluene solvent in both treatments. 104

(d) Silane IV in toluene (e) Silane IV in different solvents. 105

Figure 6.3 Elastic modulus of various disks at RH 66% (a) pure nylon, furnace cleaned untreated, piranha cleaned untreated and furnace cleaned HF treated disks , furnace cleaned Silane I (5%) treated disks (b) Silane IV disks. 108

(c) Silane III treated (from toluene) disks (d) Silane IV disks. 109

(e) Silane V treated (from toluene) composite disks 110

Figure 6.4 Strain at break of various disks at RH 66% (a) pure nylon, furnace cleaned untreated, piranha cleaned untreated and furnace cleaned HF treated disks , furnace cleaned Silane I (5%) treated disks (b) Silane IV disks. 111

(c) Silane III treated (from toluene) disks (d) Silane IV disks. 112

(e) Silane V treated (from toluene) composite disks 113

Figure 6.5 Toughness of various disks at RH 66% (a) pure nylon, furnace cleaned untreated, piranha cleaned untreated and furnace cleaned HF treated disks , furnace cleaned Silane I (5%) treated disks (b) Silane IV disks. 114

(c) Silane III treated (from toluene) disks (d) Silane IV disks. 115

(e) Silane V treated (from toluene) composite disks 116

Figure 6.6 Effectiveness factor of the different concentrations for Silane III, Silane IV and Silane V. 117

Figure 6.7 Tensile strengths for three different concentrations of Silane III, Silane IV and Silane V treated from toluene at RH 66%. 120

Figure 6.8 Comparison of the mechanical properties of silane treated disks possessing maximum properties in their respective groups. 121

Figure 6.9	Schematic representation of the tensile behavior of a composite with a nylon 6 matrix.	123
Figure 6.10	SEM of fracture surface of nylon 6 composite containing glass fibres that are (a) furnace cleaned and untreated (b) piranha cleaned and untreated.	125
Figure 6.11	SEM of fracture surface of nylon 6 composite containing glass fibres that are (a) furnace cleaned and HF treated (1 min.) (b) furnace cleaned and Silane III (2%) treated.	127
Figure 6.12	SEM of fracture surface of nylon 6 composite containing glass fibres that are (a) furnace cleaned and Silane IV (1.25% toluene) treated (b) furnace cleaned and Silane IV (1.25% ethanol) treated.	128
Figure 6.13	SEM of fracture surface of nylon 6 composite containing glass fibres that are (a) furnace cleaned and Silane IV (1.25%+CL ethanol) treated (b) furnace cleaned and Silane V (0.2%) treated.	129
Figure 6.14	Typical stress-strain curve for a nylon 6/glassfibre composite.	133
Figure 6.15	Impact strength E_s (J/m) of pure nylon and its composites with untreated and treated glassfibres at RH 63-66%.	135
Figure 6.16	(a) Impact strength E_s of composite treated with different concentrations of Silane IV in toluene (b) comparison of Impact strength, E_s and Tensile strength, σ_b of the Silane IV treated composites.	141
Figure 6.17	DSC scan for pure nylon 6 taken from circular configuration disk (a) two complete heating and cooling cycles (b) expanded region of DSC heating trace near crystalline melting regime on the first heating scan.	144
	(c) expanded region of DSC heating trace near glass transition regime on first heating scan. (d) expanded region of DSC cooling trace, near crystalline freezing regime following first heating scan.	145
Figure 6.18	DSC scan for pure nylon 6 taken from rectangular configuration disk (a) two complete heating and cooling cycles (b) expanded region of DSC heating trace near crystalline melting regime on the first heating scan.	146
	(c) expanded region of DSC heating trace near glass transition regime on first heating scan. (d) expanded region of DSC cooling trace, near crystalline freezing regime following first heating scan.	147
Figure 6.19	DSC scan for composite sample taken from ^{1}untreated disk (a) two complete heating and cooling cycles (b) expanded region of DSC heating trace near crystalline melting regime on the first heating scan.	148
	(c) expanded region of DSC heating trace near glass transition regime on first heating scan. (d) expanded region of DSC cooling trace, near crystalline freezing regime following first heating scan.	149
Figure 6.20	DSC scan for composite sample taken from ^{3}untreated disk (a) two complete heating and cooling cycles (b) expanded region of DSC heating trace near crystalline melting regime on the first heating scan.	150
	(c) expanded region of DSC heating trace near glass transition regime on first heating scan. (d) expanded region of DSC cooling trace, near crystalline freezing regime following first heating scan.	151

Figure 6.21 DSC scan for pure nylon 6 (from circular configuration disk) with a different thermal cycle. Expanded region of the DSC heating trace near the melting regime (a) first heating cycle (b) second heating cycle. 155

Figure 6.22 DSC scan for nylon 6 matrix taken from the composite 'Silane IV (1.25%) Expanded region of the DSC heating trace near the melting regime (a) first heating cycle (b) second heating cycle. 157

List of Tables

Table 1.1 Broad classification of composite materials 1
Table 2.1 Composition of glass used for fibre manufacture 9
Table 2.2 Properties of E-glass at 20°C; measured in fibre form with diameters in the range 8-14 μm 10
Table 2.3 Properties of nylon 6 and 30-35% glass fibre/nylon 6 composite 20
Table 4.1 Different plasma reactor conditions employed to etch the glass fibres 63
Table 5.1 Description of various disks fabricated in the mold 70
Table 6.1 Comparison of commercial nylon 6 and our nylon 6 100
Table 6.2 Average breaking energies from Izod type impact tests 135
Table 6.3 Different thermal properties of nylon 6 matrix in the different composites 152

Chapter 1

INTRODUCTION

1.1. Definition and Classification of composite materials

A composite material consists of two or more physically distinct and mechanically separable materials. The properties of a composite may be superior to the properties of the individual components, and possibly unique in some specific respects (*Hull, 1981, p. 3*). This synergistic feature provides the main impetus for the development of composite materials. For example, in glass fibre-reinforced plastics, glass fibres and plastics with some excellent physical and mechanical properties are combined to give a material with strength and stiffness close to that of fibres and with the chemical resistance and light weight of the plastic. The research reported here is directed toward this category of composites : glass fibre filler embedded in a polymeric matrix.

Composite materials have been classified in many ways depending on the ideas and concepts that need to be identified. These can be broadly classified as natural composite materials and man-made composite materials. Man-made composite materials can be further classified into microcomposite and macrocomposite materials. A useful and all-embracing classification is set out in Table 1.1 with some examples (*Hull, 1981, p. 1*).

Table 1.1 *Broad classification of composite materials (Hull, 1981, p. 1)*

		Examples
Natural Composite Materials		Wood Bone Muscle and other tissue
Man-made Composite Materials	**Microcomposite materials**	Metallic alloys: e.g. steels Reinforced thermoplastics
	Macrocomposites (Engineering products)	Reinforced concrete beams Galvanized steel

1.2. History and development of composite materials

Recent review articles and books refer to the technology of composite materials as one of the ancient materials technologies. Early civilizations which used laminated bows for extra strength, mixtures of straw (for the reinforcing fibre) and mud (matrix) for building bricks, and the Incas who dispersed platinum in gold and silver because they could not obtain furnace temperatures high enough to work platinum, are cited as some of the first users of composite materials (*Broutman and Krock, 1974*).

Although natural composites - wood, bones, teeth - have been in existence for many millions of years, man-made fibre-reinforced materials were not developed until the early 1940s. The impetus for the development of composite materials was born out of the challenge that structural designers laid down to the materials development community in the 1950s and 1960s. That challenge was clearly performance dominated and involved primarily the need for combined high stiffness and strength with low density. The response of the metallic segment of the materials development community was to expend much effort on developments in materials such as aluminum and titanium *(Peterson, 1980)*. There has been some success but indeed the materials advances in these areas have been incremental. The non-metals community had, over the 1940s and 1950s, labored hard on the development of glass-reinforced polymer composites with some success in selected applications. However, early attempts to fabricate glass fibre-reinforced phenolics and melamines by high pressure molding did not show much commercial promise. Glass fibre-reinforced silicones prepared in 1941 by J. F. Hyde at the Corning Glass Works were outstanding as heat resistant electrical insulation, but were too costly for structural applications. The first commercial success in this field was achieved in February, 1941, by Lynn King, at the Columbia Chemicals Division of the Pittsburgh Plate Glass Company, when he prepared glass fibre-reinforced polyester (allylglycol carbonate) resin *(Broutman and Krock, 1974, p. 2)*. Composite materials of many types are now widely employed in the transport, construction, chemical, electrical, marine, leisure, medical and aerospace industries and are a well established class of material.

1.3. Composite materials versus conventional materials

Compared with aluminum and steel, polymer composites have less weight and thermal expansion and higher fatigue resistance. If strength and stiffness alone are considered, fibre reinforced composite materials do not have many advantages compared to metals. but when we consider the stiffness per unit weight (specific stiffness) and strength per unit weight (specific strength), composite materials are superior to metals as shown in Figure 1.1. These properties make possible energy savings and higher efficiency for transport industries *(Hull, 1981, p. 4, Gaylord, 1974, p. 5)*.

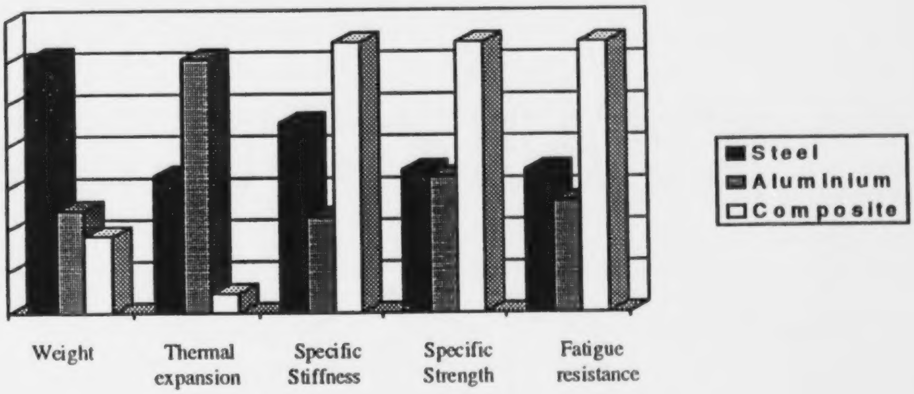

Figure 1.1. Comparison between conventional monolithic materials and composite materials *(redrawn from Chawla, 1987, p. 4)*. The "stiffness" and "strength" parameters are on a unit weight basis e.g., stiffness/weight.

1.4. General features of thermoset and thermoplastic matrices

Solid-state organic polymers, generally known as plastics, are commonly classified into two classes, thermoplastics or thermosets, depending on their behavior when heated. A thermoset polymer undergoes various degrees of cross-linking when cured by heat (or other means). The cross-linking reactions lead to the formation of an insoluble or infusible rigid product, a “set” product, in which chains are joined together to form a three-dimensional structure. The application of heat to these materials can soften them and render them flexible, but cannot convert them to liquids. In contrast, thermoplastic polymers do not undergo chemical changes during consolidation; changes are substantially physical e.g., crystallization, vitrification *(Béland, 1990, p.3)*. Thermoplastics can be liquefied by the application of heat and reprocessed, which is very useful for recycling, shaping and repairing considerations. Furthermore, the voids or defects present in thermoplastic objects (for example laminates) can often be eliminated by the application of heat and pressure, while the thermoset has to be rejected. Moreover, there is no need for adhesive bonds and mechanical fasteners, since composite parts can be thermally joined to form a composite assembly *(Béland, 1990, p.97)*. Finally, by taking advantage of the inherent nature of thermoplastic molecules to undergo thermally induced flow, shaped thermoplastic articles can be fabricated at elevated temperatures by relatively fast-processing methods *(Carlsson, 1981, p. 7)*, while thermosets require an extended in-situ curing period which lengthens the molding cycle.

The materials which are considered as new thermoplastic polymers or engineering plastics are polyketones, polyarylene sulfides, aromatic polyamides, polyimides, polysulfones, polybenzimidazoles, and polyphenylquinoxalines *(Béland, 1990, p.5)*. Most of these have not yet been utilized as matrices for polymer composites.

1.5. Goals of this work

One common thermoplastic, the polyamide nylon 6, and one familiar reinforcing agent (glass fibre type E) are selected as matrix and reinforcement, respectively, to be studied here, because of their low cost and good performance as separate materials.

The properties of polyamides make them attractive for the design engineer. Polyamides can be molded into intricate shapes or extruded, and they combine low unit cost and lightness in weight with mechanical strength and toughness, as well as resistance to abrasion, corrosion and chemical attack. In addition they have higher heat distortion and service temperatures, and lower flammability compared with polyolefins. The addition of glass fibres transforms nylon 6 from tough, relatively flexible materials to exceptionally strong and rigid materials with an extended working range. These properties, combined with other desirable features such as abrasion resistance and resistance to oils, gasoline, and other organic liquids, are responsible for nylon/glass fibre composites to be widely used in engine compartment applications involving fan blades, fuse boxes, bearings, gears, etc. *(Fernengel, 1984, Gaitskell et al., 1984)*.

1.6. Adhesion at the Interface

Fibre-reinforced plastic composite materials consist of three regions: fibre, matrix and the interface between the fibre and the matrix. The primary function of the fibre/matrix interface is to transmit stress from the polymer matrix to the high strength reinforcing fibres. So, for a composite material, desirable properties cannot be obtained merely by more mixing and dispersion of raw material; complete adhesion at the interface is also essential (*Berlin, 1985, p. 3, Yosomiya et al., 1990, p. 1, Kardos, 1983, Castle, 1988*).

One fundamental problem in producing reinforced polymers is that there is little interfacial attraction between the polymer and the glass fibre surface, so a strong physical bond between them is usually not achieved *(Szijarto and Kiss, 1985)*. This situation is further aggravated by the following conditions which act to prevent or destroy bonding: (a) The fibre surface may be contaminated, or air or other gases may be entrapped at the solid surface of the reinforcement; (b) Stress concentrations develop at the interface because of the large differences in the elastic properties and thermal expansion coefficients of the reinforcement and matrix phases (the coefficients of thermal expansion of polymers and glass differ by a factor of ten on the average, *Berlin, 1985, p. 11*); (c) Other stresses of volumetric origin arise from cure shrinkage (in thermosetting matrices) and crystallization (in crystalline thermoplastic matrices); (d) In the case of nylon 6/glass fibre systems, poor adhesion between nylon and glass fibre results partly from intrinsic incompatibility of nylon with glass, and partly from the affinity of nylon for water. Nylon absorbs moisture from the air and transmits it to the hydrophilic glass surface, where it serves to disrupt whatever weak adhesive forces would have existed between nylon and glass in a dry environment. Interfacial moisture also serves as a lubricant to reduce interphase load transfer and assists the separation of the two solid phases upon matrix rupture and subsequent fibre pull-out.

Thus, in nylon 6/glass fibre composite, adhesion between the fibre and the matrix is generally poor.

There are many ways to deliver surface treatments to improve the interfacial adhesion between the fibre surface and the matrix, to enable us to develop superior properties for a composite material. However, the extensive work in the literature dealing with fibre treatment is almost exclusively in connection with reinforced thermosets. Most fibre treatment processes for thermoplastic composites are proprietary *(Béland, 1990, p.98)*. For this reason, we have chosen to study a thermoplastic system here.

The choice of the proper fibre surface treatment is complex. It depends both on the type of fibre and on the nature of the thermoplastic involved. It may include cleaning, plasma treatment, etching and/or oxidizing of the fibres to provide reactive sites for adequate bonding to the matrix, and the application of coupling agents to the surface of the fibres.

Glass fibre-reinforced nylon 6 composites were studied extensively in our laboratory in the past. *Duangchan, 1994*, employed continuous random glass fibre mats to provide the necessary strengthening effect. The use of clean glass fibre mats without any prior surface treatment resulted in poor adhesion between the fibre and polymer, as a consequence of which there was virtually no improvement in the tensile strength of the composite material over that of pure nylon 6 fabricated by the same process. That work also involved the use of silane coupling agents as a potential means to improve interfacial adhesion. A few silanes were found to give improvement in the mechanical properties of the composite. This encouraged us to conduct further studies in the use of glass surface modification techniques to improve interfacial adhesion between nylon 6 and glass fibres.

Therefore, the objectives of this study are to improve the interfacial adhesion of glass fibre and nylon 6 by modifying the surface of glass fibres with various techniques, including the use of silanes (beyond what was done by *Duangchan*) and also using other methods not attempted by *Duangchan* (see above). We then examine whether the composite properties are thereby improved.

The sample preparation used here, similar to that of *Duangchan, 1994*, is a special form of RIM (Reaction Injection Molding), wherein the monomer is injected into a mold (with pre-loaded fibre reinforcement) and polymerized *in-situ* around the glass fibre reinforcement. Since the techniques to process thermoplastic composites are not as well established as those developed for thermoset composite materials, refinement of this molding method has value in itself *(Béiand, 1990, p.96)*. The biggest obstacles are concerned with the need to develop fabrication techniques which involve low processing temperatures and pressures and are capable of mass production methods.

This study will therefore create some knowledge about a thermoplastic composite manufacturing process as well as guidelines for enhancing the properties of thermoplastic composite materials by means of various treatments of the fibre surface.

Chapter 2

MATERIALS USED IN COMPOSITES

2.1. Glass fibres

For over 3500 years, mankind has been aware of the fact that molten glass could be drawn into fine lengths (which were originally used for both making and decorating ornamental glass objects). Late in the 19th century, it was theorized that glass drawn into very fine fibres would be suitable for use in various textile applications. Although experimental glass fibres blended with silk fibres were woven into novel dresses and gowns in France and the United States, commercial glass fibres did not become a reality until 1939 with the formation of Owens-Corning Fibreglass Corporation (an outgrowth of research efforts by Owens Illinois and Corning Glass Works) (*Knox, 1982)*.

There are different types of glass fibres for different purposes, for example, type C (C for corrosion), E (E for electrical), and S (S for higher silica content). C-glass can resist chemical corrosion better than E-glass but is more expensive and has lower strength properties. S-glass has a higher Young's modulus and is more temperature resistant but is more expensive than E-glass. Because of the price advantage of E-glass, most continuous glass fibre (about 90%) produced is of the E-glass type; it also draws well and has good strength, stiffness, electrical and weathering properties (*Knox, 1982; Holliday, 1966; Gaylord, 1974*)

Typical compositions of glasses of different types used for glass fibre in composite materials are shown in Table 2.1. Common glass fibres are based on silica (about 50-60% SiO_2) and oxides of calcium, boron, sodium, aluminum and iron.

Several specialty glass compositions have been developed to take advantage of specific properties; however, they have not become commercial fibre products. The M-glass composition was formulated to yield fibres having a high modulus of elasticity (113 GPa). Unfortunately, the presence of beryllia (beryllium oxide) in the glass prevented its commercialization. Similarly, the low-dielectric D-glass composition was developed for high-performance electronic applications and the L-glass (lead glass) composition has the advantage of radiation protection (*Knox, 1982*).

Table 2.1. *Composition of glass used for fibre manufacture (all values in wt.%) (Hull, 1981)*

Components	**C-glass**	**E-glass**	**S-glass**
SiO_2	64.4	52.4	64.4
$Al_2O_3.Fe_2O_3$	4.1	14.4	25.0
CaO	13.4	17.2	-
MgO	3.3	4.6	10.3
Na_2O, K_2O	9.6	0.8	0.3
B_2O_3	4.7	10.6	-
BaO	0.9	-	-

The surface of glass consists of randomly distributed groups of oxides and is, like the bulk, amorphous. Some of the oxides, such as SiO_2, Fe_2O_3, and Al_2O_3, interact with water vapor by forming hydroxyl groups such as –Si–OH, –Fe–OH and –Al–OH, which then act as shields by holding other water vapor molecules away from the surface with hydrogen bonds, thus preventing them from penetrating the surfaces. The hygroscopic oxides, such as Na_2O, absorb water directly at the surface and become hydrated (*Hull, 1981*). Long contact with water results in the solution of the hygroscopic elements, leaving a porous surface made up of non-hydrated oxides. Looking at the interior, we find that the two-dimensional view of the network of silica glass is as shown in Figure 2.1(a). Oxygen atoms are bonded covalently to silicon. If Na_2O is added to this glass as represented in Figure 2.1(b), sodium ions will be linked ionically with oxygen but will not join the network directly. The addition of other metal oxides will change the network structure and the bonding. As a result, the properties of this glass will be changed.

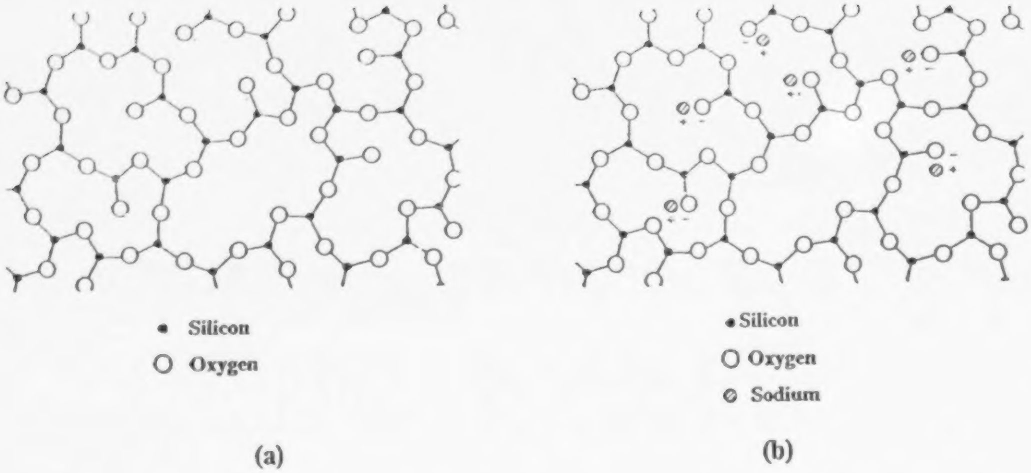

Figure 2.1. Amorphous structure of glass: (a) a two-dimensional representation of silica glass network and (b) a modified network that results when Na_2O is added to (a). Note that Na^+ is ionically linked with O^{2-} but does not join the network directly (adapted from *Hull, 1981*). An error in the original has been corrected.

The properties of glasses are quite isotropic. Young's modulus and thermal expansion coefficients are the same along the fibre axis and perpendicular to it because their three-dimensional network structure is isotropic (*Hull, 1981*). The properties of typical E-glass are shown in Table 2.2.

Table 2.2. *Properties of E-glass at 20°C; measured in fibre form with diameters in the range 8-14 μm (Hull, 1981).*

Properties	**Units**	**E-glass**
Density	10^3 kgm^{-3}	2.56
Young's modulus (tensile, along fibre axis)	GNm^{-2}	76
Modulus (perpendicular to fibre axis)	GNm^{-2}	76
Tensile strength	GNm^{-2}	1.4-2.5 (typical)*
Elongation to fracture	%	1.8-3.2
Coefficient of thermal expansion (0 to 100°C)	10^{-6}K^{-1}	4.9
Thermal conductivity (parallel to fibre axis)	Wm^{-1}K^{-1}	1.04

---

* typical of a variety of humidity conditions and ages of fibres. For freshly drawn fibres, the tensile strength is 3.5 GNm^{-2} *(Hull, 1981, p.14)*

However, the strength of glass is sensitive to process conditions and the testing environment. For example, the surface of an E-glass fibre becomes quite alkaline during heat-cleaning, due to migration of Na^+ ions to the surface. Exchange of Na^+ ions for smaller H^+ ions causes the surface to shrink, creating a tensile stress at the fibre surface. Additional externally applied tensile stress to initiate fibre failure is reduced by this amount *(Broutman and Krock, 1974, p.17)*. It is also found that tensile strength decreases when the fibres are tested in humid air, due to absorption of water on the glass surface, and when the surfaces of the fibres are in contact with mineral acids (aqueous). It is significant that the presence of water decreases the surface energy of glass fibre. As reported, glass fibre in the presence of water has a surface energy in the range of 10-20 mJm^{-2} while the dry virgin glass has a value of over 500 mJm^{-2} (*Hull, 1981*).

Fibreglass reinforcements are supplied in several forms, which allow for flexibility in cost, strength, and choice of process. The basic forms of fibreglass reinforcements are continuous and chopped strands, the latter being produced by chopping continuous-filament strands when uniform standard lengths are desired from 1/4" to over 3". Delivery of these strands can be in several different forms:

1. Rovings are cylindrically shaped packages of bundles of continuous glass fibre strands wound up in parallel, that is without twist.

2. Yarns of glass fibre are analogous to other continuous textile-fibre yarns, in that, the glass fibre strands are twisted and doubled for subsequent weaving into glass cloth.

3. Mats:

(a) Chopped strand mat is a non-woven fabric consisting of chopped glass fibre strands usually 20-50 mm in length, laid down randomly in a horizontal plane and bound together with a suitable chemical binder.

(b) Continuous strand mat consists of unchopped fine strands deposited and interlocked in spiral fashion ("swirl mats").

(c) Continuous-strand planar-random isotropic mat, with crimped strands arranged in a random pattern and assembled in mat form, such that the strands (and mat) have no preferred orientation or ordering. No binder is needed.

(d) Surfacing mat is commonly used with other glass reinforcements for high quality laminate surface appearance and weathering.

4. Milled fibres are hammermilled into a broad distribution of lengths in the range 1/32" to 1/8".

5. Fabrics and tapes: These are made from continuous filament yarns, rovings, and staple yarns. Additional processing or weaving is required to make the reinforcement available in these forms *(Loewenstein, 1983, p.19)*.

In this work, the glass fibre reinforcement used is a planar-random, isotropic, continuous E-glass mat (grade M8608), obtained in rolls from Fibreglass, Canada. Characterization data supplied by the manufacturer are: filament diameter = 20 μm, filaments/strand = 36-37, textile (strand) weight = 25 g/km, mat rest thickness = 1.02mm, mat areal weight = 450 g/m^2, σ_b = 1.86-2.0 GPa, ε_b = 4.5-4.9%, E = 69.0-72.4 GPa. This mat was compressed to the final thickness of the composite required. The sheet material thus obtained could be thermoformed to the various required shapes, having a uniform distribution of glass fibre within the polymer matrix. Thus, this technique has its attractions for the automobile industry, where sheet formation followed by thermoforming is a common operation.

2.2. Nylon 6

Nylon 6, which is also referred to as polyamide 6 or polycaprolactam, is one of the most important representatives of recyclable polymers, because it can be converted into monomeric caprolactam almost quantitatively *(Sebenda and Lanska, 1993)*.

The commercial development of nylons was an outcome of the fundamental researches into polymerization which were begun in 1929 by Carothers of E. I. du Pont de Nemours and Co. Originally a du Pont tradename, "nylon" is now a generic term for any long-chain synthetic polymer whose monomers are incorporated with amide bonds (-NH-CO-). Most of these are capable of being formed into a filament in which the structural elements are oriented in the direction of the axis (*Matthies and Seydl, 1986*).

Of the various types of nylons, nylon 66 was developed by DuPont as the first truly synthetic fibre with a broad range of applications. Soon after, about 1939/1940, nylon 6 fibres were introduced by the I. G. Farbenindustrie in Germany.

Whereas the main outlet for nylons was, and still is, the field of fibres, nylon polymers are also firmly established as engineering plastics and are suitable for a wide spectrum of applications. This is because, nylon possesses a combination of such valuable properties as, strength, stiffness, toughness, abrasion resistance and high service temperature. Further, nylon being a thermoplastic, it can be molded to give various shaped articles. The first nylon moldings were produced in 1941 but the polymer did not become well known in its present form until about 1950 (*Matthies and Seydl, 1986; Saunders, 1988; Stevens, 1990*).

Since then, both these polymers (nylon 6 and nylon 66) have been extensively used for a variety of applications. Nylon fibres characteristically have a good tensile strength and elasticity and are widely used in the manufacture of clothing, tire cord, carpets and rope. In plastic form, polyamides are used in making such items as gears, piping, wire insulation, zippers and brush bristles. Thus, the use of nylon 6 as an engineering plastic has gained added importance since the early days.

Nylon 6 is synthesized by the ring-opening polymerization of the monomer ε-caprolactam. This monomer can be prepared inexpensively from phenol as follows.

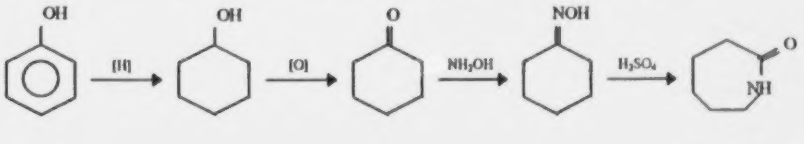

ε-caprolactam

ε-Caprolactam contains both acid (≥C=O) and amine (≥NH) groups which are divided during the ring-opening initiation but are found together in the amide bond(-NH-CO-) when polymerized. The structure of nylon 6, thus, can be written as

$$-\!\!\left[\ NH(CH_2)_5CO\ \right]_n\!\!-$$

Both batch and continuous processes are used for the production of nylon 6. In a typical batch process, a mixture of caprolactam (a ring compound), water (5-10% by weight) and acetic acid (about 0.1%) *(Saunders, 1988)* is fed into a reactor which has been purged with nitrogen (to prevent discoloration by oxygen). The mixture is heated at about 250°C for 12 hours; a pressure of about 1.5 MPa (15 atmospheres) is maintained by venting off steam. The product is then extruded as ribbon, quenched in water and chopped into chips. At this point, the material consists of high molecular weight polymer (about 90%) and low molecular weight compounds (about 10%); the latter are caprolactam (mainly), higher lactams and amino acids.

In the continuous production of nylon 6, similar reaction conditions are used. In one process, a mixture of molten caprolactam, water and acetic acid is pumped continuously to a reactor operating at about 260°C, (above the melting point of nylon, $T_m \equiv 225$°C). The feed slowly traverses through the reactor whilst steam is bled off so as to maintain atmospheric pressure. Residence time is 18-20 hours.

The water-initiated polymerization of caprolactam is believed to proceed according to the following scheme.

Initiation :

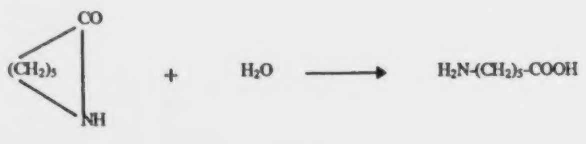

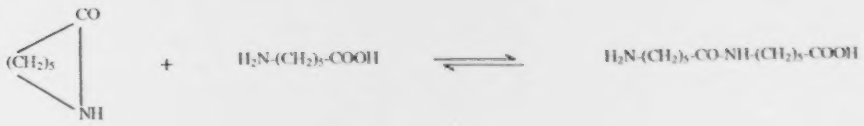

Propagation :

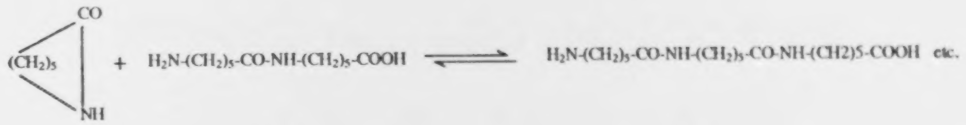
CO
(CH₂)₅
NH
+
H₂N-(CH₂)₅-CO-NH-(CH₂)₅-COOH
H₂N-(CH₂)₅-CO-NH-(CH₂)₅-CO-NH-(CH2)5-COOH etc.

Caprolactam can also be polymerized under anhydrous conditions using strong bases as catalysts. *Joyce and Ritter* at du Pont discovered in 1939 that this anionic polymerization proceeded with a much higher rate than the hydrolytic process and that it could be carried out below the melting point of the polymer to yield products of low residual monomer content, so that they needed no extraction. In spite of these obvious advantages this type of polymerization at first did not enter into commercial practice because of poor reproducibility, unstable melt viscosity and poor product color *(Matthies and Seydl, 1986*). This situation changed in 1956 when *Mottus* and co-workers at Monsanto discovered that the process could be improved by using acylated caprolactam or acylating agents (RNCO) as activators (the role of these activators is explained in the next few sections of the chapter). About 1960, the technology of activated anionic polymerization was introduced as a commercial process in the form of the so-called "monomer casting" *(Matthies and Seydl, 1986*).

In this type of polymerization, a liquid mixture of caprolactam and initiator which is usually strong base, B^-M^+, such as metal amide, metal hydride or alkali metal, is injected into a mold at a lower temperature at which the initiator is not effective. Eventually the mold temperature is raised and the polymerization is carried out. The reaction temperature is initially about 150°C but during polymerization it can rise to 200°C. The scheme of polymerization by the ring-opening anionic technique is as follows (*Odian, 1981; Stevens, 1990; Encyclopedia, 1992*).

Initiation :

Caprolactam first reacts with the base to give its metal derivative.

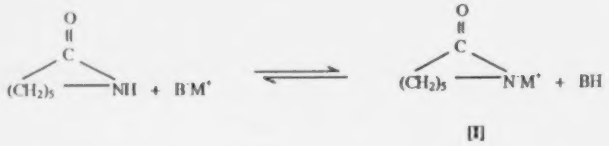

O
C
(CH₂)₅
NH + B⁻M⁺
(CH₂)₅
N⁻M⁺ + BH
[I]

The lactam anion **I** then reacts with the monomer in the second step of the initiation process by a ring-opening transamidation.

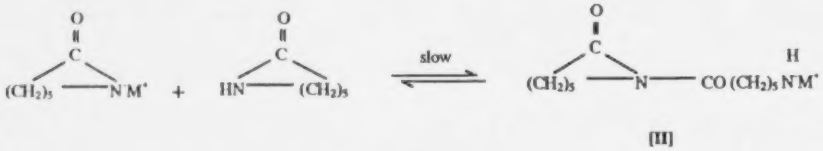

(CH₂)₅
N⁻M⁺
+
HN
(CH₂)₅
slow
N
CO (CH₂)₅ N⁻M⁺
H
[II]

The primary amine anion **II** is not stabilized by conjugation with a carbonyl group. It is highly reactive and rapidly abstracts a proton from monomer

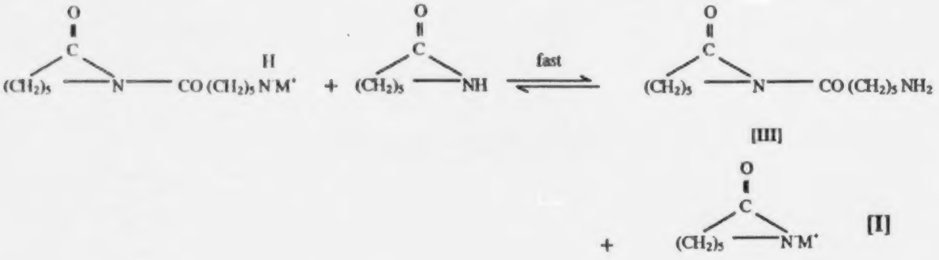

(CH₂)₅
N
CO (CH₂)₅ N⁻M⁺
H
+
(CH₂)₅
NH
fast
CO (CH₂)₅ NH₂
[III]
+
N⁻M⁺
[I]

to form the imide dimer **III**, N-(ε-aminocaproyl)caprolactam, and regenerate the lactam anion.

The imide dimer **III** is the actual initiating species necessary for the onset of polymerization. The initial induction period of the lactam polymerization is slow because the imide dimer builds up slowly.

Propagation :

Propagation is the reaction between a propagating N-acyllactam species and the lactam anion

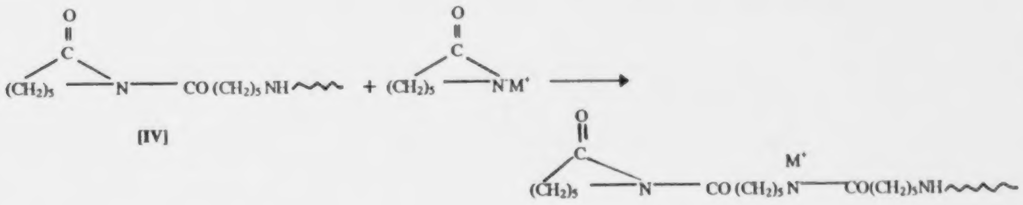

followed by fast proton exchange with the monomer

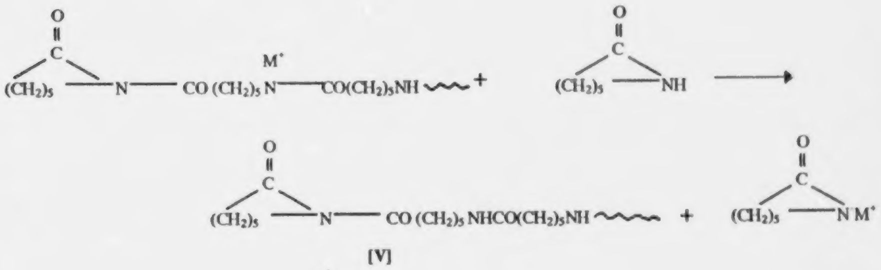

The anionic polymerization of lactams is different from other polymerizations. First, the propagating center is the cyclic amide linkage of the N-acyllactam instead of a radical, carbanion, or carbenium ion. Second, it is the monomer anion, called activated monomer, instead of monomer that adds to the propagating chain.

The concentrations of both propagating species and activated monomer are determined by the concentration of the base.

Since the induction of lactam polymerization by using a strong base alone is very slow, we can increase the rate of polymerization by adding acylating agents in the monomer. The acylation agents such as isocyanates, acid chlorides and hydrides, inorganic anhydrides, and others, will form an amide when reacting with monomer.

By reaction in presence of an isocyanate, ε-caprolactam can be converted rapidly to an N-acylcaprolactam (**VI**).

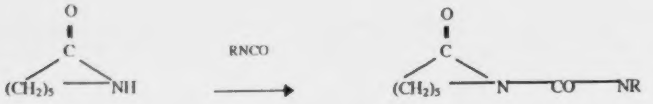

[VI]

Initiation period in this case refers to the reaction of the N-acylcaprolactam with the activated monomer followed by a fast proton exchange with monomer.

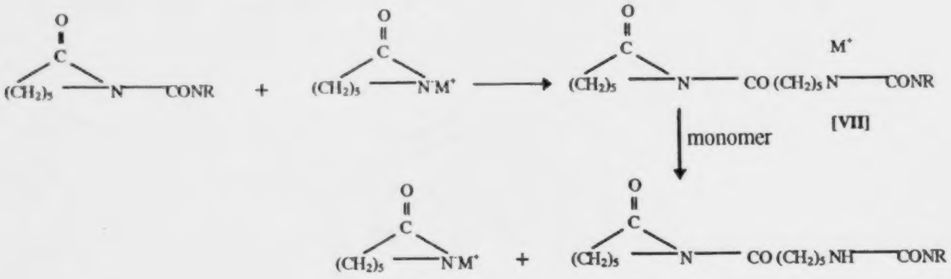

[VII]

[VIII]

The species **VII** and **VIII** correspond to species **II** and **III** in polymerization in absence of acylating agent. The use of acylating agent eliminates the induction period as a result of which the polymerization rate is higher and the reaction can be carried out at a lower temperature. Propagation follows in the same manner as for propagation of species **IV**.

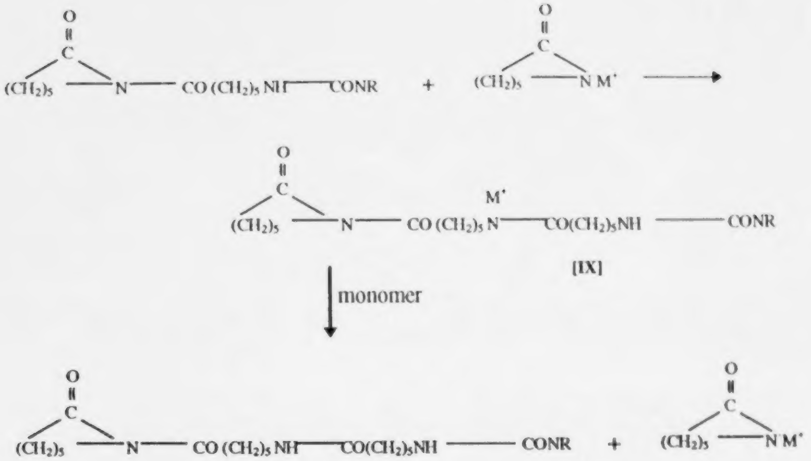

[IX]

The base is referred to as the initiator and the acylating agent as the activator. The polymerization rate depends on the concentrations of initiator and activator.

Anionic polymerization of caprolactam is utilized in casting processes, by which means it is possible to produce very large moldings, and in reaction injection molding (RIM), in which liquid components are mixed by high-pressure impingement and then injected into a mold.

Nylon 6 is a semi-crystalline polymer and has a melting point of 223°C *(Reimschuessel, 1977)*, which is rather high compared to other thermoplastic polymers. But one of the disadvantages of nylon 6 is, like all nylons, it absorbs moisture from its immediate environment. Eventually, equilibrium with the relative humidity of the atmosphere is achieved, which generally has a plasticizing effect that increases flexibility and impact resistance. The rate of atmospheric moisture absorption depends on temperature, crystallinity, humidity and thickness of samples. It absorbs large amounts of liquid water (~10% when saturated, at 20°C, see Table 2.3; ~2.5% in equilibrium with air at 50% RH and ~9.5% when saturated, at 80°C, *Encylopedia of polymer science and technology, 1985, p. 469*).

Table 2.3. *Properties of nylon 6 and 30-35 wt% glass-fibre/nylon 6 composite (Encyclopedia, 1992; Reimschuessel, 1977)*

Properties	Units	Nylon 6 [a]	Nylon 6 [b]	30-35 wt% glass fibre-reinforced [b]
Melting temperature, T_m (crystalline)	°C	223	210-220	210-220
Glass temperature, T_g (amorphous)		49	-	-
Density	g/cm^3	1.12-1.15	1.12-1.14	1.35-1.42
Tensile strength at break	MPa	48-83	41-165	165-179[c], 110[d]
Elongation at break	%	25-400	30-100[c], 300[d]	2.2-3.6[c], 6-7[d]
Tensile yield strength	MPa	-	81[c], 51[d]	-
Tensile modulus	GPa	1.0	2.6[c], 0.7[d]	8.6-10[c], 5.5[d]
Compressive strength	MPa	48-97	90-110	131-165[c]
Compressive modulus	GPa	1.7-2.4	1.7	-
Flexural strength (rupture or yield)	MPa	-	108[c], 40[d]	234-248[c], 145[d]
Flexural modulus, 23°C	GPa	2.7-2.8[c]	2.7[c], 1.0[d]	8.6-9.7[c], 5.5-6.5[d]
Izod impact (1/8-in. thick specimen)	J/m	-	32-117[c], 160[d]	112-181[c], 198-294[d]
(Izod, 0.5 in. notch)	J/m	53-294	-	-
Water absorption at saturation, 20°C	%	9-11	8.5-10.0	6.5-7.0
Thermal expansion	10^{-5}/°C	8.3	8.0-8.3	1.6-8.0

Note: Units in both references were converted to SI unit as following:
1 psi = 6894.7238 Pa
1 ft-lb./in. of notch = 53.3784 J/m of notch

a data from reference *Reimschuessel, p. 68, 1977*
b data from reference *Encyclopedia, p. 391, 1992*
c Dry, as molded (approximately 0.2% moisture content)
d As conditioned to equilibrium with 50% relative humidity

Nylon 6 has good chemical resistance to hydrocarbons, aromatic and aliphatic solvents, such as automotive oils and fuels, and refrigerants, but is attacked by strong acids, bases and phenol or even hot water (*Béland, 1990, p.39, Encyclopedia of polymer science and technology, 1985).*

Chapter 3

FIBRE - MATRIX INTERFACE

The structure and properties of the fibre-matrix interface play a major role in the mechanical and physical properties of composite materials. In particular, the large differences between the elastic properties of the matrix and the fibres have to be communicated through the interface, or, in other words, the stresses acting on the external boundaries of a specimen (i.e. on the matrix) are transmitted from the matrix to the fibre across the interface. In a simple system, bonding at an interface is due to adhesion between fibre and matrix. Adhesion can be attributed to five main mechanisms which can occur at the interface either by themselves or in combination to produce the bond. *(Hull, 1981, p. 37)*. These mechanisms are : (1) adsorption and wetting, (2) electrostatic attraction, (3) chemical bonding, (4) interdiffusion, and (5) mechanical adhesion. These are described in detail below.

3.1. Adsorption and Wetting

When two electrically neutral surfaces are brought sufficiently close together, there is a physical attraction which is best understood by considering the wetting of solid surfaces by liquids.

Wettability is defined as the extent to which a liquid would spread on a solid surface. If the net free energy of the system is reduced by liquid coverage of the solid surface, the liquid drop will spread and wet the surface completely. Wettability is most often characterized in terms of surface forces arising from surface tension. For example, for a drop of liquid resting on a plane solid surface, wettability can be measured by considering the equilibrium of forces in a system (see Figure 3.1).

For complete wettability,

$$\gamma_{LS} + \gamma_{LV} < \gamma_{SV} \qquad (3.1a)$$

where γ_{ij} represents the surface energy (energy/interfacial area) or surface tension (force/length of contact line) and LS, LV, SV designate the various surfaces (or interfaces) between bulk phases of solid (S), liquid (L), and vapor (V).

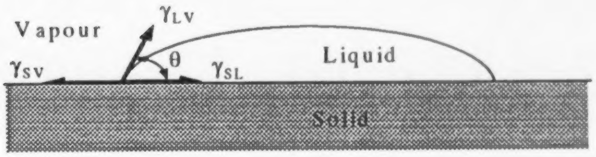

Figure 3.1. A liquid drop on a solid surface making a contact angle (θ) between the solid and the liquid. The terms γ_{LS}, γ_{LV} and γ_{SV} denote the surface energies of solid-liquid, liquid-vapor, and solid-vapor interfaces, respectively *(adapted from Hull, 1981).*

From the equilibrium of forces (Young's equation) (*Chawla, 1987, Hull, 1981*), as shown above in Figure 3.1 ,

$$\gamma_{LS} + \gamma_{LV} \cos\theta = \gamma_{SV} \tag{3.1b}$$

or

$$\theta = \cos^{-1}\left(\frac{\gamma_{SV} - \gamma_{LS}}{\gamma_{LV}}\right)$$

where θ represents contact angle.

The Dupré equation for the thermodynamic work of adhesion, W_A, of a liquid to a solid states that (*Hull, 1981)*

$$W_A = \gamma_1 + \gamma_2 - \gamma_{12} \tag{3.2}$$

where γ_1 and γ_2 are the surface free energies of the liquid and solid respectively, and γ_{12} is the free energy of the liquid-solid interface.

By putting $\gamma_1 = \gamma_{LV}$, $\gamma_2 = \gamma_{SV}$ and $\gamma_{12} = \gamma_{LS}$, we obtain

$$W_A = \gamma_{LV} + \gamma_{SV} - \gamma_{LS} = \gamma_{LV}\,(1+\cos\theta) \qquad (3.3)$$

Zisman introduced the idea of critical surface tension of wetting, γ_C (=γ_{SV}) such that only liquids with $\gamma_{LV} < \gamma_C$ will spontaneously spread on the solid. This parameter is used to evaluate the wetting of fibres by resins *(Hull, 1981)*.

Theoretical calculations *(Kelly, 1973)* indicate that a typical silicate glass fibre has a surface energy, γ_{SV} = 560 mJm^{-2} and can be wetted by liquid polyester and epoxy resin with surface energies of γ_{LV} = 35 mJm^{-2} and 43 mJm^{-2}, respectively (since, γ_{LV} = 35 and 43 are less than γ_C =560). But, since solid polyethylene has critical surface energy (γ_C) of only 31 mJm^{-2}, the above resins with $\gamma_{LV} > \gamma_C$ cannot wet it *(Hull, 1981)*.

In order to obtain complete wetting of a surface, the adhesive must initially be of low viscosity (so spreading can occur rapidly) and have a surface tension (γ_{LV}) lower than the critical surface tension (γ_c)of the solid surface *(Plueddemann, 1982)*.

Figure 3.1 shows a liquid drop on a solid surface making a contact angle between the solid and the liquid. No wetting occurs at an angle of 180° while partial wetting occurs at $0° < \theta < 180°$, and perfect wetting occurs at 0°. The contact angle depends on the nature of the surfaces; for example, the surface roughness would diminish the contact angle if the smooth surface had $\theta < 90°$ but increase it if the smooth surface had $\theta > 90°$, while adsorbed gases would increase it. Any impurities in or deliberate additions to the solid or liquid phase or a chemical reaction between the phases would affect the wettability *(Hull, 1981, p. 38)*. Fortunately, the wettability of glass can be controlled and glass made more compatible with liquid organic materials (polymers and monomers) by treating the glass surface with the proper coupling agents, such as, hydrolyzable silanes *(Plueddemann, 1982)*.

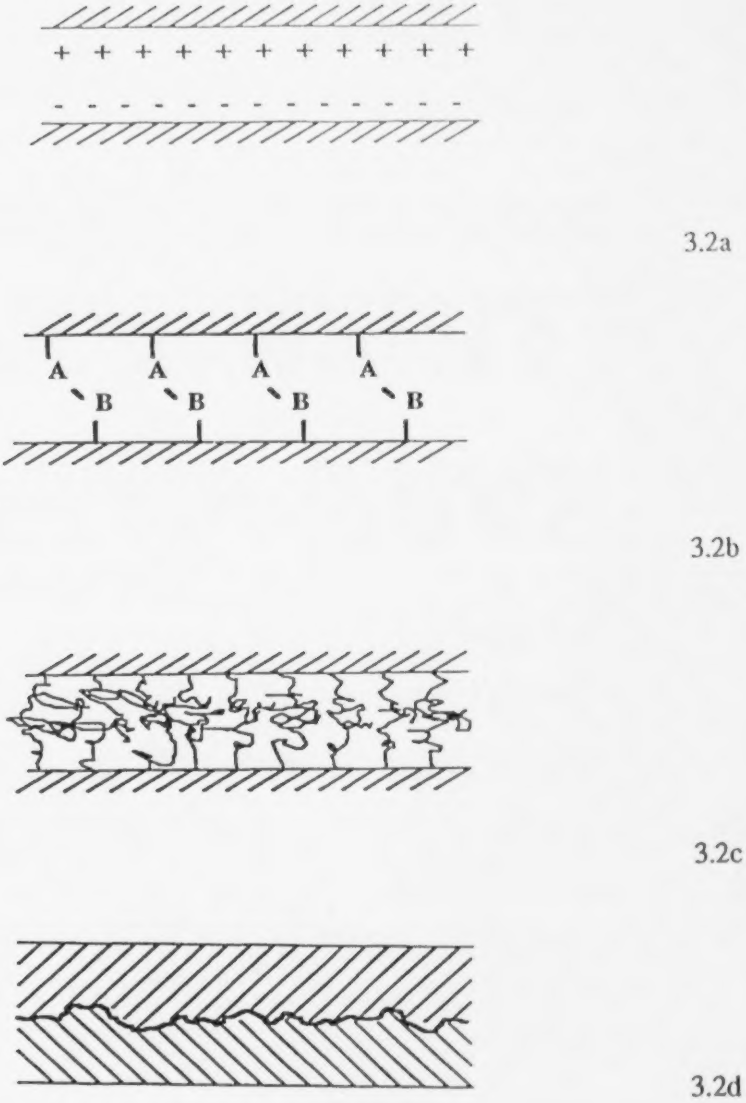

Figure 3.2. (a). Bond formed by electrostatic attraction. (b) Chemical bond formed between groups A on one surface and groups B on the other surface.(c) Bond formed by molecular entanglement following interdiffusion. (d) Mechanical bond formed when a liquid polymer wets a rough solid surface *(adapted from Hull, 1981).*

With glass fibres, the adhesion is usually the strongest in polar polymers and those with carbonyl oxygens (epoxy resins, polyesters, nylon, etc.), which are able to form hydrogen bonds with the hydroxyls on the glass fibre surface. By using coupling agents, it is possible to increase the adhesion between fibres and hydrophobic polymers *(Berlin et al., 1985).* Zisman *(Plueddemann, 1982)* concluded that good wetting of the solid surface by the liquid resin was of major importance in preparation of composites. Physical adsorption of resin on high-energy fibre surfaces could provide greater adhesive strength than the cohesive strength of organic resins, if complete wetting were obtained; localized failure would not occur at weakened interface locations, but rather within the bulk material, the highest resistance to failure that the composite could provide.

3.2. Electrostatic attraction

Forces of attraction occur between two surfaces when one surface carries a net positive charge and the other surface a net negative charge as in the case of acid-base interactions and ionic bonding (Figure. 3.2a). The strength of the interface will depend on the charge density *(Hull, 1981, p. 40).*

Although electrostatic attraction is unlikely to make a major contribution to the final bond strength of fibre-matrix composites, it could well have an important role in the way that coupling agents are laid down on the surface of glass fibres. Also, the surface may exhibit anionic or cationic properties depending on the oxides in the glass and the pH of the aqueous solution used to apply the silane coupling agents. Thus, if, ionic functional silanes are used, it is expected that the cationic functional groups will be attracted to an anionic surface and vice versa..

3.3. Chemical Bonding

This is of particular interest for fibre composite materials (Figure 3.2b)

Coupling agents are materials that improve the practical adhesive bond of polymer to the material *(Plueddemann, 1982).* They contain chemical functional groups that can react with silanol groups on glass, attached to the glass by covalent bonds. And the other different functional groups could react with the matrix during polymerization. The main function of coupling agents is to provide strong chemical links between the hydroxyl groups on the fibre surfaces and the polymer molecules of the resin *(Hull, 1981, p. 43)*.

The coupling agents used for glass fibre are usually organofunctional silanes which are hybrid organic-inorganic compounds that serve to bridge the organic-inorganic interface. The general chemical formula for the silane coupling agents is R-SiX_3. The X units represent hydrolyzable groups (an alkoxy, e.g.-OC_2H_5, or a halogen group) bonded to silicon and R is an organofunctional group. In the aqueous solution, these X groups are hydrolyzed to yield the corresponding silanol groups (Figure 3.3.b). When water is removed, the reversible condensation reaction occurs between the silanol and the surface, and between adjacent silanol molecules on the surface. The result is a polysiloxane layer bonded to the glass surface (Figure 3.3c). Therefore, the silane-coated fibre presents a surface of R groups to the monomer or unpolymerized resins. This promotes compatibility and wetting. During the polymerization process, it is desirable that reactive groups in the resin react with the organo-functional R groups, so that the R groups are strongly covalently bonded to the polymerized resin (Figure 3.3d). But one should realize that the R group must first be compatible with the *resin (Hull, 1981, p. 43)*. In our work, in which we mainly used toluene solutions instead of aqueous solutions, these X groups (on the coupling agent R-SiX_3) reacted with the OH-groups (on the glass surface) and formed covalent bonds to the glass fibre surfaces, giving HX as a byproduct (see Figure 3.4).

If no adhesion promoter is used on the glass surface, any water diffusing through the resin will eventually reach the fibre surface, which results in rapid deterioration of the untreated glass-resin interface. This will reduce the ability of the fibres to accept a transfer of stress from the polymer matrix. The basic principles of how a silane coupling agent works is illustrated in Figure 3.3, where, R-SiX_3 represents a silane coupling agent.

$$R-SiX_3 + H_2O \longrightarrow R-Si(OH)_3 + 3HX \qquad \textbf{3.3a}$$

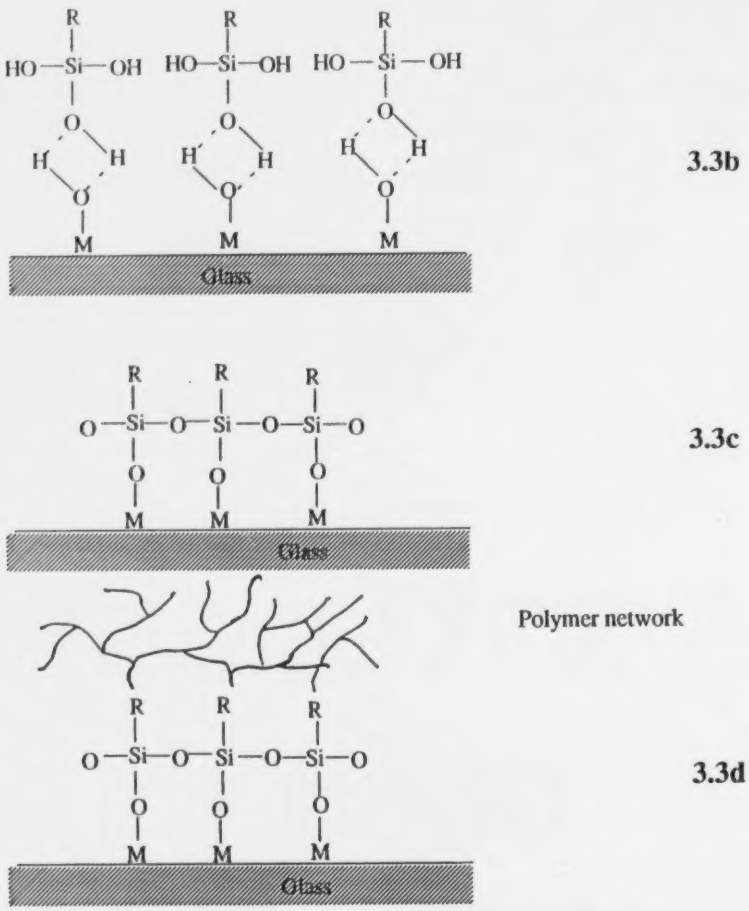
R
HO—Si—OH
O
H
M
Glass
3.3b
O—Si—O—Si—O—Si—O
3.3c
Polymer network
3.3d

Figure 3.3. Function of coupling agent (a) Hydrolysis of organo-silane to corresponding silanol. (b) Hydrogen bonding between hydroxyl groups of silanol and glass surface. (c) Polysiloxane bonded to glass surface and laterally, to neighboring coupling molecules, to form a network structure surrounding the fibre. (d) Organo-functional R group reacted with polymer matrix *(adapted from Hull, 1981, p. 44).*

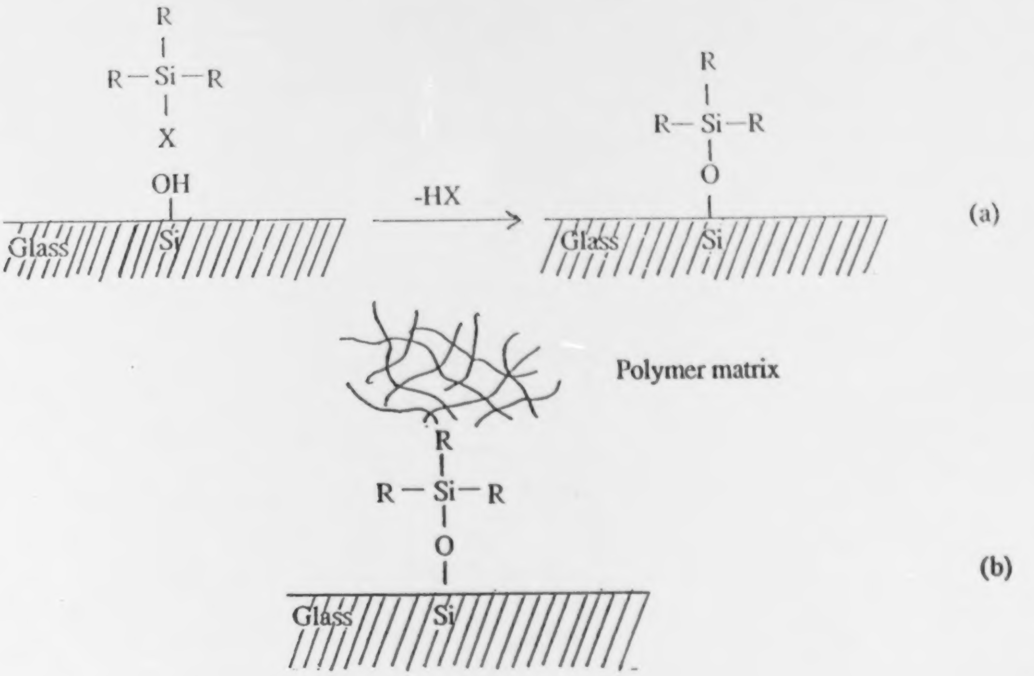

Figure 3.4. Function of coupling agent (a) Reaction between silane and hydroxyl group at glass fibre surface in toluene solution (non aqueous) (b) Organo-functional R group reacted with polymer matrix.

To explain how a silane coupling agent leads to a strong water-resistant bond, *Plueddemann (1974)* proposed that movement or displacement at the interface was able to relax the local stresses and maintain the chemical bond if a reversible bond breakage mechanism possibly occurred *(Hull, 1981, p. 45)*.

He proposed a mechanism wherein water may diffuse through the resin to the interface, after which the covalent M-O bond hydrolyses as shown in Figure 3.5. Because this process is reversible, therefore, the covalent bond can reform when the water diffuses away. If there is a simple shear stress parallel to the interface, the surfaces can slide past each other without permanent bond failure. This reversible bond process has been verified by Fourier transform infra-red spectroscopy *(Ishida and Koenig, 1980)*.

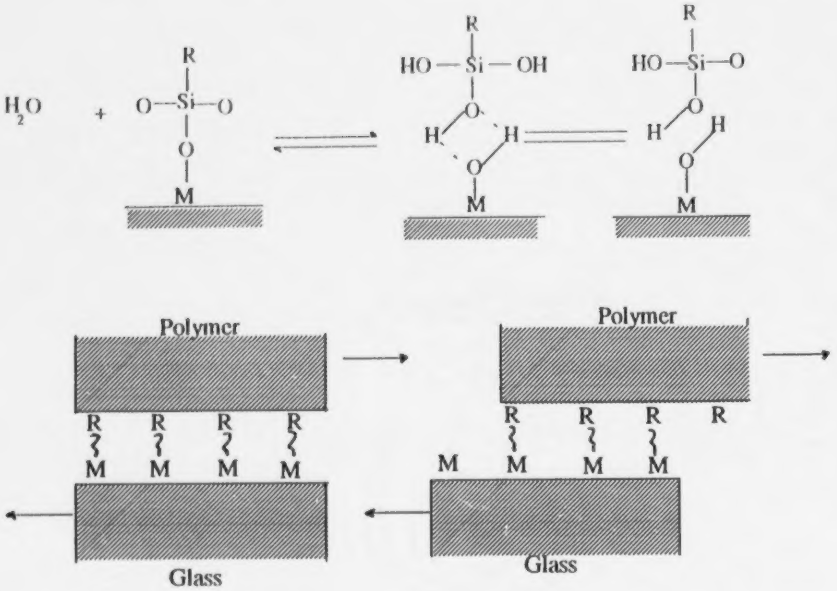

3.5a

3.5b

Figure 3.5. (a) Mechanisms of reversible bond formation associated with hydrolysis as proposed by *Plueddemann (1974)*. (b) Shear displacements without permanent damage of the interface bond. *(adapted from Hull, p. 45)*

3.4. Interdiffusion

It is possible to form a bond between two polymer surfaces by the diffusion of the polymer molecules on one surface into the molecular network of the other surface, as illustrated in Figure. 3.2c. The bond strength will depend on the amount of molecular entanglement and the number of molecules involved. Interdiffusion may be promoted by the presence of solvents and plasticising agents and the amount of diffusion will depend on the molecular conformation and constituents involved and the ease of molecular motion. Interdiffusion may account in part for the bonding achieved when fibres are pre-coated with polymer before incorporating into the polymer matrix. *(Hull, 1981)*.

Jenneskens et al (1992) studied the evidence for interfacial amide formation between surface-bound poly(3- aminopropyltriethoxysilane) and nylon 6 in composites reinforced with glass beads at 30 wt%. The glass beads were pretreated by immersing 0.5g glass beads in a mixture of toluene, water (water molar concentration three times that of the coupling agent), and 3-aminopropyltriethoxysilane (10 wt%), a molecule for which the end carbon (bonded to the amine nitrogen) was either ^{13}C or natural-abundance $^{12}C/^{13}C$. The mixture was stirred for 1 hour at room temperature and the glass beads filtered off and dried under vacuum at 100°C for 1 hour. During the pretreatment, ethoxy groups of 3-aminopropyltriethoxysilane were hydrolyzed in aqueous solution to yield silanol groups which reacted with the hydroxyl groups on glass surface and between adjacent silanol molecules on the surface, resulting in a poly(3-aminopropyltrisiloxane) network layer bonded to the glass surface (see details of reaction in chapter 3, p. 29, Figure 3.3c). These glass beads were later isolated from the composites by dissolving the matrix in trifluoroethanol. The amount of surface-bound organic on the glass beads, determined with thermogravimetry, was far greater than a mere monolayer of the glass-bonded silane molecule could account for. The analysis revealed that there had been formation of covalent chemical bonds in the polymer melt between some of the amine groups of the surface-bound poly(3-aminopropyltrisiloxane) and nylon 6 carbonyl groups (-CO-)in the interface region during composite preparation.

3.5. Mechanical Adhesion (roughening or surface interlocking)

Some bonding may occur purely by the mechanical interlocking of two surfaces as illustrated in Figure 3.2d. A resin which completely wets the fibre surface follows every detail of that surface. A quite separate factor which also relates to the roughness of the fibre surface is the potential for an increased bond strength through, for example, chemical bonding because of the larger surface area which is available *(Hull, 1981)*.

3.6. Chemical Acid Etching

Chemical etching may be used to remove surface material along with the contaminants. Etching removes surface layers such as oxides, eliminates or blunts surface cracks in brittle materials, removes contaminants that are otherwise difficult to remove, and increases surface area.

Yip and Lin, 1990, treated surfaces of five different kinds of carbon fibres with three different oxidizing chemical reagents (60% concentrated nitric acid, 15% hydrogen peroxide, and concentrated phosphoric acid) to modify surface characteristics. Scanning Electron Microscope (SEM), Scanning Auger Microprobe (SAM), and X-ray Photoelectron Spectroscopy (XPS or ESCA) techniques were used to characterize surface morphology and chemistry of these treated fibres. The chemical treatments increased both the oxygen surface concentration and surface roughness ("etching"). They found that the extent of oxidation on the carbon fibre surface depended on the chemical reagents rather than on the surface structures and the precursors of the fibres. The adhesion of carbon fibre to the epoxy resin was not promoted by the amount of oxygen or number of carbon-oxygen functional groups on the fibre surface but by the roughness at the surface which enhanced the mechanical interlocking and physical mating of carbon fibre and epoxy resin. The transverse tensile strength of fibre composites was improved up to 2.9 times (transverse tensile strength of treated/untreated).

Larena et al., 1992, investigated the bulk and surface properties of E-glass short fibres which were leached with hydrochloric acid (6M) solution. They also studied the effect of leaching on the reaction of fibre with chlorosilanes using FTIR spectroscopy and thermal analysis. Leaching removed basic oxides from the fibre, increasing fibre surface area and causing intense surface hydration as well as water diffusion into the fibre. Surface hydration was found to increase the amount of polyvinylsiloxane coating formed when the fibre was treated with vinylchlorosilane in refluxing toluene, but prevented the fibre from reacting with monochlorosilanes in toluene or aqueous solution. The coatings obtained from aqueous or toluene solutions of methylvinyldichlorosilane and vinyltrichlorosilane showed high thermal stability in a nitrogen atmosphere.

3.7. Plasma treatment

Plasma treatment of fibre surface is employed to modify the surface morphology and chemistry in order to improve adhesion between the resin and fibres.

"A plasma is a system of gaseous ions and radicals formed by radio-frequency (megahertz) induction across a gas at low pressure" *(Allcock and Lampe, 1990).*

Attributes of the plasma process include *(Mattox, 1990):*

i) removal of contaminants or weak surface layers,

ii) control over surface functional group composition and concentration,

iii) creation of active sites on the surface

iv) cross - linking the surface of polymeric fibres, or varying the surface wettability.

The plasmas can perform various functions, such as cleaning and etching or roughening, chemical surface treatment, and modifying surface chemistries. Thus the above attributes allow plasmas to be used as a tool to impart specific chemistries and characteristics on fibre surfaces to promote various adhesion mechanisms.

Gaur and Davidson, 1990, treated aramid fibre (Kevlar) with different types of plasmas: oxidizing plasma, reducing plasma, neutral plasma, and hydrophilic plasma. A small amount of epoxy resin was applied to the surface of each treated fibre, and the interfacial shear strength of these fibres tested by microbond technique. They found increments of interfacial adhesion for all the plasma-treated fibres, up to 7.9 times (interfacial shear strength of plasma-treated/untreated), irrespective of the chemical nature of the ionized gas. The adhesive bond strength was believed to be improved due to texturing of the fibre surface.

Krishnamurthy and Kamel, 1989, studied the effect of argon plasma treatment of glass surfaces by FTIR and SEM. The argon plasma on cleaned glass surfaces resulted in increased surface area due to microetching and surface rearrangement of the silicate network. They also found that the etching action of the argon plasma on the substrate surfaces facilitated the removal of the micron (μ) thick sizing from the commercial fibres accompanied by little loss in tensile strength. Plasma was also used to graft selected monomers (allylamine, hexamethyldisiloxane) on the surface of glass fibres for enhancement of bond compatibility in a composite system. The grafting treatment followed by argon etching improved the wettability further and increased the surface area.

Chang and Jang, 1990, found that pretreatment of carbon fibres with oxygen plasmas effectively improved the interfacial adhesion between the carbon fibre and bis maleimide matrix. Increase of oxygen content and polarity induced in the modified carbon fibre surface were observed. The composite transverse tensile strength increased from 2.20 MPa (untreated) to 4.71 MPa (20-minute treatment). However, exposure of fibres to the plasmas degraded the tensile strength of the fibre from 3.8 GPa (untreated) to 3.0 GPa (20-minute treatment). Therefore, an optimal treatment time was needed. They found that for short exposure time (less than half a minute) the fibre surface remained smooth (hence no external physical damage) and acquired an increase of surface free energy; this promoted wettability of fibre by matrix and produced stronger van der Waals forces. Longer exposure time caused the fibre surface to become rougher which would promote a desirable physical interlocking mechanism between the fibre and the matrix.

Chapter 4

FABRICATION OF GLASS FIBRE/NYLON 6 COMPOSITES

4.1. Equipment

The equipment consists of two parts: mold, where the polymerization takes place, and chemical feed vessel (from which the nylon monomer and other ingredients flow into the mold). The overall arrangement is shown in Figure 4.1.

4.1.1. Mold

The mold consists of a male and a female part. Major dimensions are given directly on Figure 4.2. The male part was fitted with a Viton® (du Pont, Wilmington, DE) O-ring to ensure vacuum tight conditions in the mold. This mold was machined from rectangular slabs of aluminum alloy, selected to ensure good thermal conductivity, and heated by 8 cartridge heaters (Tru-Temp Electric heat Ltd., Edmonton). Four of the heaters (400 W each) were in the male part of the mold, placed vertically and spaced at 90° intervals around the mold centerline; the other four heaters (250 W each) were in the female part of the mold, placed horizontally along radii at 90° intervals that were spaced about 22.5° to the vertical heaters above. A thermocouple was inserted into the female part, closely below the recess containing the polymerizing fluid and glass fibres (shown in Figure 4.1) and connected to a digital temperature readout and on-off controller which activated all 8 heaters simultaneously. A tapered hole was drilled through the centerline of the male part to allow the reaction mixture to fill the mold from above.

Originally, as described by *Duangchan, (1994)*, the female part was drilled from the side with a hole of diameter 3.6 mm (9/64"), connecting to a valve leading to a vacuum pump to evacuate the mold as shown in Figure 4.2, (valve "D"). The problems associated with this kind of arrangement were: (a) during the mold-filling operation, the caprolactam vapors used to flow into the vacuum pump, attacking the metal and causing frequent seizing of the pump, and (b) the composite disk which emerged from the mold was often

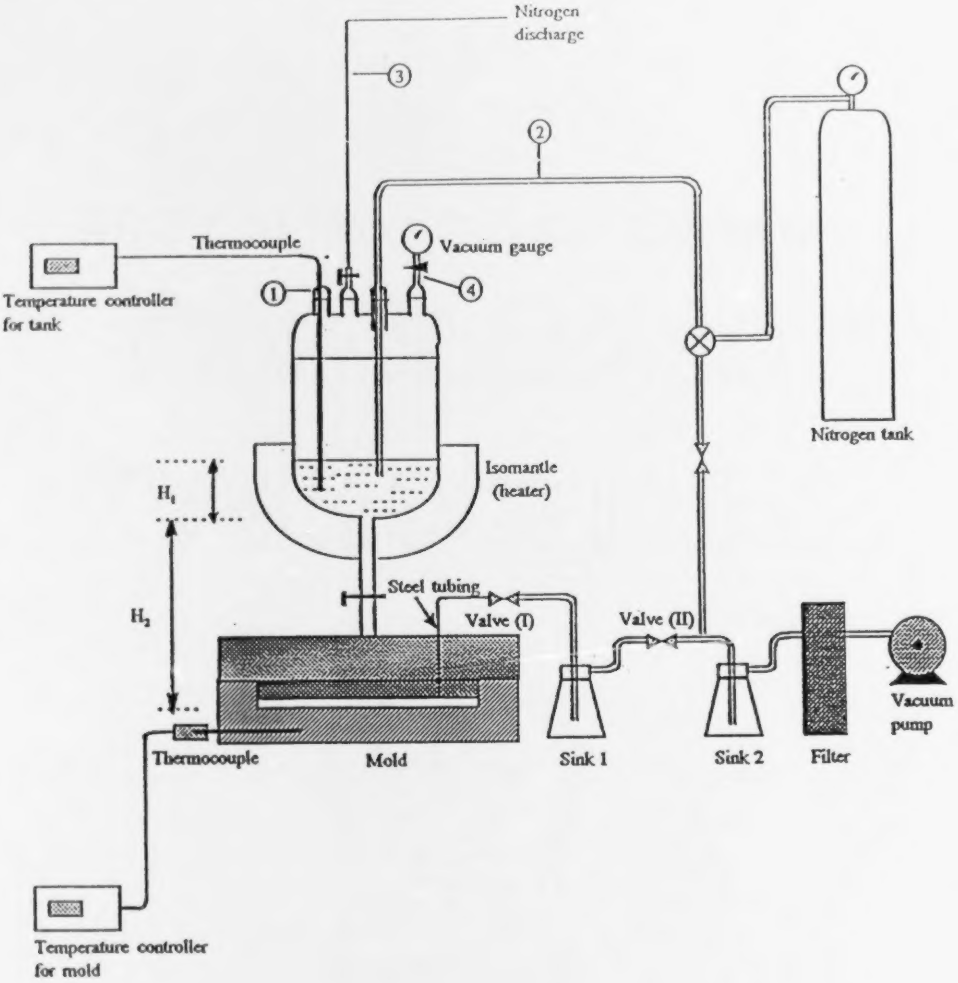
Nitrogen discharge
③
②
Thermocouple
Vacuum gauge
①
④
Temperature controller for tank
Nitrogen tank
Isomantle (heater)
H_1
H_2
Steel tubing
Valve (I)
Valve (II)
Vacuum pump
Thermocouple
Mold
Sink 1
Sink 2
Filter
Temperature controller for mold

H_1 = initial liquid level above bottom of vessel = 60 mm
H_2 = length of capillary (i.e. distance from vessel to disk entry point) = 150 mm

Figure 4.1. Diagram of experimental equipment (not to scale)

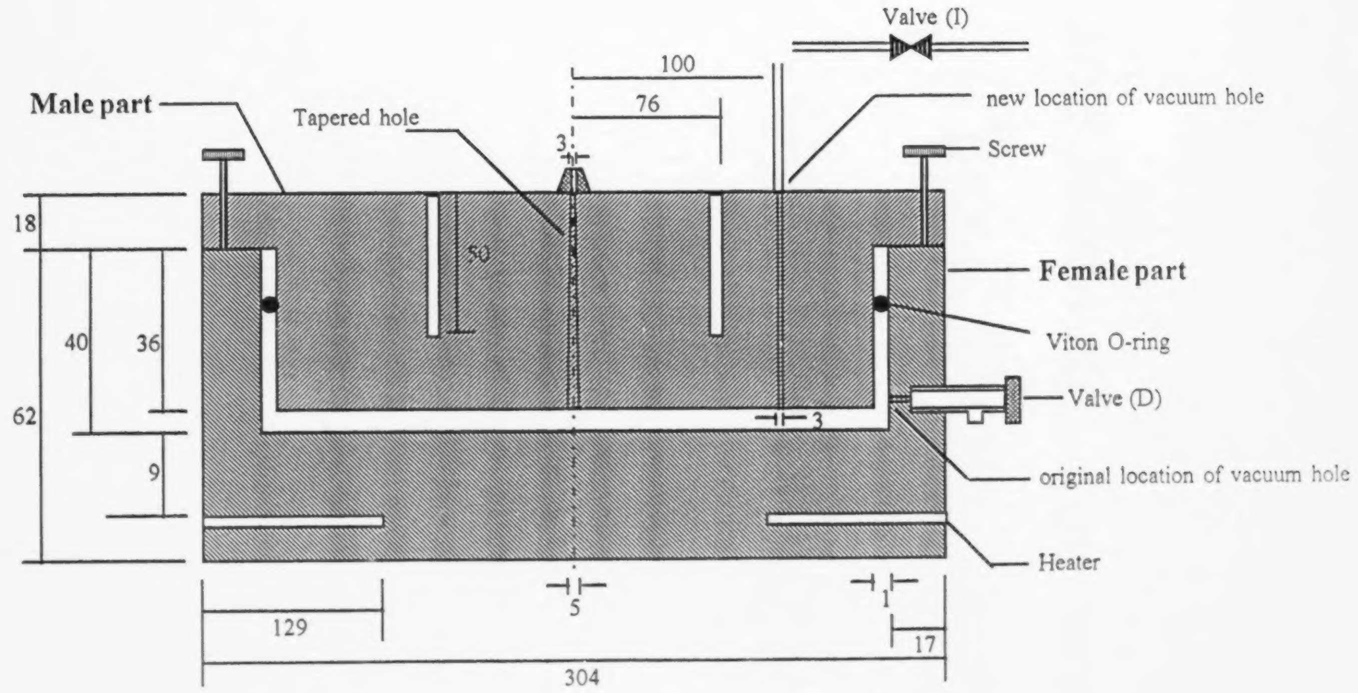
Valve (I)
100
76
Male part
Tapered hole
3
new location of vacuum hole
Screw
18
50
Female part
40
36
Viton O-ring
62
Valve (D)
3
9
original location of vacuum hole
Heater
5
1
129
17
304

Figure 4.2. Mold diagram (not to scale, Unit: mm)

marred by very apparent voids on the surface, which indicated that air or other gases were entrapped inside the mold. To overcome these problems, a hole was drilled from the top of the female part at a distance of 10 cm from the centre of the mold and it was decided to maintain the vacuum while the mold filling was carried out. The distance of 10 cm was chosen arbitrarily toward the edge of the mold, since large bubbles were obtained in this region. This hole location would thus be best suited to remove the gases that were released inside the mold. A cartridge filter, Fulflo® (Parker Filtration Division, Indiana) was also installed at the pump inlet to adsorb the vapors and prevent them from entering the pump, thus shielding the pump from chemical attack. The overall arrangement was achieved by connecting the hole to a sink through a steel tubing and valve (I), and the sink(1) was in turn connected to valve(II), followed by sink(2), then a cartridge filter, which finally led to the vacuum pump as shown in Figure 4.1.

The mold, pre-loaded with compressed glass-fibre mats that were to be encapsulated by the polymer, was held tightly shut by four C-clamps. Its outer surface was insulated by fibre glass insulating blanket J-M Glas-Mat 1200® (Canadian Johns-Manville Co. Ltd., Ontario), fibreglass cloth tape (Fisher Scientific) to minimize heat loss and temperature gradients within the polymerizing caprolactam. To open the mold, after polymerization had occurred, the 4 screws in the top of the male part were turned to exert force against the female part, breaking any polymer seal and lifting the male part up for manual removal.

Temperature inside mold

The surface temperatures inside the mold were measured with thermocouples taped to the metal along upper and the lower surfaces, at different radii and angular positions of the mold, as described by *Duangchang, 1994* and shown in Figure 4.3. Both radial and vertical temperature gradients were found. The steady-state temperature of the upper part was always slightly higher than that of the lower part, the $\Delta T(z)$ ranging from about 2° (at r = 60mm) to 5° (near rim) when the target was in the range 100°-150°C (Figures 4.4 and 4.5). The mold had higher temperature near the center and lower temperature toward the edge of the mold, the total radial gradient ΔT(r) being about 1°C across the upper surface and 4°C across the bottom surface when the overall level was 150°C

The temperature along a path directly above a lower heater position was higher than that along the path equidistant between two heaters by about 1°C. However, all these spatial variations were regarded as small enough to neglect, in the sense of being unable to cause major localized variation in the polymerization process or in final product properties. Therefore, the mold was assumed to have a uniform temperature at whatever steady-state level was set (e.g., 100°C or 150°C). This temperature distribution is further reviewed in detail by *Duangchan, 1994*.

Caption for Figure 4.3.

Locations of thermocouples on the upper and lower surfaces of the mold cavity. Their proximity to the electric heating rods, embedded in the aluminum upper and lower parts, is also given.

(a) Upper surface, seen from below. Positions are designated as "NU_n" where n is radial distance in millimeters, U refers to the upper surface, and N = 1 or 2 to indicate alignment along a radial path that passes either (1) under one of the upper vertical heaters or over one of the lower horizontal heaters, or (2) halfway between two such positions. At position $1HU_{76}$ we use N = 1H to highlight its placement directly under one of the vertical heaters, a location which has the greatest likelihood of being a "hot spot" on the upper surface.

(b) Lower surface, seen from above. Positions are designated as either "L_n" or "HL_n", where n is the same as in (a), L refers to the lower surface, and H indicates alignment on a radial path that passes directly along and above one of the lower horizontal heaters, thus possibly being a "hot line" and containing a local hot spot at r = 76 mm. The unprefixed L_n locations lie on a radius halfway between two of the HL trajectories. The dashed line represents the position of the horizontal thermocouple well beneath the surface, for insertion of the sensing control thermocouple which was always pushed to the end of the well.

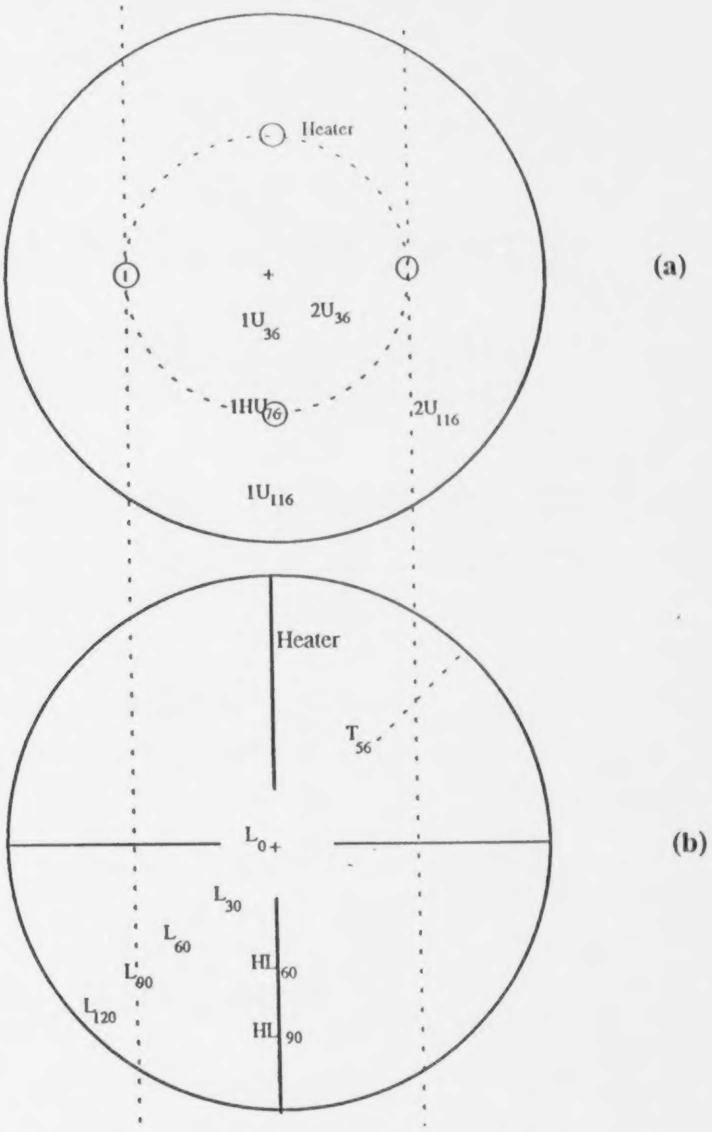
Heater
1
1
$1U_{36}$
$2U_{36}$
$1HU_{76}$
$2U_{116}$
$1U_{116}$
(a)
Heater
T_{56}
L_{0}
L_{30}
L_{60}
L_{90}
L_{120}
HL_{60}
HL_{90}
(b)

Figure 4.3. Locations of thermocouples on the (a) upper and (b) lower surfaces, of the mold cavity *(adapted from Duangchan, 1994).*

NU_n : U = Upper surface
N = Radial path, (N = 1, 1H (below heater), 2)
n = Radial distance, mm
L_n : L = lower surface
HL_n : = Lower surface above heater
T_n : = Thermocouple

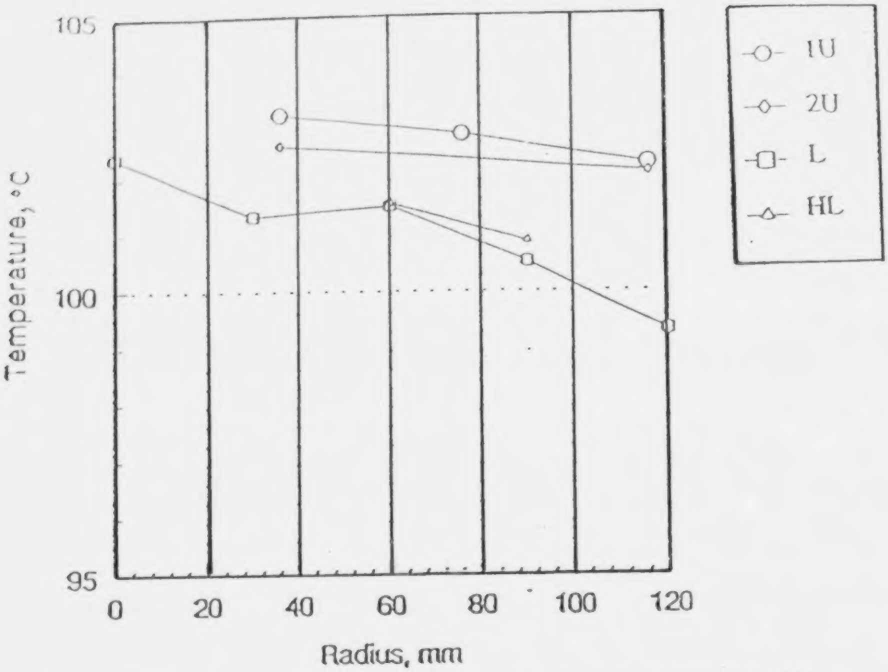

Figure 4.4. Temperature distributions on mold surfaces when nominal set point is at 100°C

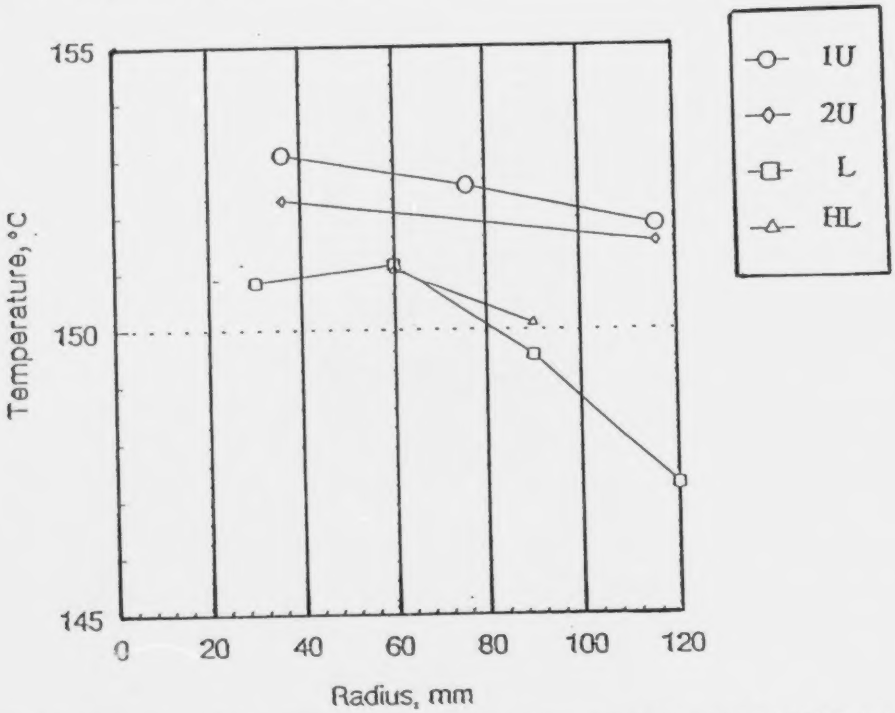

Figure 4.5. Temperature distributions on mold surfaces when nominal set point is at 150°C *(adapted from Duangchan, 1994)*

4.1.2. Chemical feed Vessel

The chemical feed vessel (Figure 4.1), used to deliver liquid monomer and catalyst to the mold, was a cylindrical-shaped glass flask with a round bottom to which was attached a valve (built-in type for vacuum purpose) followed by a short delivery glass tube (inside diameter 5 mm., length 40 mm) for delivering the flask contents to the mold below, through a short silicone rubber tube. The flow of the molten contents from the flask into the mold was controlled by the above valve. The temperature of the feed vessel liquid was maintained by a temperature controller, which received a signal from a thermocouple inserted inside the vessel and regulated power to an isomantle (heater) around the vessel to achieve the desired set point. Four access ports on top of the flask (shown in Figure 4.1) were used for the following purposes: **(1)** to insert the thermocouple for reasons stated above; **(2)** to insert a long tube extending to the flask bottom to inject N_2 and then allow it to flow out through port **(3)**, carrying with it traces of moisture and air from the molten monomer; and **(4)** to insert a vacuum gauge to measure the pressure inside the flask during the degassing operation. Port **(2)** could alternatively be used to a maintain a N_2 blanket above the liquid after the N_2 purge had been completed, or to apply a partial vacuum inside the flask for the degassing operation. Port **(3)**, the N_2 exit, was a vent to atmosphere, which could also be closed as desired.

4.2. Procedures for producing continuous-fibre composite sheet

4.2.1. Previous work

The formation of a reinforced thermoplastic sheet, followed by thermoforming to a desired shape, is a frequent procedure in the pressing operations of the automobile industry. The glass-fibre reinforced thermoplastic sheet *(Temple, 1972)* is produced by extruding molten polymer in one of two ways: (a) mixed with short glass fibres, then extruded through thick slot dies to form rectangular slabs, and then rolled to sheet dimensions; or (b) as a glass-free but highly viscous liquid onto a continuous glass (swirl) mat or chopped strand mat, then forced under high pressure (and perhaps with heating) to permeate the mat. The problems of this latter method are related to (i) nonuniformity of penetration of the mat, (ii) the difficulty of coating all surfaces of the glass fibres, and (iii) the need for high pressures (due to high viscosity of the polymer). Problems of the former method arise from undesired and non-uniform orientation of the short fibres caused by the shear flow, and associated nonuniform distribution of the glass fibres in the composite sheet (as well as high extrusion pressure). Because of these problems, there is considerable incentive to design new methods for producing long-fibre (or continuous fibre) composites.

Ishida and Rotter, 1991, have developed a new processing method, a combination of RIM (Reaction Injection Molding) and a pultrusion process, called RIM-Pultrusion, to produce composites in a continuous manner. Polyurethane was used to verify the viability of this modified process for thermosets, and nylon 6 was used for thermoplastics. For nylon 6, ε-caprolactam, phenyl isocyanate and sodium hydride were used as monomer, catalyst and initiator, respectively (see Chapter 2). It was found that the nylon 6/glass fibre (rovings) composite was successfully produced by RIM-Pultrusion. The products represented good surface quality and substantial mechanical integrity.

Otaigbe and Harland, 1988, made nylon 6 and glass fibre composites by placing a continuous strand (swirl) glass fibre mat in a mold similar to ours and then injecting under vacuum the reactive liquid mixture containing caprolactam monomer, sodium hydride, and phenyl isocyanate. The fibre volume fraction distribution across the diameter of the composite seemed to be uniform; the crystallization of the matrix was over 50% . This technique ("*in-situ* polymerization") produced a sheet of material that could be thermoformed and had uniform distribution of glass fibre in the composite.

The process used by *Otaigbe and Harland* had a number of advantages. The low-viscosity injected caprolactam permeated the mat easily, without application of pressure, and easily wet the glass fibre. The temperature for liquid processing of the caprolactam monomer was lower than that needed to process nylon 6, since $T_m = 72°C$ for the monomer and 225°C for the polymer*; moreover, the highest temperature used was the post-flow polymerization temperature (150°C) that was set in the mold. Reduction in operating cost was also achieved, because of the accumulation of all the advantages cited above.

For these reasons, it was decided that the composites in this study would be made by the same technique which is diagrammed in Figure 4.6, with some mold modifications applied to overcome operational problems.

4.2.2. Procedures used in this work to make continuous-fibre composite sheet

(A). Mold preparation

First, silicone grease and silicone mold-release spray (Dow Corning Corp.) were applied inside the mold to ensure easy post-polymerization removal of specimen disks. The grease was applied around the cylindrical surface inside the mold (female part) and around the O-ring rubber (male part), while the release spray was applied at the flat surface of both female and male parts and also in the tapered hole at the centre of the male part.

Continuous-strand glass "E"-fibre mat, non-woven and planar-random (grade M8608), was obtained in rolls from Fibreglass, Canada. Characterization data supplied by the manufacturer are: filament diameter = 20 μm, filaments/strand = 36-37, textile (strand) weight = 25 g/km, mat rest thickness = 1.02 mm, mat areal weight = 450 g/m^2, fibre tensile strength, $\sigma_b = 1.86\text{-}2.0$ GPa, fibre strain at break, $\varepsilon_b = 4.5\text{-}4.9\%$, fibre modulus, E = 69.0-72.4 GPa. From these rolls, mat disks were cut with a scissors to a diameter of 22 cm. In most commercial glass-fibre mats, chemical agents called sizing are applied to the

---

* *Rodriguez, 1989*, p.509, points out that unreacted monomer which would remain as about 10% of an equilibrium mixture with molten nylon 6 can be minimized in the final product if the reaction takes place at $T < 225°C$ (presumably because removing the polymer by immediate crystallization drives the equilibrium toward full consumption of caprolactam).

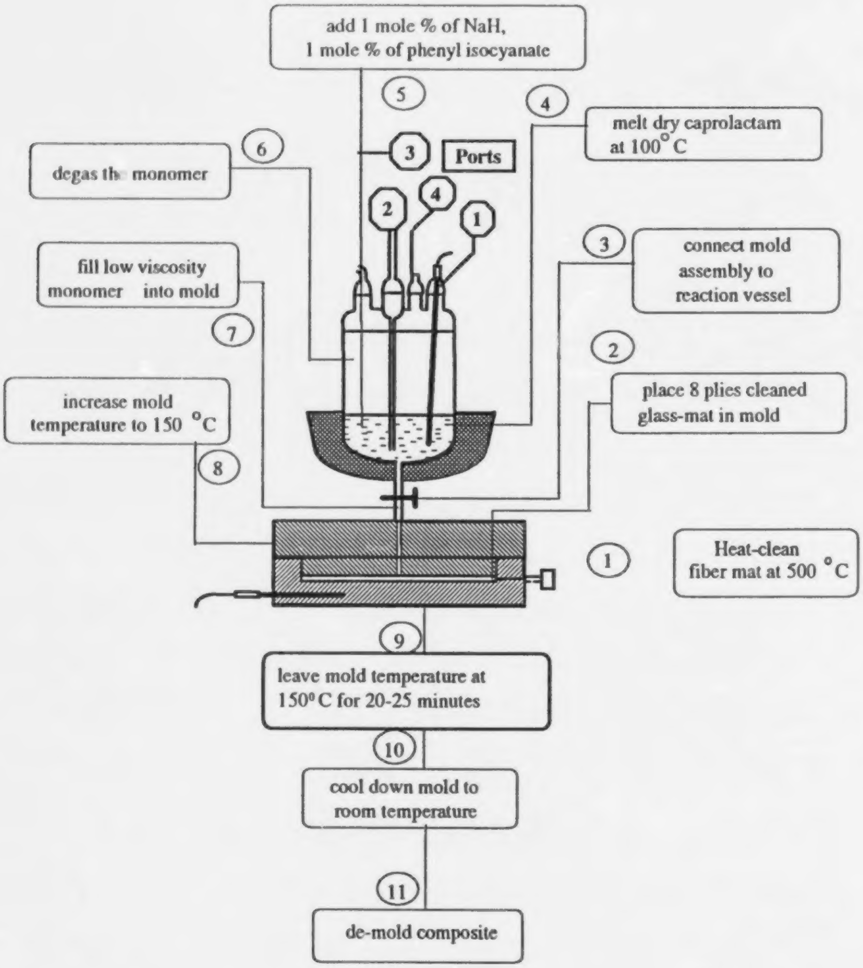
add 1 mole % of NaH,
1 mole % of phenyl isocyanate
5
4
melt dry caprolactam
at 100° C
6
degas the monomer
3
Ports
2
4
1
fill low viscosity
monomer into mold
3
connect mold
assembly to
reaction vessel
7
2
increase mold
temperature to 150 °C
place 8 plies cleaned
glass-mat in mold
8
1
Heat-clean
fiber mat at 500 °C
9
leave mold temperature at
150° C for 20-25 minutes
10
cool down mold to
room temperature
11
de-mold composite

Figure 4.6. Procedure to make nylon 6/glassfibre composite

glass surface to prevent breakage of fibres and promote fibre/matrix adhesion. The size is usually an aqueous emulsion containing processing aids, such as an anti-static agent, a lubricant, a wetting agent, a binder, and adhesion promoters. If these sizing agents are compatible with nylon 6 then, it would not be necessary to clean the glass-fibre mat. In this work, an attempt was made to use directly the glass-fibre mat with its as-received sizing to make a glass-fibre/nylon 6 composite. The resulting composite was brown due to the color of burnt sizing compound, and the composite was so brittle that it could be broken by hand. This showed that this sizing was not compatible with our nylon 6, and the glass-fibre mat had to be cleaned before use. Earlier work by *Duangchan, 1994* involved heating the glass fibre mat (already cut) in a muffle furnace, in air, at 500°C for about 1 hour to remove the sizing. In the present work, an attempt was made to clean the glass fibres chemically, too, and this will be discussed later in section **4.3.2.A(i)**

When heated in the furnace, the colour of the glass fibres turned from white to dark brown (due to colour of the burnt sizing) and then turned to white again when there was no more sizing.

Eight of the cleaned glass fibre mats were placed inside the lubricated mold. This 8-ply stack, rising above the desired sheet height of the mold, was then compressed as the mold was closed firmly by 4 C-clamps. Next, the insulator (Kaowool), which was cut in two circular-shaped pieces to cover the top and bottom part and a rectangular piece to wrap around the edge of the mold, was installed with tape. The vacuum pump was turned on, with the pinch-cock on the silicone tubing closed, to evacuate the fibre-filled mold to a pressure of about 5 kPa. The temperature of the mold was raised and maintained at 90°C by appropriate setting of the controller.

(B). Preparation of activated monomer in vessel

The polymerization of caprolactam in this experiment is anionic, using sodium hydride (Aldrich 60% dispersion in mineral oil) and phenyl isocyanate (Aldrich 98% pure) as initiator and activator, respectively. The dry caprolactam (Aldrich 99+% pure) was charged into the chemical feed vessel through access port **(3)**, then was heated to about 90-100°C by the isomantle in order to liquefy the caprolactam ($T_m \approx 72°C$, $T_b = 136\text{-}138°C$) throughout the vessel. Introducing dry nitrogen gas (from Praxair) to the other inlet tube in port **(2)**, which was above the monomer solution, provided an inert gas blanket but maintained atmospheric pressure in the vessel during the course of complete melting of the monomer. After complete melting of the monomer, the original tube to maintain the nitrogen blanket was replaced with a long tube which extended to the flask bottom to bubble dry nitrogen gas through the liquid for about 10 minutes in order to remove air, oxygen and moisture from the vessel. Following this, the original tube was reinserted in port **(2)** to restore the nitrogen blanket above the monomer solution. Equimolar concentration (1 mol% based on the weight of caprolactam used) of the initiator (sodium hydride) was then added to the molten caprolactam. For example, 0.43 gm of sodium hydride (powder form) were first added into 200 gm of ε-caprolactam*. Hydrogen bubbles occurring from the reaction of sodium hydride and caprolactam were observed. Since nitrogen gas was bubbled through the monomer, it was certain that some nitrogen gas dissolved in the solution (probably saturated, at 100°C, in melted caprolactam). Therefore, N_2 flow was stopped and the chemical vessel was evacuated to a pressure of 5kPa via a vacuum pump to degas the monomer solution. When the vacuum was first applied, a good number of bubbles were seen rising through the molten liquid. Degassing was continued

---

[*] Sodium hydride is a flammable, corrosive solid and reacts violently with oxygen (at temperatures of around 60°C), and with water at room temperature. Therefore, it is extremely important to ensure the presence of nitrogen atmosphere in the vessel before adding the catalyst. Also, proper precautions must be taken during handling of this catalyst.

until very few bubbles were seen rising through the liquid, which usually took about 15-20 minutes. Following degassing, an N_2 blanket at 1 atm was restored to the vapor space above the liquid. Equimolar concentration (1 mol% based on the weight of monomer) of phenyl isocyanate (activator) was then added to the vessel contents through port **(3)** using a syringe. Manual stirring of the flask contents was occasionally done with the help of the long rod of the thermocouple.

(C). Mold-filling, polymerization of caprolactam and removal of disk

Mold-filling: Two different techniques were employed to fill the mold. In one technique, the low-viscosity, molten monomer was allowed to flow into the mold under gravity, and in the second technique, partial vacuum was applied to the mold to pull the molten monomer into the mold. These techniques are described briefly below.

(i) In the first technique, the vacuum hole which was drilled in the top of the mold (near the outer radius) was connected to the atmosphere through a straight vertical glass tube. Mold-filling was initiated by opening the valve at the connection between the feed vessel and the mold. The molten caprolactam would first have to fill the mold completely and then rise up into the glass tube. However, this was an unacceptably slow process; even when the mold was not pre-loaded with glass fibre mats, the time taken by the molten caprolactam to fill the mold and rise into the glass tube was about 30-45 seconds. When the mold was preloaded with glass fibre mats, filling time increased to about 20-25 minutes. The latter was so long because the caprolactam had to fill the entire volume of the cavity while overcoming the resistances to flow into the crevices between the glass fibres, and only after doing so, it would rise up into the glass tube. So, to reduce the time of filling, we decided to reduce the volume of the cavity that the caprolactam had to occupy inside the mold, by placing an insert inside the female part of the mold as shown in Figure 4.7. The thickness of this insert was 4mm (same as the cavity thickness) and its diameter was slightly less than the diameter of the female part, so as to fit the former snugly. The insert had a rectangular cavity (19.0mm x 10.5mm) around the centre. This technique of placing an insert thus helped to reduce the time to fill the rectangular mold by gravity feed of the monomer to about 8-10 minutes. However, this was still not entirely satisfactory as it meant that the transfer tube, connecting the feed vessel to the mold, had to be kept warm continuously to avoid being plugged by the molten caprolactam freezing inside the tube. This warming was done by heating the tube continuously by a heat gun. This procedure was still very tedious and not practical in terms of waiting so long for the mold to be filled completely with the monomer. Furthermore the disk that emerged from the mold showed that the caprolactam had not wetted the glass fibres completely and hence there were many apparent voids on the surface (possibly because of the air or other vapours entrapped between the fibres). Also, the thickness of the disk obtained (about 5.3 mm) was greater than the 4.5 mm thickness of the disk obtained with vacuum. This is consistent with entrapment of vapor bubbles when filling is done by gravity flow at one atmosphere (as subsequent visual observation of voids confirmed); the use of a vacuum mold removes the vapor and imposes a strong suction on the upper part of the mold, bringing it down further (also observed) with great force that would serve to compress the glass mats. The problem of the transfer tube could be eliminated by wrapping it with a heating tape, thus controlling its temperature to prevent the caprolactam from freezing. However, since the disk obtained by this method was not very appealing because of the voids contained in it, we decided to use the second technique of mold - filling by vacuum, which is described below.

(ii) In the second technique, prior to the mold-filling, a vacuum was applied to the mold through valves(I) and (II), shown in Figure 4.1. Vacuum was maintained during the mold-filling operation, and both the valves (I and II) were kept open, till the molten caprolactam entered the steel tubing, shown in Figure 4.1. This was detected by touching the tubing and checking if it was warm or cold. The molten caprolactam usually took about 15-20 seconds to reach the steel tubing. As soon as the tubing became warm, valve(I) was

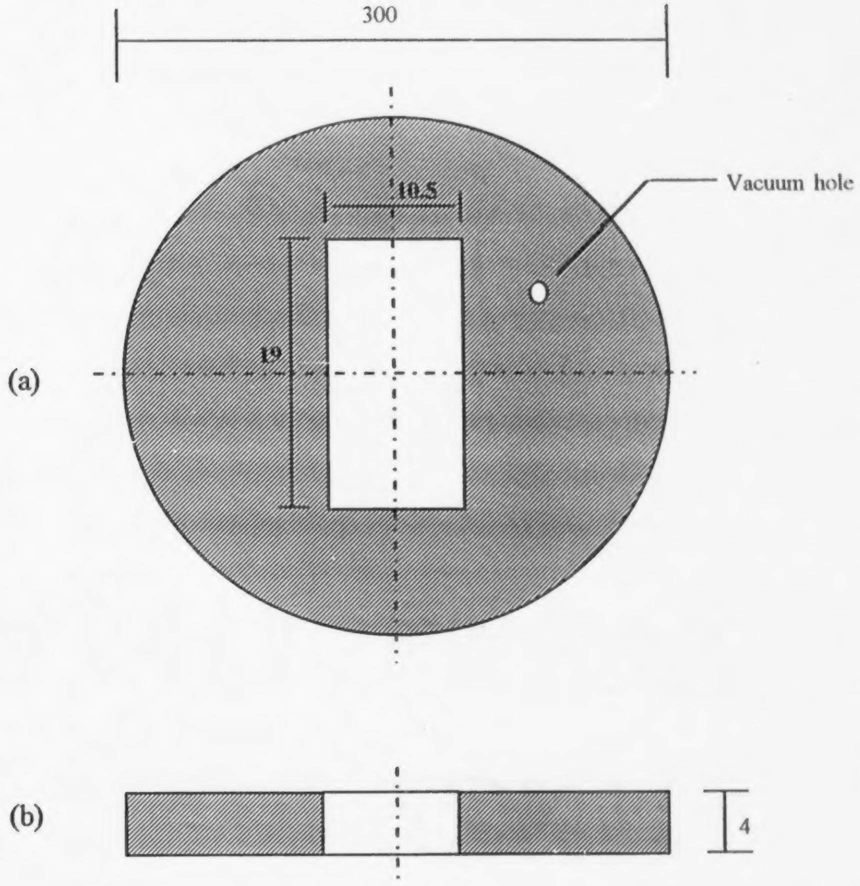
300
10.5
19
Vacuum hole
(a)
(b)
4

Figure 4.7. Diagram of insert which fits into the female part
(a) Top view (b) Front view (not to scale, Unit: mm)

immediately closed followed by valve(II). The steel tubing before the valve(I) was long enough (about 11 cm) to freeze the caprolactam inside and thus prevent the material from flowing into valve(I). In this way, we were able to maintain the vacuum during most of the mold-filling operation.

Because the mold was evacuated, if there were traces of nitrogen which were still dissolved in the monomer solution, these would be released in the mold, creating voids in the composite. In order to minimise the presence of voids, the vacuum pump continued to run while the mold filling was carried out. This was designed to aspirate any gases that were released inside the mold. The activated monomer then filled the evacuated mold, by a flow driven by atmospheric pressure (approximately 93 kPa in Edmonton, less the residual pressure in the nearly-evacuated mold--here, 5 kPa--for $\Delta P \cong 88$ kPa in this work) plus gravitational pressure, $\rho g(H_1 + H_2) \approx 2$ kPa (see Figure 4.1). As the mold filled, H_L was reduced approximately from 6 cm to 1.5 cm and pressure in the mold rose slightly as it filled with liquid. In a typical case, a total time of only about 15 - 20 seconds was needed to fill the mold. The valve(I) was closed when the monomer rose up to the steel tube. This closure was needed to prevent the monomer from being pulled completely into the sink because of the vacuum being applied. This entire process ensured that the filling operation was complete as also indicated by the change of monomer level in the reaction vessel over the course of the mold-filling operation). All composite disks in this work were prepared using this mold-filling technique, except one disk of pure nylon with the circular configuration. To fabricate the latter disk, vacuum was first applied to the mold, the valve(I) closed after a few minutes to maintain the vacuum inside the mold, and the caprolactam was then injected into the mold. This procedure prevented the caprolactam from gushing out into the steel tubing, and then into sink(1), which would result in a loss of the entire batch of molten caprolactam. So, to avoid losing the molten monomer, the valve had to be kept closed before injection of the monomer into the mold. It should be noted that the pure nylon disk with the rectangular configuration, which was made with the insert inside the mold, was made in the same fashion as the composite disks, that is, maintaining the vacuum during the mold-filling operation. In this case, the fast flow of the caprolactam into and out of the mold was slowed down by placing the insert inside the mold in such a way that, the hole connected to the vacuum faced the insert and not the molten monomer inside the mold, as shown in Figure 4.7. As a result of this, the pure nylon disks obtained in two different configurations had different surface appearance and different mechanical properties, as will be discussed in chapters 5 and 6.

Polymerization of caprolactam: After the mold was filled, it was maintained at 90°C for about 10 minutes to ensure complete wetting of the glass fibres by the monomer. During these ten minutes, the valve at the bottom of the feed vessel was closed. Some water was poured into the vessel for ease of cleaning.

Polymerization of the molten caprolactam inside the mold was initiated by increasing the temperature of the mold to 150°C in steps of 10°C, which took about 20 minutes, and this temperature was maintained for 25 minutes to ensure complete polymerization. The heater was turned off and the mold allowed to air-cool. The two pure nylon and all except one composite disks were prepared using this procedure.

One untreated glass fibre disk was prepared in a slightly different manner. For this disk, the polymerization temperature was 120°C unlike 150°C for other disks. This was carried out to explore the effect of polymerization temperature on the matrix properties and hence the properties of the composite. This effect would be more clear had the disk been made out of pure nylon instead of a composite. The caprolactam polymerization in this case was carried out as follows: after maintaining the temperature of the mold at 90°C for about 10 minutes, it was increased to 120°C in steps of 10°C, and it was maintained at 120°C, for about 15 minutes. The temperature was then increased to 150°C, and maintained at the same temperature for 25 minutes. Other procedures remained the same as for other disks. This technique of polymerization was carried out in this way, because, earlier experiments carried out in our laboratory in test-tubes (about 20 gm of monomer) revealed that the polymerization was initiated at about 120°C and the material solidified in less than 2 minutes.

Removal of the polymerized disk: The normal procedure was to remove the pure nylon or the composite disk from the mold as soon as the mold had cooled to room temperature, commonly about 24 hours. Removal was easy as long as the mold had been pre-treated with a release agent, and no damage ever occurred to any disk surface during removal. However, some bubbles or voids were always seen by casual inspection. Most of these bubbles were on the edges of the top disk surface which was mainly nylon (the glass fibre mats were cut 2.5 cm smaller than the diameter of the mold) and rarely on the bottom. In retrospect, we can presume that these bubbles probably originated from the gases/vapors released and unevacuated from the mold. Moreover the vacuum applied to the mold was not complete (~ 5 kPa), which meant that some air was always present inside the mold. As the mold was filled by a rising pool of low viscosity caprolactam, the residual air and possibly caprolactam vapors would have been either entrapped in fibre-fibre crevices or pushed to the top surface of the mold.

4.3. Fibre surface treatment

4.3.1. Review of Duangchan's work

Work done by *Duangchan, 1994* covered glass fibre surface treatments with mainly four kinds of organo-silicon compounds which were designated as Silane I, Silane II, Silane III, and Silane IV as shown below:

Silane I: 1,1,1,3,3,3,-Hexamethyldisilazane (98%, from Aldrich)

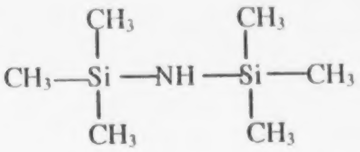

$$CH_3-\underset{CH_3}{\overset{CH_3}{Si}}-NH-\underset{CH_3}{\overset{CH_3}{Si}}-CH_3$$

Silane II: tert-Butyldimethylsilyl chloride (1.0 M solution in tetrahydrofuran from Aldrich)

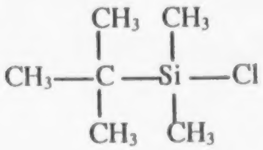

$$CH_3-\underset{CH_3}{\overset{CH_3}{C}}-\underset{CH_3}{\overset{CH_3}{Si}}-Cl$$

Silane III: Chlorotrimethylsilane (98%, from Aldrich)

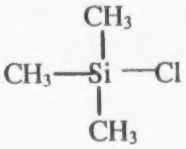

$$CH_3-\underset{CH_3}{\overset{CH_3}{Si}}-Cl$$

Silane IV: 3-Aminopropyltriethoxysilane (98%, from Aldrich)

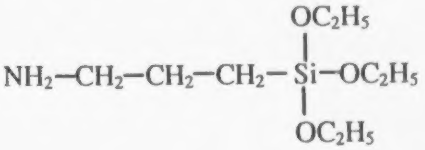

$$NH_2-CH_2-CH_2-CH_2-\underset{OC_2H_5}{\overset{OC_2H_5}{Si}}-OC_2H_5$$

These four compounds were chosen for the following reasons: Silane I, because it had -Si-NH- bonds which were expected to have some affinity for the Si-O bonds in glass, (since both groups have silicon atoms) and thus have some tendency toward physical adsorption on the glass surface, even though it had no groups which should react with hydroxyls on the glass surface; Silane III, because it had a chloride group which should react with hydroxyls on glass to form a strong covalent bond (Chapter 3), while being the smallest silane molecule that could reasonably be used in this way and have the least steric hindrance effect; Silane II, because it had the same bonding potential as Silane III but additional length which might help it to be more capable of physical intermingling with the chains of the nylon matrix, or (using its length in a different way) the additional length might interfere with neighbor molecules in gaining access to the hydroxyls on glass surface (hindrance effect); and Silane IV because it had several desirable structural features--three reactive sites (ethoxy) for bonding to either glass or to a local cross-linked network of neighbors on the glass, a backbone length of three carbons extending beyond the Si whereas Silane II had only two, and an amino tail that provided (NH) bonds that resembled those in the amide group of nylon 6. There were additional motivating factors for using Silane IV. For example, recent literature *(Jenneskens et al., 1992)* indicates that it actually reacts with caprolactam (or with nylon 6) during the polymerization process that forms nylon 6, thereby anchoring the coupling agent chemically to the matrix. Furthermore, the use of this agent *(Otaigbe, 1992; Jenneskens et al., 1992)* and possibly other amino silanes *(Hamada et al., 1992)* have produced good results with nylon as well as with epoxy matrices.

In Duangchan's work, all of the above compounds were dissolved in dry toluene (pretreated with sodium to remove water) at different concentrations and the glass mats immersed in the solutions overnight to achieve the silane coatings. The concentration range explored was 5-15 % (by volume in toluene).

In *Duangchan's* work, these compounds were found to have different effects on the composite properties. Silane I was the least effective among all of the above; it did not improve either impact or tensile properties. Silane II treated glass fibre composites showed higher impact strength and slightly lower tensile strength than Silane III treated glass fibre composites. It was speculated that, the bigger R-group of Silane II might have hindered other silane molecules from reacting with nearby hydroxyl groups on the surface of glass fibre, thereby reducing the overall bonds that could be formed between the fibre surface hydroxyl groups and the silane molecules. This led to the drop in tensile strength and an increase in impact strength of the composite compared to Silane III composite. Concentration effects were also observed with Silane III (5-15%), with the composite properties (tensile strength (σ_b), elastic modulus (E), toughness (τ) and impact strength (E_s) being higher at 5% than at other concentrations as shown in Figure 4.8. The latter result led us to believe that better properties might be expected at concentrations between 0-5% as shown by the dashed lines in Figure 4.8. Silane IV (10%) proved to be the best among all the Silanes and improved on σ_b by ~67% over pure nylon. However, only 10% concentration of Silane IV was tried in that work. This allowed the possibility that lower concentrations might give better properties, as with Silane III.

The current work, being a continuation and an overlap of the above work by *Duangchan, 1994*, has tried to address these questions and possibilities and thereby develop further insight into fibre-matrix adhesion and the role of coupling agents in assisting that adhesion.

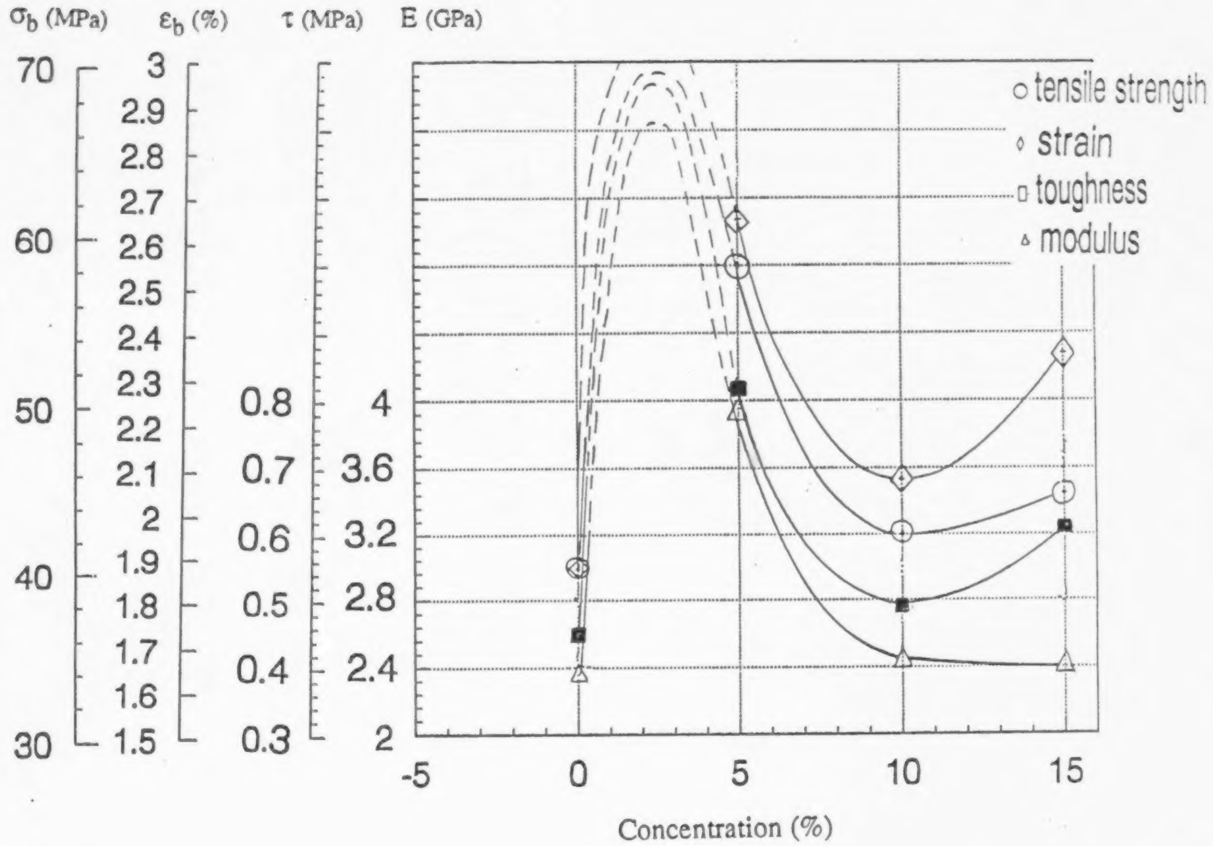

Figure 4.8. Mechanical properties from tensile test (σ_b, ε_b, τ, E) of Silane III at different concentrations (5, 10, 15%) *(adapted from Duangchan, 1994)*.

4.3.2. Fibre surface treatments employed in this work

(A) Use of different glass-fibre cleaning techniques

Few polymers adhere naturally to glass because of the molecular dissimilarity of the materials at the interface *(Shand, 1958, p. 432)*. This problem is complicated further here by the presence of sizing applied to the fibres when they are drawn and which are required in the textile processing of the strands and yarns. Textile sizings contain some form of lubricant, which obscures the glass surfaces and has an adverse effect on adhesion. The bond between glass and matrix is improved greatly by removing all sizing materials from the glass and replacing them with other coatings or films of an entirely different nature. The sizing is usually removed by a heat-cleaning treatment (air fire oxidation) in which the sizing is oxidized at a temperature of 500°C. This procedure was followed by *Duangchan, 1994* and by *Otaigbe and Harland, 1988.*

In separate work, *Shand, 1958 (p.433)*, has reported that any kind of glass reinforcement is weakened appreciably after high temperature heat cleaning, as shown in Figure 4.9. It was also reported by *Krishnanurthy and Kamel, 1989*, that a furnace treatment (650°C) to remove the sizing would reduce the strength of glass fibres since glass softens above 250°C. They speculated that this was a consequence of glass softening above 250°C. (We note, in passing, that Figure 4.9 shows a maximum strength emerging at about 350°C--even higher than the original strength--so that temperatures at this level might be optimum if some heating is performed for cleaning purposes. It remains to be seen how effective the cleaning would be at the lower temperatures, and whether controlling those temperatures could be done easily.)

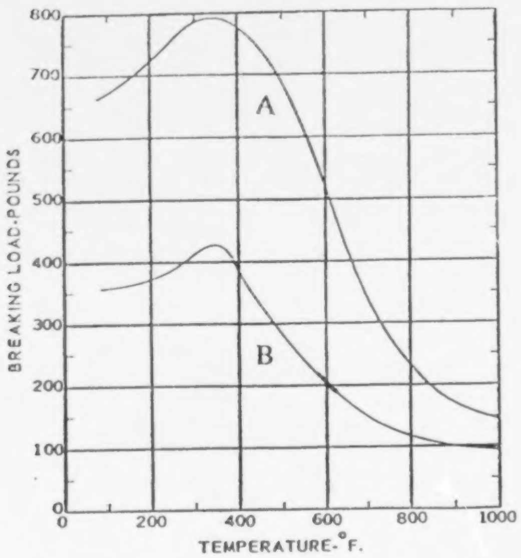

Figure 4.9 Tensile strengths of tapes as affected by heating for 1 hr at various temperatures. (A) Fibrous Glass tape, 1 by 0.015 inch (B) Fibrous Glass tape, 1 by 0.007 inch (Owens-Corning Fibreglas Corporation); *adapted from Shand, 1958, p. 416.*

In the present work, four non-heating techniques to clean glass were attempted, and these are as follows:

i) Chemical etch cleaning,

ii) Acid Oxidation,

iii) Plasma cleaning, and

iv) Cleaning with laboratory detergent.

Details of each technique are given below.

i) Chemical Etch Cleaning: This may be used to remove glass surface material along with contaminants. Etching removes surface layers such as oxides, eliminates or blunts surface cracks in brittle materials, and removes a variety of difficult-to-remove-contaminants *(Kern and Deckert, 1978).*

Common etchants for glass include sodium or ammonium bifluoride trisodium phosphate - which is a mild etchant - and hydrofluoric acid, which is a very strong etchant. Wet HF gas can also be used in vapor-phase etching, which produces better cleaning than in an HF solution as reported by *Heide et al., 1989*.

Etchants may change the surface chemistry. For example, acid etching a soda lime glass surface, which is normally basic, leaches the sodium from the surface and makes the surface acidic which changes its wetting properties *(Fowkes et al., 1988)*. Buffered solutions of acid etchants are often used to minimize changes in the hydrogen ion content (pH) as a result of chemical reactions.

In the work being reported here, only one etchant was used, which was a buffered solution, composed of a mixture of aqueous ammonium bifluoride (40%) and aqueous hydrofluoric acid (49%) in 50:1 proportion by volume (hereafter, we will refer to this as HF). However, there was no chemical reaction observed between the sizing and the etchant which indicated that the buffered solution did not attack the sizing. Nevertheless, we then tried to etch precleaned (furnace cleaned) glass fibre mats, since this etchant was also intended to roughen the glass surface which furnace-cleaning could not have done. We were successful in etching the surface as seen in Figure 1 in Appendix A. The furnace-cleaned glass fibres were treated with the mild etchant, for different lengths of time starting from 1 minute to about 45 minutes. The attack of glass surface by the etchant can be well appreciated by looking at the SEM photographs of these glass fibres; the diameter of a single glass fibre reduces from 18μ to about 5μ within about 30 minutes. This substantial loss of material would lead to loss in mechanical strength of the glass fibre. So, to avoid losing substantial mechanical strength, we decided to etch the glass fibres by immersing them in the etchant for only one minute. The etched glass fibre mat was then washed with water thoroughly to remove any traces of the etchant. The washed glass fibre mats were then dried in an oven at 125°C for 24 hours before loading them into the mold for making a composite. This work was carried out at Alberta Microelectronic Centre because of the dangerous nature of the chemicals used. When using HF, one must take extreme care to prevent the HF from getting on the skin because bad chemical burns can result.

ii) Acid Oxidation: Cleaning by oxidation relies on the formation of volatile or soluble oxidation products of the contaminants. Many acid-based systems can be used as oxidants *(Mattox, 1989, p.57)*. Hydrogen peroxide is a good oxidizing solution for cleaning glass. One system commonly used in the semiconductor industry is the "piranha solution". The piranha solution is concentrated sulphuric acid (98%) plus hydrogen peroxide (30% as purchased) mixed in 3:1 proportion by volume. Extreme care needs to be taken during the mixing of the solutions, since a considerable amount of heat of mixing is evolved.

In the current work, this solution was found to behave like the Piranha (voracious freshwater fish that eats almost any organic matter), in terms of eating all the organic contaminants on the surface of glass fibres, leaving the skeletal structure of glass intact. This is seen from the SEM photographs in Figure 2 (Appendix A), where glass fibres immersed for different lengths of time in the piranha solution, show no change in their diameter during the treatment. Thus, this solution helped in terms of offering a new way of cleaning glass fibres, without weakening them by high-temperature furnace treatment or by dissolving the glass as in HF etching.

iii) Plasma oxidation: Oxygen (or air) plasmas are very effective in removing hydrocarbons and absorbed water vapor from surfaces. The reaction of the oxygen with carbon on the surface can be tracked by using a mass spectrometer to monitor the CO and CO_2 produced *(Holland, 1964; Holland and Ojha, 1976)*.

The argon plasma treatment is also performed to clean the substrates of molecular level contaminants and to modify the surface chemistry to facilitate grafting of small molecules (e.g., monomers) introduced into the plasma field. Removal of the sizing on the commercial fibres by the argon plasma as an alternative to furnace cleaning was also studied by *Krishnamurthy and Kamel, 1989* as described in section 3.7 (chapter 3).

The equipment used in this study was located in the Alberta Microelectronic Centre. An attempt was made to clean and etch the glass fibre surface using argon plasma. However, to be able to perform the cleaning/etching task, the plasma reactor conditions need to be optimized - i.e. the plasma power level, the vacuum inside the reactor, the time of exposure, the r.f. frequency. There was not enough time available to do the optimization in this study, so - for exploratory purposes - only a few sets of conditions were employed. These are given in Table 4.1.

Table 4.1. ***Different plasma reactor conditions employed to etch the glass fibres***

Plasma Type	**Run No.**	**Base Pressure* torr**	**Pressure* mtorr**	**Power W**	**Time minutes**
Argon	I	$2.0*10^{-7}$	2	150	10
Argon	II	$2.0*10^{-7}$	10	500	10
Argon	III	$1.5*10^{-5}$	10	1000	20
Argon	IV	$1.5*10^{-5}$	30	1500	10
Oxygen	V	-	20	100	10

*** In the above table, the "base pressure" refers to the pressure at which the sample is introduced into the chamber and the pressure shown in column 4 of the table is the actual pressure during etching or sputtering.**

Samples of furnace-cleaned glass fibres were mounted on a 1″ by 3″ glass slide, and 1″ by 1″ glass was set on each end with the help of double-sided tape to hold these fibres in place. Loose fibres were pulled out or blown away with an air gun. Although, argon plasmas are known to remove the sizing also on the glass surface (cleaning), we decided to first work with the furnace-cleaned fibres to see if we were successful in etching these fibres.

The SEM micrographs of the glass fibres are shown in Appendix A (Figure 3). Run I, with a duration of 10 minutes at 150W, caused no discolouration and etching or surface roughening of the glass fibres. So, for the next sample, we increased the power level to 500W for the same duration of 10 minutes. For the high power (500W) plasma, the sample slide was mounted on a pallet which was gold-plated. After Run II, the fibres had a blackish colour, and when these were inspected under the SEM, the surface appeared a little grainy. However, this use of 500W did not cause any etching or surface pitting. Since the first two runs had minimal effect on the fibre surface, we decided to double the power and time of treatment. In runs III and IV, the argon plasmas were effective in removing the gold from the pallet surface, and the material beneath it, which was Niobium. Some of these metallic materials may have deposited onto the fibre surfaces. Some gold was visible on the edge of the glass slide. Again, SEM micrographs detected no pitting on the surface of glass fibres. The surface, however, did show some non-uniformity, but it is hard to say if it was due to etching or some pre-defects on the surface of glass fibres. Results obtained with oxygen plasma were similar to runs I and II using argon plasmas.

iv) Cleaning with Laboratory Detergent: In detergent cleaning, the detergent surrounds the foreign particles, taking them into suspension without actually dissolving the material. Wetting agents and surfactants loosen the particles from the surface. Liquid dishwasher soap is an excellent detergent for many applications. For cleaning the glass fibres, we tried using Sparkleen®, a Fisher Scientific product. Sparkleen® is the universal detergent for all laboratory glassware and equipment. It comprises of a mixture of anionic and non-ionic surfactants, and it is supposed to remove any kind of organic deposit or contaminant on glass surfaces. Hence, we used Sparkleen® to see if it could remove the organic sizing on the glass fibre surface. This was done by immersing the glass fibre mat in the detergent solution for 12 hours. This soluion was prepared by dissolving 20 gm of powder in 1 litre of water at room temperature. No agitation of the solution was carried out. The glass fibre mat was then washed in water followed by drying in air for about 2 hours. To check if the sizing was eliminated or not, we heated the glass mat in the furnace at 500°C. The glass fibres turned colour from white to black and back to white, indicating that the sizing was still present on the glass surface after detergent cleaning. Since only one set of conditions of temperature and concentration of solution was employed in this work, it would be worthwhile to investigate different conditions of temperature and concentration of solution to comment on the use of this technique for cleaning glass fibres. Nevertheless, this work did indicate how stubborn the organic contaminant (the sizing) on the glass fibre surface was, and that it could not be removed by standard treatment conditions.

B) Use of coupling agents

(1) Much of the work to be reported here deals with the mechanical performance of composites, prepared with glass fibres treated with Silane III and Silane IV, adsorbed from toluene solutions in the concentration range 0-5 % silane by volume.

Fibre surfaces were treated with the silanes in four steps:

a. Heat -cleaned glass fibre mats (circular disk, 22 cm diameter) were dried in an oven at 150°C for 4 hours in order to eliminate water at the fibre surface.

b. The glass fibre mats were immersed in a room-temperature solution of toluene and silane agent at a selected concentration in the range of interest- e.g., concentration by vol. 2% = silane 40 ml in 2000 ml of toluene. The mat and solution were contained overnight in a good sealed container (silane being very sensitive to water), to allow complete interaction of silane and glass fibre surface.

c. These glass fibre mats were washed in dichloromethane and then in acetone to get rid of all excess silane.

d. The cleaned and silane-treated glass fibre mats were dried in an oven at 100°C overnight and used the next morning to make composites.

It is very important to do the silane-surface treatment under well ventilated conditions and these silanes should be handled properly, since they are corrosive, and sensitizers (targeting eye organs).

(2) One more coupling agent has been evaluated to search for improved bonding at the interface. This is designated as Silane V and its structure is shown below:

Silane V: N-[3-(Trimethoxysilyl)propyl]-ethylenediamine

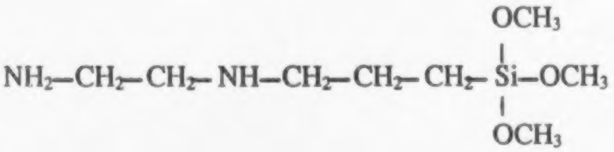

$$NH_2{-}CH_2{-}CH_2{-}NH{-}CH_2{-}CH_2{-}CH_2{-}\underset{\substack{|\\OCH_3}}{\overset{\substack{OCH_3\\|}}{Si}}{-}OCH_3$$

This silane was chosen for several reasons. First, it seemed promising because Silane IV was successful and Silane V possessed a similar structure, that is, the presence of amino tail, and three reactive (methoxy) sites to bond to glass. Second, because it has a longer backbone length which might enable the molecule to diffuse deeper into the matrix (nylon) network. Third, the presence of two (NH–) groups in the backbone offered even more bonding possibilities with polymerizing nylon 6, than for Silane IV. Concentration effects were also studied with this silane in the range 0-5% by volume in toluene, and the fibre treatment with silanes was carried out in the same way as described above in **(1)**.

(3) In Duangchan's work, all silanes were applied to glass fibres from toluene. In many commercial applications, however, the silanes are applied from aqueous solutions. In this work, we have applied Silane IV from aqueous ethanol solution, 95% (vol/vol) to see the role of solvent in the silylation of the glass surface. Only one concentration of Silane IV (1.25% by volume in the aqueous ethanol solution) was employed. The fibre surface treatment was again carried out in the same way as described in **(1)**, except that, in step (a), ethanol was used instead of toluene to dissolve the silane.

(4) Recent research by *Chaudhary et al., 1987,* and many others, has focused on imparting more durable bonding of the silane coupling agent to both the polymer and the reinforcement. Improved silane coupling agent systems have been developed by utilizing several techniques; for example, blends of hydrophobic silanes with hydrophilic silanes have been evaluated for imparting greater hydrophobic character to the inorganic substrate; use of certain additives to the silanes has been evaluated for increased siloxane crosslinking at the interface; blends of more thermally stable silanes with traditional silanes have been evaluated at elevated temperatures to seek for increased thermal stability.

The deposition of a mixture of a hexamethoxysilane additive, 1,2-bis-(trimethoxysilyl)ethane as a crosslinker and methacrylate silane onto glass from an aqueous solution was studied by *Jang et al., 1989*. This study revealed that the crosslinker showed great selectivity for adsorption on the glass surface, as a result of which, a tight siloxane network of the crosslinker was found close to the glass surface and a more diffuse methacrylate structure was formed away from the glass surface. The highly crosslinked siloxane structure close to the inorganic substrate supports the proposed mechanism for enhanced adhesion with this additive. For example, *Plueddemann and Pape, 1987,* formulated primers from blends of the hexamethoxysilane crosslinker and Silane IV, for bonding epoxy resins to glass. These primers were found to provide bonds that resisted 70°C water for more than one week, while bonds with Silane IV alone failed in less than one hour.

Because of the recent successes cited above, current work has investigated also a blend of the hexamethoxysilane crosslinker and Silane-IV as a means to improve the mechanical properties of the composite by formation of a stronger siloxane network at the interface. Silane-IV and the crosslinker were mixed in 2:1 proportion by taking 27.5ml of Silane-IV and 13.75 ml of the crosslinker and dissolving these in 2000ml of aqueous ethanol solution, 95% (vol/vol). The proportion of Silane-IV and the crosslinker was chosen, to match one of the proportions employed by *Plueddemann and Pape, 1987* in their work. Furnace-cleaned glass fibre mats were immersed in this solution overnight and then washed with dichloromethane and acetone the next day, followed by drying in the oven overnight at 100°C.

Chapter 5

STRUCTURE AND COMPOSITION OF COMPOSITE DISKS

A specialized notation will hereafter be used to identify the disks and disk types, for which results will be reported in Chapter 6 and in the Appendices. Each disk will be uniquely coded to indicate the cleaning method used to remove the sizing (e.g.FC for furnace cleaned fibres), the chemical agent used to treat the glass fibre mat (e.g., Silane IV), the concentration of that agent in the treating solution [e.g., Silane I (2%) for 2% by volume in solution], and, for nominally replicated disks molded at different times, also the sequence of those two [e.g., ^{2}Silane IV (2%)]. All disks with Silane treated fibre mats were made by dissolving the silane in toluene first and then immersing the mats in that solution. There are only two disks which did not use toluene as a solvent to dissolve the silane. In one of these disks, the silane (Silane IV), was dissolved in aqueous ethanol solution (95%) and the glass mats immersed in the same, and in the other disk, Silane IV was dissolved alongwith a crosslinking agent in 2:1 proportion in ethanol (95%). These disks are designated as Silane-IV (1.25% E) and Silane-IV (1.37%+CL) respectively.

In all, 23 disks were made, including 2 pure nylon 6 disks, and these are listed in detail in Table 5.1.

5.1. Density (ρ)

The densities of specimens of composites $(\overline{\rho_c})$ and nylon 6 $(\overline{\rho_n})$ were measured following ASTM standard D792 (described in Appendix B). Five samples at different positions (random positions) of each nylon 6 disk produced here and six samples at different fixed positions of each composite disk (shown in Figure 5.1) were measured and averaged $(\overline{\rho})$. Values of $\overline{\rho_c}$ for all specimens taken from all composite disks and values of $\overline{\rho_n}$ from the nylon 6 disks are shown in Table C-1 (Appendix C).

Table 5.1. *Description of various disks fabricated in the mold*

No.	Disk Type	Type of Surface treatment of glass fibre
1	**Pure Nylon**	Rectangular configuration with the insert in the mold.
2	**Pure Nylon**	Circular configuration without the insert.
3	**[1]Untreated (Atmospheric)** Rectangular Configuration.	Furnace cleaned, untreated glass fibres. Monomer injected inside the mold under gravity i.e. atm. condn.
4	**[1]Untreated** Circular Configuration	Furnace-cleaned, untreated glass fibres. Monomer injected with vacuum.inside the mold.
5	**[2]Untreated** Circular Configuration	Replicate of Disk no.4
6	**[3]Untreated** Circular Configuration	Furnace-cleaned, untreated glass fibres.Heating to 150°C during polymerization carried out differently.
7	**Silane-IV (0.2%)** Circular Configuration	Furnace-cleaned glass fibres, treated with Silane-IV (0.2% in Toluene).
8	**Silane-IV (0.5%)** Circular Configuration	Furnace-cleaned glass fibres, treated with Silane-IV (0.5% in Toluene).
9	**[1]Silane-IV (1.25%)** Circular Configuration	Furnace cleaned glass fibres, treated with Silane-IV (1.25% in Toluene)
10	**[2]Silane-IV (1.25%)** Circular Configuration	Replicate of Disk no.9.
11	**Silane-IV (1.25%EtOH)** Circular Configuration	Furnace-cleaned glass fibres, treated with Silane-IV (1.25%in Ethanol (95%solution))
12	**Silane-IV (1.37%+CL)** Circular Configuration	Furnace-cleaned glass fibres, treated with a 2:1 mixture of Silane-IV(1.37%) and a Crosslinking additive in Ethanol solution (95%)
13	**Silane-IV (2.0%)** Circular Configuration	Furnace-cleaned glass fibres, treated with Silane-IV (2% in Toluene)
14	**Silane-V (0.2%)** Circular Configuration	Furnace-cleaned glass fibres, treated with Silane-V (0.2%in Toluene)
15	**[1]Silane-V (1.25%)** Circular Configuration	Furnace-cleaned glass fibres, treated with Silane-V (1.25% in Toluene)
16	**[2]Silane-V (1.25%)** Circular Configuration	Replicate of Disk no.15.
17	**Silane-V (2.0%)** Circular Configuration	Furnace-cleaned glass fibres, treated with Silane-V (2.0% in Toluene)
18	**Silane-III (0.2%)** Circular Configuration	Furnace-cleaned glass fibres, treated with Silane-III (0.2% in Toluene)
19	**Silane-III (1.25%)** Circular Configuration	Furnace-cleaned glass fibres, treated with Silane-III (1.25% in Toluene)
20	**Silane-III (2.0%)** Circular Configuration	Furnace-cleaned glass fibres, treated with Silane-III (2.0% in Toluene)
21	**Silane-I (5%)** Circular Configuration	Furnace-cleaned glass fibres, treated with Silane-I (5.0% in Toluene)
22	**Piranha cleaned** Circular Configuration	Glass fibres cleaned with a Piranha solution, a 3:1 mixture of H_2SO_4 and H_2O_2
23	**HF - treated** Circular Configuration	Furnace-cleaned glass fibres, treated or etched with a buffered hydrofluoric acid solution

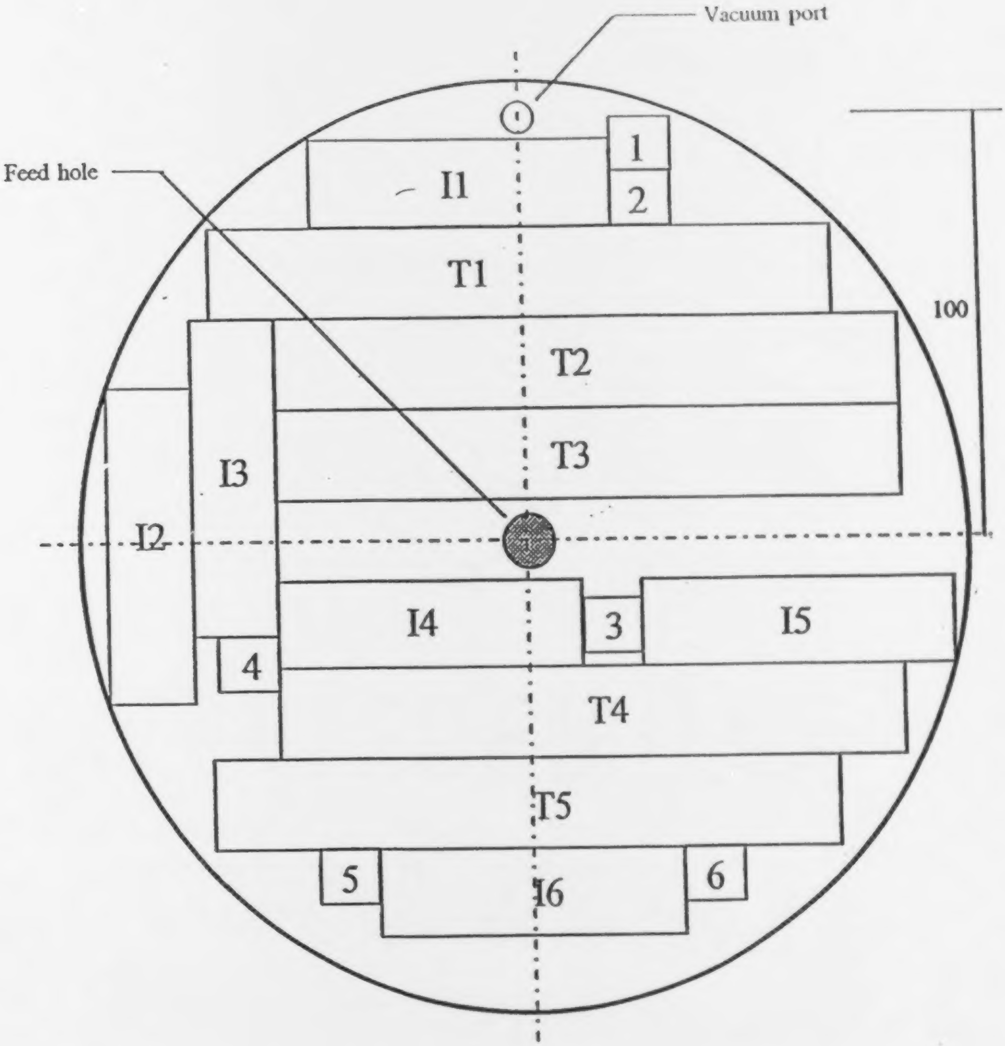
Vacuum port
Feed hole
1
2
I1
T1
T2
T3
I3
I2
100
I4
3
I5
4
T4
T5
5
I6
6

Figure 5.1. Locations of regions from which specimens were taken for obtaining data on composition (numbered 1-6), impact strength (I1-I6), and tensile behavior (T1-T5)

The densities for the pure nylon 6 disks ($\overline{\rho_n}$), were 1.128 ± 0.006 g/cm^3 for the disk with circular configuration, and 1.138 ± 0.008 g/cm^3 for the disk with rectangular configuration. The latter density was used as a standard for this study for reasons which are explained in section 5.3.1. For each composite disk, $\overline{\rho_c} > \overline{\rho_n}$ (= 1.14 g/cm^3) because the density of glass fibre (ρ_g = 2.56 g/cm^3) is higher than that of nylon. Also the measured $\overline{\rho_n}$ was found to be in the range of typical nylon 6 (1.12-1.14 g/cm^3) (*Reimschuessel,* 1977) shown in Table 2.3.

Looking at Table C-1, we find that for the disk ^{1}Silane-V(1.25%), positions 1, 2, 5 and 6 have density values higher than the average. This is because one of the cartridge heaters of the mold was not working when the disk was made and, as a result, the disk surface showed incompletely polymerized matrix in the outer regions (about 8 cm from the centre). Before conducting density measurements, the samples were dried in an oven at 100°C overnight and conditioned at 66% RH for 12 hours. When the density specimens of this disk were dried before testing, the residual monomer/oligomer vaporised leaving behind a non-uniform, porous sample. When this sample was immersed in acetone for density measurements, acetone diffused into the sample causing it to expand, and thus the reading obtained was incorrect. For this reason also, the fibre volume fractions obtained were higher than the average values. The average density for this disk was therefore computed using the more representative densities obtained for positions 3 and 4.

The second disk fabricated with Silane-V treated glass fibre with concentration of Silane-V = 1.25%, also appeared to have some incompletely polymerized regions near the outer end of the disk. When we tried to make a disk with higher concentration of Silane-V (2%), the disk obtained had a higher amount of unpolymerized matrix which in this instance covered the outer circumferential regions of the disk. Since the problem of the heater was resolved before fabricating these disks, it seemed that the presence of Silane-V on the glass fibres was hindering the polymerization of nylon 6 in some way. So, again, the densities and the volume fractions obtained for position 1 of the disk ^{2}Silane-V(1.25%)

and for positions 1, 2, 5, and 6 of the disk Silane-V (2%), were higher than the average values due to swelling by acetone.

Moving down the Table C-1, we find that the average density of all composites made (all contained 8 plies of glass fibre mat) was in the range from 1.45 to 1.55 g/cm^3, except for two disks; one disk that was chemically cleaned with the Piranha solution and the other that was etched with hydrofluoric acid. The average densities of these disks were 1.42 g/cm^3 and 1.36 g/cm^3 respectively.

As evident from the SEM photographs of glass fibres treated with the Piranha solution (see Appendix A, Figure 2), the diameter of the fibres treated in piranha solution remained unchanged with the amount of treatment time, implying that the piranha solution did not attack glass. The glass fibre mats have to be treated in a very short time after hydrogen peroxide is added to the sulphuric acid, to avoid losing the reactivity of the mixture. So, the glass fibre mats were immersed two or three at a time in the piranha solution. These fibre mats become very difficult to handle after they are immersed in the piranha solution, and they tend to fall apart. The problem gets worse during the time of washing these mats with water. So, finally when the entire cleaning is completed and the mats are kept for drying, it is hard to be able to collect exactly 8 glass fibre mats and also, the stack of these fibre mats is not uniform, in the sense, the glass fibres tend to be twisted and folded and non-uniformly distributed. This could possibly be the reason for the reasonably high deviation in the density and non-uniform distribution of glass fibres in the disk. Nevertheless, this cleaning technique could be improved upon to overcome the above problems in order to obtain a disk with uniform distribution of glass fibres. The drop in density for the HF treated disk can be explained as follows: HF is a very strong etchant for glass, and reacts with the oxides of glass, forming fluorides. This is also evident from the SEM photographs (Appendix A, Figure 1), which clearly indicate that some amount of glass is eaten away. Since the number of glass fibre mats was kept the same, it is obvious that the mass and surface area of glass decreases after the HF treatment and hence a drop in the density of the composite is observed.

5.2. Volume fraction of fibre (V_f)

5.2.1. Reproducibility and homogeneity of disks

Although the number of plies of glass fibre mat was fixed to 8 plies for each composite preparation, we were not sure how much the fibre contents in each composite varied. The method of measuring V_f is described in Appendix B. Figures 5.2 (a) and (b) show $\overline{V}_f$ of all composite disks. Values of $\overline{V}_f$ for all composites varied in the range of 23.4% - 30.5%, again exceptions being, the chemically cleaned (piranha-cleaned) disk and the HF treated disk. Small variations in the $\overline{V}_f$ for different disks might be because the roll of glass fibre mat (from which plies were cut) was not of uniform fibre arrangement.

Three composite disks with untreated glass were made, and these were all found to have the $\overline{V}_f$ in the range of 28 - 29%. These values were higher than most of the composites made with surface treated glass, by a $\Delta V_f \approx$ 3-4%. There is a trend for the composites with Silane-IV treated glass to possess lower $\overline{V}_f$ of around 24%. This drop in $\overline{V}_f$ was also observed by *Duangchan, 1994*. The lower values of $\overline{V}_f$ for the composites with chemically cleaned glass and the HF treated glass can be attributed to reasons mentioned in the above section. Also, the reasons for the occurrence of higher values of $\overline{V}_f$ for composites with Silane-V (1.25% and 2%) treated glass were explained in the previous section.

Since the fibre content affects the properties (i.e., tensile strength, impact strength) of the composite, it is necessary to look at the average V_f of each composite disk before comparing the average mechanical properties of them (the comparison of mechanical properties is shown in section 6.1). It would be even better to evaluate the average fibre fraction of each mechanical-property specimen prior to its testing.

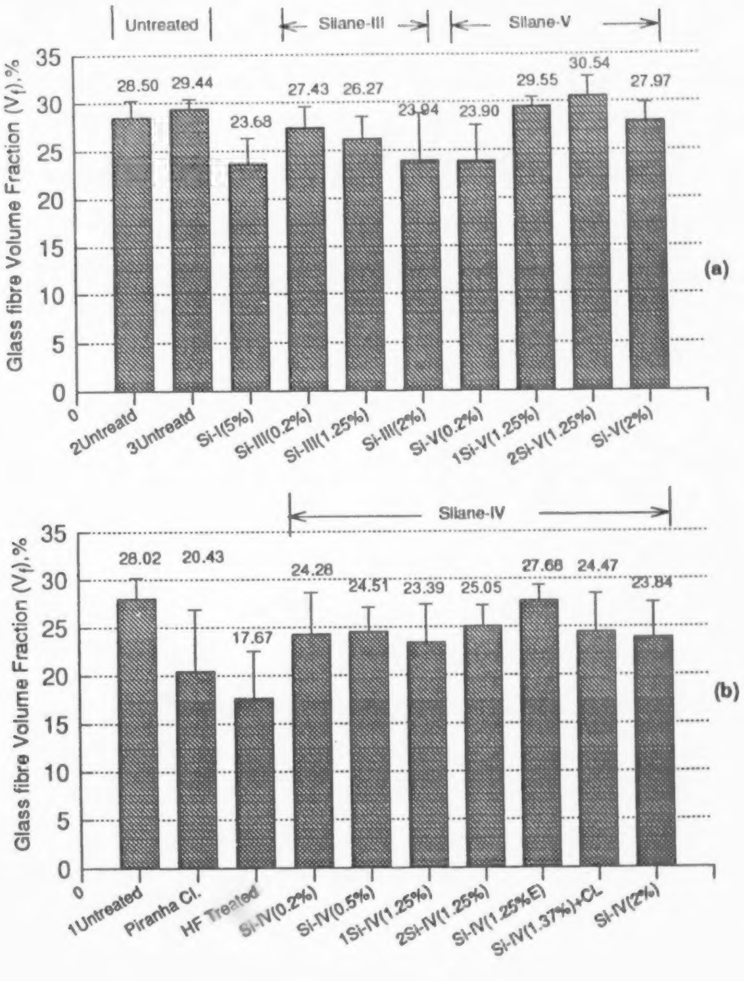

Figure 5.2 (a) and (b). Fibre volume fraction of composite disks having different glass fibre treatment and molded on different days. The abscissa "scale" groups together (by parentheses) the disks whose fibres were treated with the same chemical (e.g., Silane III). Within each group, members whose treatments were nominally identical (e.g., Silane IV in 1.25% solution) are clustered together, but always in the chronological order in which the disks were molded (e.g., ^{1}Silane IV precedes ^{2}Silane IV).

Each composite disk seemed to be fairly homogeneous with respect to V_f measured at different positions. This can be assessed from the data in Table C-2 and the corresponding "standard errors" in Figure 5.2. again exceptions to this are the chemically cleaned and the HF disks. Differences in measured V_f values at different positions are at least partially due to ordinary random data scatter, not signaling real inhomogeneity. But such variations must also be examined for consistent trends within the entire set of disk specimen data. Such trends, if present, would represent real nonuniformity and could be regarded as indicators of deficiencies in the disk-preparation procedures or the mold design. Such deficiencies would thus build into the disks an inevitable degree of patterned inhomogeneity.

One such case seems to be evident at position “1” (near one edge; see Figure 5.1), where the data show a tendency to have lower V_f than other parts. A rather consistent exception to disk uniformity in the positive direction was noted at position "3" (close to the disk center), where V_f exceeded the disk average in most of the disks. Positions 5 and 6 were also found frequently to have lower fibre contents than the average values. The position-dependence of V_f in the various disks can be examined and data for 7 disks has been presented in graphical form in Figures 5.3 (a), (b) and (c). As seen from the trendlines shown in the figures, V_f shows a trend to be higher at the centre and decreases toward the edges.

5.2.2. Masking fibre pretreatment effects with variations in V_f

Table C-2 and Figures 5.2 (a) and (b) present the average volume fraction of fibre, $\overline{V}_f$ for six specimens representing each disk prepared from untreated and treated glass fibres. Because there is some variation, the question could arise whether subsequent mechanical property variations might be due to V_f-effects or due to V_v (Void Volume fraction), or to the effects of surface chemistry and surface treatments. The effect of V_v on the mechanical properties will be discussed in the next section.

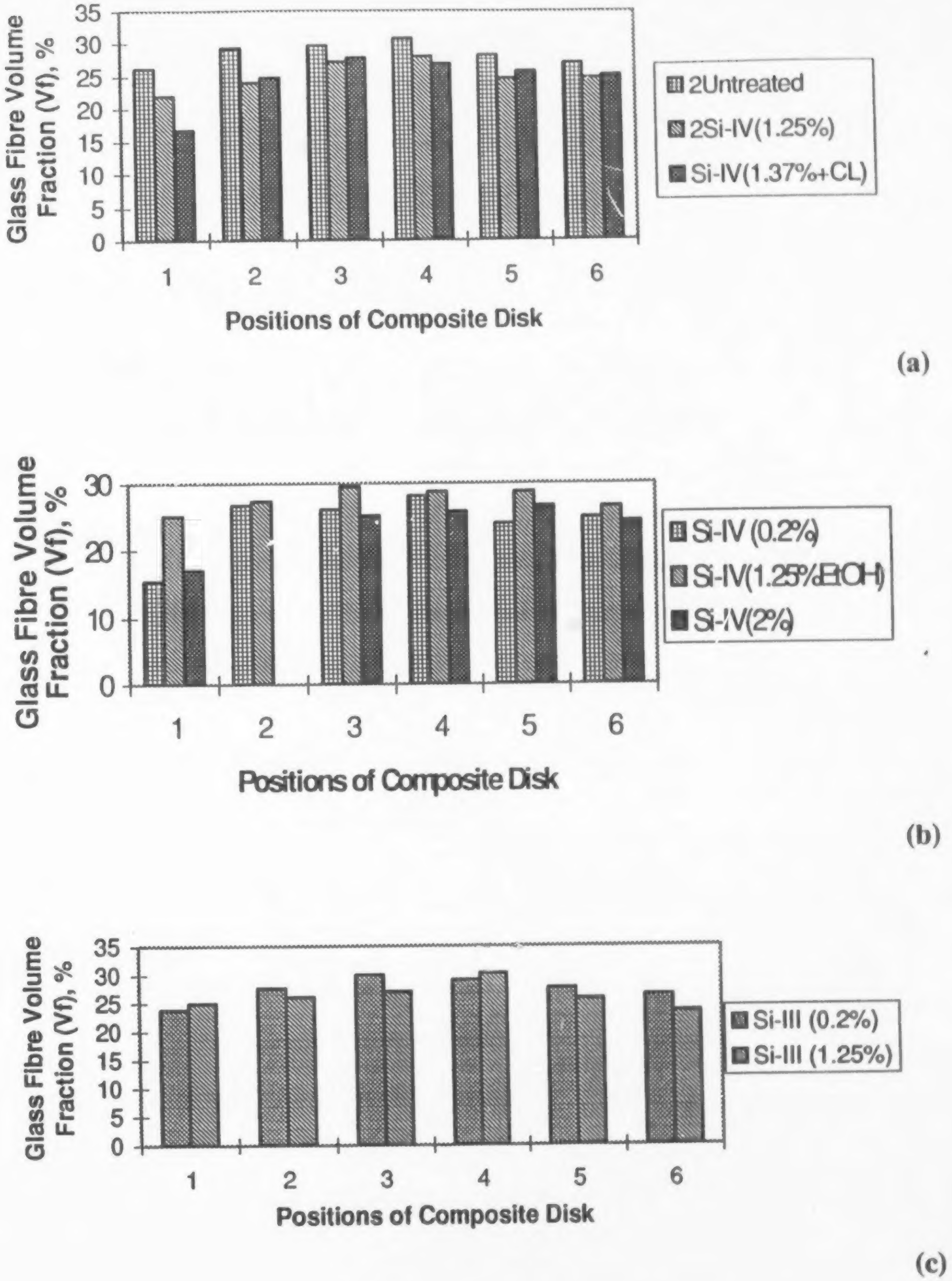

Figure 5.3 (a), (b) and (c): Fibre volume fraction at different positions in composite disks.

Inspection of the whole set of V_f values shows, fortunately, that there are several cases where disks have virtually the same $\overline{V}_f$ but differing chemicals used in fibre pretreatments, or the same $\overline{V}_f$ but different concentrations of the same coupling agent during pretreatment. In these cases, then, it is possible in principle to separate the various effects. For example, if we take a look at the disks made with different concentrations of Silane-IV in Figures 5.2 (a) and (b), we find that these disks all have $\overline{V}_f$ in the range $\cong 25\ \% \pm 2\%$. Hence, since the variation is not very large, it should not be difficult to isolate and evaluate the effect of the concentration of Silane-IV within this group. The same applies for groups with different concentrations of Silane-III and Silane-V. Also, since the variation in the V_f between these groups is not very large ($\Delta\overline{V}_f \cong 3$ - 3.5%), minor corrections for the V_f-factor variation should be possible to facilitate intergroup comparisons as well. The disks made with chemically cleaned (piranha) and HF treated glass, having $\overline{V}_f = 20.4\%$ and $\overline{V}_f = 17.7\%$ respectively, would be addressed separately in the mechanical properties section.

5.3. Void volume fraction (V_v)

It is found generally that composites tend to contain voids which reduce their maximum possible strength and diminish the advantages sought by the strategies of composite manufacture. *Fan, 1993*, studied the effect of void content on composite flexural strength and elastic modulus. In the one example displayed by Fan, a void fraction of 2.0% in the composite reduced the flexural strength by 10%, and increasing the $\overline{V_v}$ to 5.0% led to a total drop in strength of 20%. The paper by *Ghirose, 1993*, which can serve as a rare but excellent review of this topic , states that the highest quality composites should have $\overline{V_v} \leq 1\%$, but that voidage up to 5% can be tolerated (or cannot be reduced any further) in some lower-quality products.

In this study, the measurement of V_v followed ASTM: D2734-70 (described in Appendix B). The following equation was employed to calculate the void content in a composite disk

$$V_v = 100 - \rho_c\left(\frac{W_n}{\rho_n} + \frac{W_f}{\rho_f}\right)x100 \qquad (5.1)$$

where W_f and W_n are the weight fraction of fibre and nylon respectively. Table C-2 shows the void content of each disk for different positions within the disk.

As mentioned earlier in section 5.1, the density of nylon, (ρ_n) used for the calculation of void content was that obtained for the nylon disk with rectangular configuration (ρ_n = 1.14 g/cm^3). This was because the density of the nylon disk with circular configuration (ρ_n = 1.13g/cm^3), when inserted in equation 5.1 (shown above) gave negative values of void content for many disks, which is not physically possible. From Table C-2, we can see that the average void content ($\overline{V}_v$) ranges from (-0.81 ± 2.13%) for [1]Untreated to (+2:89 ± 0.42%) for Silane-IV(1.37%+CL) disk. Inspite of using the higher density of nylon 6, negative values of $\overline{V}_v$ were still obtained for two disks. These are: [1]Untreated with $\overline{V}_v$ = -0.81 ± 2.13%, and Silane-V (2%) with $\overline{V}_v$ = -0.15 ± 0.25%. Negative values of void content (V_v) were also obtained for four other disks at certain positions. These disks are as follows; Silane-V (0.2%) (positions 2 and 6); [2]Silane-V (1.25%) (position 3); and Piranha cleaned; (position 4).

Computationally, such a result (negative value for V_v) could emerge if the ρ_n value being used here were too low--i.e., if the true ρ_n in these composites was actually higher than 1.14 g/cm^3. If so, the measured mass of these composite samples could be accommodated in the calculations only if the too-low ρ_n (giving a too-low nylon mass) could be compensated by allowing additional nylon mass to be present in the only way computationally possible--i.e., "giving" more volume to the nylon by creation of negative voidage. This shows that V_v can be driven negative if (ρ_c/ρ_n) is too large--i.e., if ρ_n is erroneously too small. The possibility that $\rho_n = 1.14$ g/cm^3 could be small is supported by the fact that the published range of nylon 6 densities *(Reimschuessel, 1977)* goes as high as 1.15 g/cm^3, and the value used here is lower than the upper value of the published range.

Each composite disk had a slightly different average void content, $\overline{V}_v$, in the range of 1.81-2.64% for untreated composites (ignoring for now the two disks with negative $\overline{V}_v$); 1.72-2.72% for Silane-III treated composites; 1.16-2.89% for Silane-IV treated composites; 0.51-2.67% for Silane-V treated composites, 1.50% for HF treated composite, 0.74 for piranha cleaned composite, and 2.78% for Silane-I treated composite. A graphical display of all the $\overline{V}_v$ results, analogous to that given in Figures 5.2 (a) and (b) for $\overline{V}_f$, is presented in Figures 5.4 (a) and (b), (though the two disks with negative voidage are omitted). Since all $\overline{V}_v$ fall in the range of 0.51 - 2.89% range, it appears that $\overline{V}_v$ does not correlate with the fibre surface treatment.

5.3.1. Voidage and ρ_n uncertainty

The case of the six disks with negative void content values is perplexing because of the physical impossibility of the existence of negative voidage. Thus if we should raise the question as to why the density of nylon in the composite might be higher than the density of pure nylon ? The answer to this question is not straightforward, because, there are various factors that might influence the density of nylon in the composite. For example, one could contend that the presence of glass fibres in the nylon could promote higher fractional crystallization in the composites (more surface area for nucleation and growth) than in the pure nylon disks prepared in fibre-free molds with less solid surface area for contacting the caprolactam. Since crystals are denser than amorphous nylon, the density of the nylon in composites might be higher than that for pure nylon. The other factor that influences the nylon density is the processing history.

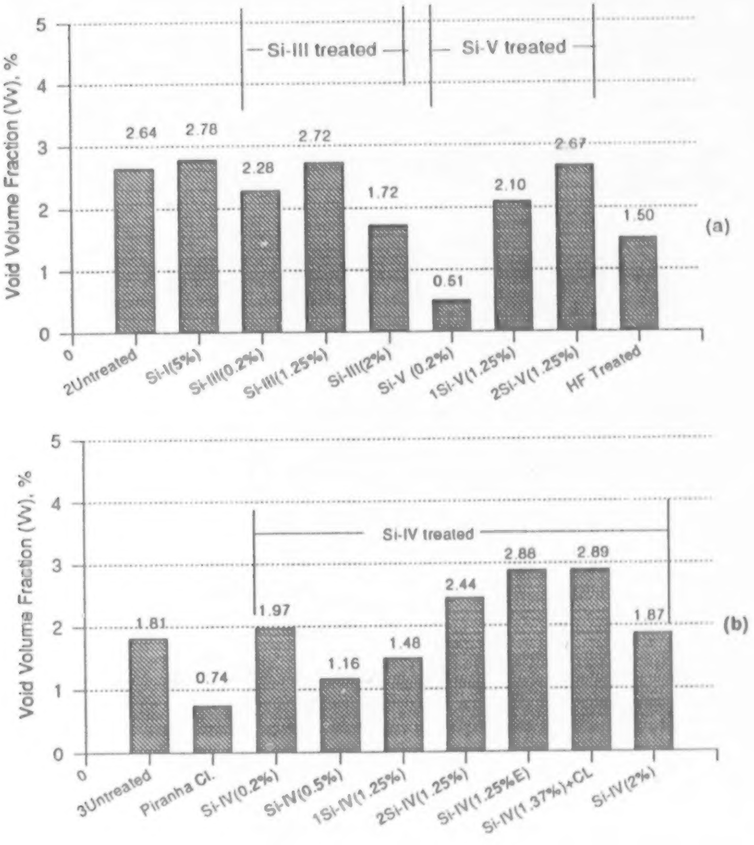

Figure 5.4 (a) and (b). Comparing void volume fraction of composites with treated and untreated glass fibres.

However, this is not a concern for us, since all the disks were made in similar fashion, with similar heating and cooling times and with the same catalyst and initiator concentrations.

One consequence of these kind of questions could be that the V_v results presented here (all obtained by calculation) could be entirely spurious. For example, one could argue that $V_v = 0$ and this would be found if the "proper" value of ρ_n were used in each type of composite. However, we find this not to be so (see following section, on SEM observations); substantial voidage did exist in these composite samples, though we cannot discern in this section precisely what it was if we cannot trust the value of $\rho_n = 1.14$ g/cm^3 used in analyzing the data of all disks and all specimens.

5.3.2. Distribution of local voidage within disks

Finally, the position-dependence of V_v in the various composite disks can be examined, analogous to what was done for V_f in Section 5.2, above. The discussion will refer in detail to Table C-2. We first note that V_v-variations differ fractionally from V_f-variations, within a single disk (the non-homogeneity problem) and marginally from disk-to-disk (discussed above, in terms of fibre surface treatment). For example, for a few disks, we find such V_v-variations as 1.39-5.36 [^{2}Untreated], 0.41-4.49% [Silane-IV(0.2%)], 1.87-5.48% [Silane-IV(1.25%EtOH)], (-1.29)-4.43% [^{2}Silane-V(1.25%)], and (-0.12)-2.86% for Silane-III (2%) disk, and a ΔV_v of 5.42% for ^{1}Untreated disk.

The distribution of voidage can also be examined. As stated earlier, for V_f, positions close to the edges (1, 2, 5 and 6) represented generally lower values for all disks, very likely because these are at the disk edge where the packing of solids (i.e., fibre mats) is sterically hindered by the mold wall and we could expect a lower V_f. Now, for V_v, we note again a trend for these positions to have lower values within their own disks, but not dramatically so (only 3 of the 9 disks show this trend). The overall picture is condensed in Figures 5.5 (a), (b) and (c), where absolute values of V_v are given for 9 disks (the disks possessing negative values of void content being omitted). There is a trend when either position 3 or position 4 or both, possess higher V_v values (11 of 18 disks, referring to Table C-2,

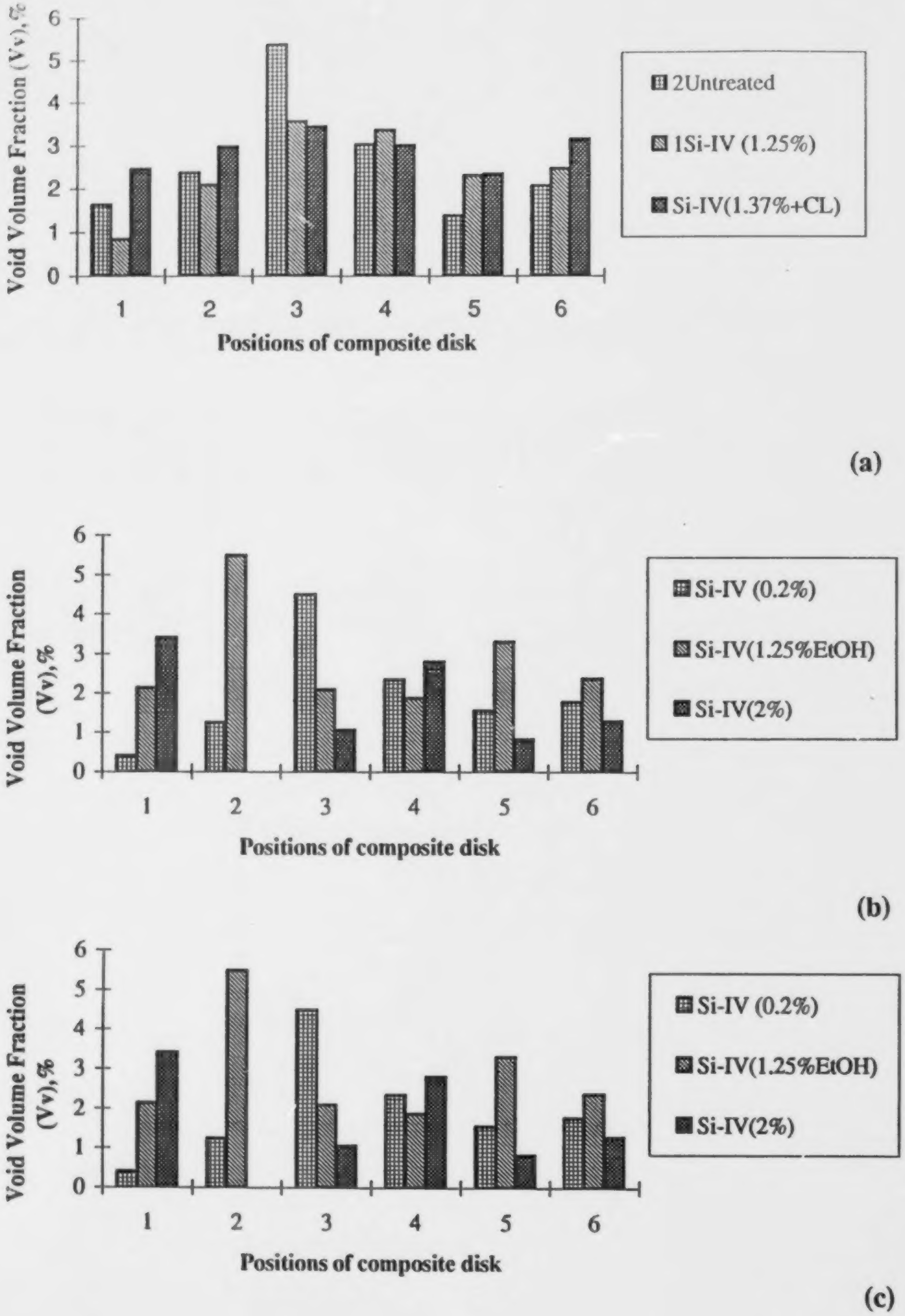

Figure 5.5.(a), (b) and (c). Void volume fraction at different positions in composite disks (see Figure 5.1). V_v values expressed as volume percents.

Appendix C). This trend is similar to that obtained for V_f, (Figure 5.3). Thus, for V_v and V_f, the distributions across the disks have some degree of similarity and could be correlated in terms of physical principles. For example, a locally higher fibre concentration would be more effective in trapping free bubbles in the caprolactam, thus capturing extra voidage (so, higher local V_f and V_v would go together).

Because Figure 5.5 tends to mask the V_v distributions with the wide discrepancies between V_v values on different disks, another graphical technique will also be used to highlight the distributions themselves. We assign numerical values (points) to the relative ranks of V_v at the six sampling positions: 6 for highest V_v value, 5 for next-highest, etc., with 1 for the position of lowest value. In these terms, the rank-distributions are displayed in Figure 5.6 (a) and (b). In these figures, the disks with negative V_v values are incorporated too. From Figure 5.6, we find that positions 3 and 4 dominate the highest ranks (5, 6) for 10 out of 18 disks; positions 1 and 2 also dominate the highest ranks (5, 6) for 10 out of 18 disks again, and positions 5 and 6 have fewer high-rankers and more in the midrange. While this presentation also indicates that voidage is not homogeneous, it does a better job than Figure 5.5 in highlighting the relative distributions.

An effort was made to establish a relationship between local V_f and V_v more quantitatively, by plots of local V_v vs. local V_f (Figure 5.7a) and corresponding averages $\overline{V}_v$ vs. $\overline{V}_f$, (Figure 5.7b). No correlations are apparent from Figure 5.7a. However, from Figure 5.7b, there appears to be a monotonic correlation band which indicates that $\overline{V}_v$ increases with the increase in $\overline{V}_f$. Since Figure 5.7a tries to represent data for 11 disks, it is difficult to highlight the trends present, if any, within this data scatter. We therefore sought to look into these trends by plotting the local V_v vs. local V_f in five different graphs (Figure 5.7 c, d, e, f, g, and h). From these figures, we again notice the appearance of the monotonic correlation bands for 11 out of 13 disks.

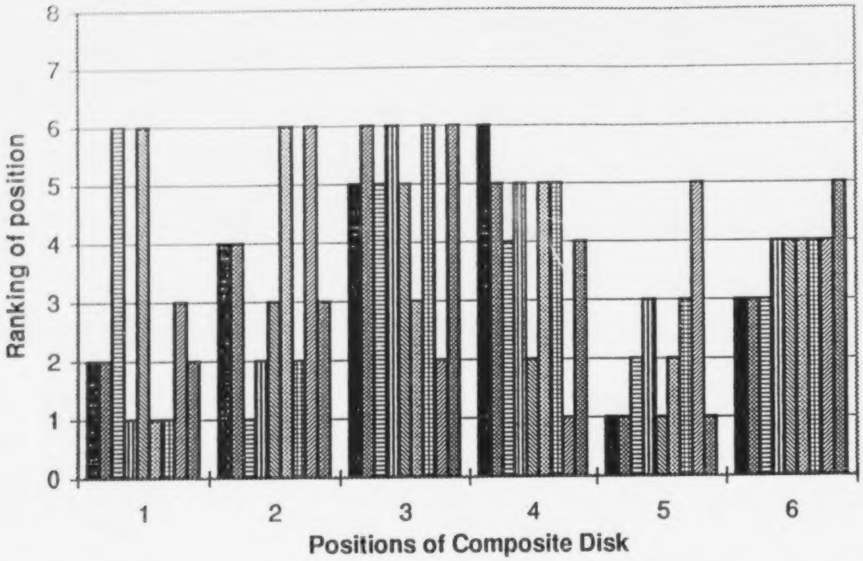

(a)

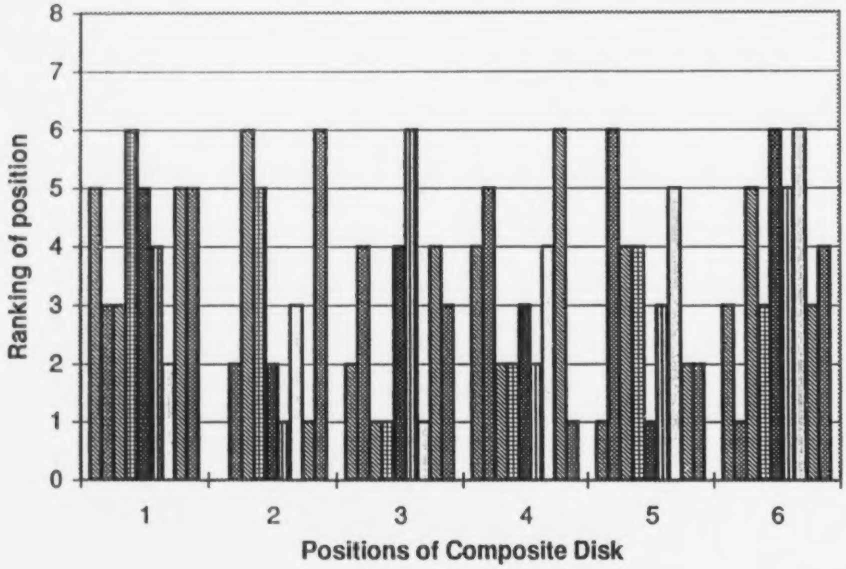

(b)

Figure 5.6 (a) and (b). Void volume fraction at different positions in composite disks (see Figure 5.1). V_v ranking, as a scale of 6-1, with 6 highest.

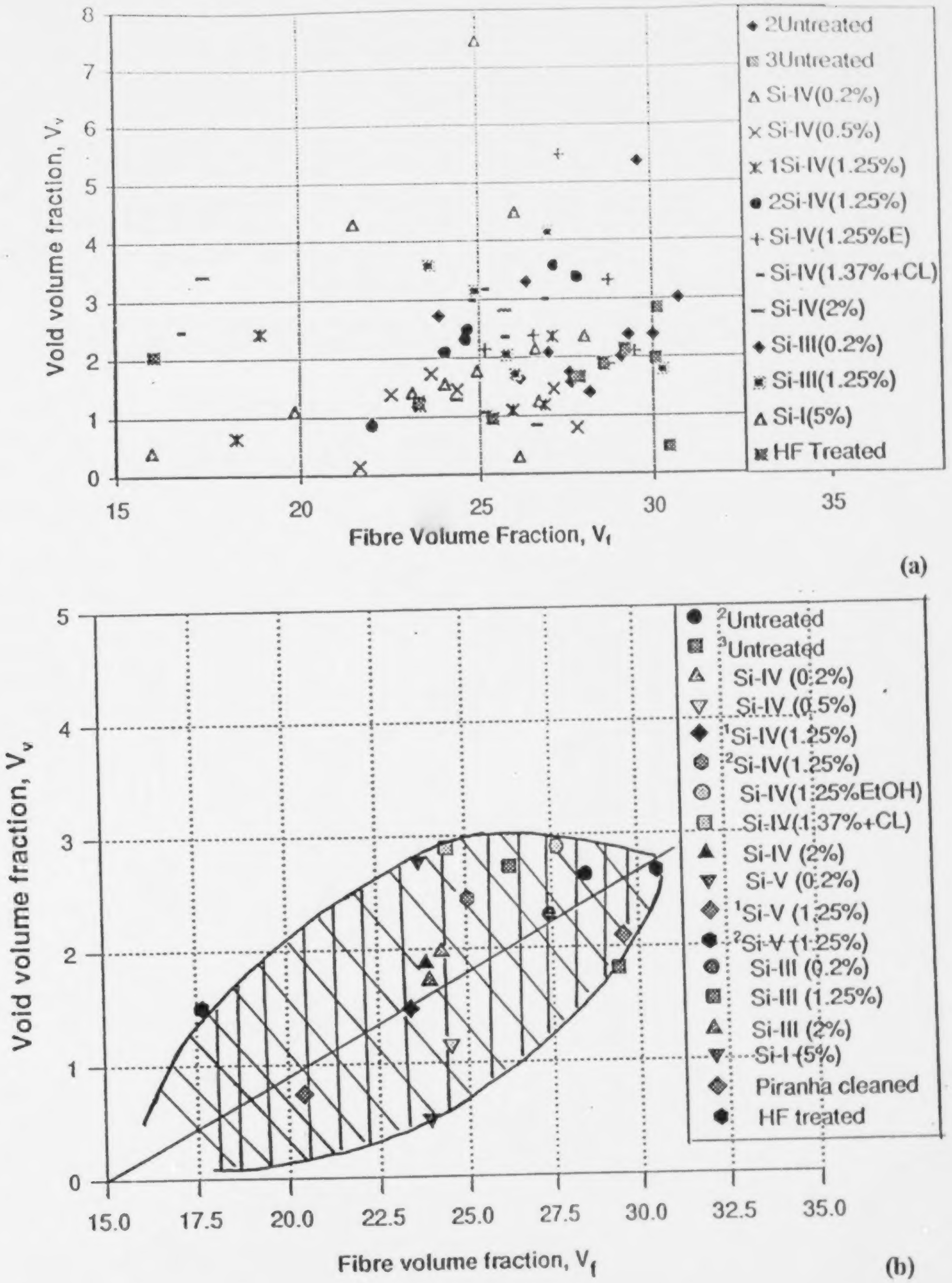

Figure 5.7 (a), (b). Fibre volume fraction (V_f) vs. void volume fraction (V_v) of composite disks. (a) Local V_v vs. local V_f for all specimens of all disks. (b) $\overline{V}_v$ vs. $\overline{V}_f$ for all disks.

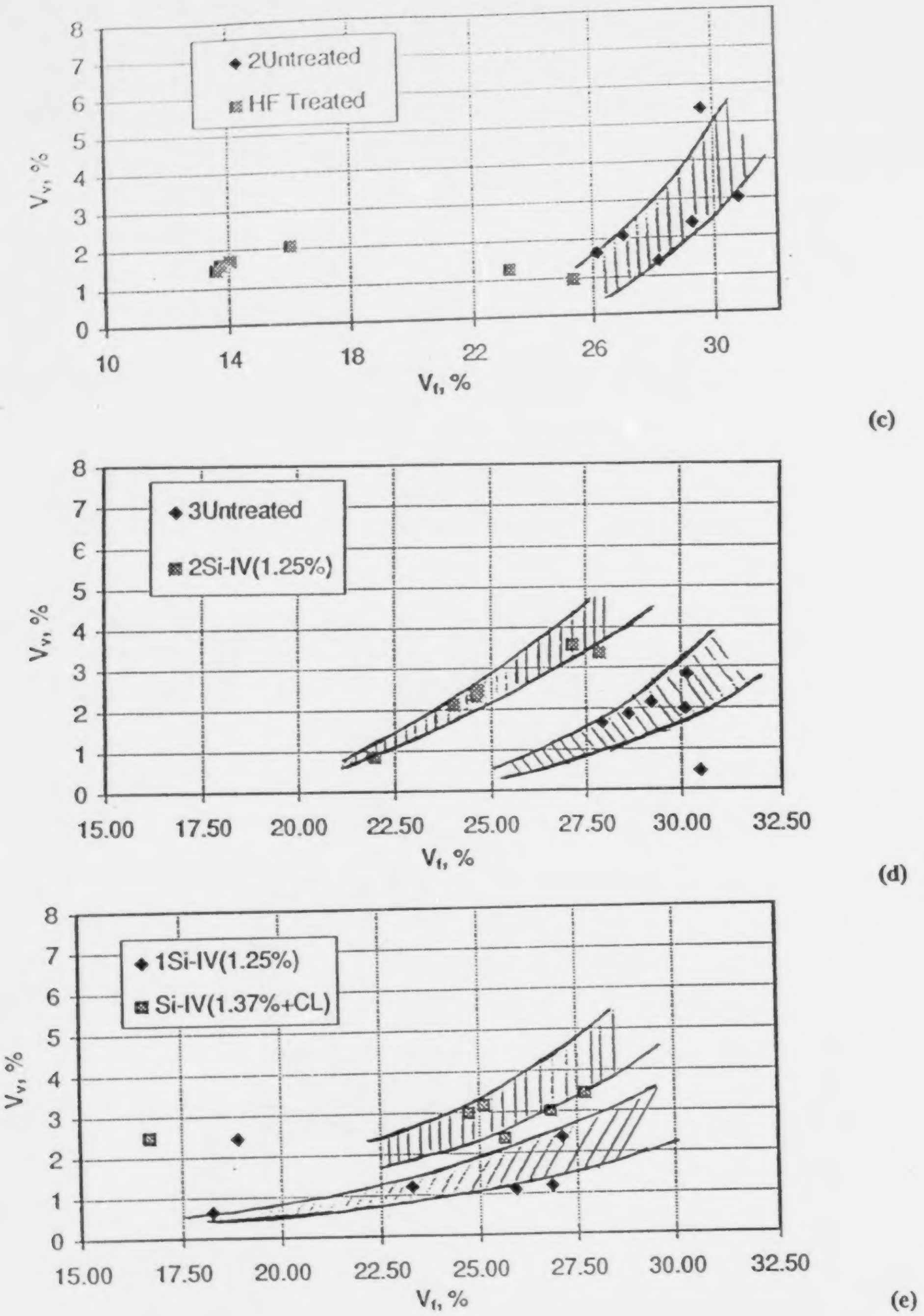

(c)

(d)

(e)

Figure 5.7 (continued). Fibre volume fraction (V_f) vs. void volume fraction (V_v) of composite disks (c), (d) and (e). Local V_v vs. local V_f for all specimens taken from disks: ²Untreated, HF treated, ³Untreated, ²Si-IV(1.25%), ¹Si-IV(1.25%), and Si-IV(1.37%+CL).

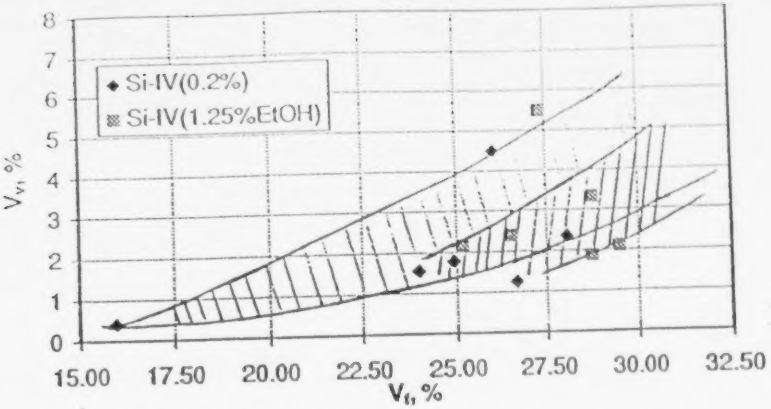

(f)

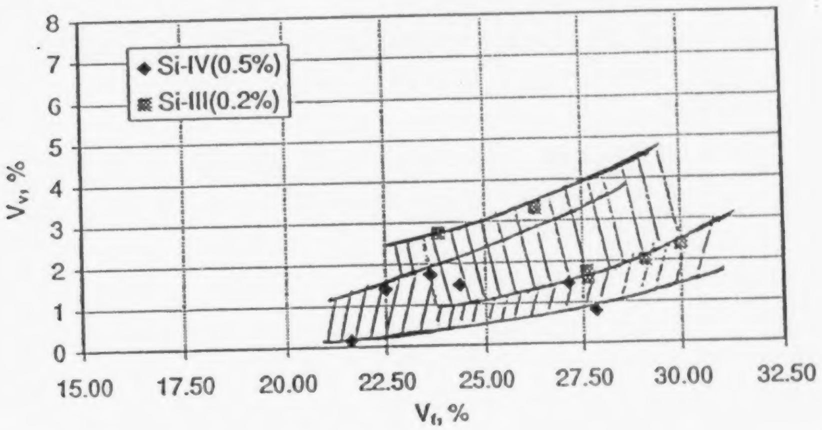

(g)

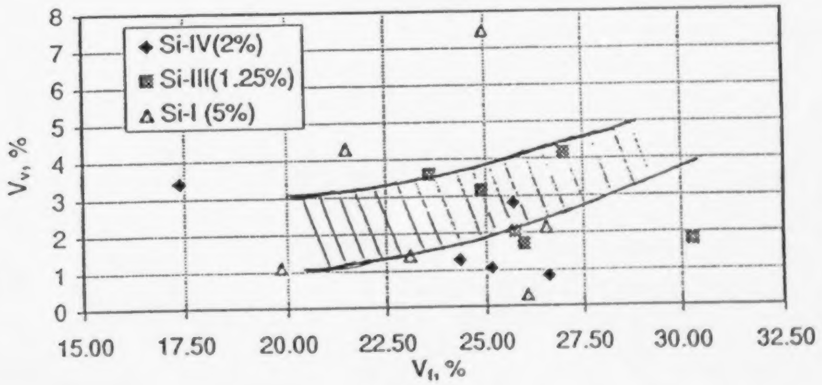

(h)

Figure 5.7 (continued). Fibre volume fraction (V_f) vs. void volume fraction (V_v) of composite disks (f), (g), and (h). Local V_v vs. local V_f for all specimens taken from disks: Si-IV (0.2%), Si-IV (1.25%EtOH), Si-IV(0.5%), Si-III(0.2%), Si-IV(2%), Si-III(1.25%) and Si-I(5%).

These tentative conclusions, of course are based on analysis of the numbers emerging in Table C-2, which may be unreliable if ρ_n is not the constant value it was originally believed to be. Other data, such as direct microstructure observation and thermal analysis (by optical microscope, SEM and DSC) and mechanical property measurement on specimens taken from different regions of the disk, can provide additional evidence on the microstructure question. These possibilities are discussed in Section 5.4 and below, and in Chapter 6.

5.4. Scanning Electron Microscope (SEM) micrographs of composites

The SEM micrographs, taken from composites with untreated fibre and composites with piranha-cleaned fibre, fibre treated with HF, Silane-III(0.2%), ^{2}Silane-IV(1.25%), and Silane-V(0.2%) are shown in Figures 5.8 (a-f). These pictures were taken at the top faces of original untested composite disks. The fracture surfaces of tensile specimens after breaking are shown in chapter 6. The faces of all unbroken composite samples appear to be similar, with identical glass fibre surfaces (smooth mainly), void size and distribution. We also find that higher void content exists in the regions where glass fibre content is high, these voids being formed at the glass fibre/nylon 6 interface. This may be due to the lack of affinity between nylon and glass fibres, as a result of which, the former always shrinks away from the glass fibres if possible. In the concentrated matrix regions, lower void content was observed. These photographs thus answer one question related to Vv = 0 in these composites. We can confirm that this is not true and that substantial voidage does exist in these composites. Now, if voids do exist, then we again ask ourselves, what must be causing the appearance of negative voidage in our system. To answer this question, we looked into the thermal analyses of these specimens to see if we could find an answer to this question of negative voidage. The thermal behavior of these composites is discussed in detail in section 6.3.

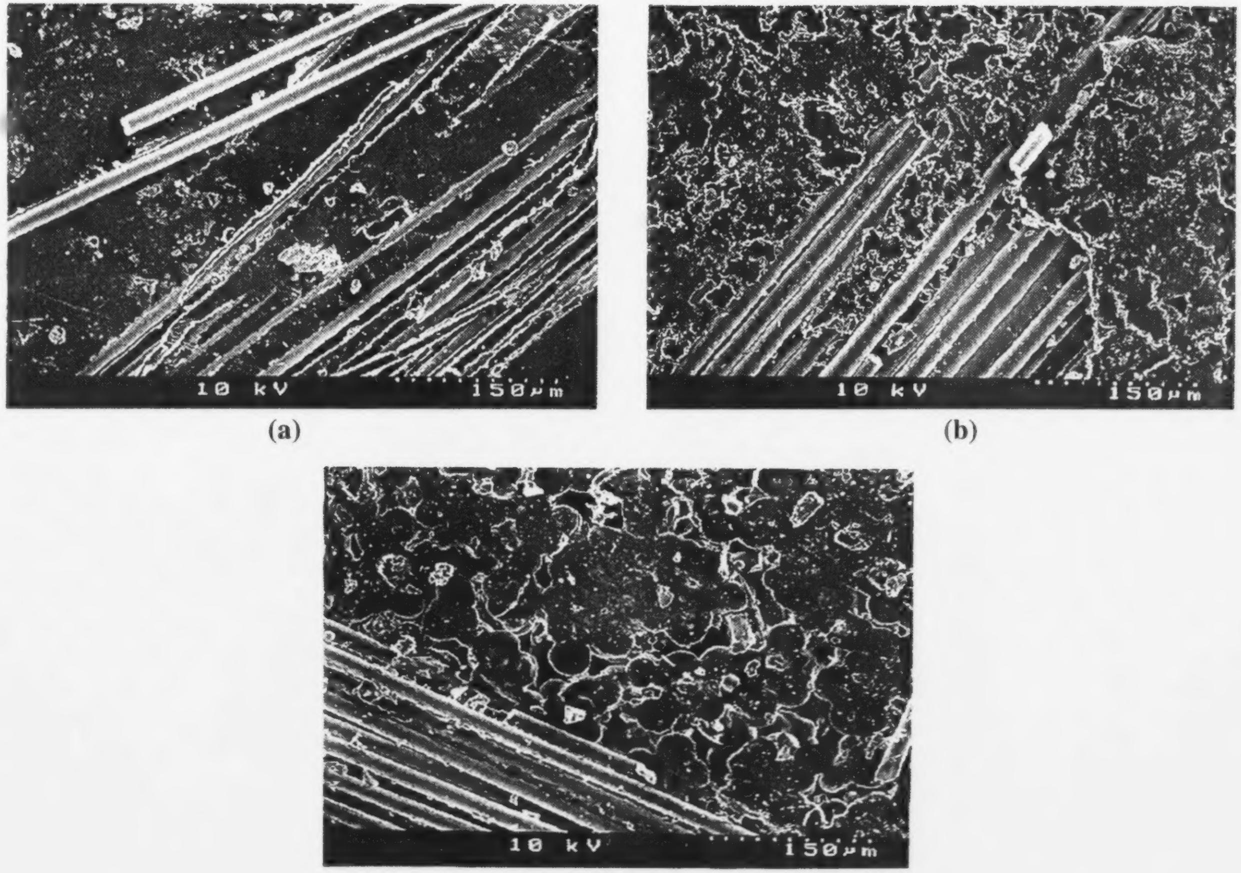
10 kV
150μm
10 kV
150μm
10 kV
150μm

(a)
(b)
(c)

Figure 5.8. Top surfaces of (a)Untreated glass fibre composite (b) Piranha cleaned glass fibre composite (c) HF treated glass fibre composite [(d), (e) and (f) continued on next page].

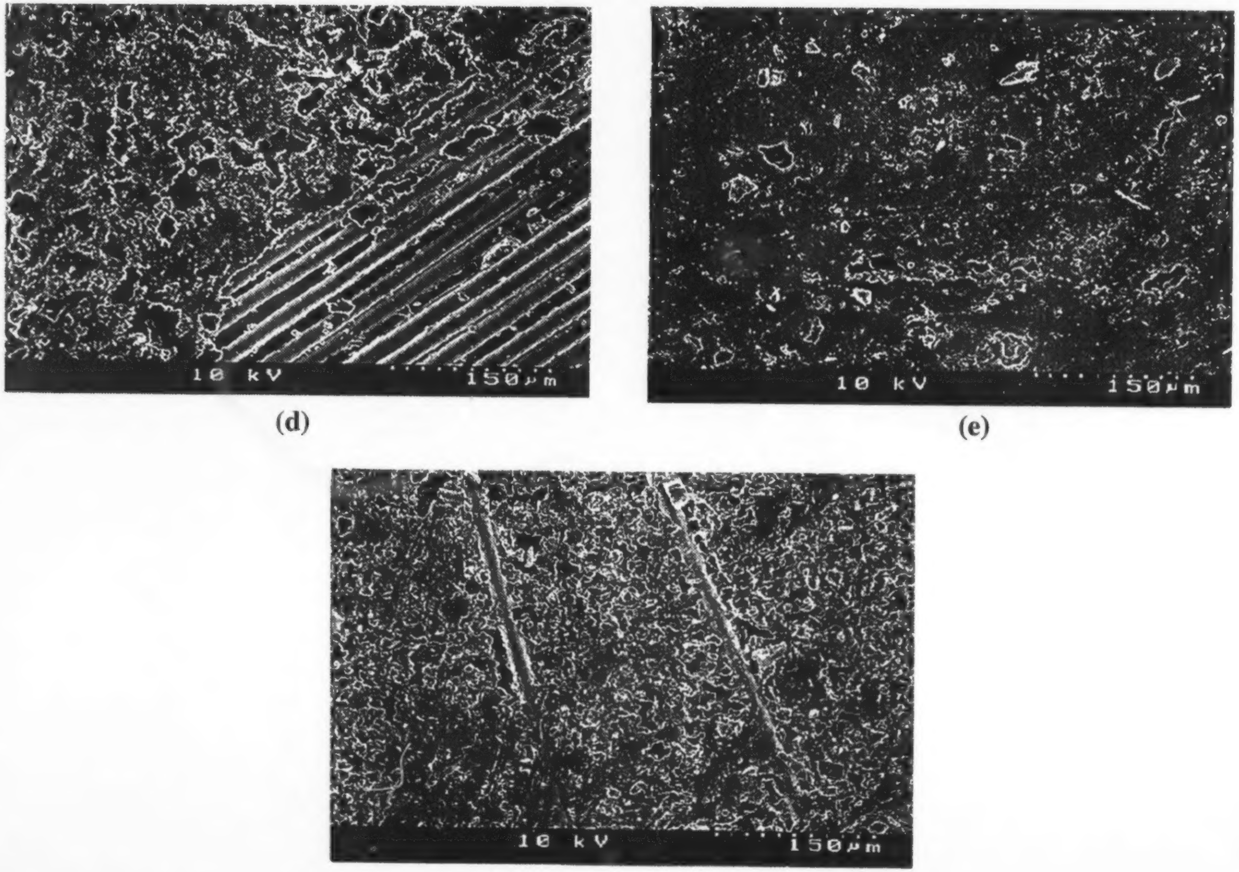
10 kV
150µm
10 kV
150µm
10 kV
150µm

(d)

(e)

(f)

Figure 5.8. Top surfaces of (d) Silane III (0.2%) treated glass fibre composite (e) ^{2}Silane IV (1.25%) treated glass fibre composite (f) Silane V (0.2%) treated glass fibre composite.

Chapter 6

MECHANICAL PROPERTIES OF COMPOSITE SPECIMENS

This section describes and discusses the mechanical properties of nylon 6 and the various composites obtained by carrying out different surface treatments of glass fibres. Both tensile and impact tests are included, with emphasis on the former. From a single tensile test four properties were obtained: tensile strength (σ_b), the stress (σ) at which the specimen breaks, tensile modulus (E), strain at break (ε_b), and toughness (τ) (breaking energy/volume at low tensile strain rates); the impact test gave only a breaking energy (E_s) (under standardized but complex strain conditions, and extremely high strain rates). The procedures for both tensile and impact tests, and samples of calculation of these properties, are shown in Appendix B.

6.1. Tensile Properties

The first set of tensile testing (12 disks) was carried out at NAIT (Plastics Engineering Department) on the Lloyds L6000R Universal Testing Machine. When access to the Lloyds machine was lost, the measurements were continued and concluded at the Mechanical Engineering Shop, University of Alberta, on an MTS tester.

Mechanical properties of nylon 6 (N6) and therefore also its glass fibre composites, are sensitive to the moisture content of the atmosphere. This is due to the high affinity of nylon 6 to water. Therefore, all the sample specimens that were tested were pre-conditioned in order to achieve equilibrium with an environment of the same relative humidity. Before doing so, the samples were dried in an oven at 110°C for about 12 hours to eliminate, or at least minimize, their moisture content. Initially, it was intended to pre-condition the samples at 50% relative humidity, since most of the literature values are cited at 50% relative humidity. The humidity in the NAIT laboratory was presumed to be controlled at 50%, and hence the writer pre-conditioned all samples in the NAIT laboratory so that no changes could occur between the storage and testing phases. However, the writer noticed that the laboratory humidity was not 50%, but was 66%.

Subsequent measurements at the Mechanical Engineering Shop were also carried out with specimens pre-conditioned at 66% relative humidity (RH) in order to maintain consistency in the testing conditions and convenience in comparing the data obtained. The latter samples were conditioned by placing them in a dessiccator, which was maintained at the desired relative humidity by placing in it a petri-dish containing a glycerol/water mixture (5:1 by volume). The relative humidity, as measured by a humidity gauge, remained almost constant over the period required for the mechanical tests. All tests were performed at room temperature (about 22°C).

Seven different types of composites were made: those with furnace-cleaned untreated (FC U) (i.e. clean glass) fibre surfaces, those with furnace-cleaned and HF etched fibre surfaces (FC HF), those with chemically-cleaned (piranha solution) untreated (CCl U) fibre surfaces, and those with Silane I (S^{I}), or Silane III (S^{III}), or Silane IV (S^{IV}), or Silane V (S^{V}) treated fibre surfaces. In all, 23 disks were made which included two pure nylon disks. These have been listed in Table 5.1. The aim of testing these materials was to see whether there was an improvement of mechanical properties when the glass fibres were given different surface treatments and to determine which surface treatment gave the greatest improvement of properties.

For each disk, five tensile specimens (cut from the disk positions T1-T5 indicated in Figure 5.1) were subjected to tensile stress-strain tests at an elongational rate of 2 mm/min. Since the gauge length of the specimen was initially 60.0 mm, the strain rate was

$$\dot{\varepsilon} = \frac{d\varepsilon}{dt} = \frac{d}{dt}\left(\frac{L - L_0}{L_0}\right) = \frac{dL}{dt}.\frac{1}{L_0} = \text{(2 mm/min)/60 mm} = 0.033\ \text{min}^{-1}.$$

Fifty of the $\sigma(\varepsilon)$ curves from among the 115 runs are contained in Appendix D. Values of σ_b, ε_b, toughness, and E were taken from each curve and are displayed for each specimen (T1→T5) of each given disk in Appendix C, in Table C-3 (specimens tested on Lloyds machine), Table C-4 (specimens tested on MTS machine). Also displayed there are the averages $\overline{\sigma}_b$, $\overline{\varepsilon}_b$, $\overline{\tau}$, and $\overline{E}$ for each disk, which will be taken as representative for that disk.

Table C-5 in Appendix C summarizes the average property values in a sequence that segregates each data set according to the surface treatment and, within that scheme, arranges results in the order of increasing concentration of the coupling agent in the treatment solution.

The Lloyds L6000R Testing Machine had an on-line computer data analysis which provided the four numerical parameters characterizing each $\sigma(\varepsilon)$ curve; hard copy of each curve was also produced. Measurements made on the MTS testing machine at U of A, did not have computerized data analysis and so the data obtained were extracted from each curve using judgement. Values of τ were obtained by scanning each $\sigma(\varepsilon)$ curve and obtaining the desired integral $\tau = \int \sigma\left(\frac{dL}{L_0}\right)$ (area under the curve), using the image analysis software. These calculations were carried out with the help of the image analysis (NIH-Image analyser) software in Dr. U. Sundararaj's polymer laboratory. Although the data were extracted by judgement and image analysis, these were found to have desirable internal consistency as seen from the small standard deviations of the values obtained for different parameters in Table C-4.

However, another unlikely complication arose later that was not apparent at the start of NAIT testing: the ε scales on the Lloyds machine and the MTS machine did not agree. *Duangchan, 1994*, encountered the same problem, when she carried out measurements on two different machines, one being an Instron machine at the U of A, and the other was the same Lloyds machine at NAIT. To our surprise, the $\sigma(\varepsilon)$ curves obtained by the writer on the same Lloyds machine at NAIT appeared different from those obtained by *Duangchan, 1994*, as shown in Appendix D. One more surprise came when we found the data obtained on the MTS machine at U of A, matched the data obtained by *Duangchan* on the Instron tester. The range of ε_b (strain at break) obtained on the Lloyds machine (for the pure nylon specimens cut from the rectangular configuration disk (ε_b = 9-10%); and for composites (4-6%)) was higher than that obtained on the MTS machine (about 4.95% for pure nylon and about 1±0.2% for composites), and closer to the range cited in literature (6-7% for N6/glass composites; see Table 2.3). This might tempt us to consider the Lloyds machine data as representative of the true properties of nylon and its composites. However, if we consider some factors listed below, we might question the verity of the data obtained on Lloyds machine. These factors are as follows:

1) A close look at the nature of the $\sigma(\varepsilon)$ curves obtained by the writer on the Lloyds machine (Appendix D) seem to show some slipping phenomenon at the grips where the specimen is clamped. Attempts to eliminate the slipping were unsuccessful; among the schemes employed were roughening the specimen surface with a sandpaper, making grooves on the specimen surface which were similar to the grooves on the grips, and gluing the specimen to another surface which would be gripped better by the jaws. This slipping phenomenon could have resulted in apparent higher values of ε_b and a similar influence on all numerical values of the ε axis (thus smaller values of $E = d\sigma/d\varepsilon\,|_{\varepsilon=0}$) being reported.

2) All specimens (including the pure nylon) showed brittle fracture (i.e. these did not yield and the failure was catastrophic). This kind of brittle fracture might be caused due to the shrinkage stresses which are developed in the material, caused by crystallization and consequent densification of nylon 6 during the in-situ polymerization process.

3) Furthermore, flask-made specimens of nylon 6, by *Sankholkar, 1996*, using the same catalyst and initiator concentrations, showed no yielding and drawing (ε_b recorded was in the range of 2.48%). However, when the same flask-made specimens were compression molded, these appeared to yield and undergo plastic flow to strains greater than 10%. It was claimed by *Sankholkar, 1996*, that this indicated the presence of shrinkage stresses in the as-made specimens, and a near-absence of residual stress in these specimens that had possibly been stress-relieved in the high-temperature molding process.

The above mentioned factors suggest that the matrix and hence the composites obtained in our laboratory are brittle, thus verifying the results obtained with the MTS and the Instron testing machines.

With all the above arguments, the fact still remains, that, the parameters involving ε cannot be compared confidently between the U of A and NAIT measurements. Nonetheless, within each set of data obtained at NAIT and at U of A, comparisons can be made and some useful conclusions can also be drawn. Further, because of the unusual nature of the $\sigma(\varepsilon)$ curves obtained at NAIT, one must exercise caution in drawing any conclusions made with respect to the parameters involving ε. However, the values of stress only (e.g., σ_b) obtained for all specimens, may be regarded as reliable and truly representative of the materials, and can be used for comparison between the two sets of data and with their respective values in literature.

However, for convenience of reference and to facilitate discussion, we shall employ here a data display, that is organized with respect to the testing machine used for all parameters, which are the tensile modulus (E), tensile strength (σ_b), strain at break (ε_b), and toughness (τ). Detailed numerical tabulations are given in Appendix C [Table C-3 and C-4], while we will present most results graphically in this Chapter.

Apart from surface treatment, the mechanical properties of a composite also depend on the glass fibre volume fraction ($\overline{V}_f$), and void content ($\overline{V}_v$) in the composite. That is,

$$\text{Mechanical property}(Y) = f\,(\overline{V}_f, \overline{V}_v, S)$$

where, S identifies the nature of the fibre surface condition after whatever treatment it has received.

Therefore, to compare surface treatment effects on mechanical properties Y, of two composite disks identified as 1 and 2, we keep the other two variables constant, that is, compare $Y_1 = f(S_1)$ and $Y_2 = f(S_2)$ at the same $\overline{V}_f$ and $\overline{V}_v$. Table C-5 (Appendix C) displays the $\overline{V}_f$, the $\overline{V}_v$ and the average tensile strengths of all composite disks having the same surface treatment, to isolate the results of the latter, to facilitate the comparisons between the disks.

6.1.1. Tensile properties of unreinforced nylon 6

As can be seen from Tables C-1 and C-2 in Appendix C, mechanical properties obtained for two different configurations of nylon 6 disks were quite different. For example, the tensile strength for the nylon disk with rectangular configuration (σ_b = 65 MPa) was more than double the tensile strength of the nylon 6 disk with circular configuration (σ_b = 27 MPa). The disk with circular configuration was more brittle than the rectangular configuration disk, [$\varepsilon_b(C^*) < \varepsilon_b(R^*)$]. The rectangular nylon disk was made with the vacuum being maintained during the mold-filling operation; the circular disk was made in a slightly different manner. The vacuum was applied to the circular mold as a first step,[•] and the molten monomer was then injected. Because of this, the entrapped air or vapors that were released inside the mold, might not have been sucked out from the mold. This meant that the circular disk might possess more voids than the rectangular disk. Indeed, visual inspection of the two disks showed the circular disk had far more voids on the surface than the rectangular one. The pattern of the voids always seemed to be radial, with small voids present near the centre, and larger ones away from the centre. This could also be one of the reasons the rectangular disk showed lesser voids, as the region the rectangular disk covered was mainly close to the centre. This macroscopic view was supported by SEM (Model Hitachi S-2700) analysis of fracture surfaces. The SEM micrographs are shown in Figure 6.1. From these photographs we can see that the rectangular disk had an uniform, dense and fine matrix and showed very minimal presence of voids. The circular disk specimens showed a non-uniform, coarser, and spongy kind of matrix. A closer view of the spongy kind of matrix region is shown in Figure 6.1 (d). The morphology of this region is very different and shows the presence of loosely bound particles held together, and the spaces between these particles represent the voids. We were also able to estimate the void content using the IPA (Image Phase Analyser, Oxford Instruments, Engiand)

[•] Hereafter, sheet specimens are identified by a prefix C (circular) or R (rectangular) to indicate the configuration of the mold in which they were polymerized.

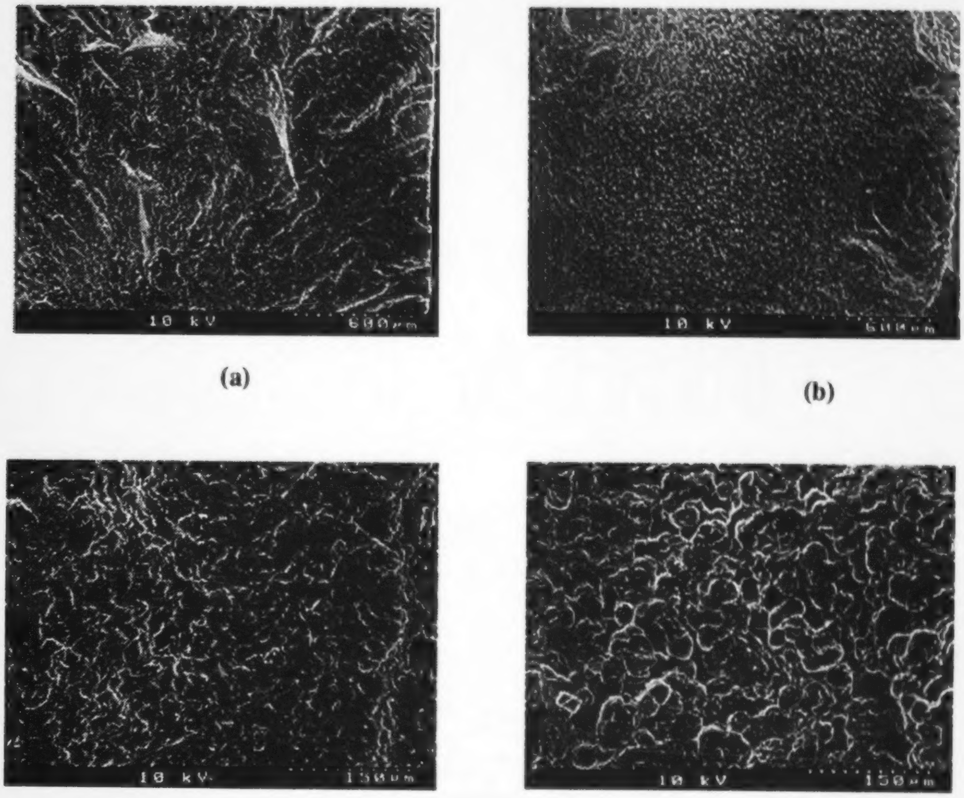
10 kV
600µm
10 kV
600µm
10 kV
150µm
10 kV
150µm

(a) (b)

(c) (d)

Figure 6.1. SEM of fracture surface of nylon from disks with
(a) rectangular configuration (600 µm) **(b)** circular configuration (600 µm)
(c) rectangular configuration (150 µm) **(d)** circular configuration (150 µm)

connected to the SEM. For each specimen, void fraction was estimated at four different regions of the fracture surface. For each region, the V_v was determined by assigning different gray scales to the image and identifying the voids by a particular gray scale. This test was subjective; nevertheless, it gave values for making comparisons between the two disks. The rectangular disk was found to have an average void content, $\overline{V_v}$ of 6 ± 1.8%, whereas, the circular disk had $\overline{V_v}$ ranging from 19 ± 2.3% in the spongy matrix regions to about 9 ± 2.8% in the dense matrix regions. The densities ($\overline{\rho_n}$) of the two disks were also found to vary slightly: $\overline{\rho_n}$ (circular) = 1.128 ± 0.006 g/cm^3, and $\overline{\rho_n}$ (rectangular) = 1.138 ± 0.008 g/cm^3. The variation in density could either be due to variation in crystallinity of nylon 6 or because of different $\overline{V_v}$ of these disks.

All of the above factors lead us to believe that the circular disk had higher void content than the rectangular disk. The question still remains as to what could have actually caused the large difference in the morphology, the void content and hence the properties of the two disks.

The next question that arises as a consequence of the above discussion is: which nylon disk should be used as a reference , with which the composites should be compared. The answer to this question could be approached by looking into various aspects. For example, let us try to compare the fabrication procedures for the various disks. All composite disks were fabricated by maintaining vacuum in the mold during the mold-filling operation. This procedure was similar to that used for making the rectangular, pure nylon disk. Secondly, if we take a look at the SEM photographs of the matrix nylon in the composite, we find that the morphology is uniform, dense, and fine and similar to that found in the rectangular, pure nylon disk. The presence of a dense morphology in the composite is also supported by the fact that the presence of glass fibres could promote higher fractional crystallization of the nylon in the composite. Further supporting evidence to this is that V_v values, obtained by using the lower density of the circular nylon disk (ρ = 1.128 g/cm^3), were negative for many composite disks (almost 45 positions out of 80 positions for various disks), probably suggesting that the density of nylon in the composite is higher than this value. Indeed, only 9 negative values of void content were obtained from that same calculation when we used the higher density of the rectangular, pure nylon disk. All the above factors do suggest that the nylon matrix in the composite is similar to that in the rectangular pure nylon disk. This reinforces our decision to use the rectangular nylon disk properties as a reference for making comparisons with the composites.

Furthermore, the nylon 6 with rectangular configuration, produced by the *in-situ* process seems to be of good quality and comparable or superior to established commercial products. Some comparisons are shown in Table 6.1. Our value of σ_b (65 MPa) is higher than most commercial values are expected to be, at the same density (crystallinity) and humidity. In contrast, our value of ε_b (5%) is much lower than the other two in Table 6.1, the published value of 30-300%, and, the value obtained for the Allied Chemicals specimens ($\varepsilon_b > 15\%$, see Table 6.1). These differences could arise from a unique crystal morphology or orientation produced by our particular *in-situ* mold polymerization and or due to the shrinkage stresses developed in the material caused by crystallization and consequent densification of nylon 6 during the polymerization process.

Table 6.1. ***Comparison of commercial nylon 6 and our nylon 6***

Properties	This study	Allied Chemicals	Table 2.3 (column b)
ρ, g/cm^3	1.13-1.14* ($\bar{\rho}$ = 1.138)	1.131-1.134* ($\bar{\rho}$ = 1.132)	1.12-1.14
σ_b, MPa	65.1** (@RH = 66%)	58.3** (@RH = 66%)	41-165
ε_b, %	4.95**	> 15	30-300
E, GPa	2.2 ** (@RH = 66%)	2.10 **(@RH = 66%)	0.7 (@RH = 50%)
Izod, E_s, J/m	38.1*** (RH = 66%)	Not obtained	32-160

* Table C-1...............** Table C-4..............***Table C-6 (a)

To see if these differences in σ_b and ε_b might be reflected in a shift of the melting point (T_m), we employed a differential scanning calorimeter (TA Instruments DSC 2910) to examine the thermal behavior of our nylon 6 and its composites. Further discussion of DSC results for nylon 6 and the various composites will be presented in section 6.3.

6.1.2. Reproducibility of composite disks

In Chapter 5, the study of microstructures of specimens taken from different disks prepared in nominally the same way permitted scrutiny of factors related to reproducibility of microstructures during the disk fabrication process. Another assessment of our control of variables in the molding process can be made by determining whether the mechanical properties in nominally identical disks can be reproduced.

Composites containing fibres that were untreated and fibres that were treated with Silane IV (1.25% in toluene) and Silane V (1.25% in toluene) were prepared twice. Reproducibility could, in principle, be evaluated from tensile data for the two untreated and two Silane-IV treated disks. However, for the Silane V-treated disks, processing conditions happened to be different for the two disks. This occurred because one of the cartridge heaters was burnt off and hence that region of the mold was not hot enough to cause complete polymerization of the caprolactam.

For the two untreated disks, all tensile properties could be evaluated for reproducibility, since both these disks were tested on the same machine (the Lloyds machine at NAIT). However, for the two Silane IV treated disks, only σ_b could be compared since these disks were tested on two different machines with different strain (ε) scales. From Tables C-3 and C-4, we see that ^{1}Untreated and ^{2}Untreated had $\overline{\sigma_b}$ = 54.60 MPa and 53.00 MPa; $\overline{E}$ = 2.36 GPa and 2.19 GPa; $\overline{\varepsilon_b}$ = 2.50% and 2.55%; and $\overline{\tau}$ = 0.71MPa and 0.68 MPa, respectively. This excellent reproducibilty is also mirrored in the two Si-IV (T) cases, for which $\overline{\sigma_b}$ = 110 MPa and 112 MPa. These results seem to confirm that the composites are reproducible in a mechanical property sense, giving $(\overline{\sigma_b})_{av} = 53.8 \pm 0.8$ MPa; $\overline{E}_{av} =$ 2.28 ± 0.09 GPa; $\overline{\varepsilon_b}_{av} = 2.53 \pm 0.13\%$; $\overline{\tau}_{av} = 0.70 \pm 0.02$ MPa for the untreated disks and

$(\overline{\sigma_b})_{av}$ = 110.82 ± 0.71 MPa for the Silane-IV treated disk. This is well within the range of experimental uncertainty for failure tests such as these.

6.1.3. Tensile properties of the composites

Figures 6.2 (a-e) display the tensile strengths of various composite disks listed in Tables C-3 and C-4 in Appendix C. The average volume fraction of glass fibres ($\overline{V}_f$) in these disks has also been shown in order to facilitate comparisons between disks with different surface treatments. The void volume fractions of all the composites were found to lie in the range 0.51-2.89%, a sufficiently narrow range so that we shall assume, for now, that void fraction is not a variable while comparing two different composite disks. The error bars in the graph represent the standard deviation of the data obtained for five different specimens of a single disk. It should be noted that only the positive deviation has been shown here.

A comparison of tensile properties of the furnace cleaned untreated glass fibre composite and pure nylon disk (rectangular configuration) in Table C-3 and C-4 shows that the tensile strength of nylon dropped to approximately 80% of its original value when glass fibres were present in the matrix at a volume fraction of approximately 28%. Similar drops for nylon/glass fibre composites were found by *Duangchan, 1994* and *Sankholkar, 1996*. All the composites were prepared in a similar fashion, that is, by carrying out polymerization at 150°C. Unlike σ_b, the elastic modulus E improved significantly upon incorporation of glass fibres in the nylon matrix (as seen in both the tables in Appendix C). We also attempted to make an untreated glass fibre composite disk by carrying out the polymerization at 120°C. The tensile strength of this disk ($\overline{\sigma_b}$ = 82 MPa) was significantly higher than the other untreated disks with $\overline{\sigma_b}$ = 53 MPa. We suspect that this improvement might be due to differences caused in the nylon microstructure in the two composites polymerized at different temperatures.

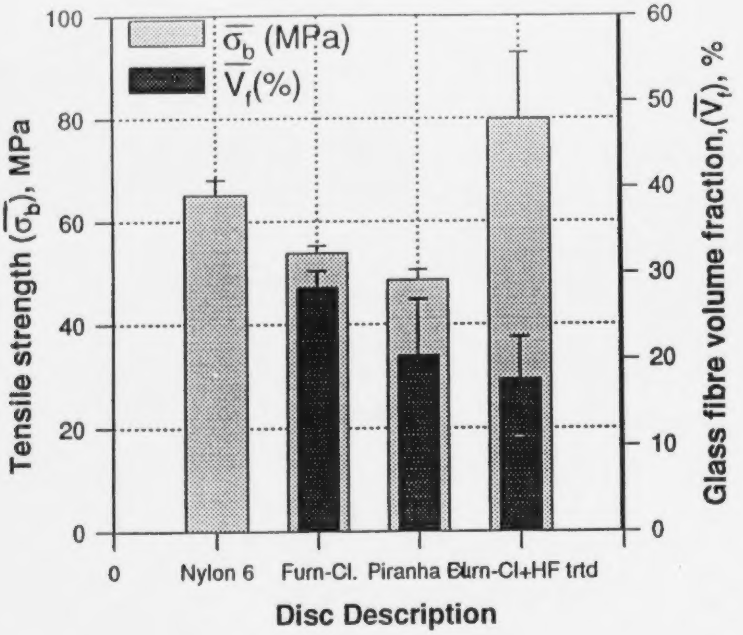

(a)

Figure 6.2(a). Tensile strengths and volume fractions of pure nylon, furnace-cleaned untreated, piranha-cleaned untreated and furnace-cleaned HF treated disks at RH 66%. No silane treated composites are represented here; Cleaning effects are emphasized here.

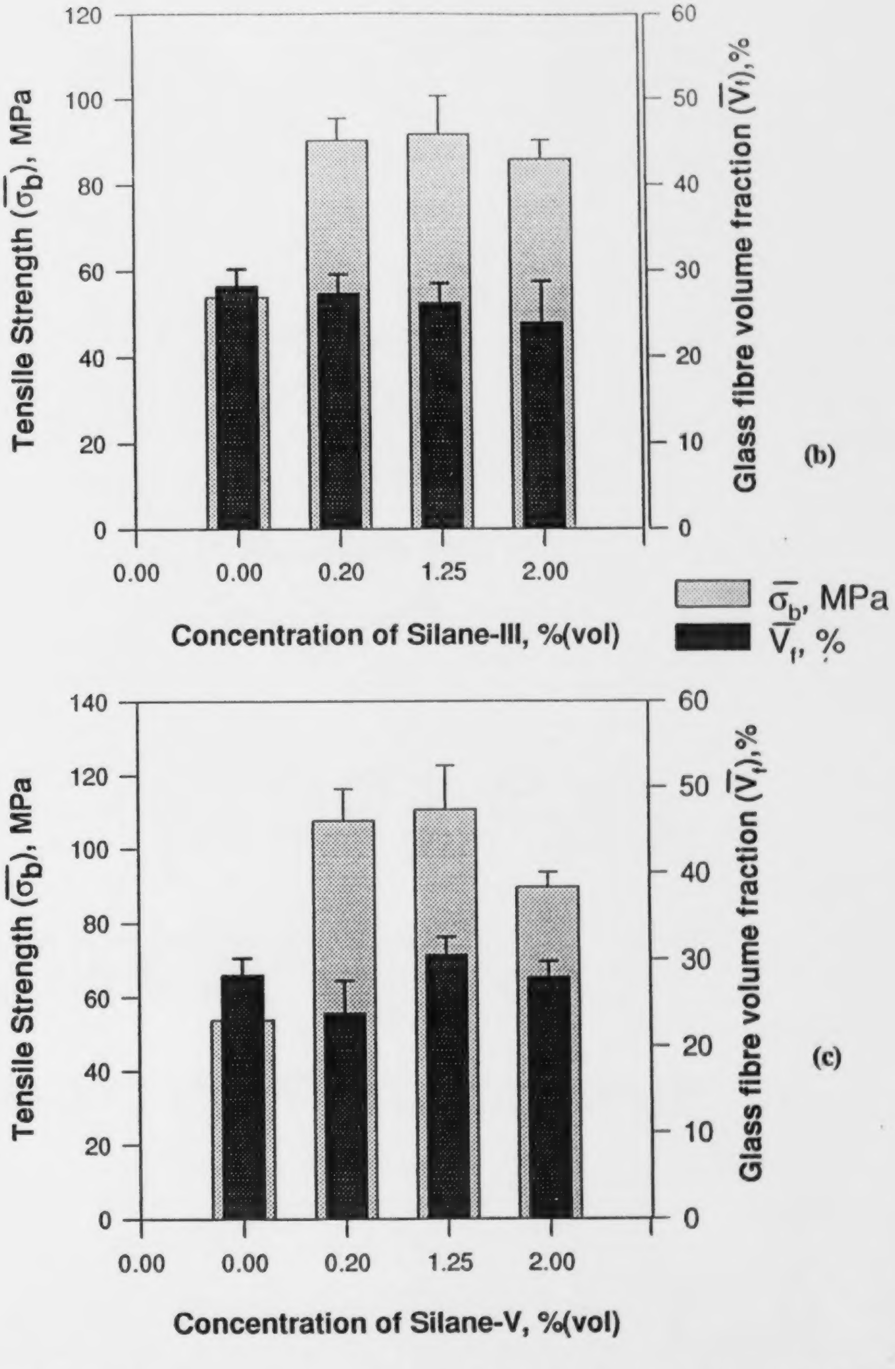

Figure 6.2 (continued). Tensile strengths and volume fractions of various silane-treated composite disks at RH 66% (b) Silane-III disks. (c) Silane-V disks. Toluene was the solvent in both treatments.

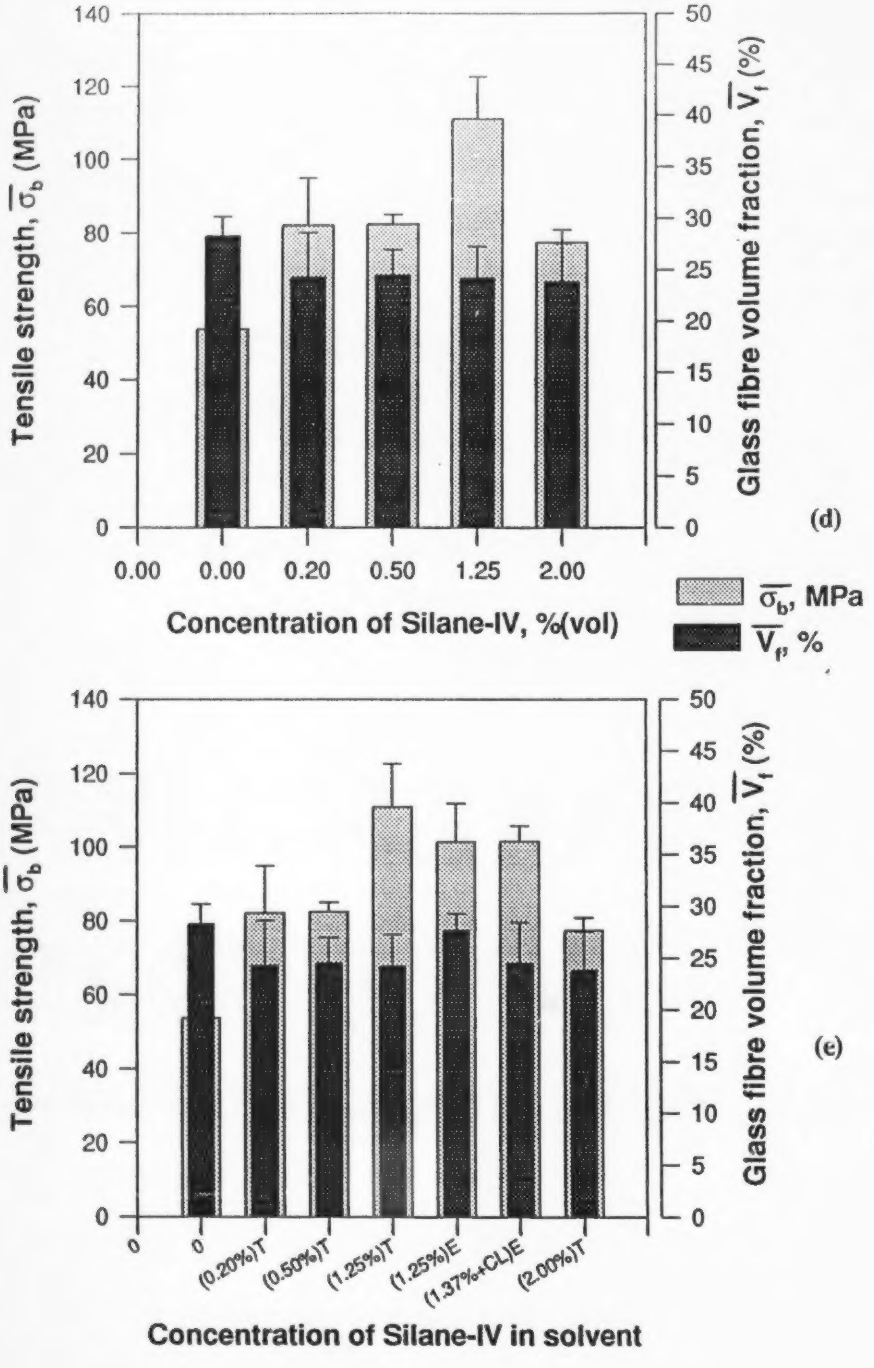

Figure 6.2 (continued) Tensile strengths and volume fractions of various silane-treated composite disks at RH 66% (d) Silane-IV in toluene (e) Silane-IV in different solvents.

Comparison of different types of surface treatment

From Figure 6.2 (a), we find that $\overline{\sigma_b}$ of the untreated composite remains unchanged when the glass fibres are either furnace cleaned or chemically cleaned (with piranha solution). One could argue that the $\overline{V_f}$ = 20% of the piranha cleaned fibres disk is lower than that of the untreated disk ($\overline{V_f}$ = 28%). So, an approximate prediction of how the piranha-cleaned composite would behave, if it had $\overline{V_f}$ = 28% would use a multiplying factor based on the ratio 28/20. When this is done, the tensile strength of the piranha treated glass fibres disk emerges to be ~59MPa. Now we must not forget that the void volume fraction might or might not increase with the volume fraction of glass fibres. This increase in the void fraction might work to bring the tensile strength of the composite lower than the extrapolated value. Thus, it is difficult to predict if the tensile strength would increase or decrease with the increase in the fibre volume fraction. Nevertheless, the tensile strength value would remain in the same range as that for the untreated disk, and we might conclude that the tensile strength remains unchanged. This implies that the chemical cleaning offers an alternative method to clean glass fibres. In the same figure, we find that HF treated glass fibre composite gives an improvement of almost 50% in $\overline{\sigma_b}$ over the untreated composite, inspite of having an abnormally low $\overline{V_f}$ of 18%. Thus, we can appreciate how enormous the improvement in tensile strength would be, had $\overline{V_f}$ been 28%, as for the untreated composite.

Figure 6.2 (b) compares tensile strengths of composites with fibres that are treated with varying concentrations of Silane III in toluene. It should be noted that $\overline{V_f}$ for all these composites lies in the same range 24-27%, and close to the untreated $\overline{V_f}$ of 28%. This enables us to make direct comparison without worrying about the $\overline{V_f}$ for these disks. The Silane III composites do show improvement in σ_b (about 66%), over the untreated composites. However, Silane III concentration effects in the tensile strengths are not very apparent, that is to say, the tensile strength remains almost the same for different concentrations of Silane-III in toluene used for treatment baths. *Duangchan, 1994*, had worked with Silane III in the concentration range 5-15%, and the values of tensile strengths that she obtained were around 60 MPa, significantly lower than the values obtained herein. However, the speculations emerging from her work with Silane-III suggested that the lower concentrations of Silane-III might give better properties. This indeed seems to be true, when one finds an increase of almost 66% in tensile strength by lowering the concentration of Silane III. Inspection of the trends in $\overline{E}$ (c), $\overline{\varepsilon_b}$ (c) and $\overline{\tau}$(c) with concentration of Silane-III show that these functions are also nearly independent of concentration in the range 0.2-2%. These plots of $\overline{E}$ (c), $\overline{\varepsilon_b}$ (c) and $\overline{\tau}$(c) are shown in Figures 6.3, 6.4 and 6.5 respectively.

Moving to Figure 6.2 (c), where, varying concentrations of Silane-V have been used, we find that the greatest improvement was obtained with two concentrations of Silane-V, viz. 0.2% and 1.25%, both of which gave an increase of ~104% over the untreated composites. Similar trends were obtained for $\overline{E}$ (c) and $\overline{\tau}$(c), while $\overline{\varepsilon_b}$ (c) was found to be constant and independent of concentration. Whereas, the increase in the tensile strength of the two composites was the same, we can comment on the effectiveness of each concentration of Silane-V in imparting the increase in tensile strength, by plotting an "effectiveness factor", which is the increase in tensile strength over the untreated composite per unit concentration, against concentration of Silane-V. This is shown in Figure 6.6. We can see that the 0.2% concentration of Silane-V has been far more effective than the 1.25% concentration, or in other words, a very small solution concentration (0.2%) leading presumably to few molecules adsorbed on the glass surface has improved the tensile strength to a very significant amount.

We also found that higher concentrations of Silane-V seemed to hinder the polymerization of nylon 6. This might be the reason for lower tensile properties obtained for Silane-V (2%T) disk.

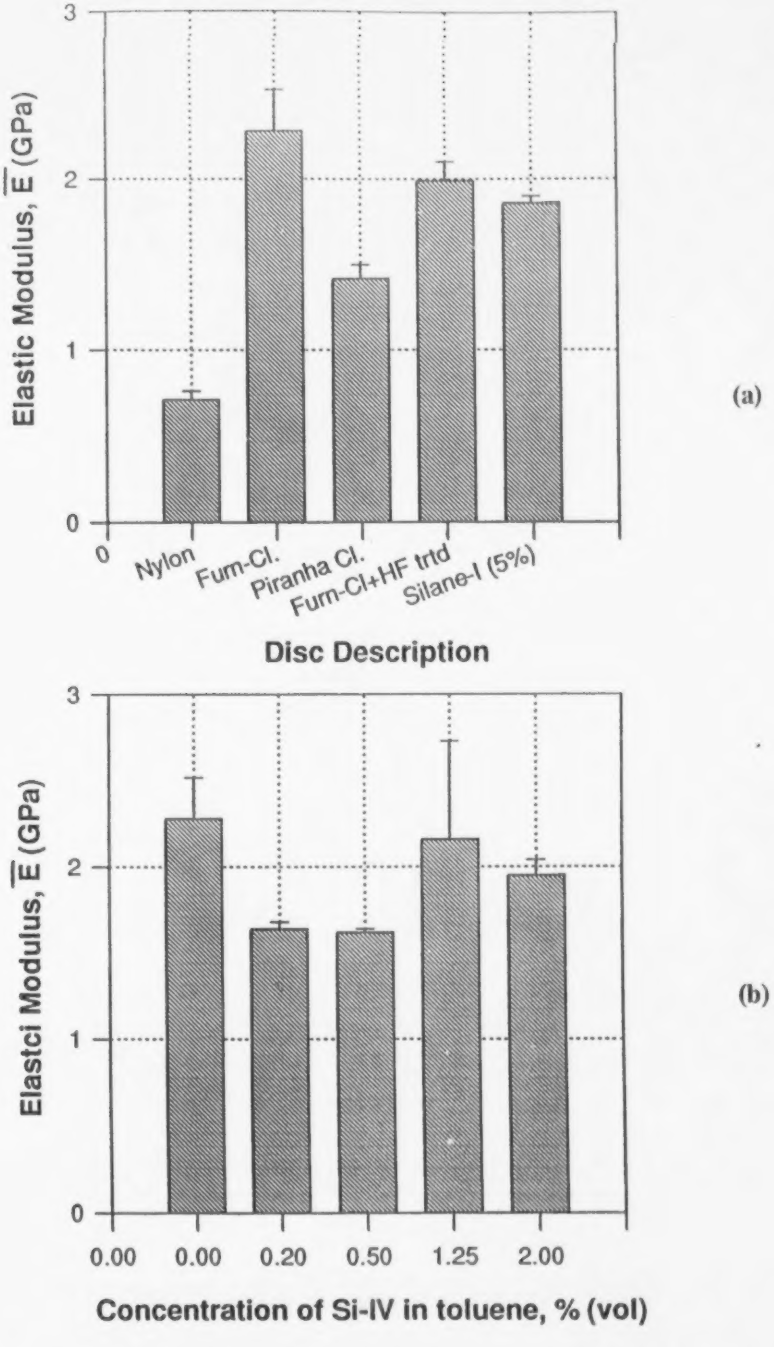

Figure 6.3. Elastic modulus of various disks at RH 66% (a) pure nylon, furnace-cleaned untreated, piranha solution cleaned untreated, furnace-cleaned HF treated, and furnace-cleaned Silane-I(5%) treated disks (b) Silane-IV disks. **Data obtained on Lloyds machine, NAIT.**

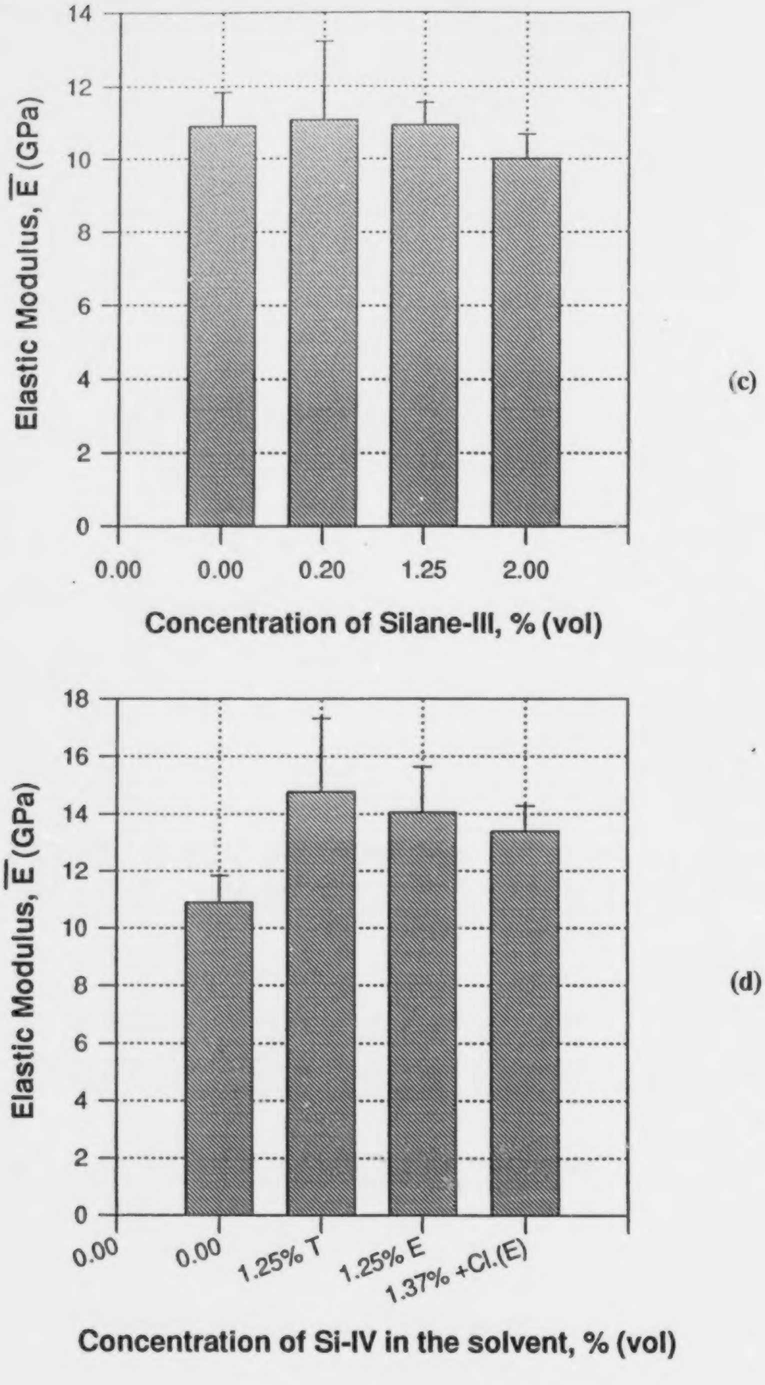

Figure 6.3 (continued). Elastic modulus of various composite disks at RH 66% (c) Silane-III treated (from toluene) disks. (d) Silane-IV disks. Data obtained from MTS tester, U of A.

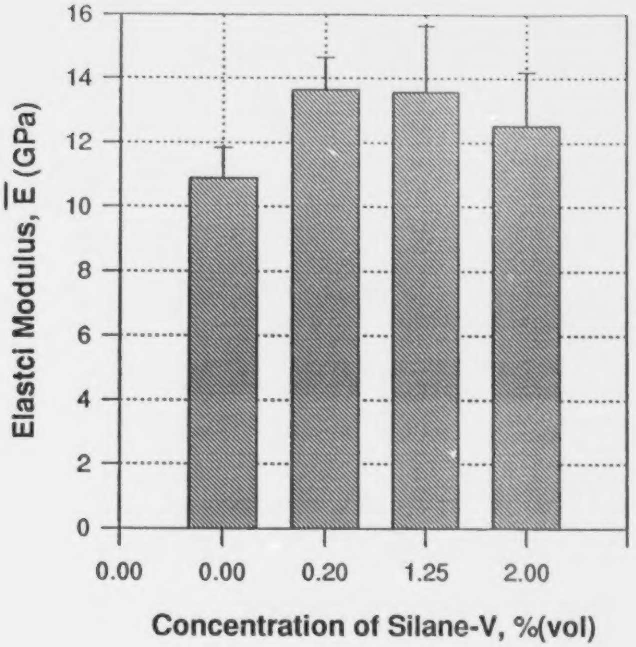

(e)

Figure 6.3 (continued) (e) Elastic modulus of Silane-V treated (from toluene) composite disks at RH 66%. **Data obtained from MTS tester, U of A**

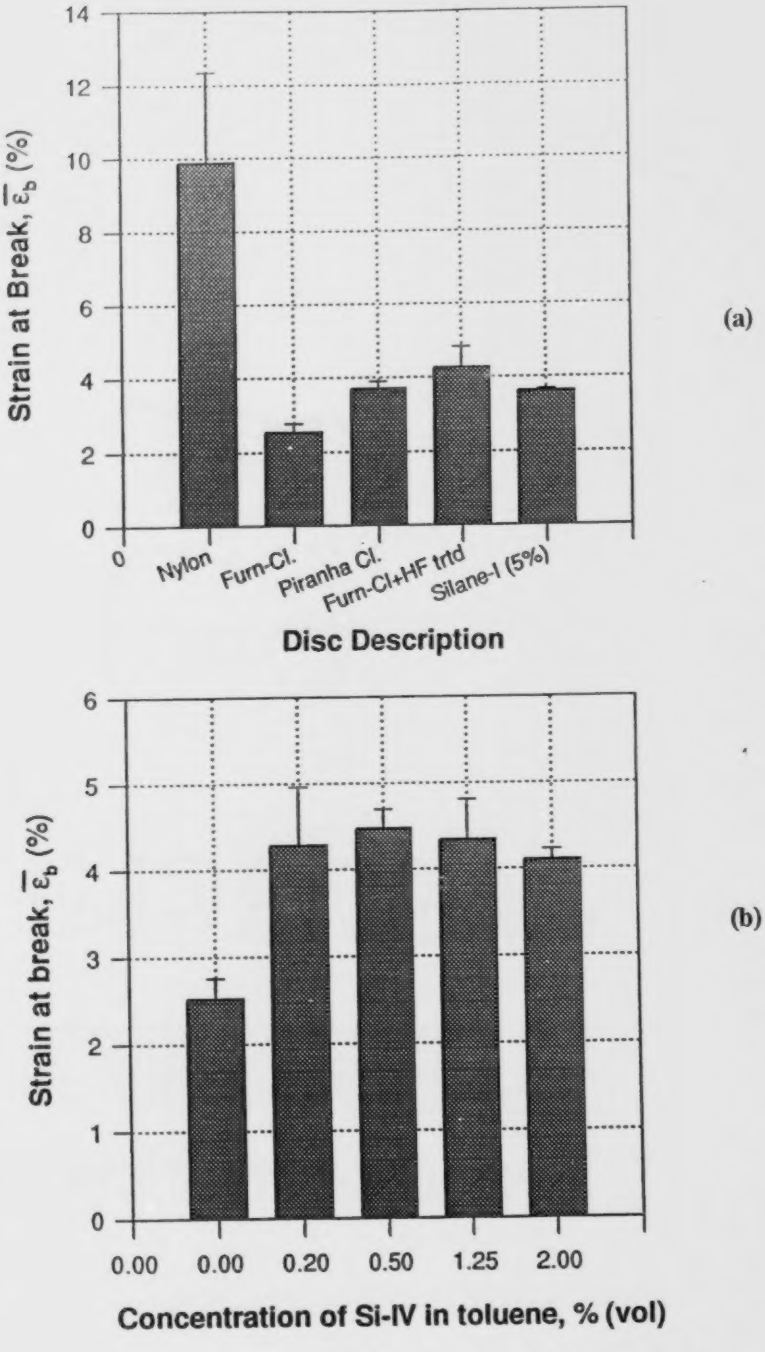

Figure 6.4. Strain at break of various disks at RH 66% (a) pure nylon, furnace-cleaned untreated, piranha solution cleaned untreated, furnace-cleaned HF treated, and furnace-cleaned Silane-I(5%) treated disks (b) Silane-IV (treated from toluene) disks. **Data obtained on Lloyds machine, NAIT.**

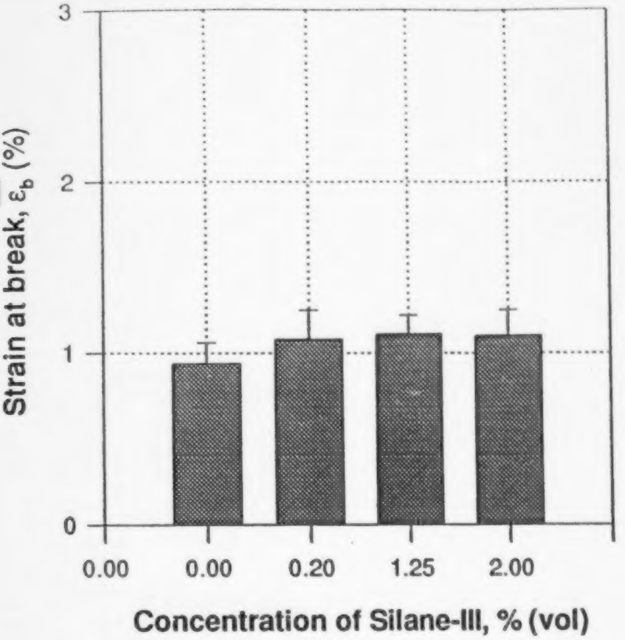

(c)

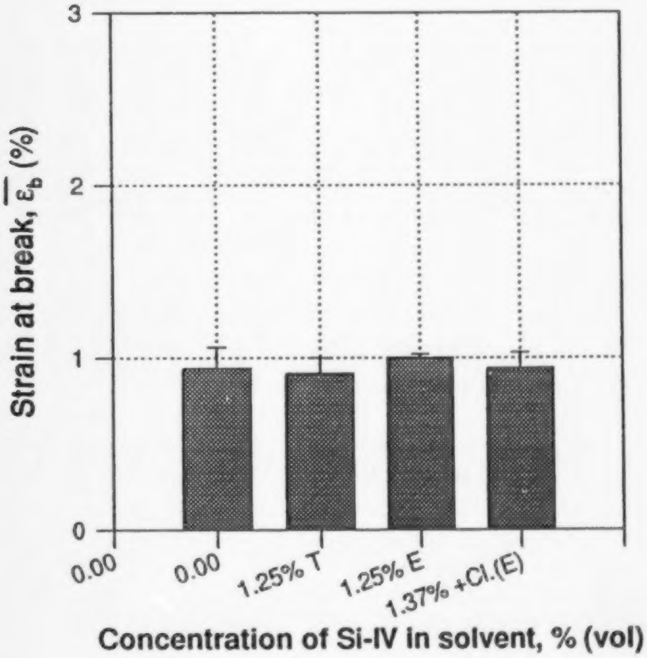

(d)

Figure 6.4 (continued). Strain at break of various composite disks at RH 66% (c) Silane-III (treated from toluene) disks. (d) Silane-IV disks. **Data obtained from MTS tester, U of A.**

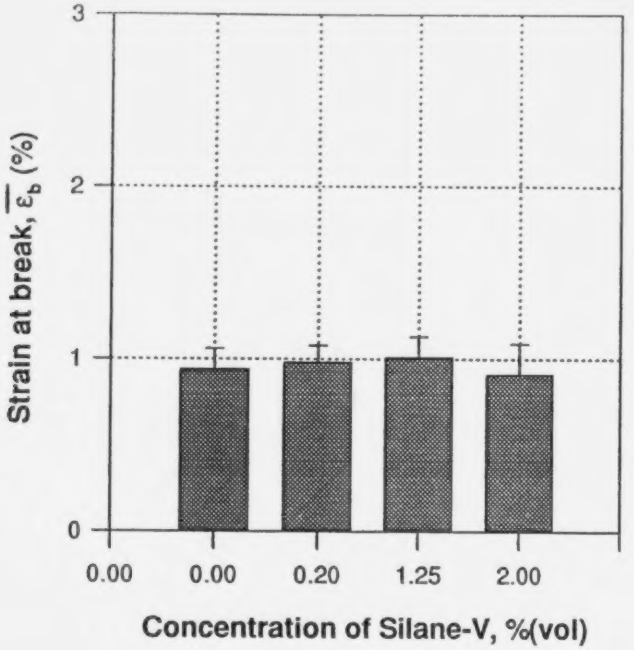

(e)

Figure 6.4 (continued) (e) Strain at break of Silane-V treated (from toluene) composite disks at RH 66%. Data obtained from MTS tester, U of A

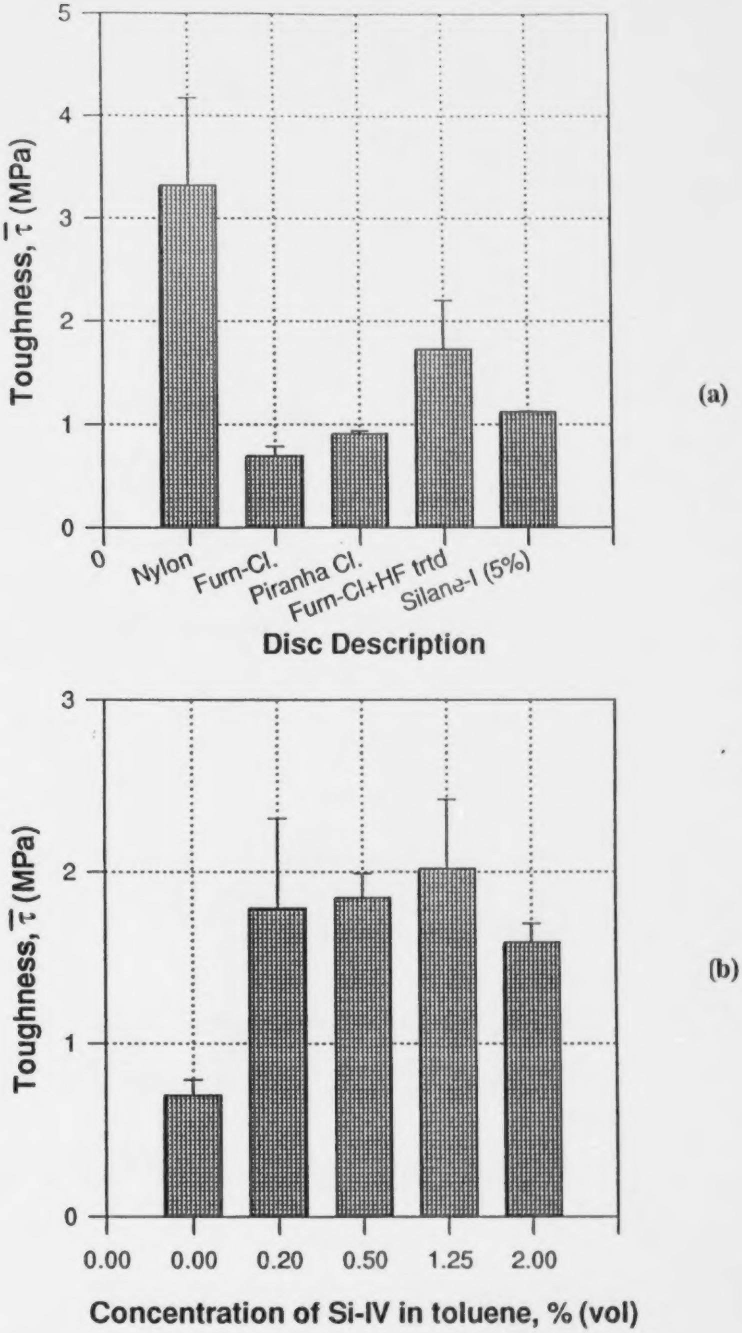

Figure 6.5. Toughness of various disks at RH 66% (a) pure nylon, furnace-cleaned untreated, piranha solution cleaned untreated, furnace-cleaned HF treated, and furnace-cleaned Silane-I(5%) treated disks (b) Silane-IV disks. **Data obtained on Lloyds machine, NAIT.**

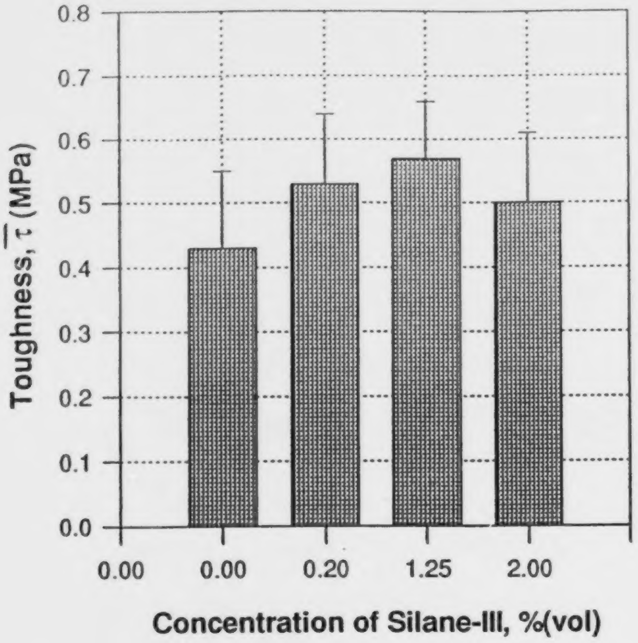

(c)

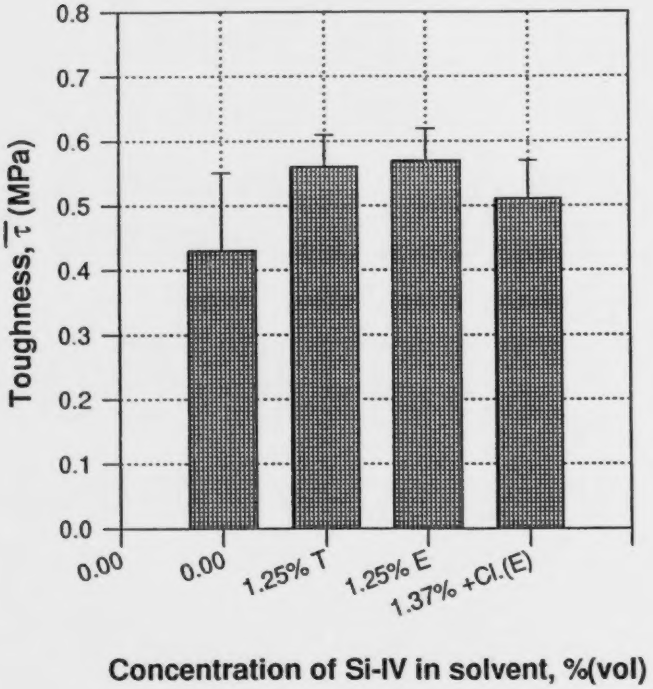

(d)

Figure 6.5. (continued). Toughness of various composite disks at RH 66% (c) Silane-III treated (from toluene) disks. (d) Silane-IV disks. **Data obtained from MTS tester, U of A.**

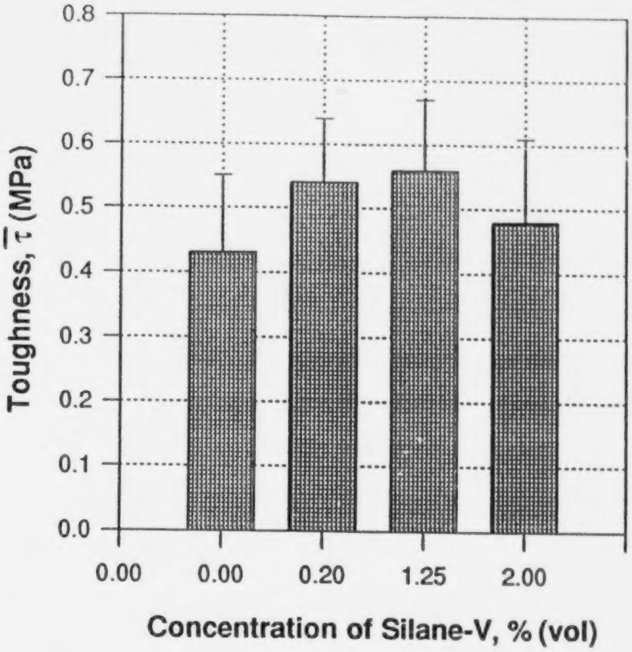

(e)

Figure 6.5 (continued) (e) Toughness of Silane-V treated (from toluene) composite disks at RH 66%. **Data obtained from MTS tester, U of A**

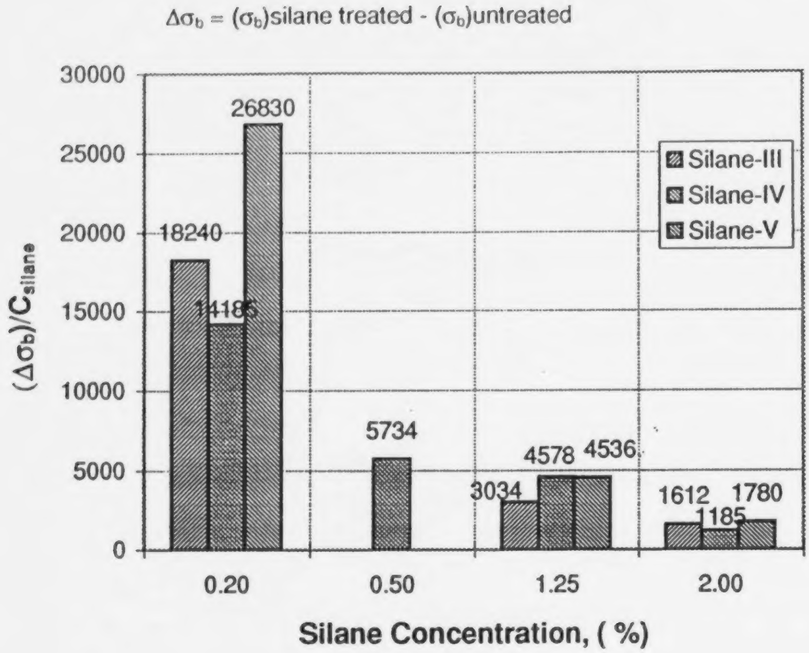

Figure 6.6. Effectiveness factor of the different concentrations for Silane-III, Silane IV and Silane-V. Effectiveness = $\Delta\sigma_b/C_{silane}$, where, $\Delta\sigma_b = (\sigma_b)_{silane} - (\sigma_b)_{untreated}$

Figure 6.2 (d) illustrates the tensile strengths of composites with varying concentrations of Silane-IV treated glass fibres. This graph shows that the Silane-IV concentration of 1.25% in toluene gives the maximum improvement in tensile strength of 104% over the untreated composite. Other concentrations of Silane-IV also gave a significant improvement in the tensile strengths of approximately 52% over the untreated glass fibre composite. We display in Figure 6.6 also the effectiveness factor for these varying concentrations of Silane-IV in improving the tensile strength of the composite. Silane-IV concentration of 0.2% again proves to be the most effective in improving the tensile strength of the composite. Figure 6.2 (e) shows varying concentrations of Silane-IV in two different solvents, namely, toluene and ethanol. These have been designated as T and E respectively in the figures. We can see that the tensile strength of the Silane-IV (1.25%T) composite was higher than the 1.25%E-treated glass fibre composite by about 10%. This suggests that toluene performed better in its role as a solvent in the silylation of the glass surface. *Wong (Broutman and Krock, 1974, p. 15)* also reported superior performance with aminoalkyl silane coupling agents applied to glass from organic solvents, instead of from water, and attributed this to the improper control of pH in the aqueous system.

The use of the crosslinking additive with Silane-IV did not cause any improvement in the tensile strength of the composite over composite made from Silane-IV alone. This we suspect is either because we did not use the right proportion of the additive with Silane-IV, or probably the additive was not compatible with the nylon matrix. Trends obtained with other properties, such as $\overline{E}$, $\overline{\varepsilon_b}$ and $\overline{\tau}$ for the various Silane-IV-treated fibre disks could not be evaluated directly by plotting them on a single graph, because these were tested on different machines. Comparisons would therefore be made by plotting the data within the same set as displayed in Tables C-3 and C-4. For example Figure 6.3(b) and 6.3(d) show the elastic moduli ($\overline{E}$) measured for disks tested on the Lloyds machine and the MTS tester respectively. The same applies for $\overline{\varepsilon_b}$ and $\overline{\tau}$, and these have been shown in Figures 6.4(b), (d), and 6.5(b), (d) respectively. The trends obtained with data from the Lloyds machine are unreliable because of the nature of the $\sigma(E)$ curves, so it is difficult to predict or draw any conclusions from these. Data obtained from the MTS tester reveal that the Silane-IV concentration of 1.25% in toluene again results in an increase in $\bar{E}$(~36%) and $\bar{\tau}$(~33%) over the untreated composite. The strain at break ($\overline{\varepsilon_b}$), however, remains constant for all the Silane-IV treated disks.

Figure 6.7 compares the role of different silane concentrations in improving the tensile strength of the composite over the untreated glass fibre composite. The effectiveness of the concentrations of each silane was displayed in Figure 6.6. We notice that the trend obtained with Silane-III seems to suggest that the maximum in properties is obtained somewhere around 2% concentration (maybe going a little higher than 2% might give higher values of tensile strength), while the trend with Silane-IV suggests a prominent maximum at concentrations very close to 1.25%. The tensile strength drops at higher concentration (2%). Silane-V trendline also shows a plateau flattening in the concentration range 0.2-1.25%. This plateau also possesses the maximum tensile strength compared to other concentrations. If we compare the effectiveness of each silane, we find that the 0.2% concentration of all silanes proves to be most effective in terms of causing an improvement in the mechanical properties of the composite. This inference might prove to be beneficial in commercial applications where both an increase in tensile strength and reduction in cost could be achieved by incorporating very small amounts (0.2%) of the expensive silanes.

Finally, to determine which silane gave the maximum improvement in properties, we evaluate which concentration of the silane gave the maximum improvement in properties. For example, 1.25% concentration of Silane-IV gave the best properties among all the other concentrations of Silane-IV that were used. Similarly, we evaluate for other silanes, and then compare the properties obtained with each silane type. This plot is shown in Figure 6.8, where all the properties (E, ε_b, σb and τ) have been plotted for the various silanes. We find that, the Silane-IV(1.25%) and Silane-V(1.25%) gave almost the same

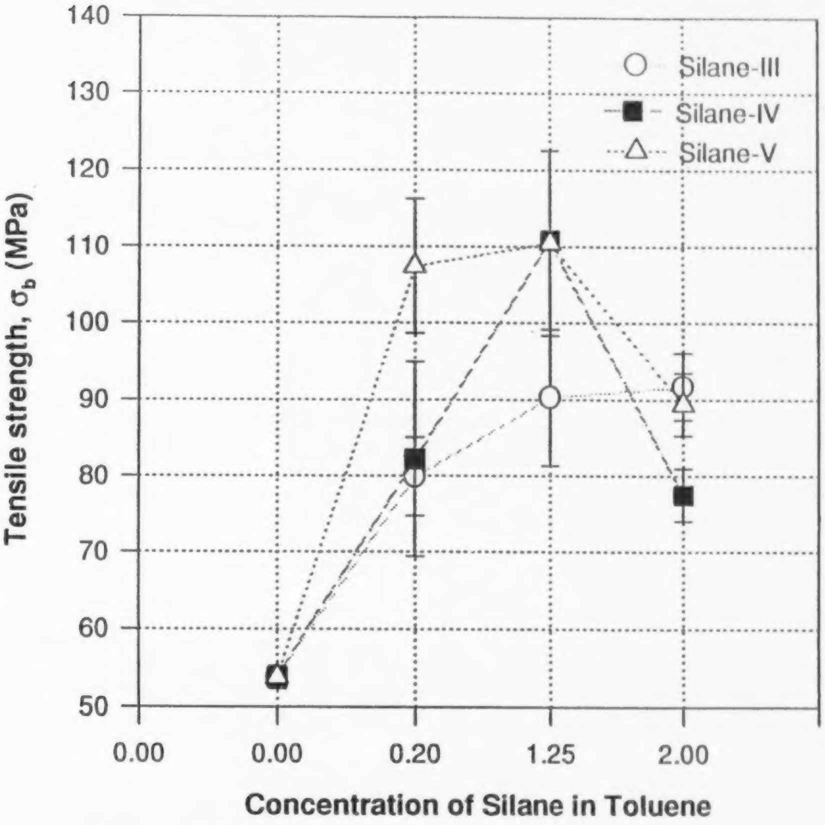

Figure 6.7. Tensile strengths for 3 different concentrations of Silane-III, Silane-IV and Silane-V treated from toluene at RH 66%.

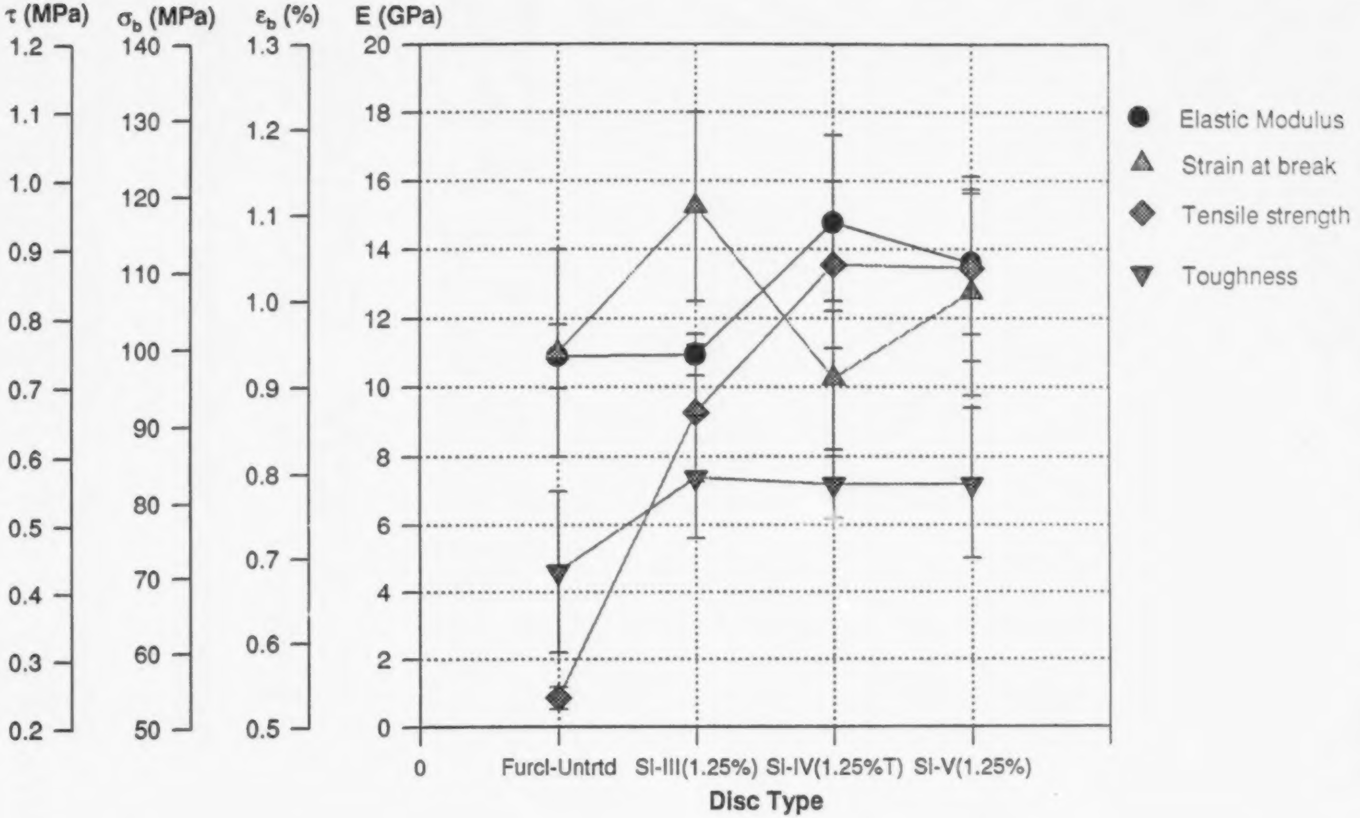

Figure 6.8. Comparison of the mechanical properties of silane treated disks possessing maximum properties in their respective groups.

improvements in tensile strengths of ~103% over the untreated composite. Silane-III(1.25%) gave the maximum strain at break (ε_b) and Silane-IV(1.25%) again gave the maximum increase in elastic modulus of 36% over the untreated composite. Intergroup comparison shows that the use of Silane-IV and Silane-V gave significant improvements in the elastic modulus of the composite (~ 32%) over that of untreated or Silane-III treated composites.

6.1.4. Role of nylon and surface treatment in glass fibre reinforcement

The decrease in the tensile strength by incorporation of glass fibres in the nylon matrix (as in the case of untreated glass fibre composite), is not always seen in composites that lack special coupling agents between fibre and matrix, but the case of nylon and glass fibre causes special problems. The nylon absorbs moisture from the air and transmits it to the hydrophilic glass interface, where it serves to disrupt whatever weak adhesive forces would have existed between nylon and glass in a dry environment.

For the sake of simplicity, let us determine the tensile strength behavior of a nylon/glass fibre composite in which the glass fibres are aligned in the direction of the applied load. We consider the properties of nylon 6 disk with rectangular configuration, as representative of the matrix nylon in the composite (properties from Table 6.2 for rectangular configuration) and the schematic stress-strain curve for this is shown in Figure 6.9. The second curve in Figure 6.9 represents the tensile behavior of glass. We can see that the strain at break of nylon (ε_b = 4.95%) is slightly higher than that of glass with ε_b = 4.5%.

On straining this composite material in a tensile test, a strain ε_{dl} (strain at delamination) is reached, when the stress σ_{dl} is sufficient to pull the fibres out of the matrix. Below this stress, it is merely mechanical bonding that keeps the fibres from getting pulled out. When pull-out occurs, the stress in the fibres is transferred to the matrix. It is possible that this stress is not enough to cause fracture in the matrix. However, the matrix thereafter behaves as if it were not reinforced with glass fibres. In fact, the composite material is now

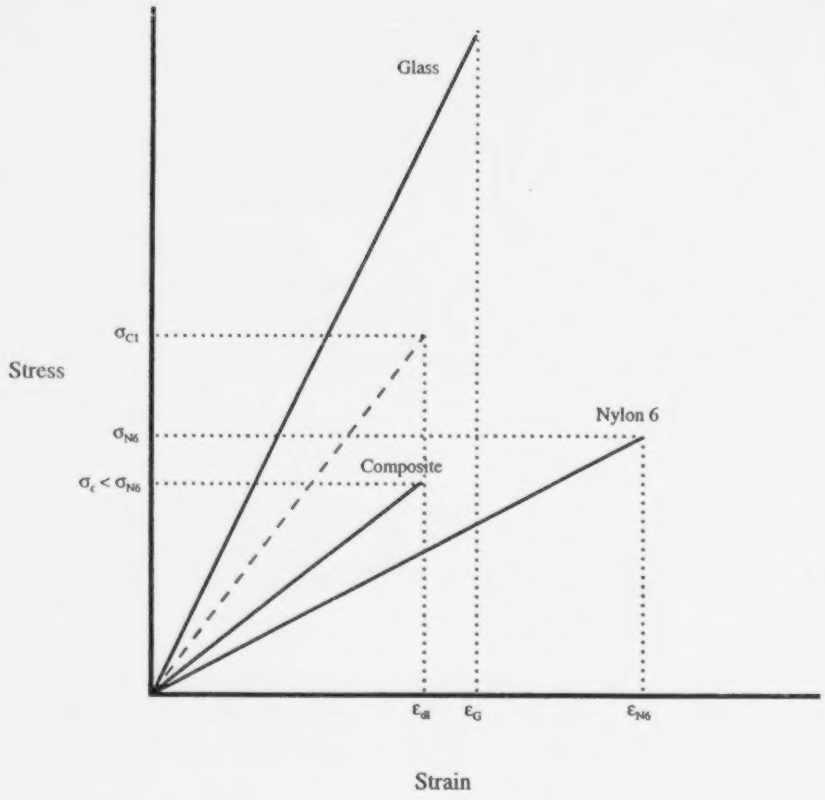

Figure 6.9. Schematic representation of the tensile behavior of a composite with a nylon 6 matrix

equivalent to having a matrix polymer with voids, the void fraction being equal to the volume fraction of the glass fibres. In Figure 6.9, it should be noted that all the stresses are defined as the tensile force developed in the material per unit cross-sectional area. However, the delamination represents a shearing condition, where the force is distributed over the matrix/fibre contact area. This is a much larger area, than the cross-sectional one, and is equal to the surface area of the glass fibres. Thus the delamination stress σ_{dl}, which has been based on the cross-sectional area is given by,

$$\sigma_{dl} = \sigma_{dl(shear)}\,(\text{surface area of glass fibres/cross-sectional area}) \qquad \text{....[6.1]}$$

where $\sigma_{dl(shear)}$ is the actual shear stress, required for delamination, based on the fibre/matrix interfacial area, i.e. the surface area of glass fibres. Thus, it is conceivable that these composites underwent delamination at the interface on application of load and displayed a tensile strength lower than that of the pure matrix polymer. This kind of fracture is also illustrated from SEM micrographs [Figure 6.10 (a)], where the fracture surface reveals the intact nature of the fibres and the total absence of "contaminating" matrix material on the fibre surfaces.

Consequently, one can notice that, since, $\sigma_{dl(shear)}$ is a property of the fibre-polymer interfacial bonding, σ_{dl} is a linear function of $\sigma_{dl(shear)}$, for a given volume fraction of the glass fibres. So, by increasing the $\sigma_{dl(shear)}$, i.e. improving the interfacial bonding for the nylon/glass system by way of surface treatment, we can increase the tensile strength of the material. The improved tensile strength curve is shown by dashed line in the Figure 6.9. This is the most simple approach to understanding the role of silane coupling agents in improving the tensile strengths of these composite materials. However, it is important to remember that all the above expressions and logic were applicable to the limiting case of unidirectional glass fibre composites. For a composite comprising of random, in-plane, continuous glass fibres, the mechanical properties are dictated by other factors as well, such as, the fibre orientation, fibre length distribution, etc.

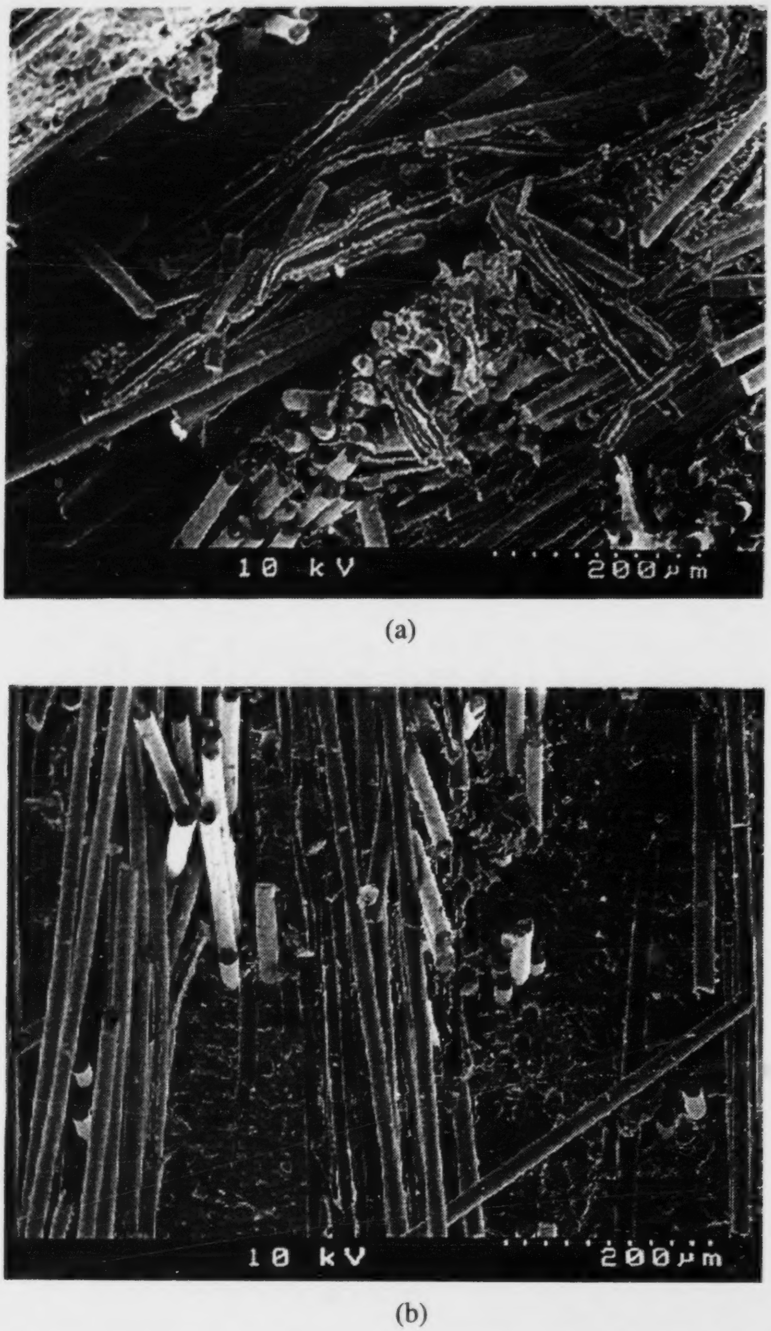
10 kV
200µm
10 kV
200µm

(a)

(b)

Figure 6.10. SEM of fracture surface of nylon 6 composite containing glass fibres that are (a) Furnace-cleaned and untreated, (b) Piranha-cleaned and untreated

Also, the observed tensile strength behavior of the various composites arise from the differences in their fracture mechanisms, which, in turn, can be predicted from the trends in tensile strength (Figure 6.2), and from the scanning electron micrographs of their fracture surfaces. As mentioned above, the SEM micrographs of the fracture surface of nylon 6/glass fibre composite revealed fibre pull-out (lack of adhesion) between the polymer and glass, whereas those of the surfaces of composites containing Silane-IV and Silane-V treated glass fibres, always showed the matrix adhering well to glass fibre even after failure of the materials. These micrographs are shown in Figures 6.10-6.13. Although the Silane-III treated glass fibre composites showed improvement in tensile strength, the SEM micrographs do not reveal significant matrix adhesion to glass fibres. Similarly the HF treated glass fibres also did not reveal any matrix adhering to them. The increase in tensile strength in this case, however, could be attributed to the mechanism of interlocking that can occur between the etched glass fibres and the matrix.

6.1.5 Role of silane coupling agents

The silane treated glass fibres were not characterized for the amounts of silane present on them. Hence, the explanation of the mechanical property trends presented here, although consistent, may not be accurate.

We found that composites comprised of glass fibres treated with Silane-IV and Silane-V seemed to show trends relating the concentration of the silane to the composite mechanical properties. Composites with Silane-IV, showed a maximum in mechanical properties at or very close to a concentration of 1.25% (vol%) in toluene. Composites with higher or lower concentrations than these showed inferior properties. What was more surprising was that composites with only 0.2% concentration of the silane, resulted in remarkable improvement in properties , although the properties were not as high as the ones obtained for 1.25% silane concentration. Similar results and trends were obtained with Silane-V, where higher mechanical properties were obtained as the concentration was reduced from 2% to 1.25%. *(Continued on p. 130)*

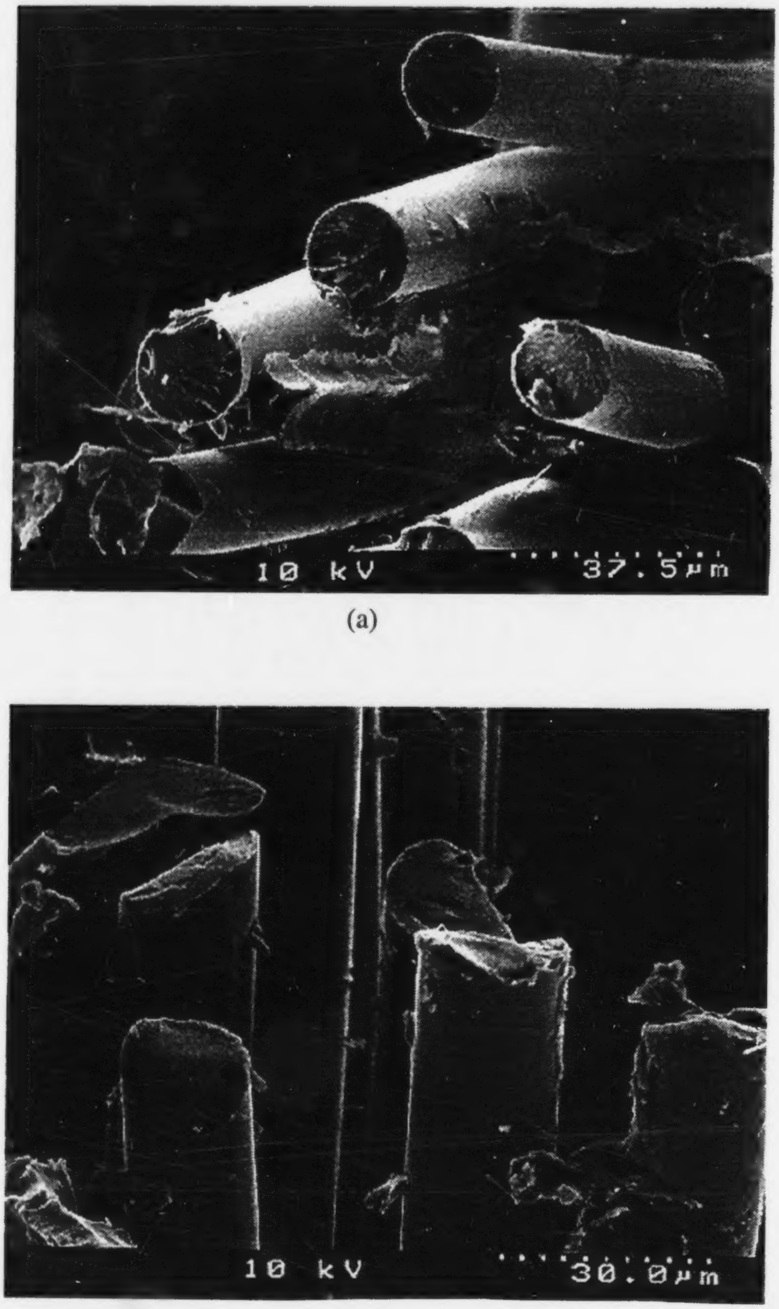
10 kV
37.5μm
(a)
10 kV
30.0μm

Figure 6.11. SEM of fracture surface of nylon 6 composite containing glass fibres that are (a) Furnace-cleaned and HF-treated (one min.) (b). Furnace-cleaned and Silane-III (2%)-treated.

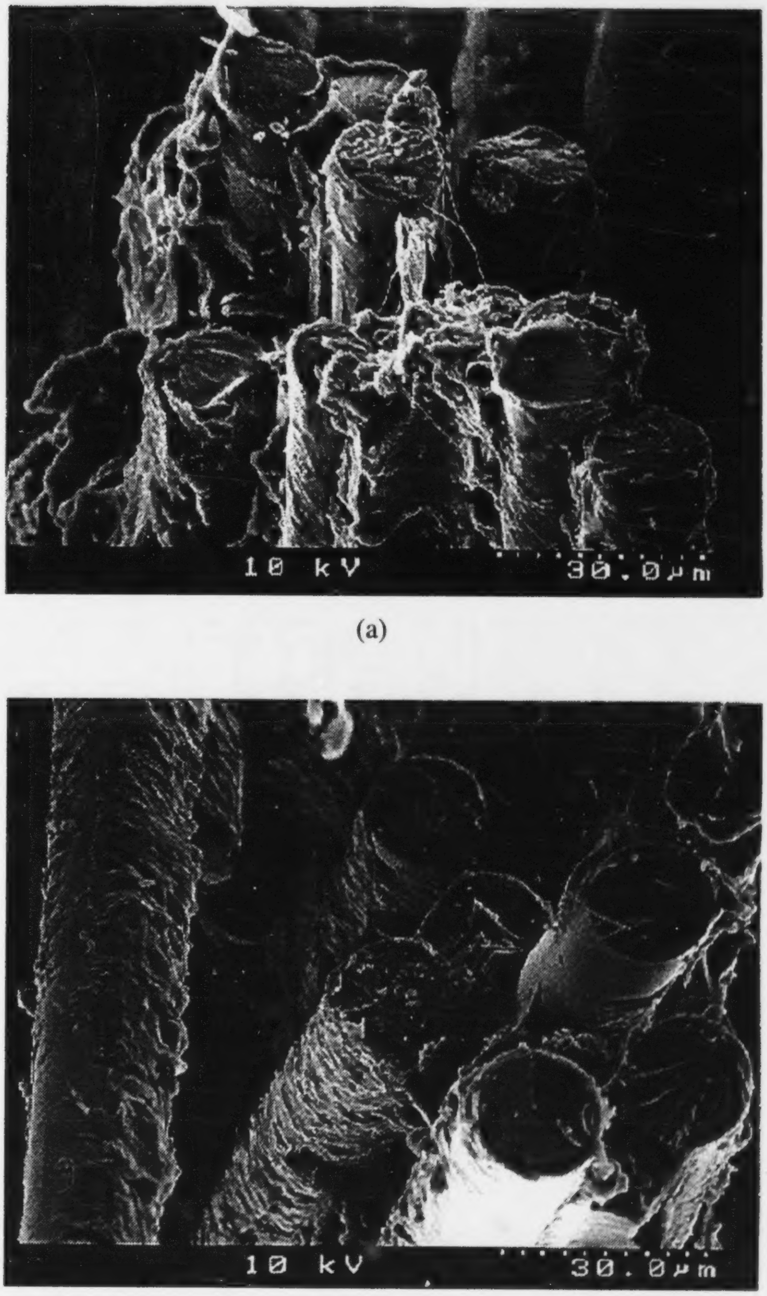

(a)

(b)

Figure 6.12. SEM of fracture surface of nylon 6 composite containing glass fibres that are (a) Furnace-cleaned and Silane-IV (1.25% toluene)-treated (b) Furnace-cleaned and Silane-IV(1.25% ethanol)-treated.

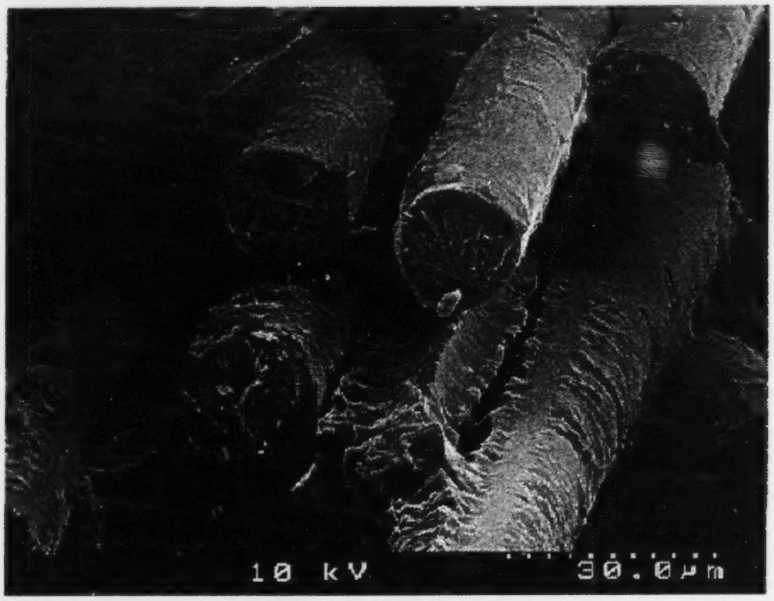

(a)

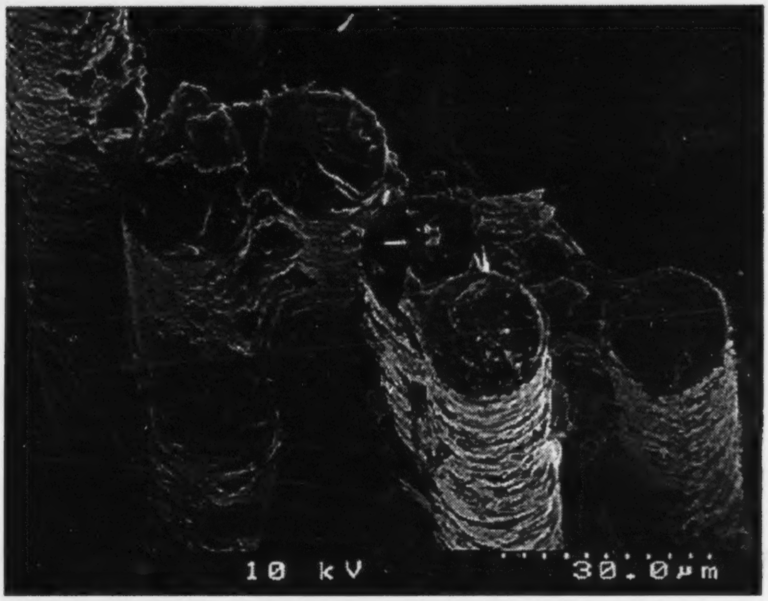

(b)

Figure 6.13. SEM of fracture surface of nylon 6 composite containing glass fibres that are (a) Furnace-cleaned and Silane-IV (1.25%+CL ethanol)-treated (b) Furnace-cleaned and Silane-V (0.2%)-treated.

This marked improvement in properties imparted to the glass-nylon 6 composites by traces of appropriate reactive silanes at the interface suggests that an understanding of the nature of adhesion through silane coupling agents might be the key to understanding the general mechanism of adhesion. The microstructure, morphology and mechanical properties of the interphase region adjacent to the silane-modified surface of the substrate and to the matrix are important considerations. While the subject of silane chemistry and its interaction with both the glass surface and the polymer matrix have been extensively studied, little fundamental information relating sizing application to composite mechanical properties has been published *(Drown et al., 1991)*.

The nature of adsorbed coupling agent films deposited on glass has been studied by numerous investigators and discussed critically by *Zisman, 1969*, as reported by *Broutman and Krock, 1974*. It is deduced that silane coupling agents are not generally deposited on glass as simple oriented monomolecular films, but as multi-layers with variable orientation depending upon conditions of deposition.

The phenomenon of a concentration which gives optimum properties has been observed by (*Sung et al., 1982; Graf et al., 1972; Wong, 1972)* as reported by *Ishida, 1983*. Concentrations higher than this optimum concentration resulted in inferior strengths. This concentration dependence could be understood by considering the deposited silane film to possess a structural gradient. This gradient is made up of various layers such as, the physically adsorbed (or the physisorbed) layer, and the chemically adsorbed (or the chemisorbed) layer. The physically adsorbed layers exist in the outermost layers of the silane interphase. These can be removed by washing with appropriate solvent. The chemisorbed layers consist of two layers- (I) a monolayer, in which the silanol groups of the silane molecules usually condense with the surface hydroxyl groups and the silane molecules become part of the substrate, and (ii) the second and above layers that are loosely chemically bound. In this region, the remaining silanol groups may condense with adjacent silanols to form a siloxane layer or remain partly uncondensed at the surface. The chemisorbed portion of silane may be mainly responsible for the reinforcement mechanisms. The role of the physisorbed silanes on the mechanical properties is not known. Nevertheless, it is known that these layers play a significant role in determining the mechanical properties of the composite.

Aminosilanes are known to self-catalyze condensation reactions with the mineral hydroxyl groups or with silanol groups in the solution *(Kaas and Kardos, 1976)*. Thus high concentrations of this silane in solution would result in the formation of oligomeric polysiloxanols. In fact, it has been reported by *Culler et al., 1983*, that the aminosilane molecules exist as oligomers in solutions of aminosilane at concentrations exceeding 1% (wt.) and that at concentrations less than 1% (wt.), the aminosilane molecules exist as silanetriols. On the other hand, *Ishida, 1984*, reported that aqueous solutions of aminosilanes at concentrations exceeding 0.2%, contain primarily oligomeric polysiloxanols formed in self-catalyzed condensation reactions. Consequently, it can be concluded that the self-catalyzation of the amine group of γ-APS leads to oligomer formation in the silane solution prior to adsorption. The silanols may be needed to produce the chemisorbed monolayer, whereas, the oligomers do not produce a high yield of chemisorbed silane resulting in the very high content of the physisorbed silane as observed by *Culler et al., 1983*. This implied that, high concentrations of aminosilanes result in high concentrations of physisorbed silanes, and concentrations lower than 1% might result in higher chemisorbed layers.

The physisorbed silanes , if not completely removed, may result in inferior properties of the composite. *Graf et al.* obtained lower flexural strengths for the E-glass γ-Methacryloxypropylsilane (MPS) composite with higher content of physisorbed silane *(Ishida, 1983)*. *Duangchan, 1994*, also observed similar trends, where she found that higher concentration of silanes resulted in inferior properties of the composite. Thus, there is a possibility that the physisorbed silanes act as lubricants and help in fibre pull-out. Thus, better properties of composites may be expected at lower concentrations of silanes.

Then the question arises as to why the properties of the composite are inferior at very low concentrations. One answer to this could be that, the low concentration might result in the formation of an incomplete chemisorbed monolayer on the fibre surface. Hence, in absence of a complete monolayer which determines to a great extent the mechanical properties of the composite, the resulting properties of the composite are inferior *(Broutman and Krock, 1974, p.8)*.

Summarizing the entire discussion, we understand that an optimum concentration of the aminosilane is required to achieve optimum properties of the composite. This optimum concentration may vary depending on the conditions of deposition of the silane onto glass (such as temperature, type of solvent, pH of solution, etc.). Characterizations of the treated glass fibres using various spectroscopic techniques should therefore help to develop a better understanding of the mechanism of adhesion induced by the presence of silanes on the glass surface.

6.1.7. Failure mechanism of glass fibre/nylon 6 composites

A typical stress-strain curve of a nylon/glass fibre composite material made in our laboratory is shown in Figure 6.14. This curve is representative of all the curves obtained for the various composite disks in this work. We notice that a three stage mechanism can be can be identified in this curve. (i)The material behaves in a linear elastic manner to a strain in the range 0.15-0.3%, the deviation from this behavior being due to onset of cracking or debonding of the transversely oriented fibre bundles (ii) onset of matrix cracking at a strain of 0.6% corresponding to the most pronounced change in slope in the stress-strain curve, and (iii) further debonding, shear cracking, and resin fracture until complete failure of the composite at a strain of ~ 1%. *Hull and coworkers, 1981*, had also reported a similar three stage failure mechanism for dry polyester resin reinforced with chopped strand glass fibre mat (volume fraction of fibres was 17%).

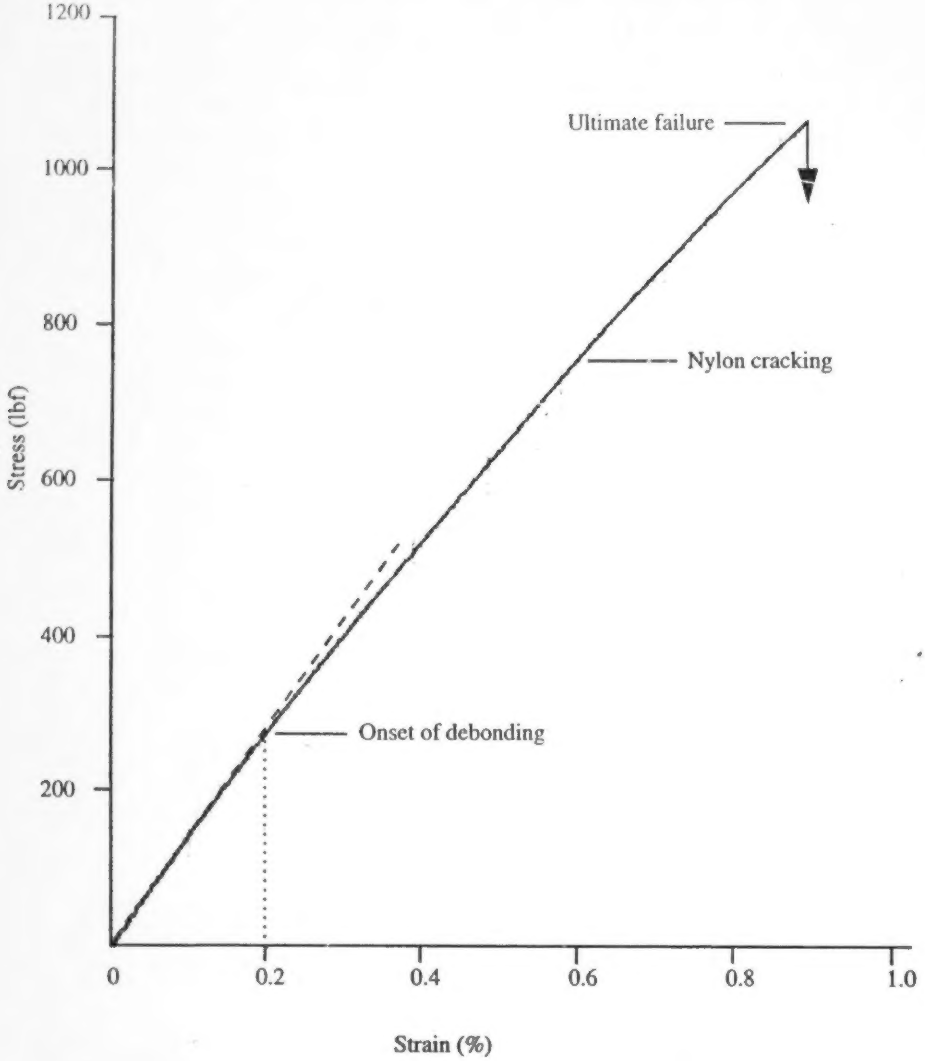

Figure 6.14. Typical stress-strain curve for a nylon 6/glassfibre composite.

6.2. Impact properties

All composite disks and two nylon disks were evaluated for their impact properties on two different days, at NAIT, where the laboratory temperature was 22-23°C. The samples were pre-conditioned at RH of 66%, in the same manner as the tensile specimens. However, the relative humidity inside the desiccator in which the samples were stored was found to drop from 66% to about 63% during testing. Since this drop is not very large, we have assumed that humidity did not affect the impact properties, and that variations in the impact properties could be attributed to other factors such as the different fibre surface treatments, the glass fibre content, and the void content of these composites.

Although all composite disks (23) were tested for impact properties, quantitative values were obtained for only 10 disks including 2 pure nylon disks. This was because of the malfunctioning of the impact tester at NAIT. One point to be noted is that the impact tester showed problems throughout the testing, and hence in spite of testing six specimens from each disk, an average of only 3 readings were obtained for each of the 10 disks. Nevertheless, the values obtained did provide information that was consistent with the trends observed in tensile properties. For other disks for which quantitative values were not obtained, readings representing the type of failure (partial or complete) of the impact specimen was recorded. This would thus give us an idea of the nature of the adhesion between the glass fibres and nylon in the composite, as explained in the later sections.

From each disk, specimens were cut from the same positions (Figure 5.1). Over a period of several weeks, all disks were processed in this way and the specimens preserved in a desiccator at about 66% RH until tested together with a Tinius Olsen Izod Testing Machine (25-lb.). The average E_S value of all 6 specimens represented the impact strength of a composite disk. These average values, for 10 disk preparations, are shown in Table 6.2, their graphical presentation is displayed in Figure 6.15, along with the glass fibre content of each disk. The procedures and sample calculations of impact properties are shown in Appendix B and the raw data for all impact specimens is presented in Table C-6 (a), Appendix C.

Table 6.2. Average breaking energies from Izod type impact tests
(RH : 63-66%; Temperature: 22-23°C)

Type of Disk	Breaking energy (average), Es, per notch width (J/m)
Pure nylon 6 (rectangular)	38.09 ± 3.26
[1]Untreated	187.58 ± 12.12
[2]Untreated	198.36 ± 18.93
Piranha cleaned	215.59 ± 19.71
HF treated	142.66 ± 20.56
Silane-I (5%)	282.06 ± 21.21
Silane-IV (0.2%)	184.90 ± 17.34
Silane-IV (0.5%)	174.72 ± 14.54
[1]Silane-IV (1.25%)	116.47 ± 16.89
Silane-IV (2%)	148.68 ± 15.53

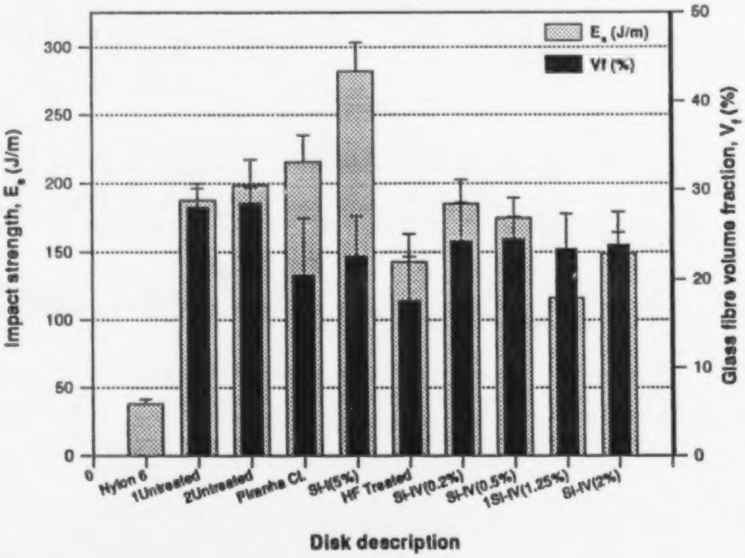

Figure 6.15. Impact strength E_s, (J/m) of pure nylon and its composites with untreated and treated glass fibres at RH 63-66%.

6.2.1. Improvement of E_s by glass-fibre reinforcement

From Table 6.2, we can see that the impact strength for pure nylon 6 (rectangular configuration) is much lower than the literature values, which lie in the range, 58-294 J/m (see Table 2.3). This low value suggests that the nylon we obtained, in our laboratory is relatively brittle, thus agreeing with the tensile results, where we obtained comparitively low ε_b values for nylon 6 specimens. A zero E_s value was obtained for the nylon disk with circular configuration. However, it is hard to say if this value was obtained because of malfunctioning of the machine (since the machine was found to do this often with other specimens also), or because the circular disk specimens were more brittle than the rectangular specimens (as confirmed from the tensile results) or simply had impact strengths too low to be detected on the impact scale of the machine.

Table 6.2 also shows that E_S was enormously enhanced by the presence of untreated glass-fibre. Comparison of pure nylon 6-E_S value with those of the two untreated composites, gives improvement factors $E_S^U/E_S^N \approx 5$ for the two untreated composites ($\overline{V}_f \approx 28$ %, $\overline{V}_v \approx 1.4$%). This enormous improvement could be because of fibre pull-out effects and debonding, which tend to dissipate high amounts of energy. It should also be understood that these improvement factors are considerably higher than is usually associated with glass reinforcement of the short fibre commercial type. For example, Modern Plastics Encyclopedia reports an improvement ratio of only about 2 in E_S when chopped glass fibres are present in nylon 6 at the 30-35% level. Use of the long fibres associated with the mats ("continuous fibres") may be the key to such large improvement found in the present work.

One must remember that, "improvement" in impact strength does not always imply an improvement in other mechanical properties *(Hull, 1981)*. In fact, the reverse is often true; good impact strength is commonly associated with poor tensile performance, and good impact behavior is often a sign of easy fibre/matrix delamination. For example, if there exists a good adhesion between the fibres and the matrix, then the impact load is transferred from the matrix to the glass fibres directly, and since glass is brittle, it will fail or break with the impact, and thus the crack formed in the specimen will propagate without dissipating energy in the form of friction, thereby giving the appearance of a smaller amount of energy being required to cause fracture of the specimen. On the other hand, in the absence of adhesion between the glass fibres and the matrix, delamination will occur. Such delamination in an impact test allows the fibre to "pull out" of its matrix sheath without breaking and dissipate energy in sliding friction energy, that would otherwise be used to form matrix cracks. One can therefore appreciate the opposite trend which is observed in tensile testing, that is, easy delamination (in absence of good adhesion) leads to easy tensile (low σ_b) failure at low strain (ε_b). These trends in impact testing, however, represent ideal conditions. In reality, there are many other factors that affect the impact strength of the specimen, such as the rate of loading, notch-sensitivity (the notch width and notch radius of curvature), thickness of the sample, etc. (*Shah, 1984, p. 52*). These factors could lead to a large scatter of data obtained with these kinds of failure tests.

6.2.2. Effect of different surface treatments on E_S

In focusing on chemical influences, we should examine E_S values for composites; again, not forgetting the influence of glass fibre content in these. It is difficult to predict how the impact strength would vary with the glass content, because the impact strength also depends on the nature of adhesion between the two phases. For example, in absence of adhesion, if the glass fibre content would increase, the impact strength value would also increase due to higher amount of energy needed to pull the fibres out of the matrix. On the contrary, we see that in presence of good adhesion, if the glass fibre content is increased the impact strength would drop, due to the sample being dominated by the impact strength of the brittle glass fibres. Hence, comparisons merely on fibre content or on surface treatment is not possible here. So, let us first compare the impact strengths of different composites, based on identical glass fibre content. From Figure 6.15, we isolate the cases of two disks with extremely low fibre content, the HF treated disk ($\overline{V}_f$ = 17.7%) and the chemically cleaned (piranha) disk ($\overline{V}_f$ =20.4%) from all the other disks, which have their

$\overline{V}_f$ in the range 23.7-28.5%. It is clear that silanes used in this study (Silane-I and Silane-IV), yielded composites with impact properties superior to those N6 without reinforcement.

We can see from Figure 6.15 that the best impact performance emerges from Silane-I treated glass fibre composite (with E_s = 282.1 J/m). Further, this composite was found to undergo partial failure, the fracture surface of which showed many fibres sticking out, indicating fibre pull-out in this composite. Also appearing in Figure 6.15 is the poor impact performance of all composites treated with Silane-IV compared to the untreated fibre composites. However, in all these (Silane-IV treated) composites, the $\overline{V}_f$ ($\approx$ 25%) was slightly lower than in the untreated ones (with $\overline{V}_f \approx 28\%$), so true comparison is not possible. For an approximate prediction of how the Silane-IV composites would behave if these had 28% fibres, we would use a multiplying factor based on the ratio 28%/25%. The $\overline{V}_f$-correction gives E_s = 184.9 × (28%/25%) = 207.1 J/m for Silane-IV (0.2%). Similarly, the corrected values of E_s for other Silane-IV treated disks turn out to be 195.68 J/m for Silane-IV(0.5%), 130.45 J/m for Silane-IV(1.25%), and 166.52 J/m for Silane-IV(2%) composite disks. Thus, we find that, two of the four Silane-IV treated disks emerge with equal or better impact performance than the untreated disks, whereas the other two Silane-IV treated disks still show poorer properties. Since Silane-IV (1.25% and 2%) gave good improvement in tensile properties, this indicated that there was good adhesion between the fibres and matrix in these composites (as was also evident from the SEM micrographs). Because of good adhesion, the impact strengths should drop as was explained above. Now, one could argue that, even the disks with Silane-IV (0.2% and 0.5%) showed improvement in tensile properties over the untreated composites, and so why did we get higher impact values for these disks ? The answer to this could be that the impact strengths of these disks, although higher than the impact strength of the untreated disk, were not significantly higher than the untreated disks, and these emerged to be equal or better only when the correction in $\overline{V}_f$ was made. Prior to making these corrections, all disks showed poorer impact performance than the untreated disks. Further, these specimens showed complete failure, unlike the untreated fibre composites The lower impact performance thus serves to highlight the significance of achieving good adhesion between the fibre and the nylon matrix through Silane-IV coupling agent.

Moving to the HF treated glass composite, we find that this disk also shows poorer impact properties (E_s = 142.66 J/m) than the untreated disks. However, the $\overline{V_f}$ for this disk (17.67%) was significantly lower than the untreated fibre disk (with $\overline{V_f}$ = 28%). So, if we apply the $\overline{V_f}$ correction factor again, the E_s value turns out to be 226 J/m, which is significantly higher than the impact properties of the untreated disks. The failures observed for these specimens were not the same; two specimens showed complete failure and the other two specimens showed partial failure. This non-uniformity in composite failure might have resulted because of the non-uniformity in the fibre content in the disk (as pointed out in chapter 5). Regions with higher fibre content (positions 3 and 4 in Figure 5.1), gave rise to higher impact values for the specimens I3 and I4, and regions with lower fibre content (positions 1 and 5 in Figure 5.1) gave lower impact values for specimens I1 and I6 respectively. This trend does not necessarily mean that the impact values increased because the fibre content increased. This might partly be the reason for it, but a rather different justification to this behavior could be as follows: the higher fibre content in these positions indicated that the etching of the glass fibres in this region was not very high, indicating that the fibre surface must have been smooth and thus this part of the disk might have behaved like the untreated glass fibre composite case with no adhesion between the glass fibres and the matrix nylon. Consequently, the failure occurred by delamination and fibre pull-out, thereby rendering high values of impact strength to the specimens. This lack of adhesion is further confirmed with slightly lower values of tensile strengths of the tensile specimens, T3 and T4, compared to other specimens in the same disk. Next, we find that the impact performance of the piranha cleaned disk (Es = 215.59 J/m) is already higher than the Untreated fibre composite.

6.2.3. Dependence of E_S on the concentration of Silane-IV solutions used for treatment of fibres in composites.

Coating fibres from solutions with 0.2%, 0.5%, 1.25% and 2% of Silane IV in toluene at various times led to fabrication of composite disks on Day I, Day II , Day III and Day IV. We compare E_S for Silane IV applied from the above solutions with the E_s for the Untreated disks (represented by "0% concentration" on the plot). This plot is shown in Figure 6.16 (a). All the above disks had $\overline{V}_f$ in the range 23.4-24.5%, which is a sufficiently narrow range. Hence we compare the impact values as obtained and do not incorporate any $\overline{V}_f$ corrections in these. We shall also plot the tensile strengths of these disks to determine any trends if present between the two properties (i.e. impact and tensile). This plot is shown in Figure 6.16 (b). From Figure 6.16 (a), we find that E_s values are lowest for Silane-IV concentration of 1.25%. The E_s also seems to be higher for Silane-IV concentration of 0.2%. The upward trend at Silane-IV concentration of 2%, suggests that the E_s values might increase for concentrations beyond 2%. Figure 6.16 (b) is a very interesting plot in that, the inverse relationship appears to exist between σ_b and E_s. These trends thus support the previously-mentioned generalizations of the two properties.

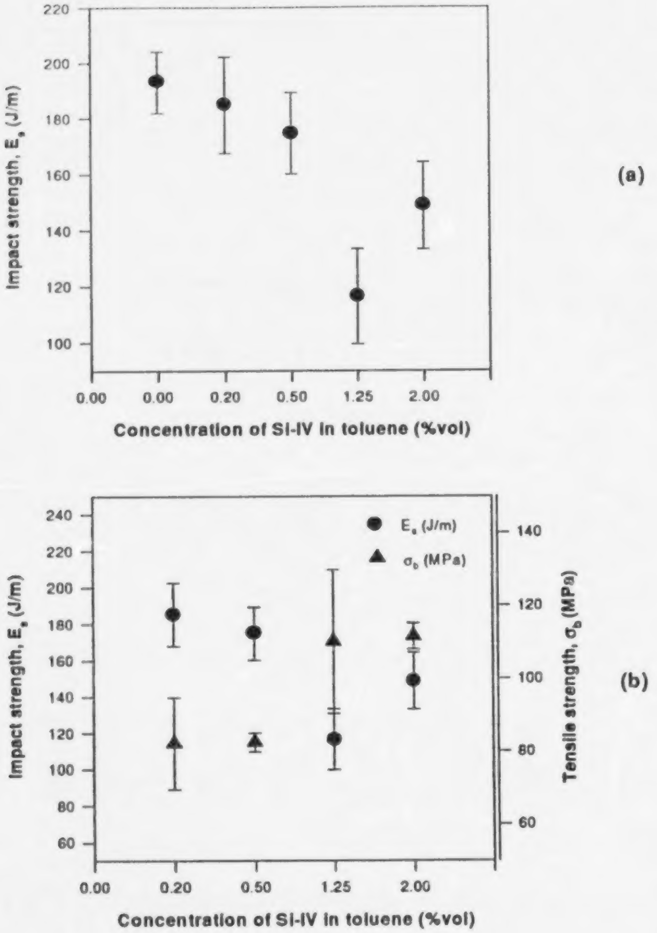

Figure 6.16 (a). Impact strength (E_s) of composite treated with different concentrations of Silane-IV in toluene (Note: The 0 % concentration represents the E_s of Untreated fibre composite), (b) Comparison of Impact strength (E_s).and Tensile strength (σ_b) of the Silane-IV treated composites.

6.2.4. Qualitative results from other composite specimens

Because the Izod impact tester did not function properly in the next set of testing, we were not able to obtain any quantitative values for the impact strength. So, we decided to report just the type of failure that we observed for each specimen. These are given in Table C-6 (b) in Appendix C. As mentioned earlier, the type of failure also signifies to certain extent, the nature of adhesion between the matrix and the glass fibre. Partial failure would occur due to debonding and pull-out of fibres. This would therefore indicate lack of adhesion between the matrix and the glass fibre. On the other hand, if complete failure occurred, then it is more likely that the fracture occurred due to fracture of the glass fibres. This would therefore represent good adhesion between the glass fibre and the matrix. Based on these arguments, we find that all composites [shown in Table C-6 (b)], except the Silane-III treated glass fibre composites underwent complete failure most of the times, and thus possessed good adhesion between the fibres and the matrix. In the Silane-III composites, we find occurrence of both, the partial and complete fracture mechanisms, indicating the presence of non-uniform adhesion in the composite disk. This kind of analysis helps us to relate the type of failure to the nature of adhesion between the glass fibres and the matrix, thereby providing useful qualitative information without having quantitative at hand.

Apart from strength and structural properties, other characterizations, such as DSC thermal analyses, molecular weight measurements of the composites were also employed. The experimental setup, procedure and the intrinsic viscosity measurements for molecular weight determination of nylon 6 prepared in our laboratory and of commercial nylon 6 samples, have been described in detail in Appendix E. DSC data are discussed in the following, section 6.3.

6.3. Thermal behavior of nylon 6 and its composites

As seen in sections 6.1 and 6.2, the different surface treatments of glass fibres led to a remarkable difference in the tensile properties of the respective composites. The differences caused in the adhesion of the glass fibres to the matrix nylon was evident from the scanning electron micrographs of the fracture surfaces of the tensile specimens. To see if these differences could arise from variations in crystal morphology or orientation produced by the glass fibre surface treatment, we employed a differential scanning calorimeter (TA Instruments DSC 2910) to examine the thermal behavior of nylon 6 and its composites.

The speed of scanning was maintained at 10°C per minute and the materials were subjected to two complete scans (each scan consisting of heating and cooling between 0 and 250°C). Figures 6.17-6.20 display the different scanning calorimetric curves (heating and cooling scans) of the nylon (rectangular and circular configuration) disk specimens, and the two furnace-cleaned, untreated glass fibre disk specimens. From each heating and cooling scan, the following data was sought: the melting point (T_m) of nylon, the glass transition temperature (T_g), the crystallinity of the sample in the first and second cycles. The results obtained from these measurements are shown in Table 6.3. The heat of fusion (ΔH_f) was calculated from the area enclosed by the endothermic region of the scan and the baseline. For the pure nylon samples, this value was divided by the ΔH_f value of a hypothetical 100% crystalline nylon 6 (188 J/g, *Polymer Handbook*) to obtain the percent degree of crystallinity. For composites however, the ΔH_f value obtained from the curves was divided by the average weight fraction of the matrix in the composite ($\overline{\omega_m}$ obtained from Table C-2) and this corrected value was then divided by the ΔH_f value of a 100% crystalline nylon 6 to obtain the percent crystallinity of the nylon in the composite. The drop in crystallinity represents the loss of the area enclosed by the curve during the two scans. This topic will be discussed in detail later in this section.

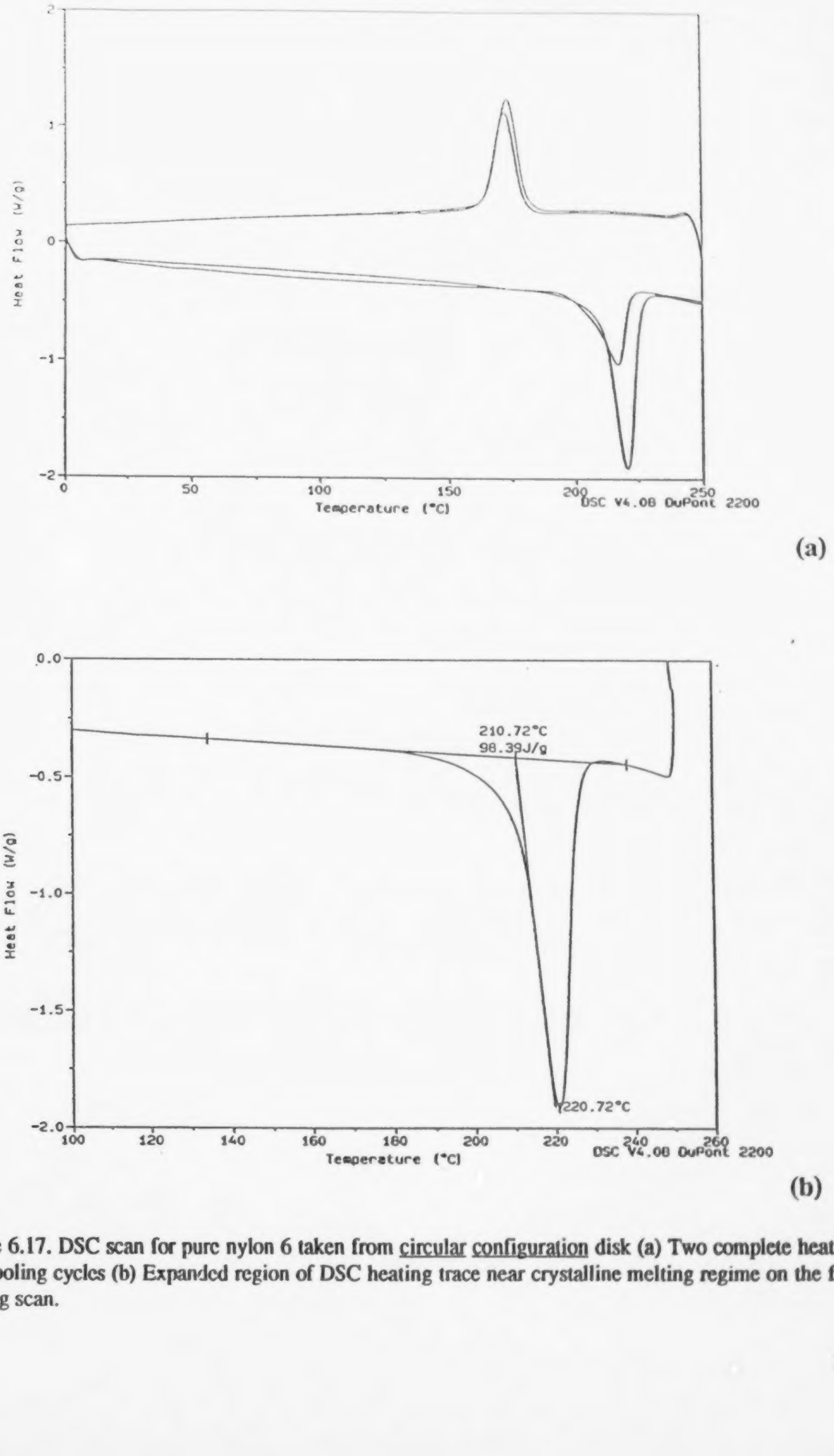

Figure 6.17. DSC scan for pure nylon 6 taken from circular configuration disk (a) Two complete heating and cooling cycles (b) Expanded region of DSC heating trace near crystalline melting regime on the first heating scan.

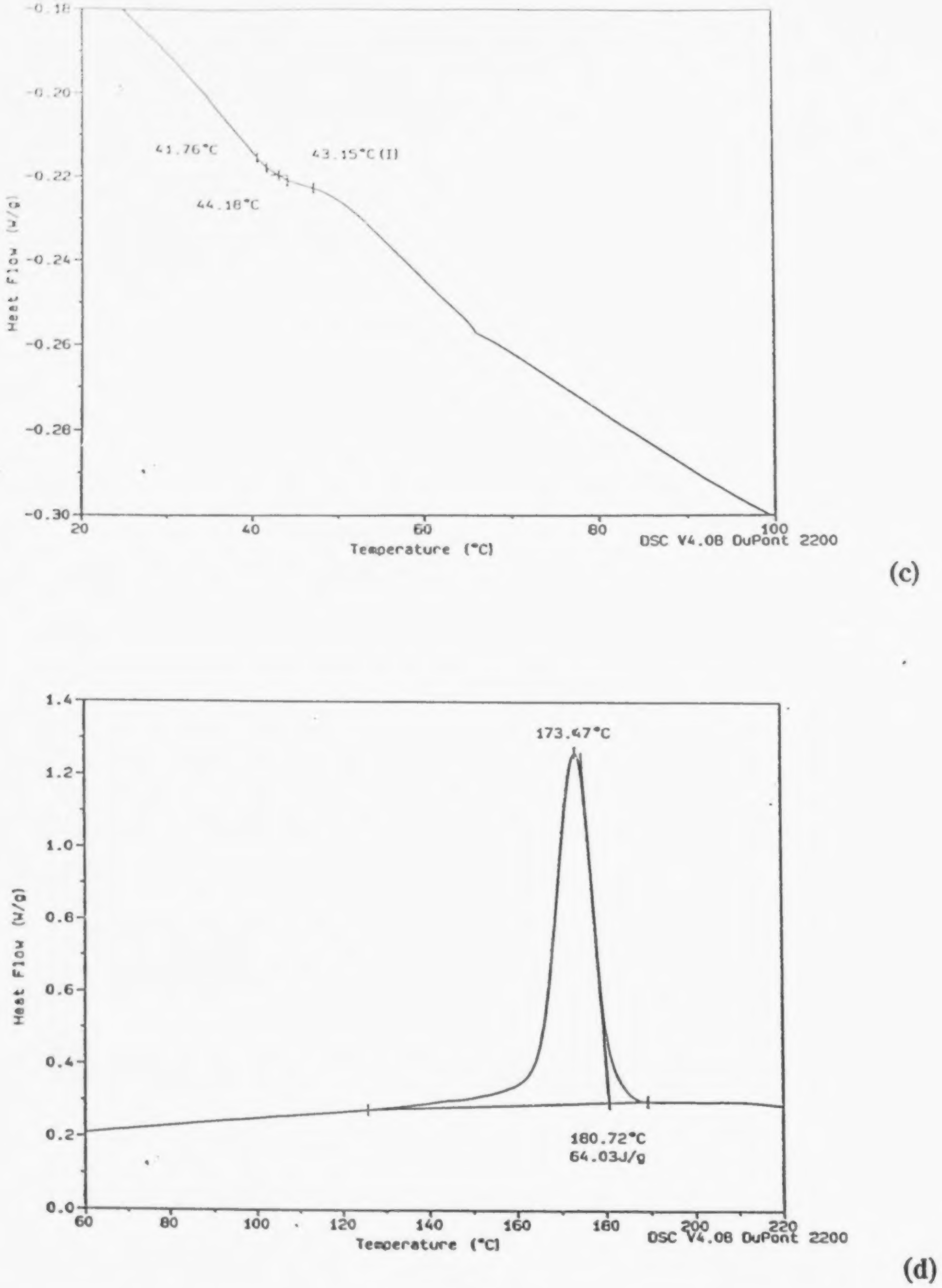

Figure 6.17. (Continued) (c) Expanded region of DSC heating trace, near glass transition regime on first heating scan (d) Expanded region of DSC cooling trace, near crystalline freezing regime following first heating scan.

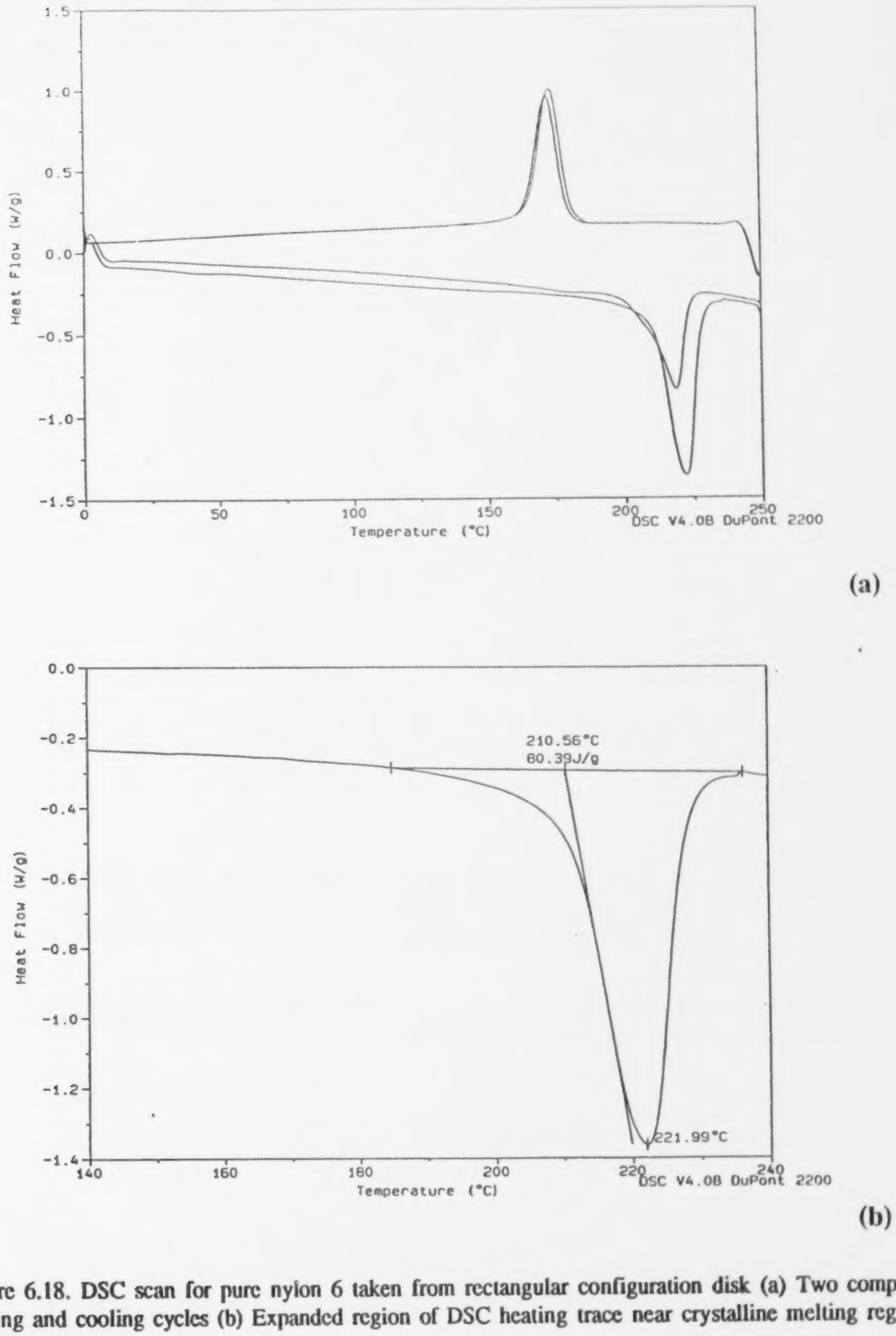

Figure 6.18. DSC scan for pure nylon 6 taken from rectangular configuration disk (a) Two complete heating and cooling cycles (b) Expanded region of DSC heating trace near crystalline melting regime (first heating scan).

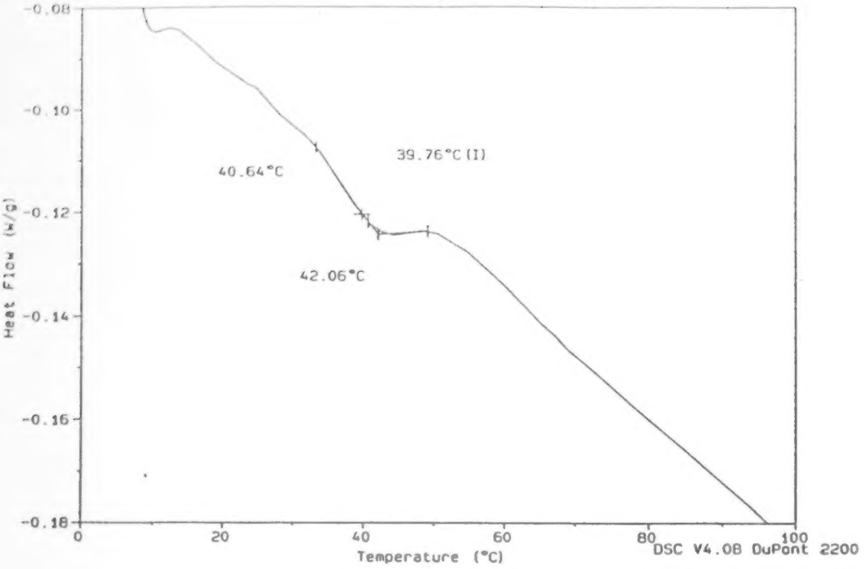

(c)

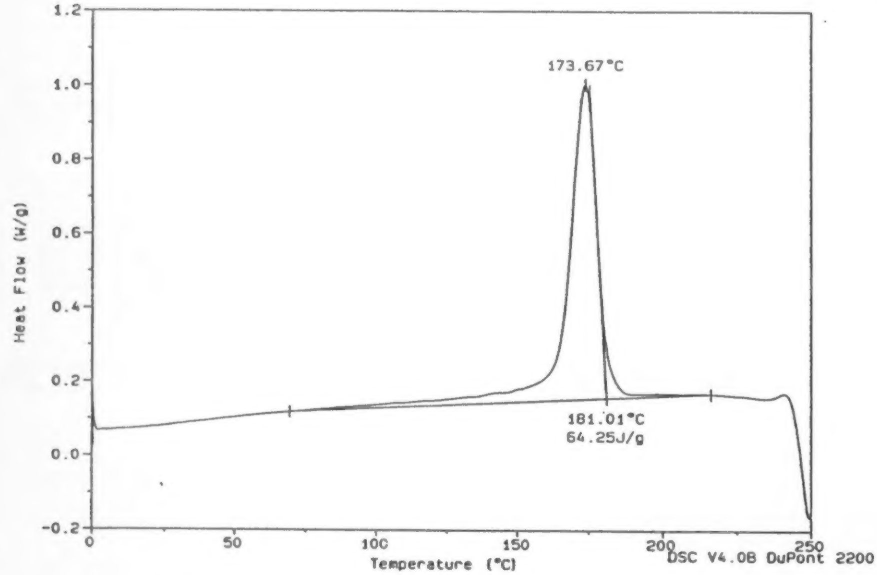

(d)

Figure 6.18. (Continued) (c) Expanded region of DSC heating trace, near glass transition regime (first heating scan) (d) Expanded region of DSC cooling trace, near crystalline freezing regime (following first heating scan).

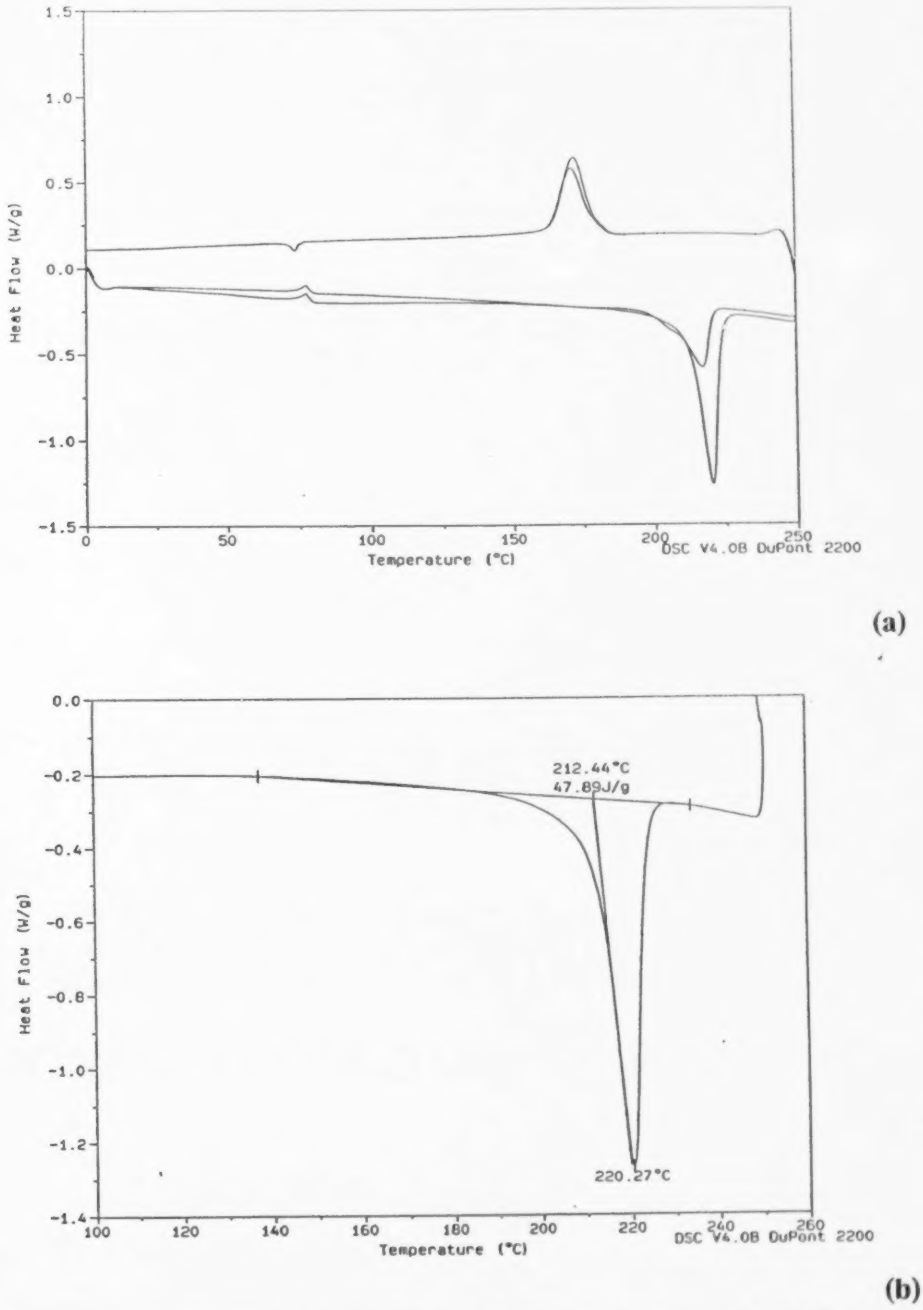

Figure 6.19. DSC scan for composite sample taken from specimen of [1]Untreated disk (a) Two complete heating and cooling cycles (b) Expanded region of DSC heating trace near crystalline melting regime (first heating scan).

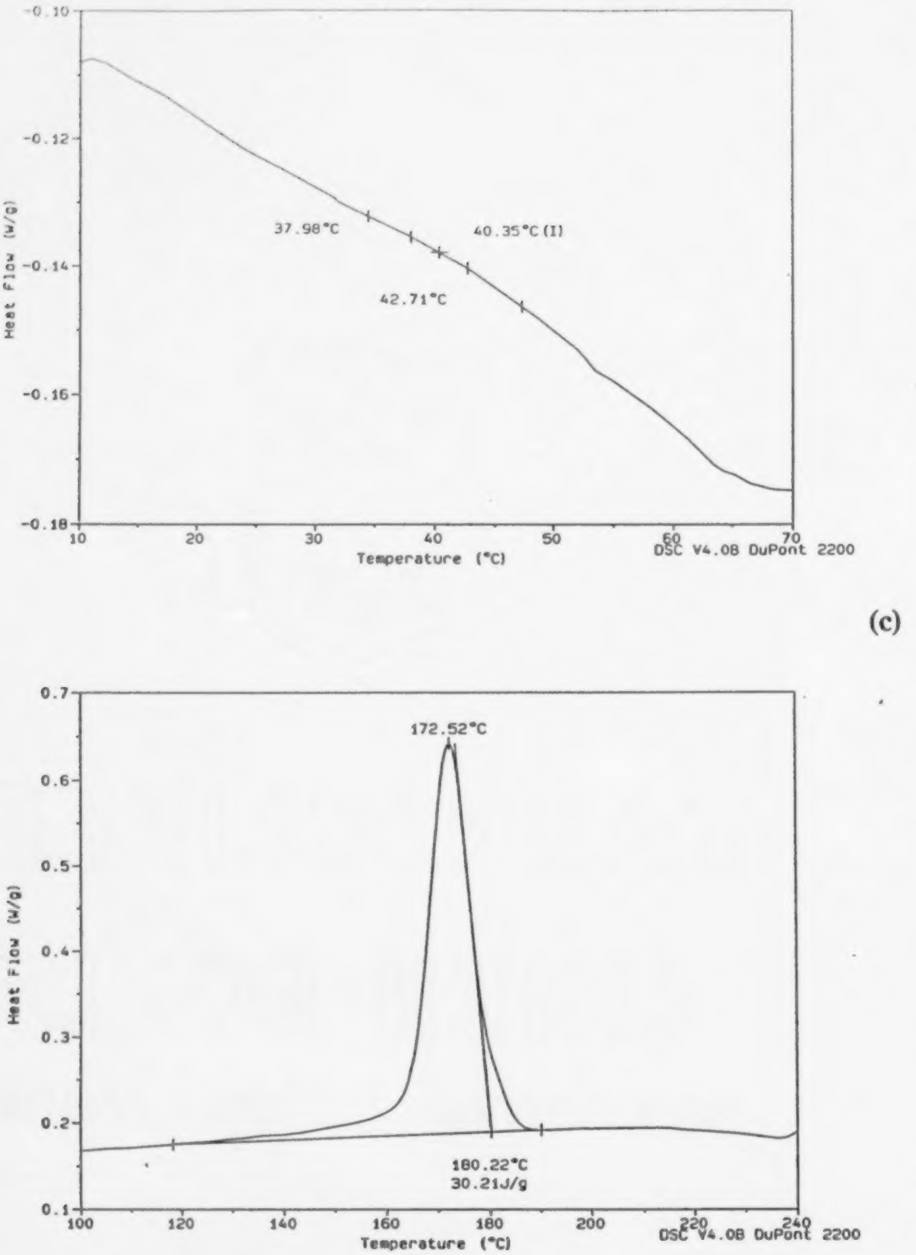

Figure 6.19. (Continued) DSC scan for composite sample taken from specimen of ^{1}Untreated disk (c) Expanded region of DSC heating trace, near glass transition regime (first heating scan) (d) Expanded region of DSC cooling trace, near crystalline freezing regime (following first heating scan)

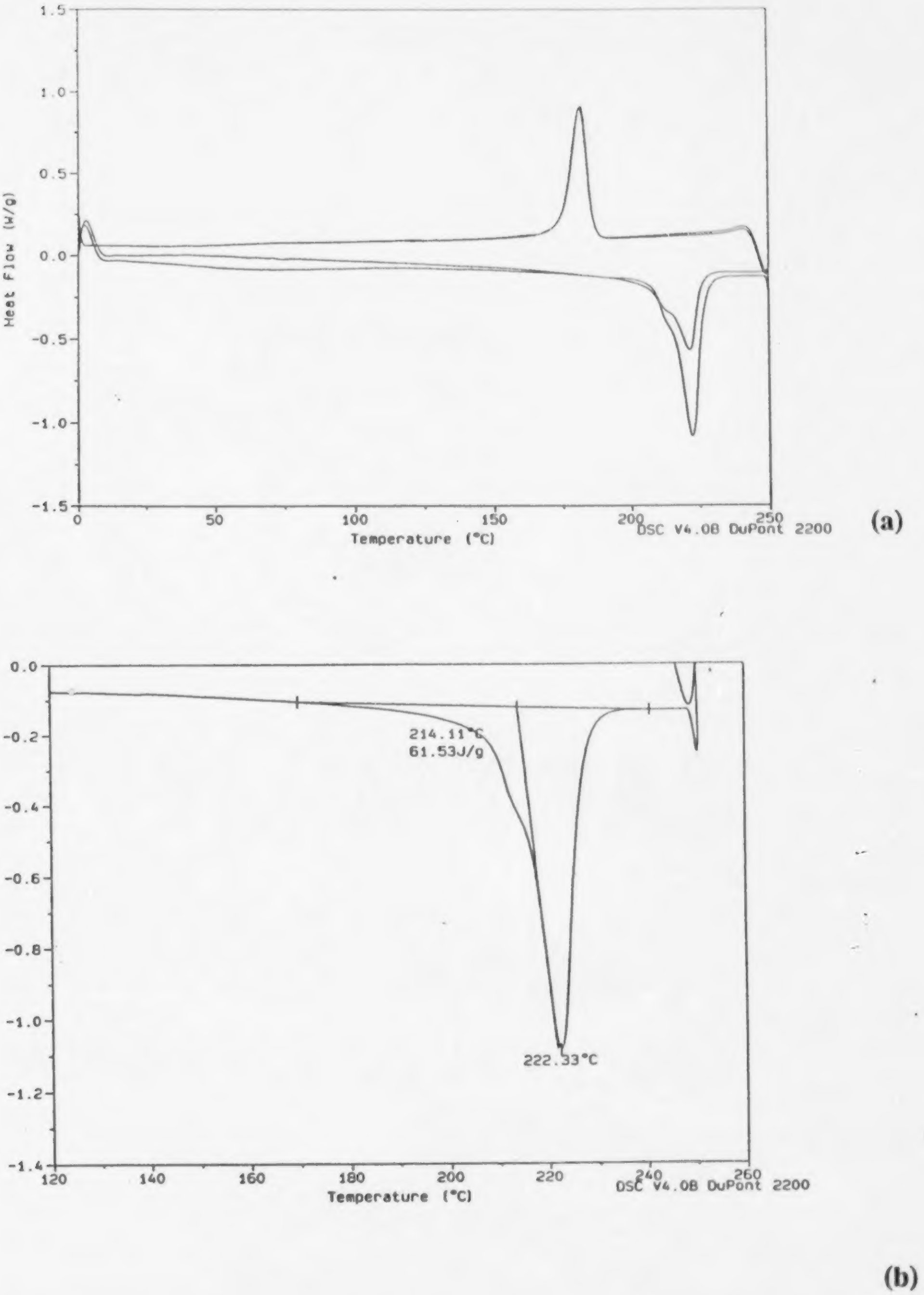

Figure 6.20. DSC scan for composite sample taken from specimen of ^{3}Untreated disk (a) Two complete heating and cooling cycles (b) Expanded region of DSC heating trace near crystalline melting regime (first heating scan).

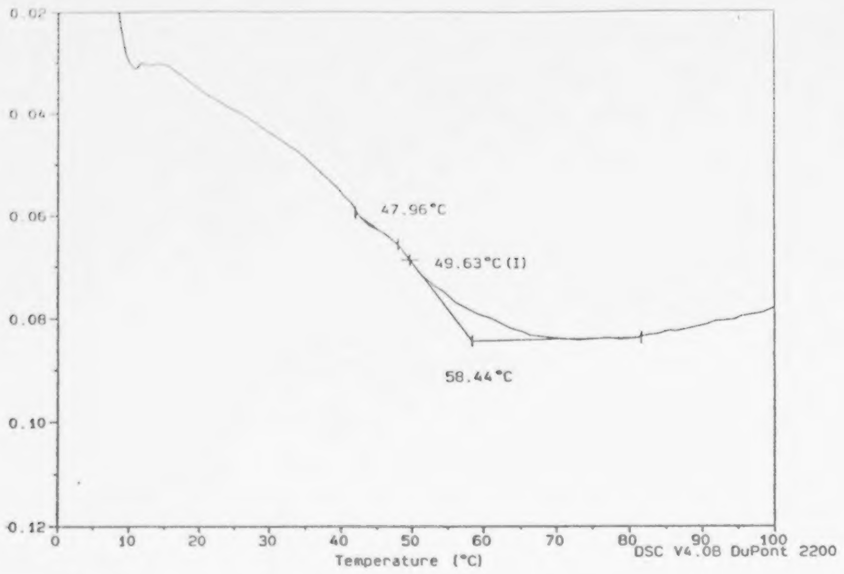

(c)

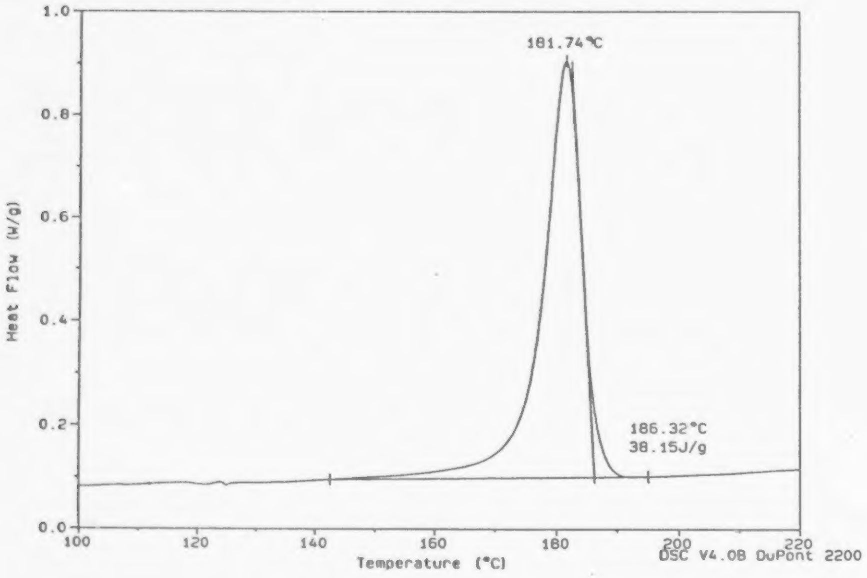

(d)

Figure 6.20. (Continued) DSC scan for composite sample taken from specimen of ³Untreated disk (c) Expanded region of DSC heating trace, near glass transition regime (first heating scan) (d) Expanded region of DSC cooling trace, near crystalline freezing regime (following first heating scan).

Table 6.3. Different thermal properties of nylon 6 matrix in the different composites. Scanning rate: 10°C/minute

Type of Disk	Tm (Ist Run) (°C)	Tg (Ist Run) (°C)	Crystallinity (Ist Run), C_1 (%)	Crystallinity (IInd Run), C_2 (%)	Drop in Crystallinity $(C_1-C_2)/C_1$ (%)
Pure nylon(R)	221.99	39.76	42.8	23.3	45.6
Pure nylon (C)	220.72	43.15	52.3	31.6	39.6
Pure nylon[a]	220.52	40.23	49.0	33.9	30.8
Nylon from [1]Si-IV(1.25%) composite	221.82	45.30	53.8	37.9	29.6
[1]Untreated	220.27	40.35	48.9	28.2	42.3
[3]Untreated	222.33	49.63	64.2	48.4	24.6
Piranha-Cleaned	217.01	43.39	39.9	27.4	31.3
HF-Treated	221.22	63.50	56.3	41.1	27.0
Si-III (0.2%)	220.26	59.30	54.5	43.7	19.8
[1]Si-IV (1.25%)	222.62	46.73	53.8	35.9	33.2
Si-IV (1.37%+CL)	218.49	48.30	54.0	45.4	15.9
[2]Si-V (1.25%)	218.58	41.97	54.5	33.7	38.1

Results of DSC testing, shown for the pure nylon 6 (circular and rectangular) in Figures 6.17 and 6.18 are in good agreement with reports in the literature. The overall performance of the material on a full heating/cooling cycle indicates a strong endothermic peak in the range 220-225°C which we assign to crystalline melting, identifying the peak position as T_m. There is also a small inflection visible in the 40-50°C range, which we interpret as the glass transition and label the midpoint as T_g. From the former, we find that $T_m \equiv 222°C$ is in perfect agreement with the commercial product reports in Table 2.3 and $T_g \equiv 42°C$, is somewhat below the 49°C from Table 2.3 (*Reimschuessel, 1977).* The cooling peak in Figure 6.17 and 6.18 is displaced to a temperature (≈175°C) well below the heating peak, but this is normal with polymer crystallizations. One interesting point we notice is that, the crystallinity of the circular nylon disk is slightly higher than that of the rectangular nylon [$\frac{C_1(C)}{C_1(R)} = \frac{52.3}{42.8} = 1.2$] . Could this difference in crystallinity be due to the error caused in choosing the baseline for the rather broad melting range ? If this is not the case, then, why did the less crystalline nylon (R) possess higher tensile strength than the more crystalline nylon (C) ? This is because, even if the circular nylon showed higher crystallinity, the fact that it possessed much higher void content (~ 14.3%) than the rectangular nylon disk (~6%), offers good reason for the material (circular configuration nylon) to be weaker than the rectangular configuration nylon. Consequently, the circular configuration nylon also had lower density than the rectangular configuration nylon disk (since for a given mass of the specimen, the volume occupied by the sample is much higher because of the presence of voids). While the reason for the difference in crystallinity could be attributed to the different procedures employed to fabricate these disks, the question remains as to what could have caused such a difference in the crystallinity of the two nylon disks.

The observed drop in crystallinity of the nylon (~42%) in the second scan can be explained by the differences in the thermal history of the as-polymerized *(in-situ)* and the DSC-polymerized sample. In the former, the microphase structure corresponds to the one formed as a result of in-situ polymerization and crystallization at 150°C, while in the latter, the microphase structure corresponds to the reprocessed polymer, which has been formed by recrystallization at around 200°C. For lactam polymerizations, the polymer is in equilibrium with the residual monomer and cyclic oligomers. This equilibrium is a function of temperature and is displaced toward the monomer and its cyclic oligomers as the temperature is increased, as a result of transamidation reactions (*Otaigbe and Harland, 1988)*. These low molecular weight substances are capable of altering the crystallization process in the nylon 6 by kinetically hindering the nucleation and growth of extended chain crystals from the melt. This decrease in crystallinity may also be attributed to the presence of Na in the nylon matrix, as pointed out by *Sankholkar, 1996*. He speculated that the loss in crystallinity was due to the degradation of the nylon sample because of the presence of

Na in the matrix. This sodium reacted exothermally with water vapor, causing localized hot spots in the sample, which caused chemical degradation of nylon. In addition to the above reasons, there could be one more reason for the loss in crystallinity. The crystallization rate is different in the DSC run from the crystallization phenomenon in the mold. We investigated this matter further and carried out the DSC scan in a slightly different fashion (shown in Figure 6.21). For example, after the first heating scan (0 to 250°C, we let the temperature cool to about 210°C at a rate of 10°C/minute and then changed the scanning rate to 1°C/minute, in order to give sufficient time for the crystals to form and grow in the molten polymer. The scan rate was resumed to 10°C/minute after the temperature dropped to 170°C. When the drop in crystallinity was examined for this cycle, we found that the drop in crystallinity still occurred although it was lower (~31%) (see Table 6.3) than the one obtained from the original scan (~42%). This result suggests that the crystallization kinetics can have a possible influence on the crystallinity of the polymer. *Sankholkar, 1996*, did not notice this kind of drop in crystallinity in his nylon samples which were prepared with Mg-based catalyst, so this behavior could also be attributed to the difference in the equilibrium concentrations of the polymer and the monomer/oligomer, caused in presence of two different catalysts. The equilibrium concentration of the polymer in presence of the Na catalyst might be lower than that in presence of Mg-based catalyst, suggesting higher concentrations of monomer/oligomer in the Na-based catalyst nylon. This in turn would have resulted in the chemical degradation or shift toward higher equilibrium concentrations of monomer/oligomer concentrations at high temperatures, resulting in overall drop of crystallinity of nylon.

Moving to the composites, two examples are presented of DSC analysis of the untreated composites in Figures 6.19 and 6.20. These are the ^{1}Untreated (^{1}U)and the ^{3}Untreated (^{3}U) disks. The ^{1}Untreated disk was prepared in the same fashion as the rectangular pure nylon disk, and hence a comparison of its properties with pure nylon suggests a small shift in T_m toward slightly lower temperature of 220.72°C, a slight increase in T_g to 43°C, and

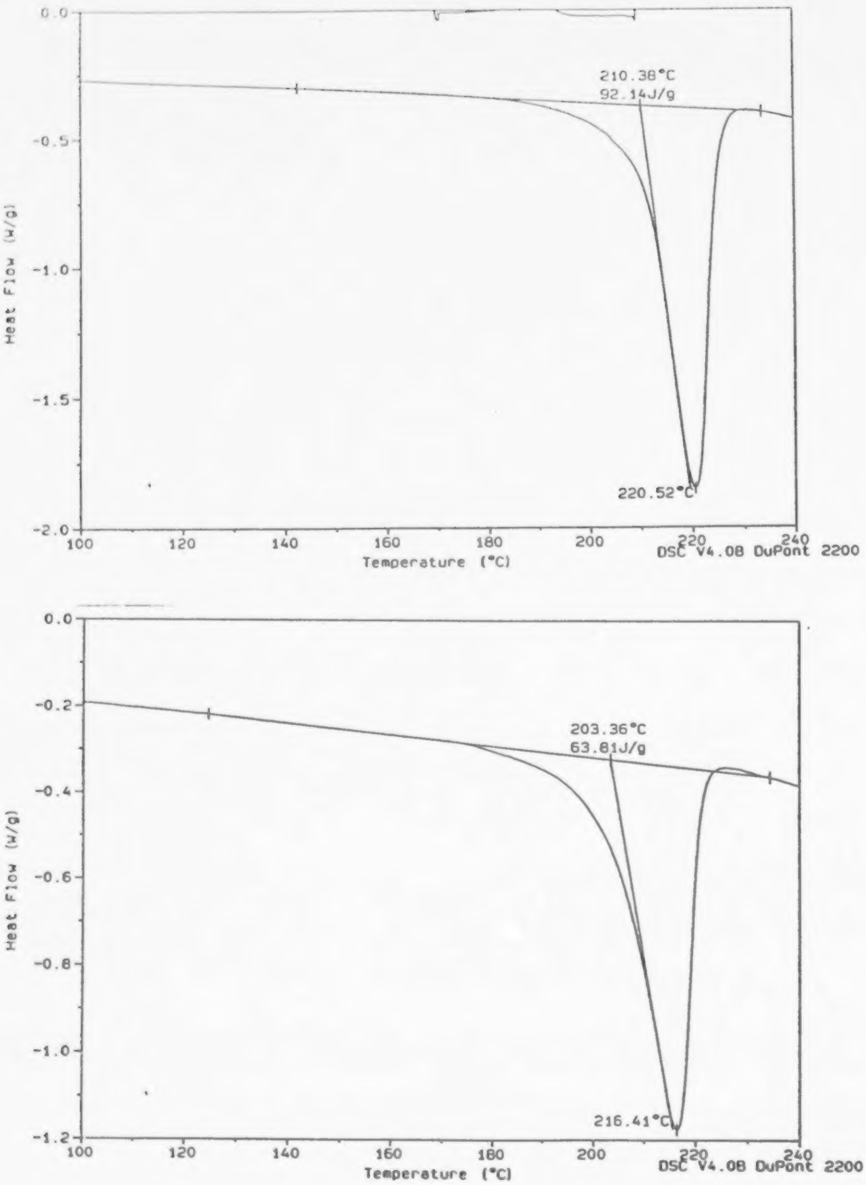

(a)

(b)

Figure 6.21. DSC scan for pure nylon 6 (from circular configuration disk) with a different thermal cycle Expanded region of the DSC heating trace near the melting regime in (a) First heating cycle (b) Second heating cycle

an increase in crystallinity of the matrix nylon in the composite. This supports our assumption of having denser nylon matrix in the composite caused by the presence of glass fibres. This idea is further supported when we carried out the DSC analysis of the nylon obtained from the composite disks (sample taken from the circumferential region where no glass fibre is present). This curve is shown in Figure 6.22. The nylon sample was taken from the ^{1}Si-IV (1.25%T) composite disk. We found this nylon to possess higher crystallinity (~53.8%) than that of pure nylon (~42.3%(R); 52.3%(C)), thus supporting our assumption of existence of higher density matrix nylon in the composite.

The other disk (^{3}U) was prepared in a slightly different fashion, in that the polymerization of the monomer was carried out at 120°C, unlike the ^{1}U disk, where the polymerization was carried out at 150°C. From the curves, we see that the ^{3}Untreated composite disk had slightly higher T_m (222.3°C) and T_g (49.6°C) than the ^{1}Untreated composite disk with T_m = 220.3°C and T_g = 40.4°C. The crystallinity of the ^{3}Untreated disk was also higher than the ^{1}Untreated disk, the ratio being $[C_I(^3U)/C_I(^1U)] = 1.3$ and the drop in crystallinity for the former disk (^{3}U) was lower (~24.6%) than that for the latter disk (^{1}U) (~42.3%). These results suggest that indeed the polymerization of the polymer is supported at lower temperatures and that the lower drop in crystallinity between the two runs for ^{3}U nylon 6 suggests that the equilibrium concentration of polymer is higher at lower temperatures (notice the caprolactam peak, $T_m \approx 72$°C in the ^{1}U sample, Figure 6.19(a), which shows that the caprolactam is degrading). Since, the void content in the both the above disks was in the same range, the increase in crystallinity acted to increase the tensile properties of the ^{3}Untreated disk by formation of a stronger matrix nylon.

6.3.1. Effect of surface treatment on the thermal properties of nylon matrix in composite

To determine the effect of surface treatment on the thermal behavior of nylon matrix in the composite, we carried out thermal analyses for six different samples. These are listed in

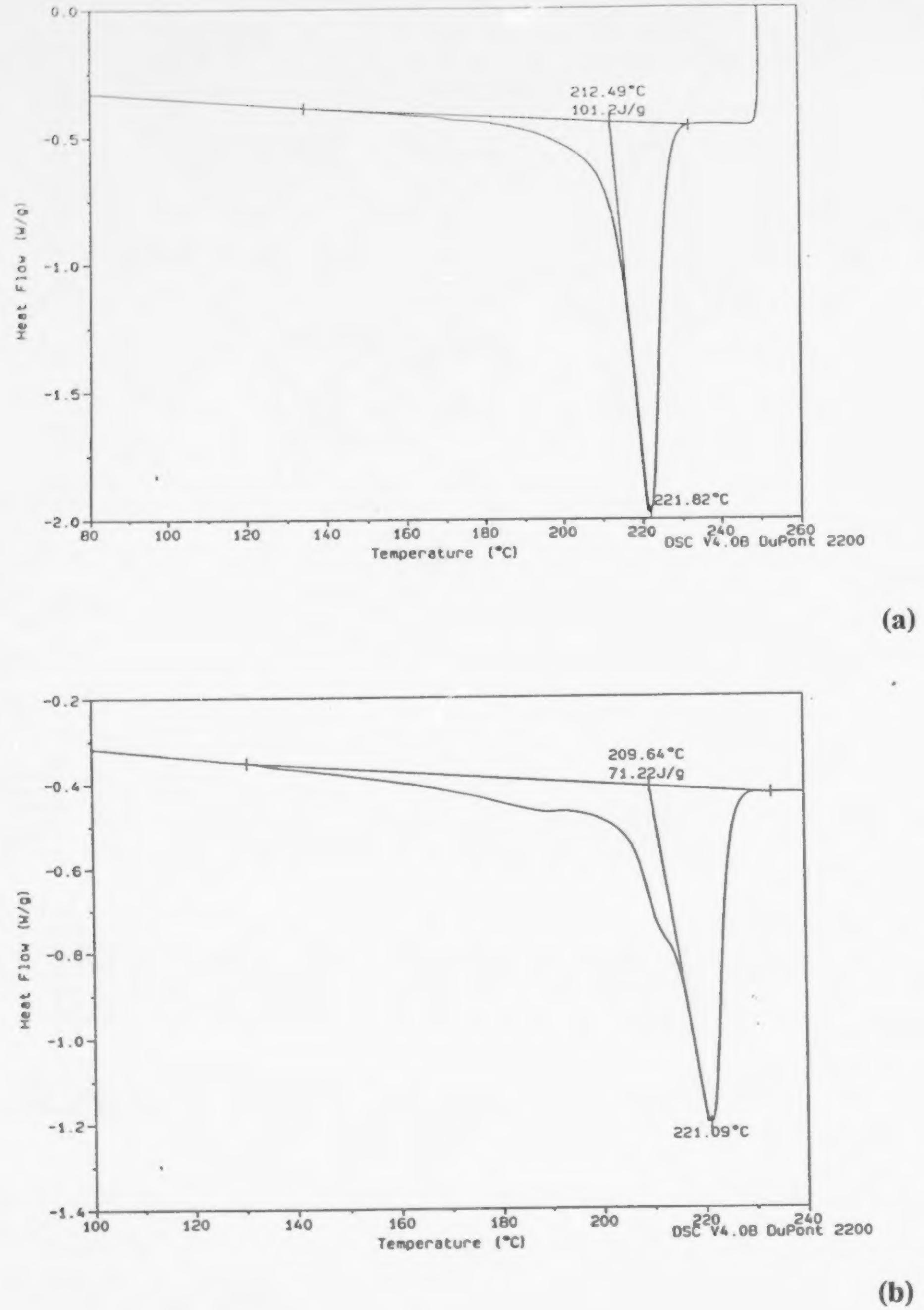

Figure 6.22. DSC heating scan for nylon 6 matrix taken from the composite ^{1}Silane-IV (1.25%). Expanded region of the DSC heating trace near the melting regime in (a) First heating cycle (b) Second heating cycle

Table 6.3, and the curves are shown in Appendix F, Figures 1-6. Only one sample for each silane-type was tested.

We find that for the piranha-cleaned disk, the chemical treatment did alter the crsytallization process in the mold, enough to drop the average T_m by 5°C. The detailed analysis is shown in Table 6.3. We can see that there was not a very significant change in T_g (which was 43.4°C). The major difference caused by the chemical cleaning was in causing a drop in the crystallinity of the nylon in the composite [C_l=39.9% < 48.9%(^{1}U)]. This meant that the chemical cleaning modified the surface chemistry of the glass fibres in such a way so as to promote less crystal formation in the matrix. The reason for such a behavior is difficult to explain. Possibly, the chemical cleaning might have rendered the surface an excess of hydrogen ions, which might have hindered the crystal growth and formation. Alternatively, this might have shifted the equilibrium of polymerization reaction to the left, leading to higher equilibrium concentration of the monomer/oligomers. This is evident from the figure, where the appearance of a small peak at around 75°C corresponds to the caprolactam melting range, suggesting the existence of a fair amount of residual monomer in the nylon. It is difficult to predict if the presence of monomer would cause plasticizing effects, thereby reducing the tensile strength and the elastic modulus of the composite, because the overall performance of the composite is also governed by other factors such as, fibre content, adhesion at fibre/matrix interface, void content, etc.

Moving to Figure 2 in Appendix F, we find that the HF-treated fibres have worked in the reverse way, that is, it promoted crystal formation (C_l = 56.3%), but did not alter the T_m (of 221.2°C) and the appearance of an inflection around 65°C is perplexing, because of the fact that the T_g cannot be so high, and this again lies in the lower end of the melting range of caprolactam (65-75°C).

Figures 3-6 in Appendix F display DSC scans for the silane-treated glass fibre composite disks. From Table 6.3, we find that all the disks possess crystallinity in the range 53.8-54.5%, which is higher than that for the ^{1}Untreated composite disk. However, the melting points were different for the nylon from each disk. For example, T_m for Silane-III treated disk was 220.3°C; T_m [^{1}Si-IV(1.25%)] = 222.6°C; T_m [Si-IV(1.37%+CL)] = 218.5°C and T_m [^{2}Si-V(1.25%)] = 218.6°C. It was difficult to identify the Tg for Si-III and Si-IV (1.37%+CL) composite disk, so no comments can be made on the glass transition behavior of these disks.

Chapter 7

CONCLUSIONS AND RECOMMENDATIONS

7.1. Conclusions

Improved mechanical properties of composites were obtained by altering the surfaces of glass fibres with different treatment techniques.

Differences in properties (both structural and mechanical) were also observed when pure nylon 6 was fabricated with different mold configurations. The rectangular configuration nylon 6 (RN6) was found to have a dense, uniform and fine morphology, whereas the circular configuration nylon 6 (CN6) showed a coarse, non-uniform morphology. A rough estimate of the void volume fraction in RN6 gave values of ~6%, while the values of void fraction obtained for CN6 were ~14%. Consequently, the density of RN6 (ρ = 1.14 g/cm^3) was slightly higher than that obtained for CN6 (ρ = 1.13 g/cm^3). Although, this difference in densities could be considered minor, the effect of a slightly higher density was found to be pronounced in void volume fraction calculations; increasing the density of nylon from 1.13 to 1.14 changed the physically impossible negative numbers of V_f to meaningful positive numbers. Further, the higher void content in CN6 rendered it inferior in mechanical properties. The σ_b for CN6 was lower than RN6 by almost 50%. Although we would have expected all properties of CN6 to be inferior compared to RN6, one property showed a reverse trend: the crystallinity of nylon in the circular configuration was found to be higher for CN6 (52.3%) than RN6 (42.8%). This meant that the CN6 could have performed superior or equal to RN6 in all the properties, had there not been so many voids in it. However, it is difficult to explain the large difference in properties arising from fabricating nylon 6 in the two mold configurations. It is also important to note that the RN6 properties compared favorably with other reports for nylon 6; in particular, it possessed a higher σ_b than commercial samples at the same range of density.

The structural properties of the composites made by *in-situ* polymerization were quite reproducible. Densities of composites were always in the range, ρ = 1.45-1.55 g/cm^3 (except HF-treated fibre composite with ρ = 1.36 g/cm^3 and piranha-cleaned fibre composite with $\rho = 1.42$ g/cm^3). The glass fibre volume fractions, V_f of all composites, were in the range 23.4-30.5%, with differences probably due to non uniformity of the fibreglass mat in the roll, and not from the fabrication process. However, the HF-treated fibre composite and the piranha-cleaned fibre composite had significantly lower V_f compared to the remaining composite disks. The lower values obtained for ρ and V_f for the HF-treated composite could be attributed to the etching action of HF on glass fibres, which resulted in a loss in mass of the glass fibres. For the piranha-cleaned fibre composite, the difficulty in handling the glass fibre mats after the cleaning could have resulted in the non-uniformity of fibre distribution and content.

The void volume fraction V_v, obtained for all composites was consistently at the level of 2% or less, and this level is well within acceptable industry standards. Further, no effect of surface treatment on the void fraction was observed. In each composite disk, there were local variations in V_f, V_v, and ρ. Indications (not very strong) were that higher V_v was found in regions of higher V_f. This may be because there was higher resistance to flow of molten caprolactam and less penetration, especially around the area where most fibres were highly packed, usually at the centre of the mold.

The ρ of nylon 6 was believed to differ between bulk nylon 6 and composite matrices due to a change of crystal morphology when glass fibre was present. From DSC analysis, pure nylon 6 in disks without reinforcement showed lower crystallinity than the nylon 6 in composite disks. This high and effective crystallization of nylon 6 in composites may result from a very slow cooling rate (air-cool), and from the contact of molten nylon 6 with the glass fibre surface (this can nucleate the crystal structure of polymer). Thus, higher crystallinity of nylon 6 in the composites gives additional evidence to verify our belief of obtaining higher densities of nylon in composites than in pure nylon. This proves to be critical when calculating the void content V_v.

Tensile tests on furnace-cleaned, untreated composites revealed that the nylon 6/glass-fibre composite possessed a lower σ_b (53.8 MPa) than the nylon alone (62.5 MPa), indicating very poor adhesion between glass fibre and matrix. The SEM micrographs of the fracture surfaces of the tensile specimens offered additional evidence, in that the surfaces of the pulled-out glass fibres were smooth and there was no matrix adhering to them. In such an absence of bonding between the glass fibres and matrix, increase in V_f might result in worse properties than unreinforced (pure) polymer, since no stress transfer takes place from matrix to the fibre. Moreover, there is less matrix to support the load than in pure nylon, thus resulting in poor performance of the composite. However, if the bonding is good, the presence of glass fibres would result in improved properties of the composite. This relatively poor performance seen when the composite nylon 6 was polymerized at 150°C was not duplicated when T_p=120°C. The untreated fibre composite disk fabricated with T_p = 120°C showed superior properties to the untreated composite with T_p = 150°C. This improvement could be attributed to the matrix properties because the SEM micrographs showed no evidence of adhesion between glass fibre/nylon 6 again. Further, the composite polymerized at 120°C also showed higher crystallinity than the one polymerized at 150°C.

Tensile performances of the variously treated fibre composites ranked as follows:

HF-treated fibre composites gave improved strength properties of σ_b (49%) over the Untreated fibre composite, even with a very low V_f of 18%. Also, the crystallinity of the matrix nylon in this composite was higher than that of pure nylon. This suggests that a short etching time (with little loss of glass) would give tremendously improved properties if the nominal V_f was actually achieved as intended (30%). The piranha-cleaned fibre composite showed no improvement in properties compared to the furnace-cleaned, but offers a simple and inexpensive alternative way of cleaning glass fibres.

Silane I gave slightly improved properties, σ_b being 15% higher than the Untreated composite. The physical adsorption between -Si-NH of Silane I and -Si-OH of the glass surface seemed to be very weak, unlike the presence of chemically reacting groups on other silanes. Hence, a significant improvement in properties was not expected.

Silane-III improved σ_b by almost 66% and τ by 33% over the Untreated fibre composite, thus suggesting the formation of a strong covalent bonding by reaction of the chloride group of Silane-III with the hydroxyl group on the glass surface. However, no concentration effects were observed in the range 0.2-2% for Silane-III in toluene. Also evident from the SEM micrographs was the lack of any matrix nylon adhering to the glass surface. This probably suggests that although the bonding between the silane and glass is improved, it is not sufficient to resist failure by delamination, which is revealed by leaving the glass fibre surfaces intact and smooth.

Silane-IV gave significantly higher improvements in properties compared to Silane-I and Silane-III. For example, it improved σ_b by ~104%, E by 36% and τ by 30% over the Untreated fibre composite. This might be because the Silane-IV molecule had all the desirable features of a coupling agent such as, being able to bond covalently with the hydroxyl groups on the glass surface, or to form a local cross-linked network of neighbors on the glass, and the presence of the amino tail that could react with the caprolactam during polymerization process. In fact because of the last feature, an interphase can be formed at the glass fibre/nylon interface, which comprises glass fibre bonded Silane-IV molecules, and other chemically adsorbed/cross-linked molecules, surrounded by or bonded to matrix nylon molecules. The properties of this interphase are different from those of the bulk, and to some extent determine the properties of the composite. For example, the formation of a strong interphase might cause the composite to behave differently even at very low strains, since the system is now slightly different from the non-adhered nylon/glass fibre system. This might be the reason for an increase in the elastic modulus of the Silane-IV treated fibre composite over the Untreated. The SEM micrographs revealed matrix well to the glass fibres even after the failure of the materials. Concentration effects were observed for Silane-IV, with a maximum in strength properties obtained at 1.25% Silane-IV in toluene.

Concentration effects could be related to the nature of the multilayers formed on the surface of glass fibres by treatment with different concentrations of silanes. For example, higher concentrations of Silane-IV might lead to higher amounts of polysiloxane formation in the bulk solution (these aminosilanes being self-catalytic), which results in a loss of the silanols that are needed to form the chemisorbed monolayer. These oligomers then form the physisorbed layers, which are known to lower the strength properties of the composite by acting as plasticisers and thereby helping in the debonding at the glass fibre/matrix interface. The extremely low concentration used in preparing the fibres for Silane-IV samples probably results in the formation of an incomplete, chemisorbed monolayer, and a weaker interphase, which lacks the strength to support the load, thus resulting in a composite with inferior properties.

The Silane-IV deposited from ethanol did not perform as well as when it was deposited from toluene. Nevertheless, this treatment gave a composite with improved properties of σ_b (88%), E (29%) and τ (33%) over the Untreated fibre composite. The deposition and the nature of the deposited silane molecules depends on factors such as, concentration of silane in the solution, water concentration, pH of the solution, temperature, aging time, etc. It is difficult to comment as to which factor would have affected the deposition of the silane on glass surface, but we could eliminate the factors of temperature, aging time, since these were not different for the two treatments. Thus, the concentration of water and pH of the solution are the potential factors that might have affected the deposition of the silane on glass surface, as a result of which, difference in the strength properties were observed. Because of lack of sufficient data on the above factors, at this point, it is difficult to find the right answer to the question.

The composite obtained by depositing the blend of crosslinking additive and Silane-IV gave similar improved properties of σ_b (89%), E (23%) and τ (19%) over the Untreated. Whereas, the crosslinking additive was chosen to provide a stronger crosslinked network at the interface, this failed to do so. This might be because we did not use the right concentration of the crosslinking additive.

Silane-V treated composites also showed significant improvements in the strength properties. The best properties were again obtained with Silane-V concentration of 1.25%

in toluene, which gave improved properties of σ_b (105%), E (25%) and τ (30%) over the Untreated composite. This improvement in properties can again be attributed to the desirable features that this silane has in common with Silane-IV. Further, the long backbone might permit it to diffuse deeper into the matrix nylon, thereby acting as a bridge between the two phases. Concentration effects were again observed, but the maxima in the range 0.2-1.25% were not as sharp, and dropped abruptly above 1.25%. We therefore speculate that Silane-V at higher concentrations hinders the polymerization of nylon 6, thereby resulting in the drop in properties. Furthermore, at high concentrations, the presence of physisorbed Silane-V molecules might increase, and these molecules because of their long chains, might hinder crystal formation and growth.

The most interesting observation among all the silane-treated composites was that the increase in the tensile strength of the composite was not accompanied with an increase in ε_b, which is a very desirable property in composites, as in all advanced materials; high strength but not brittle.

E_s for all the composites were almost five times over the unreinforced nylon. The improvement was due partly to the intrinsic strength of glass and partly to fibre pull-out effects which apparently dissipated considerable energy and made even the poorly bonded fibre systems effective (indeed, this seems to explain much of the inverse relationship found between E_s and σ_b).

7.2. Recommendations

7.2.1. Mold improvements

Although significant improvements were made in the mold design and the entire experimental setup, there are still some pockets that need to be filled in to be able to carry out an efficient reaction injection molding process. One of these is in the heating of the feed vessel, for which purpose an isomantle is used. The temperature of the flask contents was maintained by a temperature controller, which received a signal from a thermocouple inserted inside the vessel and regulated power to the isomantle around the vessel to achieve the desired set point. Since there is no agitation inside the flask, there exists a temperature gradient in the flask contents, with the maximum temperature close to the walls of the flask, and the temperature gradually decreases toward the centre. Also, the liquid around the thermocouple is stationary and its temperature is not truly representative of the temperature inside the flask. Thus, the signal delivered to the controller is always for lower temperature and the controller therefore gives out a high power signal to the isomantle, as a result of which the temperature inside the flask now shoots up. This leads to longer waiting times to bring the temperature down, and hence the heating process takes more time than it would normally do. This difficulty can be overcome by having a stirrer inside the flask, which would keep the temperature inside the flask uniform.

Further, because the chemical reaction is accelerated and completed over a small temperature range (somewhere, not exactly known, between 100°C and 150°C), it is possible that the relatively small temperature variations across the upper and lower mold surfaces--and between upper and lower surfaces--could be creating some problems of matrix inhomogeneity, internal stress and separation of matrix from fibre. An effort should be made to reduce these internal temperature variations $\Delta T(r,z)$ still further, to less than 1° C. Better external insulation should be used, and with an entirely new insulating layer should be built into the mold as well. With a new mold, too, the number of heaters and their placement could be altered--i.e., use more of them, spaced more uniformly (especially around the rim)--in order to reduce the temperature gradients that now exist. Most importantly, one should not forget to introduce thermocouples into female as well as the male part of the mold (unlike what we have currently, only the female part has a thermocouple inserted into it) to ensure uniform heating of the mold.

Opening and closing this mold seems unnecessarily difficult. For opening, each lifting screw must be turned in small increments in sequence with the other three screws. If these are not turned properly, the male part of the mold will become tilted and bind, so the mold cannot open. If so, the whole procedure must be reversed and tried once more: loosen all screws, use C-clamps to close the mold, tighten screws, release C-clamps, and then repeat the opening sequence. This process is wasteful of time and is potentially damaging to some parts of the mold, since aluminum is soft and could be harmed by the metal-to-metal binding and use of force. The mold closing procedure is also awkward, requiring struggle with the large ungainly C-clamps. For many reasons, then, a redesign of the mold opening and closing processes is desirable. Hydraulic mechanisms would be preferred. If mold-opening by hand is preferred, using the four-screw system is still an appropriate method. However, to make this an easily managed step (i.e. to reduce the physical resistance), the O-ring seal should be relocated to the exterior lip of the mold where the male part and female part make a flush contact with each other. In this work, the O-ring could not be relocated because the exterior lip was too narrow; greater width at this point would be needed in an upgraded design.

In this work, the glass tube and valve connection between the feed vessel and the mold was kept warm by good insulation. However, caprolactam was still found to freeze occasionally inside the tube. This problem should be overcome by wrapping a heating tape around the tube and then controlling the temperature of the tube by means of a controller. This would thus make the procedure simpler and easier to work with.

7.2.2. New experiments

Since we obtained superior properties by polymerizing the caprolactam at 120°C, composite disks with silanes must be made at this polymerization temperature, which offers major improvements for the composite independent of fibre treatment.

Now, DSC evidence for the crystallinity of nylon obtained with NaH as the catalyst decreased in the second heating cycle, which suggests that inferior properties of the composite would result after it is thermoformed. This drop can be attributed to either the catalyst (causing chemical degradation) or to the crystallization kinetics of nylon in the melt. Now, this problem can be eliminated completely by using other catalysts such as isobutylmagnesium bromide, which have been reported *(Sankholkar. 1996)* to not cause any degradation of the polymer in the second heating cycle. It would be preferable if all composites made here in the future were made using this catalyst or trying some other catalyst superior to NaH.

Since only one concentration of the crosslinking additive with Silane-IV was studied in this work, future work must investigate the effect of other concentrations.

Recent research has focused on developing improved silane coupling agent systems to obtain specific desired properties, such as using blends of hydrophobic silanes with hydrophilic silanes to impart greater hydrophobic character to the fibre surface; use of more thermally stable silanes to obtain increased thermal stability, use of additives to give increased siloxane crosslinking, etc. There have been some successes in the use of these different techniques with mainly polyester composites *(Pape and Plueddemann, 1987)*. These techniques must be investigated with our nylon/glass fibre composite system to see if improved properties are obtained.

Since concentration effects were observed with Silanes IV and V, this behavior should be further investigated to see what is actually happening by depositing different concentrations of silanes. This can be done by characterizing the silane-treated glass fibre surfaces. Various spectroscopic techniques, such as the XPS, the SSIMS, or even a FTIR analysis might characterize the surface chemistry more completely.

On a general basis, all treated glass fibres should first be characterized in terms of modified surface chemistry, wetting characteristics with the molten monomer and the polymer, with water. Further, since silane deposition is dependent upon such factors as, concentration in solution, water concentration, pH of the solution, aging time, etc., the effect of these variables on the silane deposition should be studied.

Next, find new silanes that are similar to Silane IV ($H_2N(CH_2)_3Si(OCH_3)_3$) but potentially better because of having a C=O and perhaps more NH_2 groups, and also with a longer chain and branches to enhance entanglements. One candidate to try is (3-Chloropropyl)trimethoxysilane, $Cl(CH_2)_3Si(OCH_3)_3$, which has three methoxy groups to bond with the glass surfaces (as does Silane IV) and also one Cl group which can react with the NH group in nylon 6 chain or with the glass.

Other techniques to measure adhesion between the glass fibres and nylon should be used. One such test is the pull-out test. By this method, the other variations in the full composite structure will be eliminated, leaving only the interfacial adhesion to be measured without complication. Thus, this technique will facilitate testing of small samples of surface-treated fibres, and will be a quick and convenient method to obtain values of adhesion for different systems. This technique will be most useful for plasma treated glass fibres, where only a few fibres can be etched/treated at a time. Further studies should be conducted in optimizing the plasma reactor conditions (such as power, plasma type, time of exposure, etc.) to clean, etch or modify the glass surface and these should then be tested for adhesion with nylon using the above pull-out test.

Use other methods to measure voids, such as optical image analysis or acoustical analysis, and compare the results with the value obtained from calculation with measured densities. The dilute solution viscometry apparatus should be modified and the method standardized in order to obtain consistent values of intrinsic viscosities and hence the molecular weights.

References

1. Allcock, H. R., and Lampe, F. W., *Contemporary Polymer Chemistry*, 2nd ed., New Jersey, p. 115, **1990**.

2. Béland, S., *High Performance Thermoplastic Resins and Their Composites*, Noyes Press, New Jersey, p. **1990**.

3. Berlin, A. A., Volfson, S. A., Enikolopian, N. S., Negmatov, S. S., *Principles of Polymer Composites*, Springer-Verlag, New York, **1986**.

4. Bonfield, S. J., Berger, M. H., Bunsell, A. R., Watts, J. F., Greaves, S. J., Grosjean, F., Rosenberg, E. and Bain, J. M. "Influence of the Fibre/Matrix Interface on the Behaviour of Thermoplastic Composites: The Fibre/Size Interphase", *J. Comp. Polym.*, 5, n 3, p. 161-172, **1992**.

5. Broutman, L. J. and Krock R. H., *Composite materials, Volume 6, Interfaces in Polymer Matrix Composites* (ed. E.P Plueddemann), Academic Press, New York, **1974**.

6. Carlsson, L. A., *Thermoplastic Composite Materials, Volume 7, Composite Materials Series* (ed. R.B. Pipes), Elsevier Science Publishers B.V., Amsterdam, **1991**.

7. Castle, J. E. and Watts, J. F. "The Study of Interfaces in Composite Materials by Surface Analytical Techniques", *Interfaces in Polymer, Ceramic, and Metal Matrix Composites*, (ed. H. Ishida), Elsevier Science Publishers, p.57-71, **1988**.

8. Chang, T. C. and Jang, B. Z., "The Effects of Fibre Surface Treatmenst by a Cold Plasma in Carbon Fibre/Bismaleimide Composites", *Materials Research Society Symposium Proceedings*, 170, 321, **1990**.

9. Chaudhary, M. K., Gentle, T. M., and Plueddemann, E. P., "Study of Adhesion through Interdiffusion and IPN formation in the Interphase Region of Composites", *Journal of Adhesion Science and Technology*, 1(1), p. 23-38, **1987**.

10. Chawla, K. K., *Composite Materials*, Springer-Verlag, New York, **1987**.

11. Culler, S. R., Ishida, H., and Koenig, J. L., *Proceedings of 15th National Technical Conference, SAMPE,* October, **1983**.

12. Duangchan, A. T., "Glass-Fibre and Nylon 6: An Advanced Composite Material", *MSc Thesis, University of Alberta*, **1994**.

13. Encyclopedia'92, *Modern Plastics*, Mc Graw Hill, mid-October, **1991**.

14. Fan, T. C., "Design Consideration of Composites with Voids", *J. SAMPE*, 29(4), 15, **1993**.

15. Fernengel, R., "Plastics in the Engine Compartment", *Creative Use of Plastics in Cars*, VDI-Verlag GmbH Publishers, Duesseldorf, West Germany, p.65-82, **1984**.

16. Fowkes, F. M., Dwight, D. W., Manson, J. A., and Lloyd, T. B., "Enhancing mechanical properties of polymer composites by modification of surface acidity or basicity of fillers", *Adhesion in Solids*, p. 223, *MRS Symposium Proceedings*, Vol. 119, MRS Publications, **1988**.

17. Gaitskell, J. N., Herring, J. M., Williams, I. G., "Polyamides - Development of Mechanical Properties by Glass Fibre Reinforcement, Mineral Filling and Rubber Toughening", *Seminar on Plastics - Development and Prospects,* Cracow, Poland, Sep. 17-21, p.432-34, **1984**.

18. Gaur, V. G., and Davidson, T., "Interfacial Effects of Plasma Treatment on Fibre Pull-Out", *Materials Research Society Symposium Proceedings*, 170, 309, **1990**.

19. Gaylord M. W., *Reinforced Plastics: Theory and Practice*, Cahners Publishers, Massachusetts, **1974**.

20. Ghirose, S. R., "Effect of Void Content on the Mechanical Properties of Carbon/Epoxy Laminates", *SAMPE Quarterly*, 24(2), 54-59 **1993**.

21. Gillespie, L. H., Jr., "Engineering Plastics: The Concept that launched an Industry", *Polymer Preprints, American Chemical Society*, v 27, n 1, p. 470-71, **1986**.

22. Hamada, H., Coppola, J. C., and Hull, D., "Effect of Surface Treatment on Crushing Behaviour of GlassCloth/Epoxy Composite Tubes", *Composites*, 23, 2, March, **1992**.

23. Heide, P. A. M., Baan Hofman, M. J., and Ronde, H. J., "Etching of thin SiO_2 layers using wet HF gas", *Journal of Vacuum Science Technology*, A7(3), p. 1719, **1989**.

24. Holister, G. S., Thomas, C., *Fibre Reinforced Materials*, Elsevier Publishing Co. Ltd., New York, **1966**.

25. Holland, L. and Ojha, S.M., " The Chemical Sputtering of Graphite in an Oxygen Plasma", *Vacuum*, 26(2), 53, **1976**.

26. Holland, L., "Wetting Glass Surfaces", Chapter 6 in The Properties of Glass Surfaces, Wiley **1964**;

27. Holliday, L., *Composite Materials*, Glass Systems, K.L. Loe Wentein, Elsevier Publishers, New York, **1966**.

28. Hull, D., *An Introduction to Composite Materials*, Cambridge University Press, Cambridge, U.K., **1981**.

29. Ishida, H., "Structural Gradient in the Silane Coupling Agent Layers and its Influence on the Mechanical and Physical Properties of Composites", *Molecular Characterization of Composite Interfaces*, (ed. Ishida, H. and Kumar, G.), Plenum Press, New York, p. 25, **1983**.

30. Ishida, H. and Rotter, G., "RIM-Pultrusion of Thermoplastic Matrix Composites", *J. Comp. Polym.*, 4,1, p. 1-11, **1991**.

31. Ishida, H., and Koenig, J. L., "Hydrolytic Stability of Silane Coupling Agents on E-Glass Fibres Studied by Fourier Transform Infrared Spectroscopy", *Proceedings of the*

35th SPI/RP Annual Technology Conference, paper 23-A Society of the Plastics Industry, New York, **1980**.

32. Jang J., Ishida, H., Plueddemann, E. P., "Adsorption Behavior and Molecular Structure of the Mixed Silane with a Crosslinking Additive on the Substrate", *44th Reinforced Plastics/Composites Conference, Society of Plastics Industry*, Paper 9-B, **1989**.

33. Jenneskens, L. W., Venema, A., Veenendaal, N. V., and Huysmans, W. G. B., "Evidence for Interphasial Amide Formation between Surface-Bound Poly(3-Aminopropyltrisiloxane) and Polyamide-6 in Glass Bead Reinforced Polyamide-6 Model Composites", *Journal of.Polymer.Science.: Part A: Polymer Chemistry*, 30, p. 133-136, **1992**.

34. Kardos, J. L., "The Role of the Interface in Polymer Composites - Some myths, mechanisms, and modifications", *Molecular Characterization of Composite Interfaces*, (ed. H. Ishida and G. Kumar), Plenum Press, New York, **1983**.

35. Kelly, A., *Strong Solids*, Clarendon Press, Oxford, **1973**.

36. Kern, W., and Deckert, C. A., "Chemical Etching", *Thin Film Processes*, Chapter V-1, edited by John L. Vossen and Werner Kern, Academic press, **1978**.

37. Knox, C. E., "Fiberglass Reinforcement", in *Handbook of Composites* (ed. G. Lubin), Van Nostrand Reinhold Co., New York, **1982**.

38. Krishnamurthy, V., and kamel, I., L., "Argon Plasma Treatment of Glass Surfaces", *Journal of Materials Science*, 24(9), p. 3345-52, **1989**.

39. Larena, A., Urreaga, J., M., and De La Orden, M. U., "Effects of Previous Leaching with Hydrochloric Acid of E-Glass Short Fibre on the Fibre Reaction with Chlorosilanes", *Materials Letters*. 12, p. 415-418, **1992**.

40. Leeser, D. and Banister, B., "Amorphous Thermoplastic Matrix Composites for New Applications", *21st International SAMPE Technical Conference*, Sept. 25-28, p.507-13, **1989**.

41. Matthies, P. and Seydl, W. F., "High Performance Polymers: Their Origin and Development", *Proceedings of the Symposium, Presented at the 91st meeting of the American Chemical Society*, Elsevier Publ., New York, p. 39-53, **1986**.

42. Mattox, D. M., "Surface Preparation For Thin Film Deposition", *The Short Course Executive Committee American Vacuum Society*, **1991**.

43. Mattox, D. M., "UV/O3 and other oxidative cleaning methods", *Society of Vacuum Coaters* 32nd Technical Conference Proceedings, p.7, **1989**.

44. Odian, G., *Principles of Polymerization*, 3rd ed., John Wiley & Sons, New York, **1981**.

45. Otaigbe, J. U., "Effect of Coupling Agent and Absorbed Moisture on the Tensile Properties of a Thermoplastic RRIM Composite", *Journal of Applied Polymer Science*, 45, p.1213-1221, **1992**.

46. Otaigbe, J. U.,and Harland, W. G., "Studies in the Properties of Nylon 6-Glass Fibre Composites", *Journal of Applied Polymer Science*, 36, p.165-175, **1988**.

47. Peterson, G. P., "Advanced Composites: Past Perspective and Future Strategy", *Advances In Composite Materials, 3rd International Conference on Composite Materials*, (ed. Bunsell et al.), Paris, v1, p.4, **1980**.

48. Plueddemann, E. P., Mechanism of Adhesion Through Silane Coupling Agents, *Composite Materials*, Academic Press, New York, 6, p.174-216, **1974**.

49. Plueddemann, E. P., *Silane Coupling Agents*, Plenum Press, New York, **1982**.

50. Reimschuessel, H. K., "Nylon 6 Chemistry and Mechanisms", *J. Polym. Sci. Macromol. Rev.*, 12, 68, **1977**.

51. Rodriguez, F., *Principles of Polymer Systems*, 3rd ed., Hemisphere Publishing Corp., New York, p. 509, **1989**.

52. Sankholkar, Y. D., "Copolymers of Nylon 6 and Polycarbonate for Advanced Composite Materials", *MSc Thesis*, *University of Alberta*, **1996**.

53. Saunders, K. J., *Organic Polymer Chemistry*, Chapman and Hall, New York, **1988**.

54. Sebenda, J. and Lanska, B., "Effect of Polymerization Conditions on the Thermooxidation of Nylon 6", *Journal of Macromolecular Science - Pure and Applied Chemistry*, v A30, n 9-10, p. 669-78, **1993**.

55. Shah, V., "Handbook of Plastics Testing Technology", John Wiley & Sons, New York, **1984**.

56. Shand, E. B. , *Glass Engineering Handbook*, The Maple Press Company, York, PA, p.416, **1958**.

57. Stevens, M. P., *Polymer Chemistry*, Oxford University Press, New York, **1990**.

58. Sung, N. H., Kaul, A., Chin, I., and Sung, C. S. P., *Polymer Engineering Science*, 22, p. 637, **1982**.

59. Szijarto, K. and Kiss, P., "Filling of Polymers with the Aid of Coupling Agents", *Polymer Composites, Proceedings 28th Microsymposium on Macromolecules Prague, Czechoslovakia,* (ed. B. Sedlacek), p.473-77, Walter de Gruyter, Berlin, New York, **1986**.

60. Temple, C. S., et al., (to PPG Industries, Inc.) *U.S. Pat.3*, 684, 645 **1972**.

APPENDIX A

SEM micrographs of glass fibres subjected to different cleaning techniques

Figure 1. Effect of HF treatment on glass fibres after, (a) 0 mins., (b) 10 mins., (c) 30 mins., and (d) 45 mins.

Figure 2. Effect of piranha solution treatment on glass fibres after, (a) 0 mins.,(b) 5 mins., (c) 10 mins., and (d) 15 mins.

Figure 3. Effect of plasma treatment on glass fibres, (a) Argon plasma treated fibre (150W, 10 mins.), (b) Argon plasma treated fibre (500W, 10 mins.), (c) Argon plasma treated fibre (1000W, 20 mins.), (d)Argon plasma treated fibre (1500W, 10 mins.), and (e) Oxygen plasma treated fibre (100W, 10 mins.).

APPENDIX A

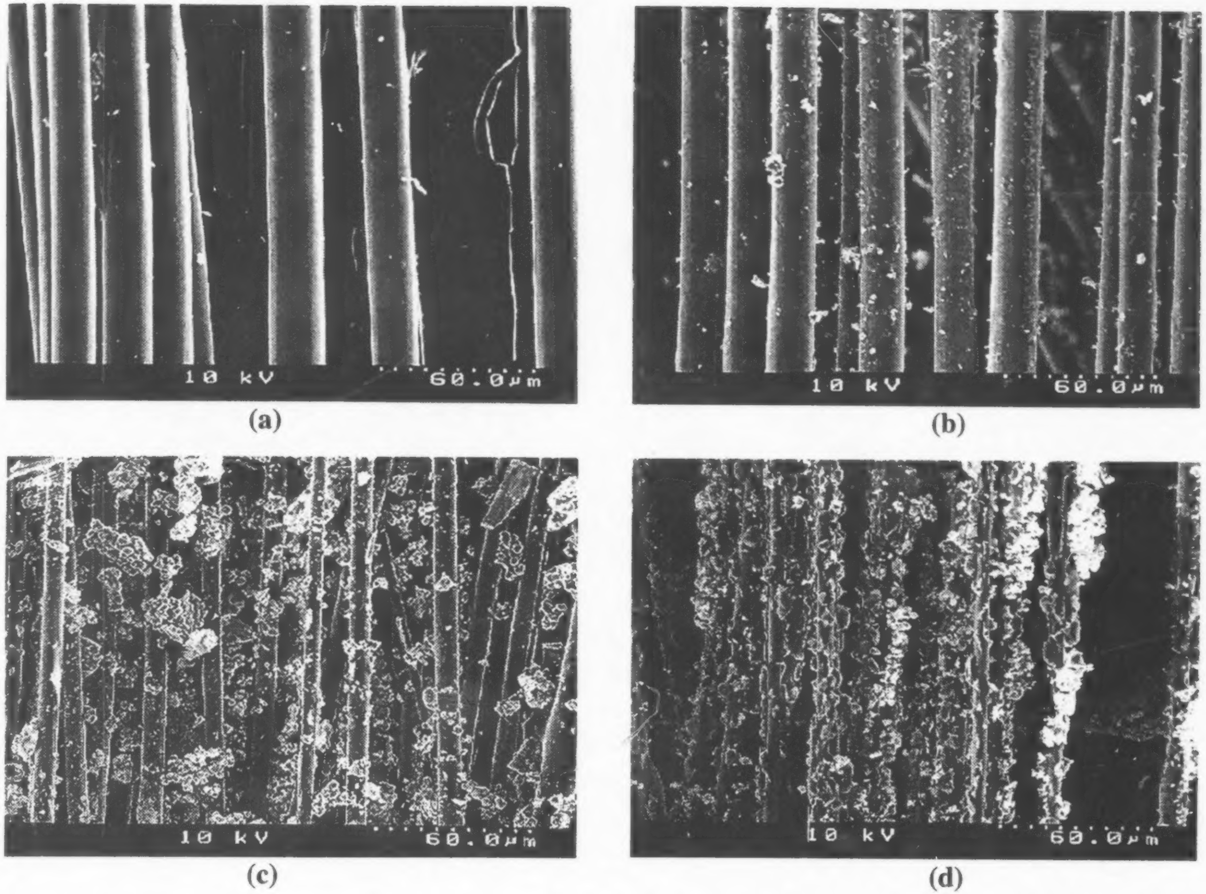
10 kV
60.0µm
10 kV
60.0µm
10 kV
60.0µm
10 kV
60.0µm

(a)

(b)

(c)

(d)

Figure 1. Effect of HF treatment on glass fibres after, (a) 0 mins., (b) 10 mins., (c) 30 mins., and (d) 45 mins.

APPENDIX A

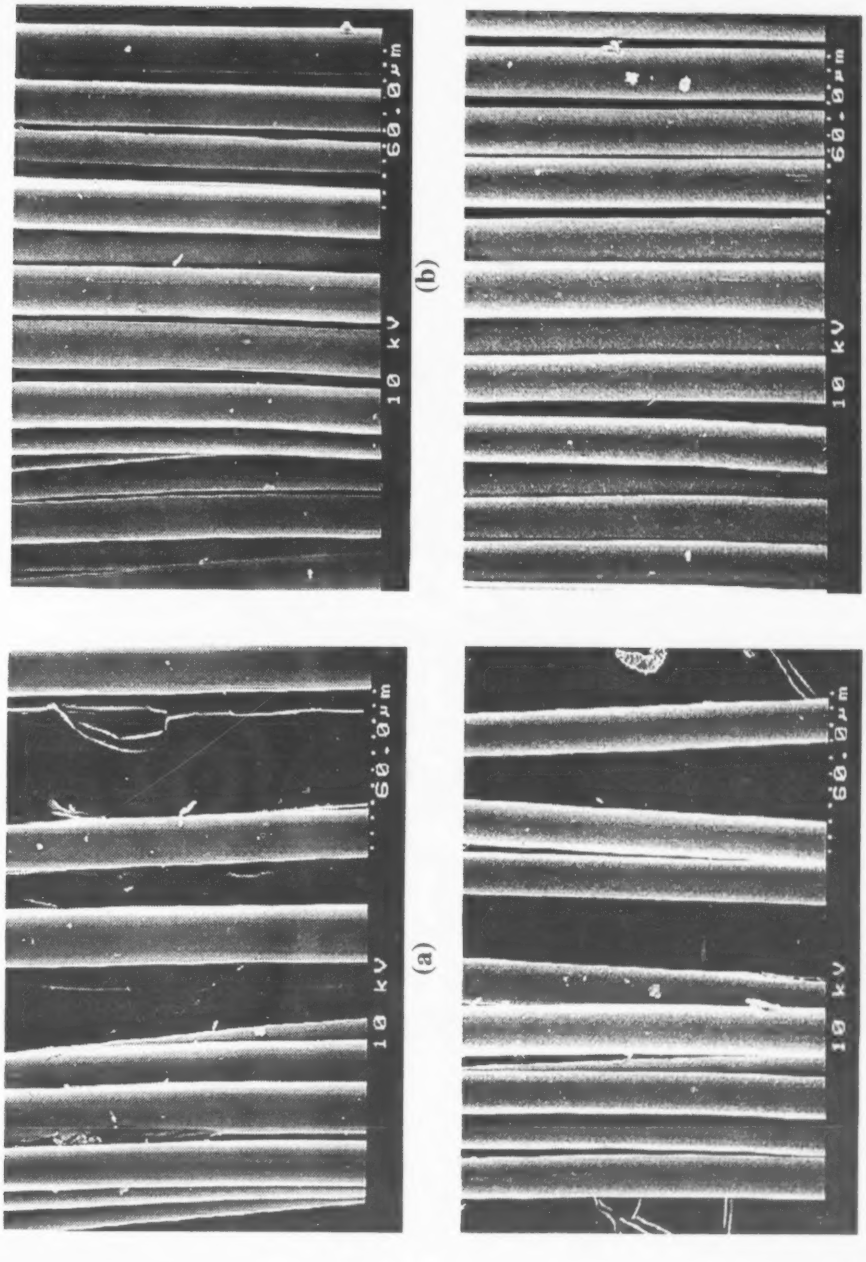
(a)
10 kV
60.0µm
(b)
10 kV
60.0µm
(c)
10 kV
60.0µm
(d)
10 kV
60.0µm

Figure 2. Effect of piranha solution treatment on glass fibres after, (a) 0 mins., (b) 5 mins., (c) 10 mins., and (d) 15 mins.

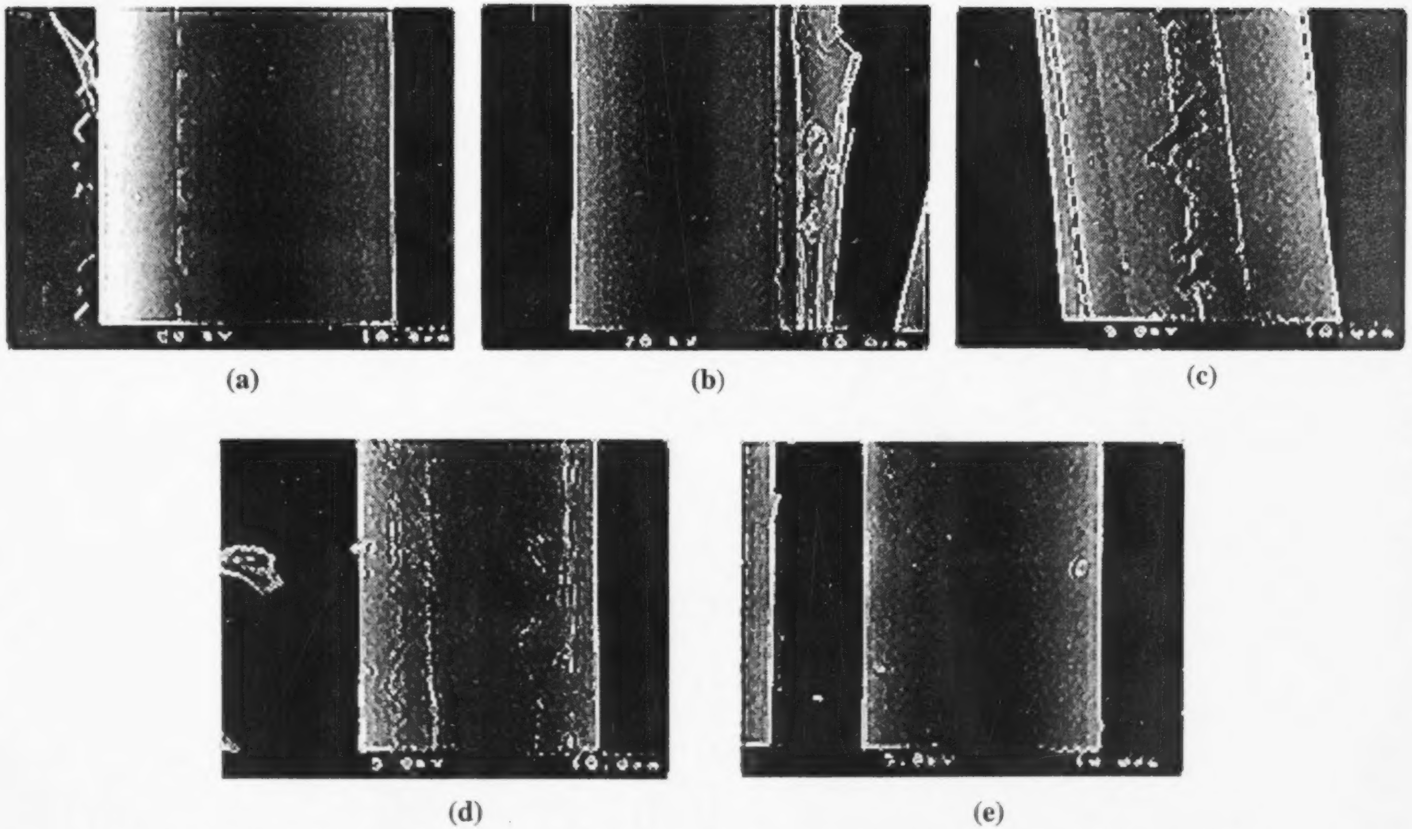

(a) (b) (c)

(d) (e)

Figure 3. Effect of plasma treatment on glass fibres, (a) Argon plasma treated fibre (150W, 10 mins.), (b) Argon plasma treated fibre (500W, 10 mins.), (c) Argon plasma treated fibre (1000W, 20 mins.), (d) Argon plasma treated fibre (1500W, 10 mins.) and (e) Oxygen plasma treated fibre (100W, 10 mins.).

APPENDIX B

B-1. Mechanical Properties of Composite Samples Determination

B-1.1: Tensile properties obtained from the Lloyds machine at NAIT

B-1.2: Tensile properties obtained from the MTS tester at U of A

B-2. Fibre and Void Volume Fraction Determination

B-2.1: Fibre volume fraction determination

B-2.2: Void volume fraction determination

B-1. Mechanical Properties of Composite Samples

B-1.1. Tensile properties obtained from the Lloyds machine at NAIT

The tensile properties were determined according to ASTM D638. The Lloyds machine at NAIT was used to perform the tensile tests on the dumb-bell shaped specimens under the following conditions of testing:

cross-head speed = 2 mm/ min

gauge length = 60 mm

strain rate = 3.0 % / min (i.e, cross-head speed / gauge length * 100)

The load (F)-extension (X) curve obtained from the Lloyds machine for the specimen ^{2}Untreated$_{T5}$ ($^2U_{T5}$) is shown below. This curve is representative of all other curves that were obtained from the Lloyds machine for other specimens.

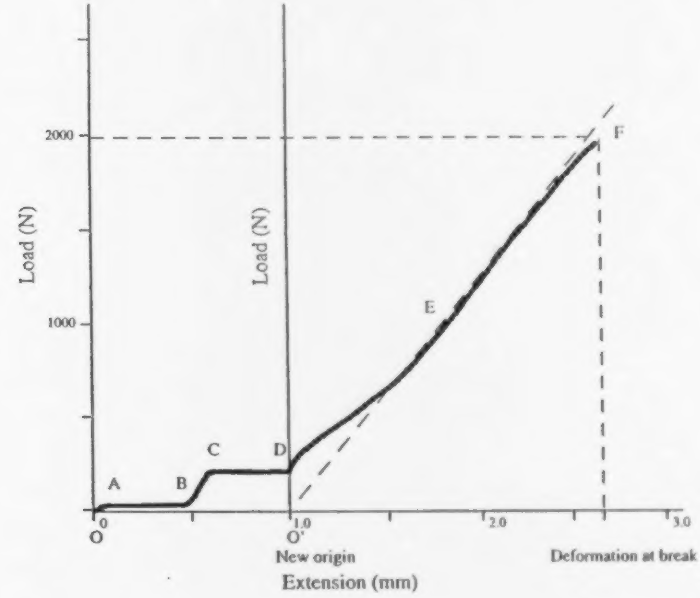

Figure 1. Tensile stress-strain curve obtained from LLOYDS Machine at NAIT.

As seen from the curve, the region CD apparently showed some slip occurring between the grips and the specimen, and the slip continued till the point E, beyond which the curve shows linearity. Because of the unusual nature of this curve, it was difficult to determine the tensile properties with confidence. Nevertheless, we chose a standard procedure to evaluate the curves, and thus be able to compare these curves. This procedure is outlined below:

The linear region (EF) of the curve was extrapolated (shown by dashed lines in the figure) to the extension axis and the point of intersection was considered as the new origin (O′). All the properties were determined from this new curve (O′EF). As is evident from the figure, the tensile load (load at break) remains unchanged even with the new origin.

The tensile properties were calculated as follows:

(i) Elastic modulus, E

$$E = \left|\frac{d\sigma}{d\varepsilon}\right|_{\varepsilon \to 0}$$

$$= \text{slope of tangent to the curve at limit of zero strain}$$

$$\text{For sample } {}^{2}U_{T5}\text{: } E = \frac{790}{4.35 \times 10^{-5} \times 0.5 / 60} \text{ Pa}$$

$$\therefore \quad E = 2.18 \times 10^{9} \text{ Pa}$$

$$= 2.18 \text{ GPa}$$

(ii) Tensile strength is the stress at which the material fails in a tensile test,

$$\sigma_b = F_b/A$$

where, A is the cross-sectional area,

For Sample: ${}^{2}U_{T5}$ (shown above),

F_b, load at breaking point = 2566 N

$A = 4.35 \times 10^{-5}$ mm2

$$\sigma_b = \frac{2566\,\text{N}}{4.35 \times 10^{-5}\,\text{m}^2}$$

$$= 59.00 \times 10^6 \ \frac{\text{N}}{\text{m}^2}$$

$$= 59.00 \text{ MPa}$$

(iii) Strain at break, ε_b

Strain at break is the strain at which the material fails in a tensile test.

The strain was determined by measuring distance from O′ to breaking point on x-axis, say d_b (deformation at break). This is divided by the gauge-length to obtain the value of strain at break (ε_b). Thus, for sample $^2U_{T5}$,

d_b (deformation at break) = 1.738mm

$$\varepsilon_b \text{ (strain at break)} = \frac{1.738\text{mm}}{60.00\text{mm}} = 0.0288 = 0.0288 \times 100 = 2.88\%$$

(iv) Toughness

Toughness is measured by measuring the area under the stress-strain curve from zero to breaking point.

Cross sectional area of the specimen, $^2U_{T5}$ = 4.35×10^{-5} m2

The area under the curve is assumed to be the same as the area under the triangle which is calculated using the formula,

$$\text{Area} = \frac{1}{2} \times \text{base} \times \text{height} = \frac{1}{2} \times \varepsilon_b \times \sigma_b$$

$$= \frac{1}{2} \times 0.0288 \times 59.00\,\text{MPa}$$
$$= 0.85\ \text{MPa}.$$

B-1.2. Tensile properties obtained from the MTS tester at U of A

A typical stress-strain curve obtained from the MTS tester at U of A is shown in the figure below. From these, the tensile properties were calculated as follows:

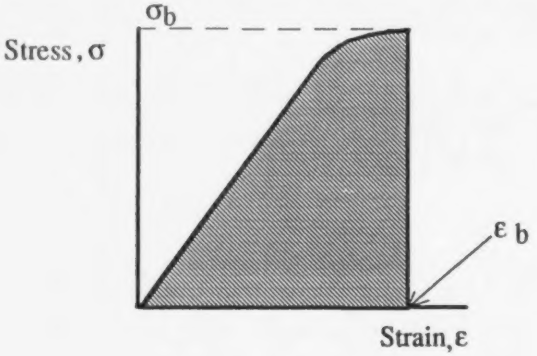

Sample calculations:

For sample ${}^3U_{T3}$

(i) Elastic modulus, E

$$E = \left|\frac{d\sigma}{d\varepsilon}\right|_{\varepsilon \to 0}$$

$$= \text{slope of tangent to the curve at limit of zero strain}$$

For sample ${}^3U_{T3}$ from Figure D-1 (Appendix D),

$$E = \frac{200(\text{lbf}) \times 4.4482(\text{N / lbf})}{(10.05 \times 4.53)(\text{mm}^2) \times (0.0047 - 0.0031)} \left[\frac{\text{N}}{\text{mm}^2}\right]$$

$$\therefore \quad E = 12.20 \times 10^9\ \text{Pa}$$

$$= 12.20\ \text{GPa}$$

(ii) Tensile strength, σ_b

F_b, load at breaking point = 810 lbf

$$A = 4.55 \times 10^{-5} \quad mm2$$

$$\sigma_b = \frac{810 lbf}{4.55 \times 10^{-5} m^2} \times 4.4482 \frac{N}{lbf}$$

$$= 79.14 \times 10^6 \quad \frac{N}{m^2}$$

$$= 79.14 \text{ MPa}$$

(ii) Strain at break, ε_b

The strain axis was: 1cm = 0.1%.

Accordingly, the strain at break ε_b was read out directly from the curve, and for the sample $^3U_{T3}$, this was 0.84%. Thus,

$$\varepsilon_b = 0.84 \%.$$

(iv) Toughness

Toughness is measured by measuring the area under the stress-strain curve from zero to breaking point.

The area under the stress-strain curve was obtained by a scanning technique with the aid of a computer.

For $^3U_{T3}$,

$$\text{Area} = 33.77 \text{ cm}^2$$

Calibration of the original chart paper: $1 \text{ cm}^2 = 0.1 \text{ lbf}$

$$\therefore \tau = \frac{33.77(\mathrm{cm}^2) \times 0.1(\mathrm{lbf} / \mathrm{in}^2) \times 4.4482(\mathrm{N} / \mathrm{lbf})}{4.55 \times 10^{-5}(\mathrm{m}^2)}$$

$$= 0.33 \times 10^{+6}\ \mathrm{Pa}$$

$$= 0.33\ \mathrm{MPa}.$$

B-2. Fibre and Void Volume Fraction Determination

Fibre and void volume fraction were determined by burning the known weight of samples (using crucible as containers) in the muffle furnace at 600°C for 30 minutes, putting the crucible into a desiccator, and allowing the heated samples to cool down to room temperature before weighing.

B-2.1. Fibre volume fraction, V_f(%)

The fibre volume fraction was calculated by the following equation:

$$V_f = \underline{\frac{W_f}{\rho_f}\cdot\rho_c \times 100}$$

where V_f = fibre volume fraction

W_f = fibre weight fraction

ρ_f = fibre density = 2.56 g/cm3 (ASTM:D 2734 - 70)

Sample $^1U_1$: W_f = 0.480

ρ_c = 1.55 g/cm3

ρ_f = 2.56 g/cm3

$$\therefore V_f = \frac{0.48}{2.54} \times 1.55 \times 100$$

$$= 28.96\ \%$$

***B-2.2**. Void volume fraction calculation, V_v (%)*

The void volume fraction was calculated by the following equation:

$$V_v = 100 - \rho_c\left(\frac{W_m}{\rho_m} + \frac{W_f}{\rho_f}\right) \times 100$$

where W_m = weight fraction of matrix, %

ρ_m = density of matrix (nylon 6), g/cm^3

ρ_c = density of composite, g/cm^3

For Sample $^1U_1$: W_m = 0.52

ρ_m = 1.14 g/cm^3

ρ_c = 1.55 g/cm^3

$$Vv = 100 - 1.55 \times \left(\frac{0.52}{1.14} + \frac{0.48}{2.56}\right) \times 100$$

$$= 0.08\ \%$$

APPENDIX C

Table C-1. Density, ρ

Table C-2. V_f and V_v

Table C-3. Average tensile properties of pure nylon and its composites (Data obtained from **Lloyds machine at NAIT**)

  Table C-3.1. Tensile properties for all specimens of pure nylon and its composites

Table C-4. Average tensile properties of pure nylon and its composites (Data obtained from **MTS tester at U of A**)

  Table C-4.1. Tensile properties for all specimens of pure nylon and its composites

Table C-5. $\overline{V_f}$, $\overline{V_v}$ and σ_b for pure nylon and its composites

TABLE C-1

Density Measurements

Type of Sample	Sample No.	Wt. of comp(C) in air (g)	Wt. of wire(W) in air (g)	Wt. of (C+W) densitomtr (g)	Corrected wt in acetone (g)	Density of composite (g/cm^3)	Average density (g/cm^3)	Standard deviation (g/cm^3)
Nylon 6	1	1.25	0.01	1.26	0.39	1.13		
(Circular config.)	2	1.49	0.01	1.49	0.45	1.12		
	3	1.25	0.01	1.25	0.39	1.13		
	4	1.48	0.01	1.48	0.46	1.13		
	5	2.33	0.01	2.33	0.72	1.13	**1.13**	**0.01**
Nylon 6	1	1.28	0.01	1.29	0.41	1.15		
(Rectangular config.)	2	1.32	0.01	1.33	0.41	1.14		
	3	1.45	0.01	1.46	0.45	1.13		
	4	1.64	0.01	1.64	0.51	1.13	**1.14**	**0.01**
[1]Untreated (Furn. Cl.)	1	1.00	0.01	1.01	0.49	1.53		
	2	1.42	0.01	1.43	0.71	1.55		
	3	2.15	0.01	2.15	1.04	1.52		
	4	2.96	0.01	2.96	1.45	1.53		
	5	1.16	0.01	1.16	0.61	1.63		
	6	1.24	0.01	1.24	0.61	1.53	**1.55**	0.04
[2]Untreated (Furn. Cl.)	1	1.03	0.01	1.03	0.50	1.49		
	2	1.20	0.01	1.20	0.59	1.53		
	3	1.19	0.01	1.19	0.57	1.50		
	4	1.45	0.01	1.46	0.72	1.54		
	5	1.44	0.01	1.44	0.70	1.52		
	6	1.33	0.01	1.33	0.64	1.50	**1.51**	**0.02**
[3]Untreated (Furn. Cl.)	1	0.84	0.01	0.84	0.42	1.54		
	2	1.11	0.01	1.11	0.56	1.57		
	3	1.12	0.01	1.13	0.55	1.53		
	4	1.13	0.01	1.13	0.56	1.54		
	5	1.06	0.01	1.06	0.52	1.52		
	6	0.99	0.01	0.99	0.48	1.52	**1.54**	**0.02**
Silane- IV (0.2%)	1	1.38	0.01	1.38	0.57	1.32		
	2	1.65	0.01	1.65	0.79	1.50		
	3	2.16	0.01	2.16	1.00	1.46		
	4	2.02	0.01	2.03	0.98	1.51		
	5	1.75	0.01	1.76	0.82	1.46		
	6	1.56	0.01	1.57	0.74	1.47	**1.46**	**0.05**
Silane-IV (0.5%)	1	2.06	0.01	2.06	0.95	1.46		
	2	2.11	0.01	2.11	0.97	1.44		
	3	2.25	0.01	2.25	1.08	1.51		

TABLE C-1 *(Continued p. 2)*

Density Measurements

Type of Sample	Sample No.	Wt. of comp(C) in air (g)	Wt. of wire(W) in air (g)	Wt. of (C+W) densitomtr (g)	Corrected wt in acetone (g)	Density of composite (g/cm^3)	Average density (g/cm^3)	Standard deviation (g/cm^3)
Silane-IV (0.5%)	4	1.95	0.01	1.96	0.95	1.53		
	5	1.55	0.01	1.55	0.71	1.45		
	6	2.23	0.01	2.21	1.05	1.47	**1.47**	**0.03**
^{1}Silane-IV (1.25%)	1	2.13	0.01	2.13	0.93	1.39		
	2	2.23	0.01	2.23	0.97	1.38		
	3	1.67	0.01	1.67	0.81	1.51		
	4	2.03	0.01	2.02	0.97	1.50		
	5	2.55	0.01	2.55	1.22	1.50		
	6	1.81	0.01	1.81	0.84	1.46	**1.46**	**0.04**
^{2}Silane-IV (1.25%)	1	0.85	0.01	0.85	0.39	1.44		
	2	0.98	0.01	0.98	0.46	1.46		
	3	1.22	0.01	1.23	0.58	1.49		
	4	0.97	0.01	0.97	0.47	1.50		
	5	0.89	0.01	0.89	0.42	1.46		
	6	1.01	0.01	1.01	0.47	1.46	**1.47**	**0.02**
Silane-IV (1.25%EtO	1	2.03	0.01	2.03	0.96	1.47		
	2	1.67	0.01	1.68	0.78	1.47		
	3	1.52	0.01	1.53	0.75	1.53		
	4	1.35	0.01	1.35	0.66	1.53		
	5	1.80	0.01	1.81	0.87	1.51		
	6	1.53	0.01	1.53	0.73	1.49	**1.50**	**0.03**
Silane-IV (1.37%+CL	1	1.15	0.01	1.16	0.49	1.35		
	2	1.66	0.01	1.67	0.78	1.46		
	3	1.73	0.01	1.73	0.83	1.49		
	4	1.79	0.01	1.79	0.85	1.49		
	5	1.84	0.01	1.84	0.87	1.48		
	6	1.65	0.01	1.65	0.77	1.46	**1.45**	**0.05**
Silane-IV (2%)	1	1.11	0.01	1.11	0.46	1.32		
	2		**Sample Misplaced**					
	3	0.89	0.01	0.89	0.43	1.48		
	4	0.78	0.01	0.78	0.37	1.47		
	5	1.39	0.01	1.39	0.67	1.51		
	6	1.40	0.01	1.40	0.66	1.47	**1.45**	**0.04**
Silane-V (0.2%)	1	1.16	0.01	1.16	0.51	1.38		
	2	1.80	0.01	1.81	0.88	1.53		
	3	1.87	0.01	1.88	0.91	1.52		
	4	1.36	0.01	1.37	0.65	1.48		

TABLE C-1 *(Continued p. 3)*

Density Measurements

Type of Sample	Sample No.	Wt. of comp(C) in air (g)	Wt. of wire(W) in air (g)	Wt. of (C+W) densitomtr (g)	Corrected wt in acetone (g)	Density of composite (g/cm³)	Average density (g/cm³)	Standard deviation (g/cm³)
Silane-V (0.2%)	5	1.38	0.01	1.39	0.64	1.44		
	6	1.90	0.01	1.90	0.90	1.49	**1.47**	**0.04**
[1]Silane-V (1.25%)	1*	1.35	0.01	1.35	0.73	1.68		
	2*	1.03	0.01	1.04	0.57	1.73		
	3	1.41	0.01	1.42	0.70	1.55		
	4	1.04	0.01	1.05	0.51	1.52		
	5*	0.98	0.01	0.99	0.52	1.63	**1.54**	**0.02**
[2]Silane-V (1.25%)	1*	1.44	0.01	1.44	0.74	1.60		
	2	1.49	0.01	1.50	0.73	1.53		
	3	2.02	0.01	2.03	1.02	1.58		
	4	1.37	0.01	1.37	0.67	1.53		
	5	1.41	0.01	1.42	0.72	1.58		
	6	0.98	0.01	0.98	0.47	1.50	**1.55**	**0.04**
Silane-V (2%)	1*	1.48	0.01	1.48	0.79	1.67		
	2*	1.33	0.01	1.34	0.70	1.63		
	3	1.99	0.01	2.00	0.97	1.52		
	4	1.78	0.01	1.79	0.89	1.56		
	5*	1.18	0.01	1.18	0.64	1.71		
	6*	1.17	0.01	1.17	0.65	1.73	**1.54**	**0.02**
Silane-III (0.2%)	1	1.05	0.01	1.05	0.49	1.45		
	2	1.22	0.01	1.23	0.60	1.51		
	3	1.29	0.01	1.29	0.64	1.54		
	4	1.19	0.01	1.19	0.58	1.53		
	5	1.35	0.01	1.35	0.66	1.51		
	6	1.23	0.01	1.23	0.58	1.48	**1.50**	**0.03**
Silane-III (1.25%)	1	0.98	0.01	0.98	0.46	1.46		
	2	1.04	0.01	1.04	0.50	1.49		
	3	0.96	0.01	0.97	0.46	1.48		
	4	1.15	0.01	1.15	0.57	1.55		
	5	1.30	0.01	1.30	0.62	1.48		
	6	1.13	0.01	1.13	0.52	1.43	**1.48**	**0.04**
Silane-III (2%)	1	1.24	0.01	1.24	0.49	1.30		
	2	1.39	0.01	1.39	0.66	1.49		
	3	0.92	0.01	0.93	0.46	1.55		

* Reading may be incorrect, because the sample was incompletely polymerized, and so the residual monomer/oligomer got burnt off when sample was dried , before carrying out density measurements

TABLE C-1 *(Continued p. 4)*

Density Measurements

Type of Sample	Sample No.	Wt. of comp(C) in air (g)	Wt. of wire(W) in air (g)	Wt. of (C+W) densitomtr (g)	Corrected wt in acetone (g)	Density of composite (g/cm³)	Average density (g/cm³)	Standard deviation (g/cm³)
Silane-III (2%)	4	1.25	0.01	1.25	0.60	1.50		
	5	1.24	0.01	1.24	0.59	1.49		
	6	1.26	0.01	1.27	0.55	1.38	**1.46**	**0.05**
Silane-I (5%)	1	2.75	0.01	2.76	1.14	1.39		
	2	4.13	0.01	4.13	1.98	1.51		
	3	2.92	0.01	4.73	1.39	1.49		
	4	4.72	0.01	3.05	2.10	1.41		
	5	3.04	0.01	3.05	1.35	1.41		
	6	3.52	0.01	3.52	1.62	1.45	**1.45**	**0.04**
Piranha Cleaned	1	2.92	0.01	2.93	1.34	1.44		
	2	2.49	0.01	2.49	1.24	1.55		
	3	3.21	0.01	3.21	1.35	1.35		
	4	2.51	0.01	2.51	1.13	1.42		
	5	2.79	0.01	2.79	1.15	1.33		
	6	3.01	0.01	3.02	1.37	1.43	**1.42**	**0.08**
HF Treated	1	1.94	0.01	1.95	0.72	1.24		
	2	2.49	0.01	2.50	1.04	1.34		
	3	4.15	0.01	4.16	1.92	1.46		
	4	3.40	0.01	3.41	1.62	1.49		
	5	3.51	0.01	3.51	1.43	1.32		
	6	5.00	0.01	5.00	2.02	1.32	**1.36**	**0.08**
Allied Composite	1	1.20	0.01	1.20	0.33	1.07		
	2	1.01	0.01	1.01	0.28	1.07		
	3	0.81	0.01	0.81	0.22	1.07		
	4	0.66	0.01	0.66	0.18	1.07	**1.07**	**0.00**
Untrtd.(Atmospheric)	1	1.58	0.01	1.58	0.72	1.44		
	2	1.45	0.01	1.45	0.68	1.46	**1.45**	**0.02**

TABLE C-2

Glass Fibre Volume Fraction and Void Volume Fraction

Type of Sample	Sample No.	Weight of composite (g)	Weight fibre (g)	Wt.fracn fibre (ωm)	Wt fracn Nylon (ωn)	Vol. fracn fibre V_f(%)	Vol.fracn Voids V_v(%)
[1]Untreated (Furn. Cl.)	1	0.999	0.42	0.42	0.58	25.33	-2.74
	2	1.42	0.68	0.48	0.52	28.96	0.08
	3	2.1464	0.99	0.46	0.54	27.19	0.90
	4	2.9601	1.41	0.48	0.52	28.45	1.43
	5	1.1589	0.57	0.49	0.51	31.48	-3.99
	6	1.2386	0.55	0.45	0.55	26.70	-0.55
Average				**0.46**	**0.54**	**28.02**	**-0.81**
Standard Deviation				**0.03**	**0.03**	**2.13**	**2.13**
[2]Untreated (Furn. Cl.)	1	1.034	0.46	0.45	0.55	26.12	1.64
	2	1.1971	0.59	0.49	0.51	29.30	2.38
	3	1.1866	0.60	0.51	0.49	29.64	5.36
	4	1.4526	0.74	0.51	0.49	30.74	3.00
	5	1.4369	0.68	0.47	0.53	28.20	1.39
	6	1.3269	0.61	0.46	0.54	26.99	2.08
Average				**0.48**	**0.52**	**28.50**	**2.64**
Standard Deviation				**0.02**	**0.02**	**1.73**	**1.45**
[3]Untreated (Furn. Cl.)	1	0.8376	0.42	0.50	0.50	30.15	2.83
	2	1.1086	0.55	0.50	0.50	30.47	0.45
	3	1.1212	0.55	0.49	0.51	29.21	2.13
	4	1.1261	0.56	0.50	0.50	30.09	1.97
	5	1.056	0.50	0.47	0.53	27.91	1.65
	6	0.9862	0.47	0.48	0.52	28.60	1.86
Average				**0.49**	**0.51**	**29.41**	**1.81**
Standard Deviation				**0.01**	**0.01**	**1.01**	**0.78**
Silane- IV (0.2%)	1	1.3762	0.41	0.30	0.70	15.96	0.41
	2	1.6476	0.75	0.45	0.55	26.68	1.25
	3	2.1551	0.98	0.46	0.54	26.03	4.49
	4	2.0222	0.96	0.48	0.52	28.06	2.35
	5	1.7513	0.74	0.42	0.58	24.01	1.55
	6	1.5621	0.68	0.43	0.57	24.92	1.77
Average				**0.42**	**0.58**	**24.28**	**1.97**
Standard Deviation				**0.06**	**0.06**	**4.31**	**1.39**
Silane-IV (0.5%)	1	2.0562	0.85	0.42	0.58	23.61	1.73
	2	2.1121	0.84	0.40	0.60	22.51	1.38
	3	2.248	1.04	0.46	0.54	27.15	1.46
	4	1.9534	0.91	0.47	0.53	27.83	0.79
	5	1.5494	0.59	0.38	0.62	21.62	0.15
	6	2.2303	0.95	0.42	0.58	24.33	1.45
Average				**0.42**	**0.58**	**24.51**	**1.16**
Standard Deviation				**0.03**	**0.03**	**2.50**	**0.58**

TABLE C-2 (Continued p.2)

Glass Fibre Volume Fraction and Void Volume Fraction

Type of Sample	Sample No.	Weight of composite (g)	Weight fibre (g)	Wt.fracn fibre (ωm)	Wt fracn Nylon (ωn)	Vol. fracn fibre V_f(%)	Vol.fracn Voids V_v(%)
[1]Silane-IV (1.25%)	1	2.1304	0.72	0.34	0.66	18.25	0.64
	2	2.2264	0.78	0.35	0.65	18.91	2.43
	3	1.6664	0.76	0.46	0.54	26.86	1.18
	4	2.0265	0.94	0.46	0.54	27.12	2.35
	5	2.5521	1.13	0.44	0.56	25.92	1.09
	6	1.8095	0.74	0.41	0.59	23.29	1.19
Average				**0.41**	**0.59**	**23.39**	**1.48**
Standard Deviation				**0.06**	**0.06**	**3.97**	**0.73**
[2]Silane-IV (1.25%)	1	0.8517	0.33	0.39	0.61	21.98	0.85
	2	0.9762	0.41	0.42	0.58	24.02	2.10
	3	1.2195	0.57	0.47	0.53	27.18	3.55
	4	0.9678	0.46	0.48	0.52	27.86	3.35
	5	0.8896	0.38	0.43	0.57	24.60	2.31
	6	1.0079	0.44	0.43	0.57	24.66	2.47
Average				**0.44**	**0.56**	**25.05**	**2.44**
Standard Deviation				**0.03**	**0.03**	**2.16**	**0.97**
Silane-IV (1.25%EtOH)	1	2.0317	0.89	0.44	0.56	25.17	2.14
	2	1.6747	0.80	0.48	0.52	27.38	5.48
	3	1.5245	0.75	0.49	0.51	29.48	2.09
	4	1.3451	0.65	0.48	0.52	28.73	1.87
	5	1.8041	0.88	0.49	0.51	28.76	3.31
	6	1.5313	0.70	0.46	0.54	26.54	2.37
Average				**0.47**	**0.53**	**27.68**	**2.88**
Standard Deviation				**0.02**	**0.02**	**1.62**	**1.37**
Silane-IV (1.37%+CL.)	1	1.1538	0.37	0.32	0.68	16.73	2.46
	2	1.6632	0.72	0.43	0.57	24.75	2.97
	3	1.7288	0.82	0.47	0.53	27.73	3.43
	4	1.7904	0.83	0.46	0.54	26.84	2.99
	5	1.8356	0.82	0.44	0.56	25.66	2.34
	6	1.6486	0.73	0.44	0.56	25.12	3.16
Average				**0.43**	**0.57**	**24.47**	**2.89**
Standard Deviation				**0.06**	**0.06**	**3.95**	**0.42**
Silane-IV (2%)	1	1.1099	0.37	0.33	0.67	17.38	3.40
	2	**Sample Misplaced**					
	3	0.8883	0.39	0.43	0.57	25.14	1.06
	4	0.7801	0.35	0.45	0.55	25.73	2.80
	5	1.3925	0.63	0.45	0.55	26.62	0.83
	6	1.4039	0.59	0.42	0.58	24.32	1.28
Average				**0.42**	**0.58**	**23.84**	**1.87**
Standard Deviation				**0.05**	**0.05**	**3.71**	**1.15**

TABLE C-2 (Continued, p.3)

Glass Fibre Volume Fraction and Void Volume Fraction

Type of Sample	Sample No.	Weight of composite (g)	Weight fibre (g)	Wt.fracn fibre (ωm)	Wt fracn Nylon (ωn)	Vol. fracn fibre V_f(%)	Vol.fracn Voids V_v(%)
Silane-V (0.2%)	1	1.1567	0.37	0.32	0.68	17.48	0.68
	2	1.8005	0.82	0.46	0.54	27.16	-0.14
	3	1.8743	0.87	0.46	0.54	27.60	1.03
	4	1.3645	0.59	0.43	0.57	24.95	1.14
	5	1.3834	0.58	0.42	0.58	23.85	3.00
	6	1.8978	0.73	0.38	0.62	22.36	-2.63
Average				**0.41**	**0.59**	**23.90**	**0.51**
Standard Deviation				**0.05**	**0.05**	**3.72**	**1.85**
[1]Silane-V (1.25%)	1	1.3467	0.93	0.69	0.31	45.70	8.79
	2	1.0296	0.75	0.73	0.27	49.43	9.85
	3	1.4075	0.70	0.50	0.50	30.16	1.88
	4	1.0409	0.51	0.49	0.51	28.94	2.32
	5	0.9841	0.71	0.72	0.28	46.00	14.01
Average				**0.49**	**0.51**	**29.55**	**2.10**
Standard Deviation				**0.01**	**0.01**	**0.87**	**0.32**
[2]Silane-V (1.25%)	1	1.4405	0.81	0.56	0.44	34.96	3.17
	2	1.4929	0.77	0.52	0.48	30.98	4.43
	3	2.0234	0.97	0.48	0.52	29.60	-1.29
	4	1.3696	0.68	0.49	0.51	29.47	2.51
	5	1.41	0.77	0.55	0.45	33.92	3.64
	6	0.9775	0.48	0.49	0.51	28.71	4.05
Average				**0.51**	**0.49**	**30.54**	**2.67**
Standard Deviation				**0.03**	**0.03**	**2.06**	**2.32**
Silane-V (2%)	1	1.4757	0.95	0.64	0.36	41.86	5.51
	2	1.3319	0.79	0.59	0.41	37.83	3.74
	3	1.9906	0.89	0.45	0.55	26.67	-0.33
	4	1.7839	0.86	0.48	0.52	29.27	0.02
	5	1.1815	0.76	0.64	0.36	42.97	3.73
	6	1.174	0.74	0.63	0.37	42.43	1.48
Average				**0.47**	**0.53**	**27.97**	**-0.15**
Standard Deviation				**0.02**	**0.02**	**1.84**	**0.25**
Silane-III (0.2%)	1	1.0487	0.44	0.42	0.58	23.83	2.72
	2	1.2248	0.57	0.47	0.53	27.61	1.73
	3	1.287	0.64	0.50	0.50	30.01	2.37
	4	1.1857	0.58	0.49	0.51	29.11	2.00
	5	1.3532	0.63	0.47	0.53	27.64	1.57
	6	1.2284	0.56	0.46	0.54	26.34	3.29
Average				**0.47**	**0.53**	**27.43**	**2.28**
Standard Deviation				**0.03**	**0.03**	**2.18**	**0.65**

TABLE C-2 (Continued, p.4)

Glass Fibre Volume Fraction and Void Volume Fraction

Type of Sample	Sample No.	Weight of composite (g)	Weight fibre (g)	Wt.fracn fibre (ωm)	Wt fracn Nylon (ωn)	Vol. fracn fibre V_f(%)	Vol.fracn Voids V_v(%)
Silane-III (1.25%)	1	0.9796	0.43	0.44	0.56	24.91	3.13
	2	1.039	0.46	0.45	0.55	26.01	1.70
	3	0.9607	0.45	0.47	0.53	27.02	4.13
	4	1.1484	0.57	0.50	0.50	30.29	1.77
	5	1.3031	0.58	0.45	0.55	25.78	2.04
	6	1.1331	0.48	0.42	0.58	23.58	3.57
Average				**0.45**	**0.55**	**26.27**	**2.72**
Standard Deviation				**0.03**	**0.03**	**2.29**	**1.03**
Silane-III (2%)	1	1.2381	0.38	0.31	0.69	16.49	1.07
	2	1.3865	0.62	0.45	0.55	26.10	1.80
	3	0.921	0.44	0.47	0.53	28.69	-0.12
	4	1.2489	0.57	0.46	0.54	26.79	2.15
	5	1.2402	0.56	0.46	0.54	26.42	2.56
	6	1.2635	0.45	0.36	0.64	19.16	2.86
Average				**0.42**	**0.58**	**23.94**	**1.72**
Standard Deviation				**0.07**	**0.07**	**4.89**	**1.10**
Silane-I (5%)	1	2.751	0.91	0.33	0.67	21.50	4.28
	2	4.1291	1.83	0.44	0.56	26.08	0.30
	3	2.9242	1.33	0.46	0.54	26.58	2.14
	4	4.7224	2.14	0.45	0.55	24.98	7.46
	5	3.0411	1.10	0.36	0.64	19.85	1.10
	6	3.5184	1.43	0.41	0.59	23.08	1.40
Average				**0.41**	**0.59**	**23.68**	**2.78**
Standard Deviation				**0.05**	**0.05**	**2.67**	**2.66**
Piranha Cleaned	1	2.9214	1.15	0.39	0.61	22.21	1.04
	2	2.4894	1.29	0.52	0.48	31.49	3.09
	3	3.207	0.91	0.28	0.72	15.01	0.15
	4	2.5079	0.88	0.35	0.65	19.59	-0.38
	5	2.7887	0.71	0.26	0.74	13.25	0.05
	6	3.0133	1.13	0.38	0.62	21.05	0.49
Average				**0.36**	**0.64**	**20.43**	**0.74**
Standard Deviation				**0.09**	**0.09**	**6.44**	**1.25**
HF Treated	1	1.9431	0.54	0.28	0.72	13.59	1.45
	2	2.4896	0.76	0.31	0.69	16.03	2.04
	3	4.149	1.70	0.41	0.59	23.25	1.26
	4	3.4037	1.48	0.44	0.56	25.35	0.95
	5	3.5112	0.96	0.27	0.73	14.06	1.69
	6	4.9989	1.33	0.27	0.73	13.74	1.58
Average				**0.33**	**0.67**	**17.67**	**1.50**
Standard Deviation				**0.07**	**0.07**	**4.87**	**0.37**

TABLE C-2 (Continued, p.5)

Glass Fibre Volume Fraction and Void Volume Fraction

Type of Sample	Sample No.	Weight of composite (g)	Weight fibre (g)	Wt.fracn fibre (ωm)	Wt fracn Nylon (ωn)	Vol. fracn fibre V_f(%)	Vol.fracn Voids V_v(%)
Allied Composite	1	1.1997	0.00	0.00	1.00	0.10	6.28
	2	1.0072	0.00	0.00	1.00	0.09	6.13
	3	0.8068	0.00	0.00	1.00	0.09	6.00
	4	0.6592	0.00	0.00	1.00	0.10	5.99
Average				**0.00**	**1.00**	**0.09**	**6.10**
Standard Deviation				**0.00**	**0.00**	**0.00**	**0.14**
Untrtd.(Atmospheric)	1	1.581	0.62	0.39	0.61	21.91	1.22
	2	1.4503	0.59	0.41	0.59	23.28	0.73
Average				**0.40**	**0.60**	**22.60**	**0.98**
Standard Deviation				**0.01**	**0.01**	**0.97**	**0.35**

Table C-3. Average tensile properties of pure nylon 6 and its composites

Data obtained on Lloyds Machine at NAIT

(RH: 66%; Temperature: 22° C)
E: Elastic modulus; σ_b: Tensile strength; ε_b: Strain at break; τ: Toughness

Type of Disk	E (GPa)	σ_b (MPa)	ε_b * (%)	τ (MPa)
Pure nylon 6 (R)	0.71 ± 0.05	65.93 ± 7.08	9.90 ± 2.46	3.32 ± 0.85
Pure nylon 6 (C)	1.12 ± 0.20	27.39 ± 5.44	1.48 ± 0.36	0.88 ± 0.35
[1]Untreated	2.36 ± 0.27	54.60 ± 2.16	2.50 ± 0.36	0.71 ± 0.16
[2]Untreated	2.19 ± 0.12	53.00 ± 0.77	2.55 ± 0.10	0.68 ± 0.02
[1]Untreated (Atm.)#	0.69 ± 0.16	48.11 ± 1.38	7.75 ± 1.66	1.87 ± 0.43
Piranha Cleaned	1.42 ± 0.08	48.56 ± 1.95	3.70 ± 0.19	0.91 ± 0.03
HF treated	1.99 ± 0.11	79.88 ± 12.95	4.26 ± 0.56	1.73 ± 0.47
Silane-I (5%)	1.86 ± 0.04	61.73 ±2.01	3.62 ± 0.06	1.12 ± 0.01
Silane-IV (0.2%)	1.64 ± 0.04	82.17 ± 12.74	4.29 ± 0.67	1.79 ± 0.52
Silane-IV (0.5%)	1.62 ± 0.02	82.47 ± 2.56	4.48 ± 0.22	1.85 ± 0.14
[1]Silane-IV(1.25%)	2.16 ± 0.57	110.13 ± 19.73	4.35 ± 0.46	2.02 ± 0.40
Silane-IV (2%)	1.95 ± 0.09	77.49 ± 3.45	4.11 ± 0.12	1.59 ± 0.11

*** affected strain because of slippage of jaws as described on p. 95, chapter 6**

R Rectangular configuration nylon disk

C Circular configuration nylon disk

# Disk fabricated with gravity feed of monomer into the mold

TABLE C-3.1

Tensile properties for all specimens of pure nylon 6 and its composites

Data obtained on Lloyds Machine at NAIT

RH: 66%; Temperature: 22^0 C

E: Elastic modulus; σ_b: Tensile Strength; ε_b: Strain at break; τ: Toughness

Type of Disk	**Specimen**	E (GPa)	σ_b (MPa)	ε_b (%)	τ (MPa)	**Width (mm)**	**Breadth (mm)**
Pure nylon 6 (R)	T2	0.76	62.25	7.61	2.37	3.28	4.48
	T4	0.70	74.10	9.6	3.57	3.28	4.36
	T8	0.67	61.45	12.5	4.02	3.26	1.71
Average		0.71	65.93	9.90	3.32	3.27	3.52
Standard deviation		0.05	7.08	2.46	0.85	0.01	1.57
Pure nylon 6 (C)	T1	0.93	24.78	2.56	0.80	10.44	4.14
	T3	1.31	23.75	1.81	0.58	10.45	4.03
	T5	1.13	33.65	3.02	1.27	10.33	4.05
Average		1.12	27.39	2.46	0.88	10.41	4.07
Standard deviation		0.20	5.44	0.61	0.35	0.07	0.06
[1]Untreated	T1		Data not saved by the computer				
(Furnace-cleaned)	T2		Data not saved by the computer				
	T3	2.66	52.30	2.10	0.55	10.13	4.51
	T4	2.17	56.58	2.78	0.86	10.09	4.49
	T5	2.25	54.92	2.63	0.72	10.00	4.48
Average		2.36	54.60	2.50	0.71	10.07	4.49
Standard deviation		0.27	2.16	0.36	0.16	0.07	0.02
[2]Untreated	T1	2.44	54.90	2.36	0.65	9.95	4.24
(Furnace-cleaned)	T2	2.10	52.20	2.60	0.68	10.06	4.28
	T3	**1.94**	**45.18**	**2.40**	**0.54**	**10.00**	**4.25**
	T4	2.20	53.19	2.57	0.68	10.10	4.32
	T5	2.18	59.00	2.88	0.85	10.02	4.34
Average		2.19	53.00	2.55	0.68	10.01	4.26
Standard deviation		0.12	0.77	0.10	0.02	0.08	0.03
[1]Untreated (Atm.)	T1	0.88	46.59	5.82	1.36	3.30	5.25
(Furnace-cleaned)	T2	0.76	49.61	7.26	1.80	3.32	5.35
	T3	0.62	47.36	8.14	1.93	3.27	5.38
	T5	0.51	48.89	9.79	2.40	3.30	5.49
Average		0.69	48.11	7.75	1.87	3.30	5.37
Standard deviation		0.16	1.38	1.66	0.43	0.02	0.10

All bold-faced readings ignored because these showed small stones at their fracture surface, and hence did not represent the true value for the specimen.

TABLE C-3.1 *(Continued, p.2)*

Tensile properties for all specimens of pure nylon 6 and its composites

Data obtained on Lloyds Machine at NAIT

RH: 66%; Temperature: 22^0 C

E: Elastic modulus; σ_b: Tensile Strength; ε_b: Strain at break; τ: Toughness

Type of Disk	**Specimen**	**E (GPa)**	**σ_b (MPa)**	**ε_b (%)**	**τ (MPa)**	**Width (mm)**	**Breadth (mm)**
Piranha-cleaned	T1	1.27	53.49	4.72	1.26	10.12	4.63
	T2	1.29	45.10	3.65	0.82	10.55	4.58
	T3	1.45	40.86	2.95	0.60	10.11	4.56
	T4	1.56	47.97	3.23	0.77	10.43	4.52
	T5	1.56	56.74	3.82	1.08	10.22	4.46
Average		1.42	48.56	3.70	0.91	10.12	4.60
Standard deviation		0.08	1.95	0.19	0.03	0.01	0.05
HF-treated	T1	**1.52**	**51.23**	**3.58**	**0.92**	**9.98**	**4.53**
	T2	1.90	78.60	4.41	1.73	9.95	4.51
	T3	2.14	92.02	4.58	2.11	10.25	4.47
	T4	1.98	86.59	4.62	2.00	10.20	4.53
	T5	1.92	62.30	3.44	1.07	9.84	4.48
Average		1.99	79.88	4.26	1.73	10.06	4.50
Standard deviation		0.11	12.95	0.56	0.47	0.20	0.03
Silane-I (5%)	T1	2.04	63.00	3.44	0.96	10.35	4.76
	T2	1.89	63.35	3.47	1.10	10.52	4.75
	T3	1.83	63.42	3.58	1.13	10.40	4.73
	T4	1.77	62.70	3.68	1.15	10.41	4.66
	T5	1.73	57.62	3.89	1.26	10.33	4.63
Average		1.89	62.02	3.67	1.11	10.34	4.70
Standard deviation		0.22	2.48	0.32	0.21	0.01	0.09
Silane-IV (0.2%)	T1	1.63	87.03	4.62	2.01	10.24	4.51
Toluene solvent	T2	1.65	93.69	4.83	2.26	10.22	4.53
	T3	1.59	76.80	4.10	1.59	10.12	4.60
	T4	1.70	71.17	3.60	1.30	10.15	4.61
	T5	**1.64**	**63.72**	**3.30**	**1.06**	**10.17**	**4.62**
Average		1.64	82.17	4.29	1.79	10.18	4.57
Standard deviation		0.04	12.74	0.67	0.52	0.04	0.05

All bold-faced readings ignored because these showed small stones at their fracture surface, and hence did not represent the true value for the specimen.

TABLE C-3.1 *(Continued, p.3)*

Tensile properties for all specimens of pure nylon 6 and its composites

Data obtained on Lloyds Machine at NAIT

RH: 66%; Temperature: 22° C

E: Elastic modulus; σ_b: Tensile Strength; ε_b: Strain at break; τ: Toughness

Type of Disk	**Specimen**	**E** **(GPa)**	**σ_b** **(MPa)**	**ε_b** **(%)**	**τ** **(MPa)**	**Width** **(mm)**	**Breadth** **(mm)**
Silane-IV (0.5%)	T1	**4.21**	**51.31**	**0.03**	0.79	**10.12**	**4.50**
Toluene solvent	T2	1.62	85.46	4.69	2.00	10.12	4.52
	T3	1.58	83.41	4.60	1.91	10.12	4.52
	T4	1.63	79.48	4.20	1.68	10.12	4.55
	T5	1.63	81.53	4.41	1.80	10.15	4.55
Average		1.62	82.47	4.48	1.85	10.13	4.54
Standard deviation		0.02	2.56	0.22	0.14	0.01	0.02
[1]Silane-IV (1.25%)	T1	3.01	132.50	4.10	1.83	10.10	4.55
Toluene solvent	T2	**1.89**	**83.11**	**3.92**	**1.63**	**10.13**	**4.57**
	T3	1.81	102.7	4.97	2.55	10.12	4.58
	T4	1.92	95.19	4.40	2.08	10.13	4.60
Average	T5	2.16	110.13	4.35	2.02	10.12	4.58
Standard deviation		0.57	19.73	0.46	0.40	0.01	0.02
Silane-IV (2%)	T1	1.84	72.37	3.96	1.43	10.20	4.71
Toluene solvent	T2	1.93	78.92	4.2	1.65	10.25	4.70
	T3	**1.93**	**60.37**	**3.3**	**1.00**	**10.22**	**4.70**
	T4	2.04	78.75	4.06	1.60	10.15	4.63
	T5	1.97	79.93	4.2	1.68	10.25	4.59
Average		1.95	77.49	4.11	1.59	10.21	4.66
Standard deviation		0.09	3.45	0.12	0.11	0.05	0.06

All bold-faced readings ignored because these showed small stones at their fracture surface, and hence did not represent the true value for the specimen.

Table C-4. Average tensile properties of pure nylon 6 and its composites

Data obtained on MTS tester, University of Alberta

(RH: 66%; Temperature: 22° C)
E: Elastic modulus; σ_b: Tensile strength; ε_b: Strain at break; τ: Toughness

Type of Disk	E (GPa)	σ_b (MPa)	ε_b (%)	τ (MPa)
Pure nylon (R)[#]	2.18	62.54	4.95	0.86
[3]Untreated	10.90 ± 0.94	82.14 ± 4.20	0.94 ± 0.12	0.43 ± 0.12
Silane-III (0.2%)	11.07 ± 2.15	90.28 ± 5.17	1.08 ± 0.17	0.53 ± 0.11
Silane-III (1.25%)	10.94 ± 0.61	91.72 ± 8.92	1.11 ±0.11	0.57 ± 0.09
Silane-III (2%)	10.02 ± 0.67	86.03 ±4.39	1.10 ± 0.15	0.50 ± 0.11
[2]Silane-IV(1.25%)	14.77 ± 2.56	111.55 ±3.60	0.91 ± 0.09	0.56 ± 0.05
Silane-IV(1.25%EtOH)	14.05 ± 1.59	101.32 ± 10.48	1.00 ± 0.02	0.57 ± 0.05
Silane-IV(1.37%+CL)	13.39 ± 0.88	101.63 ± 4.18	0.94 ± 0.09	0.51 ± 0.06
Silane-V (0.2%)	13.66 ± 1.00	107.46 ± 8.75	0.98 ± 0.10	0.54 ± 0.10
[1]Silane-V (1.25%)	10.65 ± 1.22	67.90 ± 7.89	0.83 ± 0.18	0.30 ± 0.10
[2]Silane-V (1.25%)	13.59 ± 2.05	110.51 ± 12.12	1.01 ± 0.12	0.56 ± 0.11
Silane-V (2%)	12.53 ± 1.68	89.40 ± 4.13	0.91 ± 0.18	0.48 ± 0.13
Alld Chem. pure nylon 6[#]	2.10	58.32	> 15%	6.20
Allied Chemicals nylon 6 composite[#]	2.02	47.18	> 15%	4.29

# Only one sample available for testing.

TABLE C-4.1

Tensile properties for all specimens of pure nylon 6 and its composites

Data obtained on MTS tester, U of A

RH: 66%; Temperature: 22^{0} C

E: Elastic modulus; σ_b: Tensile Strength; ε_b: Strain at break; τ: Toughness

Type of Disk	Specimen	E (GPa)	σ_b (MPa)	ε_b (%)	τ (MPa)	Width (mm)	Breadth (mm)
Pure nylon 6 (R)	T6	2.2	62.54	4.95	0.86	3.27	4.35
[3]Untreated	T1	11.20	78.42	0.84	0.34	10.04	4.52
	T3	12.20	79.14	0.84	0.33	10.05	4.53
	T5	9.67	82.68	1.05	0.58	10.11	4.55
	T2	11.04	81.45	0.88	0.36	9.93	4.51
	T4	10.40	89.00	1.10	0.52	9.93	4.53
Average		10.90	82.14	0.94	0.43	10.01	4.53
Standard deviation		0.94	4.20	0.12	0.12	0.08	0.01
Silane-III (0.2%)	T1	10.30	85.72	1.10	0.54	10.00	4.80
	T3	10.97	90.00	1.23	0.67	10.02	4.76
	T5	9.41	84.68	1.08	0.52	10.08	4.69
	T2	14.77	95.99	0.80	0.37	10.04	4.80
	T4	9.90	94.99	1.20	0.55	10.02	4.72
Average		11.07	90.28	1.08	0.53	10.03	4.75
Standard deviation		2.15	5.17	0.17	0.11	0.03	0.05
Silane-III (1.25%)	T1	11.18	86.97	0.98	0.47	10.00	4.68
	T3	11.82	83.21	0.99	0.50	10.03	4.69
	T5	10.16	85.94	1.17	0.56	9.95	4.63
	T2	10.79	99.14	1.20	0.67	10.11	4.66
	T4	10.73	103.33	1.20	0.65	9.97	4.62
Average		10.94	91.72	1.11	0.57	10.01	4.66
Standard deviation		0.61	8.92	0.11	0.09	0.06	0.03
Silane-III (2%)	T1	11.16	85.40	0.87	0.33	10.06	4.66
	T3	9.90	80.91	1.04	0.46	10.06	4.70
	T5	9.38	83.95	1.23	0.56	10.09	4.70
	T2	9.91	92.72	1.20	0.60	10.14	4.66
	T4	9.77	87.15	1.14	0.53	10.00	4.67
Average		10.02	86.03	1.10	0.50	10.07	4.68
Standard deviation		0.67	4.39	0.15	0.11	0.05	0.02

TABLE C-4.1 *(Continued, p.2)*

Tensile properties for all specimens of pure nylon 6 and its composites

Data obtained on MTS tester, U of A

RH: 66%; Temperature: 22^{0} C

E: Elastic modulus; σ_b: Tensile Strength; ε_b: Strain at break; τ: Toughness

Type of Disk	**Specimen**	**E** **(GPa)**	**σ_b** **(MPa)**	**ε_b** **(%)**	**τ** **(MPa)**	**Width** **(mm)**	**Breadth** **(mm)**
[2]Silane-IV (1.25%)	T1	13.01	107.53	1.01	0.58	9.97	4.73
	T3	19.26	109.26	0.77	0.48	10.09	4.64
	T5	14.33	114.15	0.91	0.57	10.04	4.58
	T2	13.51	116.31	0.93	0.60	10.03	4.69
	T4	13.72	110.48	0.95	0.56	10.11	4.58
Average		14.77	111.55	0.91	0.56	10.05	4.64
Standard deviation		2.56	3.60	0.09	0.05	0.05	0.07
Silane-IV(1.25%EtOH)	T1	**14.96**	**65.90**	**0.45**	**0.14**	**10.30**	**4.62**
	T3	15.66	115.12	1.02	0.65	10.32	4.68
	T5	12.31	103.06	0.98	0.54	9.72	4.72
	T2	15.10	96.28	0.98	0.55	10.20	4.62
	T4	13.11	90.81	1.00	0.54	10.24	4.64
Average		14.05	101.32	1.00	0.57	10.12	4.67
Standard deviation		1.59	10.48	0.02	0.05	0.27	0.04
Silane-IV (1.37%+CL)	T1	12.92	98.32	1.04	0.56	10.15	4.68
	T3	13.83	96.17	0.87	0.42	10.16	4.78
	T5	13.79	103.49	1.00	0.56	10.19	4.80
	T2	14.31	106.06	0.82	0.47	10.13	4.72
	T4	12.10	104.10	0.96	0.53	10.28	4.78
Average		13.39	101.63	0.94	0.51	10.18	4.75
Standard deviation		0.88	4.18	0.09	0.06	0.06	0.05
Silane-V (0.2%)	T1	14.40	106.26	1.04	0.58	10.23	4.53
	T3	13.58	117.84	1.02	0.65	10.22	4.58
	T5	13.93	98.96	0.84	0.44	10.22	4.53
	T2	14.41	99.21	0.92	0.42	10.14	4.51
	T4	11.98	115.01	1.10	0.60	10.20	4.55
Average		13.66	107.46	0.98	0.54	10.20	4.54
Standard deviation		1.00	8.75	0.10	0.10	0.04	0.03

All bold-faced readings ignored because these showed small stones at their fracture surface, and hence did not represent the true value for the specimen.

TABLE C-4.1 *(Continued, p.3)*

Tensile properties for all specimens of pure nylon 6 and its composites

Data obtained on MTS tester, U of A

RH: 66%; Temperature: 22^0 C

E: Elastic modulus; σ_b: Tensile Strength; ε_b: Strain at break; τ: Toughness

Type of Disk	**Specimen**	**E (GPa)**	**σ_b (MPa)**	**ε_b (%)**	**τ (MPa)**	**Width (mm)**	**Breadth (mm)**
[1]Silane-V (1.25%)	T1	12.01	77.85	0.79	0.32	10.15	4.56
	T3	10.51	72.62	1.04	0.44	10.12	4.60
	T5	11.54	57.71	0.56	0.16	10.12	4.57
	T2	10.30	68.33	0.83	0.30	10.12	4.49
	T4	8.88	63.01	0.91	0.30	10.24	4.55
Average		10.65	67.90	0.83	0.30	10.15	4.55
Standard deviation		1.22	7.89	0.18	0.10	0.05	0.04
[2]Silane-V (1.25%)	T1	12.53	101.55	1.08	0.59	10.23	4.53
	T3	16.92	122.72	0.94	0.60	10.10	4.45
	T5	13.79	113.25	1.04	0.58	10.15	4.45
	T2	11.50	120.41	1.15	0.66	10.18	4.50
	T4	13.21	94.61	0.85	0.38	10.09	4.45
Average		13.59	110.51	1.01	0.56	10.15	4.48
Standard deviation		2.05	12.12	0.12	0.11	0.06	0.04
Allied Chmcl.nylon 6		2.10	58.32	> 15%	6.20	10.17	3.15
Allied Chmcl.nylon 6 Composite		2.02	47.18	> 15%	4.29	9.98	3.07

Table C-5. Average glass fibre volume fraction (Vf, %), Void volume fraction (Vv, %), and Tensile strength (σ_b) for pure nylon 6 and its composites

(RH: 66%; Temperature: 22° C)

Disc Description	Glass fibre volume fraction, V_f, (%)	Void volume fraction, V_v, (%)	Average Tensile strength, (σ_b), (MPa)
Pure nylon 6 (R)[#]	0	6.00 ± 2.67	62.54
Pure nylon 6 (R) [*]	0	6.00 ± 2.67	65.93 ± 5.83
Pure nylon 6 (C) [*]	0	14.25 ± 12.14	27.39 ± 5.44
^{1}Untreated	28.02 ± 2.13	-0.81 ± 2.13	54.60 ± 2.16
^{2}Untreated	28.50 ± 1.73	2.64 ± 1.45	53.00 ± 0.77
^{3}Untreated	29.41 ± 1.01	1.81 ± 0.78	82.14 ± 4.20
^{1}Untreated (Atm.)	22.60 ± 0.97	0.98 ± 0.35	48.11 ± 2.06
Piranha Cleaned	20.43 ± 6.44	0.74 ± 1.25	48.56 ± 1.95
HF treated	17.67 ± 4.87	1.50 ± 0.37	79.88 ± 12.95
Silane-I (5%)	23.68 ± 2.67	2.78 ± 2.66	61.73 ± 2.01
Silane-III (0.2%)	27.43 ± 2.18	2.28 ± 0.65	90.28 ± 5.17
Silane-III (1.25%)	26.27 ± 2.29	2.72 ± 1.03	91.72 ± 8.92
Silane-III (2%)	23.94 ± 4.89	1.72 ± 1.10	86.03 ±4.39
Silane-IV (0.2%)	24.28 ± 4.31	1.97 ± 1.39	82.17 ± 12.74
Silane-IV (0.5%)	24.51 ± 2.50	1.16 ± 0.58	82.47 ± 2.56
^{1}Silane-IV(1.25%)	23.39 ± 3.97	1.48 ± 0.73	110.13 ± 19.73
^{2}Silane-IV(1.25%)	25.05 ± 2.16	2.44 ± 0.97	111.55 ± 3.60
Silane-IV(1.25%EtOH)	27.68 ± 1.62	2.88 ± 1.37	101.32 ± 10.48
Silane-IV(1.37%+CL)	24.47 ± 3.95	2.89 ± 0.42	101.63 ± 4.18
Silane-IV (2%)	23.84 ± 3.71	1.87 ± 1.15	77.49 ± 3.45
Silane-V (0.2%)	23.90 ± 3.72	0.51 ± 1.85	107.46 ± 8.75
^{1}Silane-V (1.25%)	29.55 ± 0.87	2.10 ± 0.32	67.90 ± 7.89
^{2}Silane-V (1.25%)	30.54 ± 2.06	2.67 ± 2.32	110.51 ± 12.12
Silane-V (2%)	27.97 ± 1.84	-0.15 ± 0.25	89.40 ± 4.13
Allied Chemicals pure nylon	0.00	Not analysed	58.32
Allied Chemicals nylon 6 composite[#]	0.10	6.10 ± 0.14	47.18

# data obtained on MTS tester, University of Alberta.

**** data obtained on Lloyds machine, NAIT.***

TABLE C-6.1(a)

Izod impact tests of all specimens

RH:63- 66%; Temperature: 22-23° C

Es: Breaking energy per notch width

Type of Disk	FAILURE CODE	A mm	E mm	W mm	E_s (J/m)
Pure nylon 6 (R)	C	10.85	12.67	4.46	37.53
	C	10.72	12.53	4.42	41.57
	C	10.82	12.63	4.40	35.18
Average					38.09
Standard deviation					3.26
Pure nylon 6 (C)	C	10.80	12.61	4.04	0.00
	C	10.78	12.59	4.01	0.00
	C	10.82	12.64	4.07	0.00
Average					0.00
Standard deviation					0.00
[1]Untreated	P	10.87	12.65	4.50	174.46
Furnace-cleaned	P	10.86	12.66	4.55	0.00
	P	10.93	12.72	4.50	198.28
	P	10.72	12.66	4.51	190.01
	P	10.93	12.69	4.45	0.00
	P	10.76	12.67	4.46	0.00
Average					187.58
Standard deviation					12.12
[2]Untreated	P	10.8	12.79	4.23	0.00
Furnace-cleaned	P	10.91	12.76	4.27	0.00
	P	10.83	12.77	4.27	180.11
	P	10.93	12.77	4.29	217.88
	P	10.86	12.78	4.30	197.12
	P	10.96	12.76	4.42	0.00
Average					198.36
Standard deviation					18.93
Piranha-cleaned	P	10.56	12.6	4.66	235.30
	P	10.38	12.45	4.55	195.86
	P	10.32	12.37	4.46	0.00
		SAMPLE MISPLACED			
	P	10.41	12.34	4.56	215.60
	P	10.39	12.32	4.56	0.00
Average					215.59
Standard deviation					19.72

TABLE C-6.1(a) *(Continued p.2)*

Izod impact tests of all specimens

RH:63- 66%; Temperature: 22-23 ^{0} C

Es: Breaking energy per notch width

Type of Disk	FAILURE CODE	A mm	E mm	W mm	E_s (J/m)
Silane-I (5%)	P	10.4	12.33	4.74	267.00
	P	10.29	12.31	4.65	0.00
	P	10.36	12.39	4.7	0.00
	P	10.3	12.5	4.64	297.12
	P	10.27	12.5	4.65	0.00
	P	10.42	12.36	4.58	0.00
Average					282.06
Standard deviation					21.30
HF-treated	C	10.41	12.46	4.45	119.5
	P	10.35	12.32	4.44	0
	P	10.28	12.37	4.47	161.35
	P	10.3	12.38	4.45	166.21
	P	10.51	12.33	4.48	0
	C	10.34	12.34	4.42	123.56
Average					142.66
Standard deviation					20.56
Silane-IV (0.2%)	P	10.25	12.56	4.52	165.42
	P	10.32	12.35	4.53	0.00
	P	10.19	12.46	4.58	188.25
	P	10.35	12.48	4.55	0.00
	P	10.48	12.62	4.54	201.02
	P	10.32	12.28	4.55	0.00
Average					184.90
Standard deviation					18.04
Silane-IV (0.5%)	P	10.28	12.56	4.51	0.00
	P	10.18	12.51	4.52	0.00
	P	10.23	12.61	4.52	0.00
	P	10.25	12.66	4.55	184.91
	P	10.41	12.54	4.55	164.52
	P	10.21	12.59	4.54	0.00
Average					174.72
Standard deviation					14.42
[1]**Silane-IV (1.25%)**	P	10.28	12.66	4.56	134.35
	C	10.42	12.53	4.6	114.25
	C	10.26	12.54	4.57	0.00
	C	10.32	12.58	4.49	100.81
	C	10.36	12.34	4.56	0.00

TABLE C-6.1(a)*(Continued, p.3)*

Izod impact tests of all specimens

RH:63- 66%; Temperature: 22-23° C

Es: Breaking energy per notch width

Type of Disk	**FAILURE** **CODE**	**A** **mm**	**E** **mm**	**W** **mm**	**E_s** **(J/m)**
[1]Silane-IV (1.25%)	P	10.35	12.46	4.55	0.00
	P	10.23	12.59	4.54	0.00
Average					116.47
Standard deviation					16.89
Silane-IV (2%)	C	10.27	12.42	4.72	0.00
	C	10.36	12.08	4.71	130.91
	P	10.47	12.58	4.78	159.76
	P	10.32	12.55	4.70	0.00
	P	10.42	12.21	4.63	155.32
	P	10.29	12.37	4.56	0.00
	P	10.29	12.23	4.65	0.00
Average					148.66
Standard deviation					15.53

TABLE C-6.2

Izod impact tests on all specimens

RH: 63-66%; Temperature: 22-23^0 C

Type of Disk	Failure code	Type of Disk	Failure code
[3]Untreated	P	Silane-IV (1.37%+CL)	P
	P		C
	P		C
	P		P
	P		P
			C
Silane-III (0.2%)	P	Silane-V (0.2%)	C
	P		C
	P		P
	P		P
	P		C
	C		P
Silane-III (1.25%)	C	[1]Silane-V (1.25%)	P
	P		P
	P		P
	P		P
	P		P
	P		P
Silane-III (2%)	P	[2]Silane-V (1.25%)	C
	P		C
	P		C
	P		P
	C		P
	P		C
[2]Silane-IV (1.25%)	C	Allied Chmcl.nylon 6	P
	C		
	P	Allied Chmcl.nylon 6	P
	C	Composite	
	C		
	C		
Silane-IV(1.25%EtOH)	C		
	C		
	C		
	P		
	P		

APPENDIX D

Load-strain Curves of Nylon 6/Glass fibre composites
(using MTS tester at U of A)

Figure 1.	(a) ^{3}Untreated glass fibre composite (b) ^{2}Silane-IV(1.25%)-treated glass fibre composite
Figure 2.	(a) Silane-III (1.25%)-treated glass fibre composite (b) Silane-III (0.2%)-treated glass fibre composite
Figure 3.	(a) Silane-III (2.00%)-treated glass fibre composite
Figure 4.	(a) Allied Chemicals pure nylon 6 and its glass fibre composite
Figure 5.	Silane-V (0.2%)-treated glass fibre composite on different scales (a) inch scale (b) Centimetre scale
Figure 6.	^{1}Silane-V (1.25%)-treated glass fibre composite on different scales (a) inch scale (b) Centimetre scale
Figure 7.	Silane-V (2.00%)-treated glass fibre composite on different scales (a) inch scale (b) Centimetre scale
Figure 8.	Silane-IV (1.25% EtOH)-treated glass fibre composite on different scales (a) inch scale (b) Centimetre scale
Figure 9.	^{2}Silane-V(1.25%)-treated glass fibre composite on different scales (a) inch scale (b) Centimetre scale
Figure 10.	Silane-IV(1.37%+CL)-treated glass fibre composite on different scales (a) inch scale (b) Centimetre scale

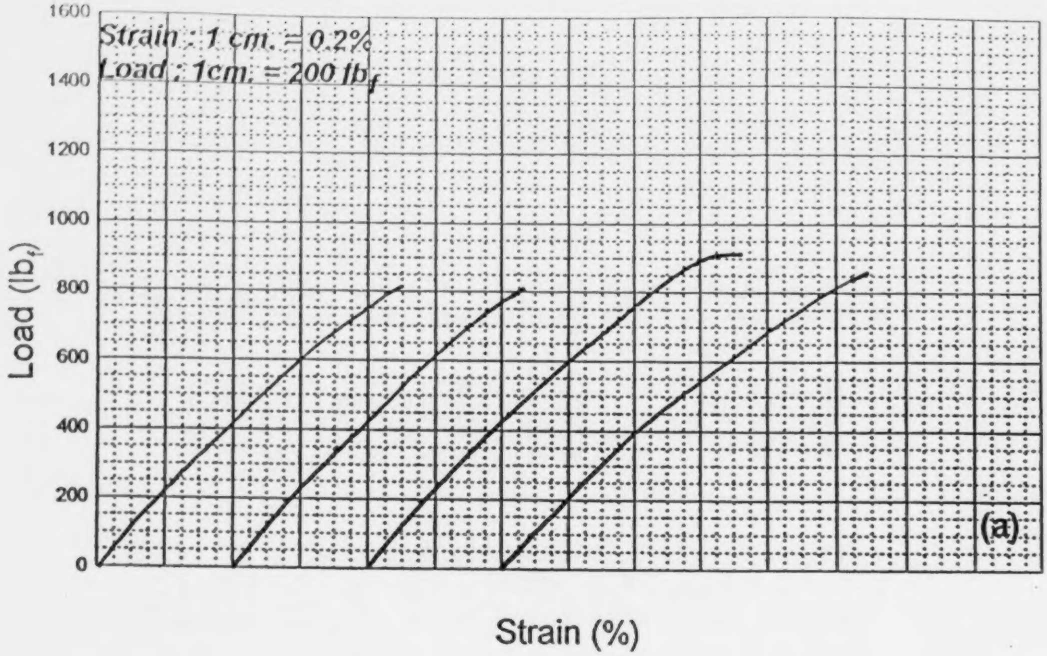

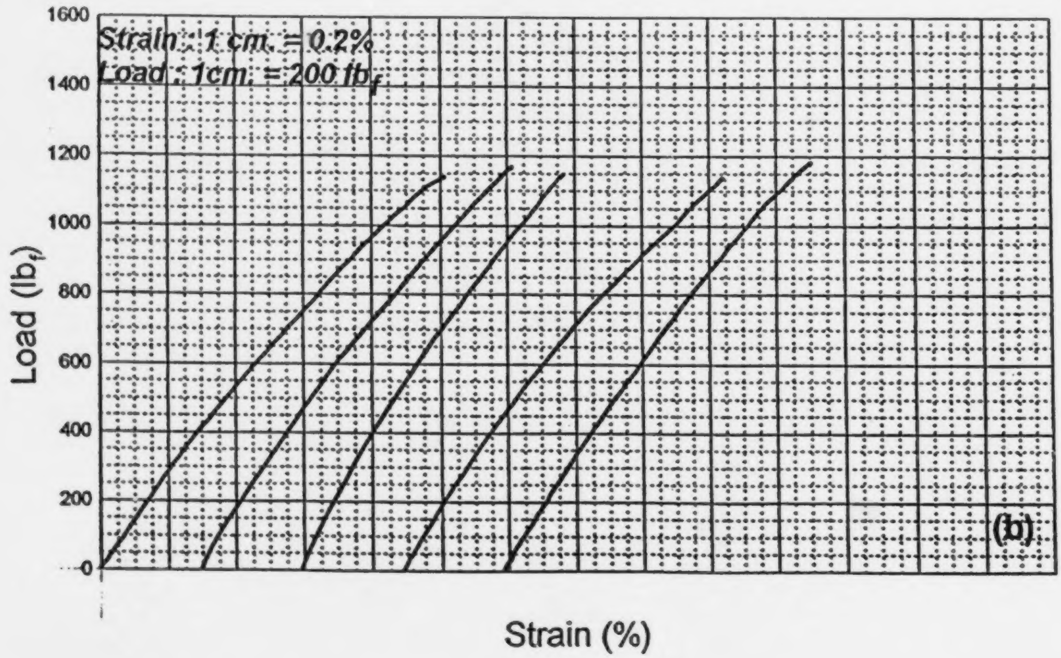

Figure 1 (a-b). Load-versus strain curves for (a) [3]Untreated glass fibre composite (b) [2]Silane-IV (1.25% toluene)-treated glass fibre composite.

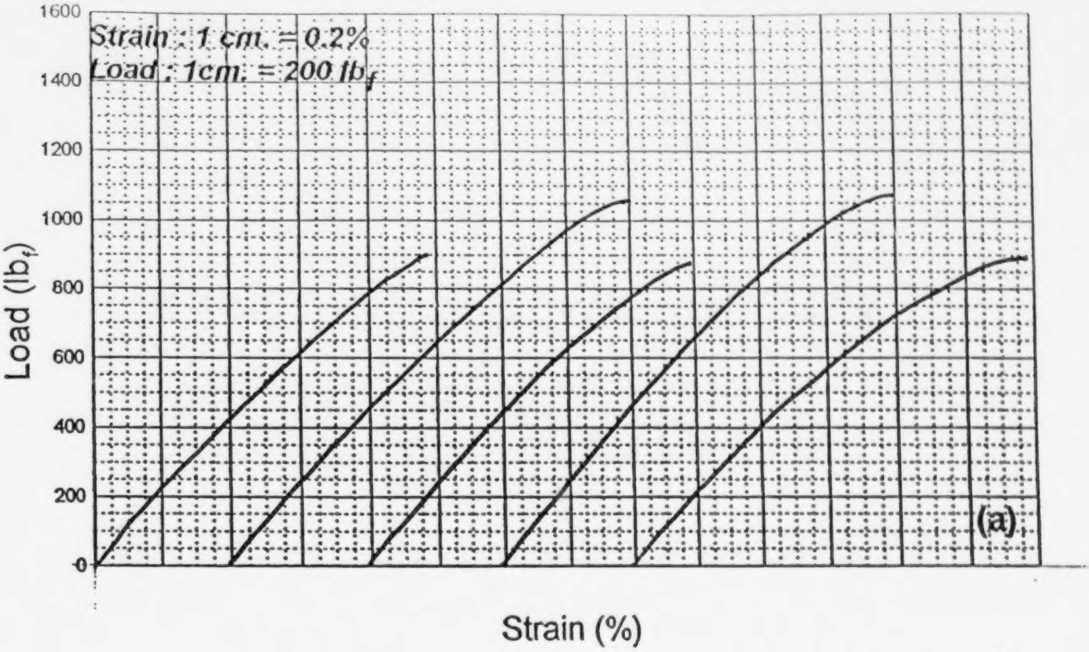

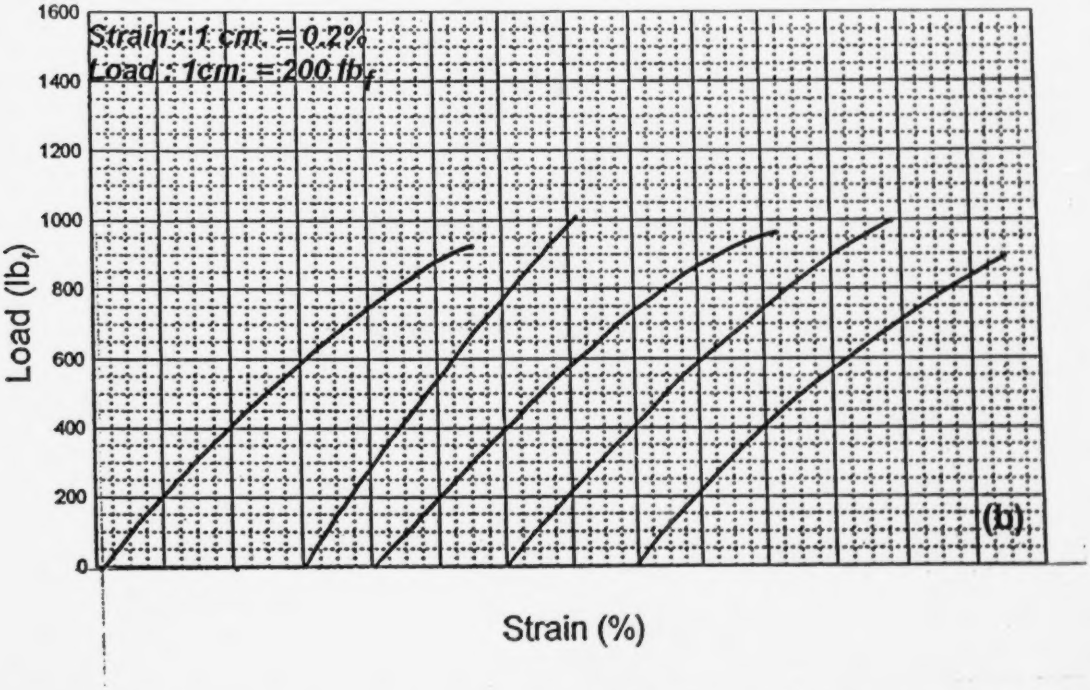

Figure 2 (a-b). Load-versus strain curves for (a) Silane-III (1.25%)- treated glass fibre composite (b) Silane-III (0.2%)-treated glass fibre composite.

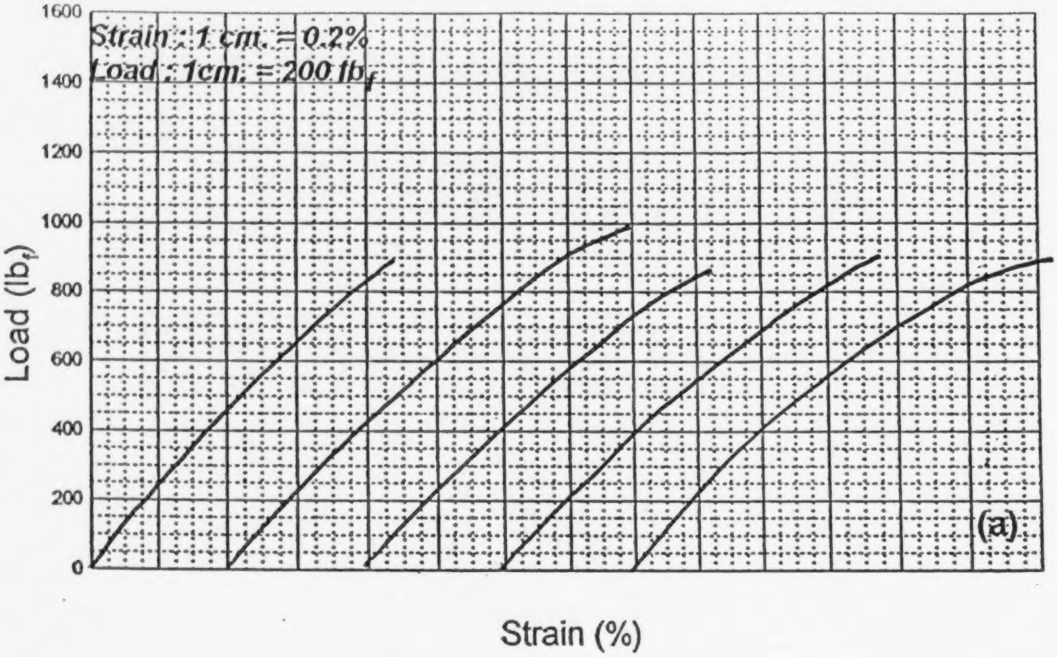

Figure 3 (a). Load-versus strain curves for (a) Silane-III (2.00%)- treated glass fibre composite.

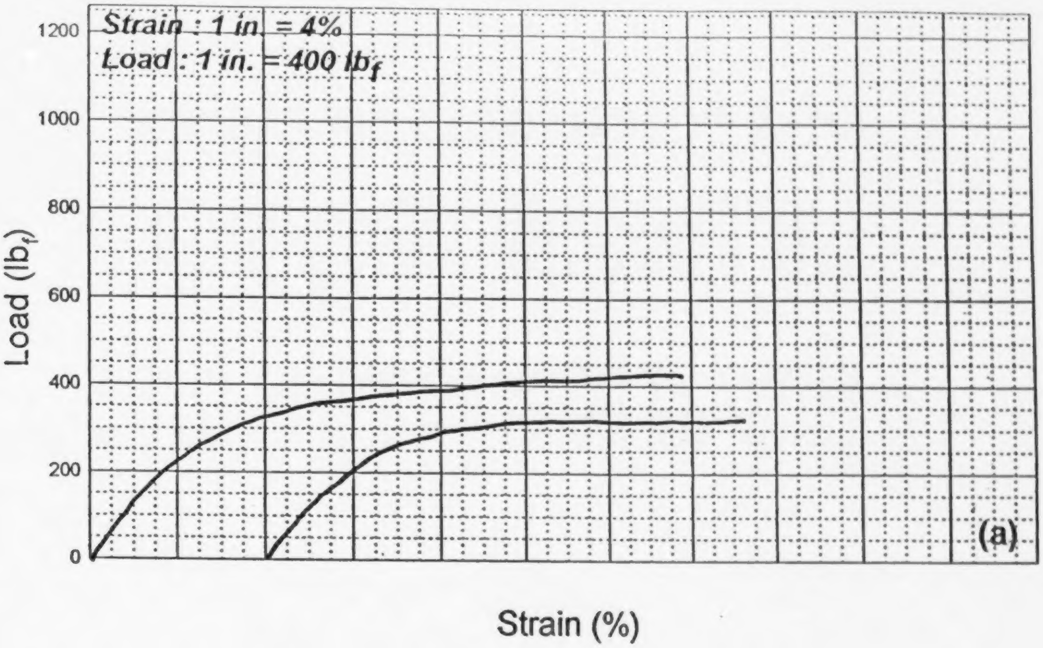

Figure 4 (a). Load-versus strain curves for (a) Allied Chemicals pure nylon 6 (left) and nylon6/glass fibre composite (right).

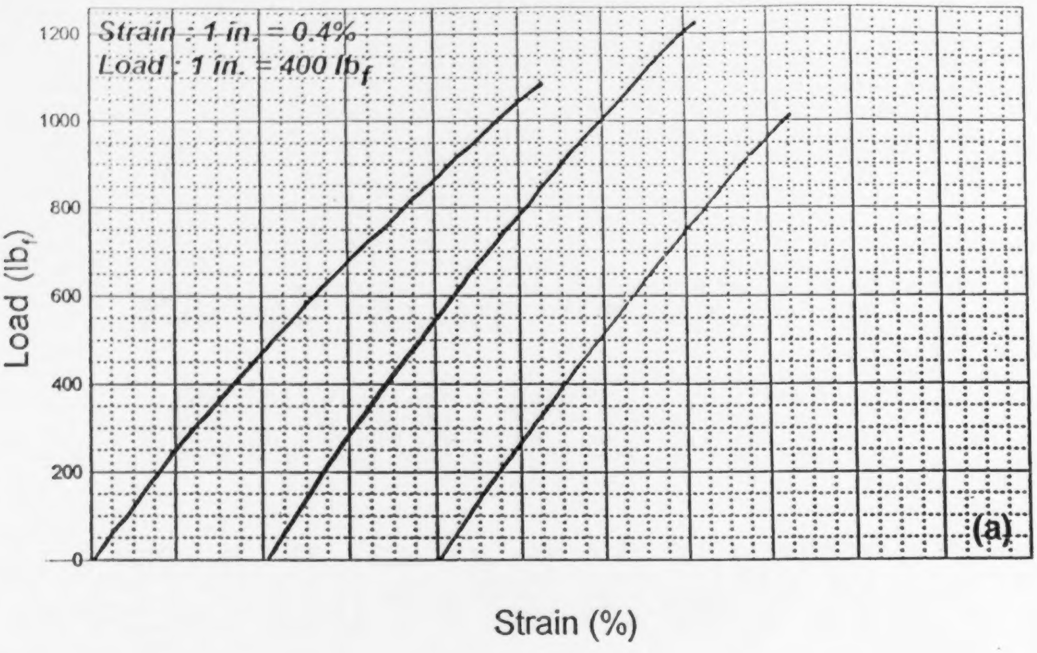

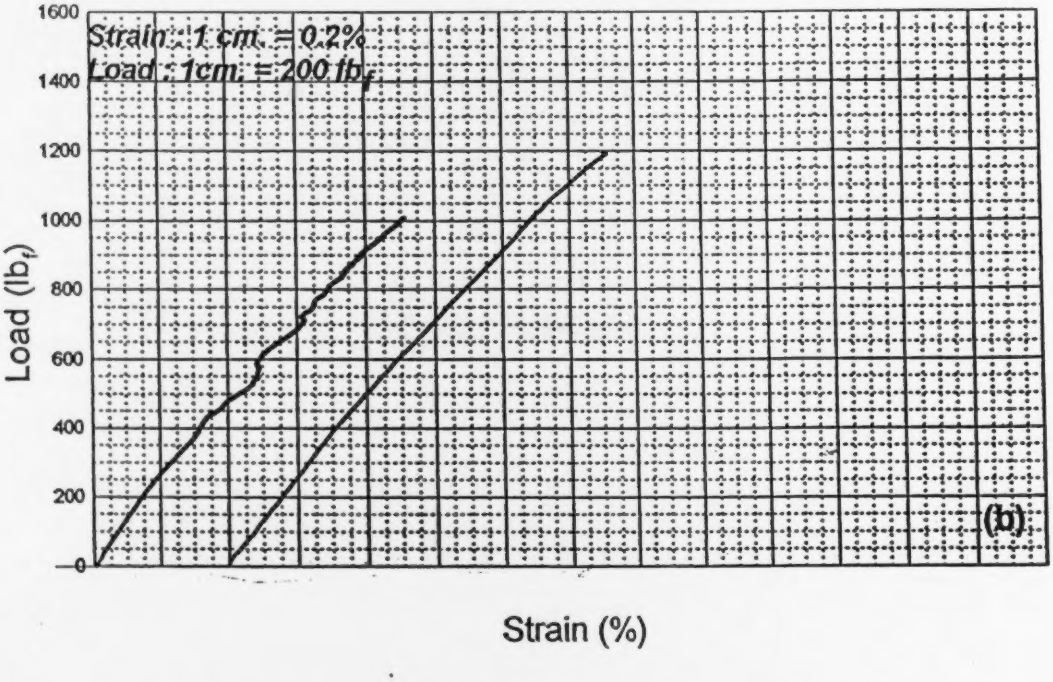

Figure 5 (a-b). Load-versus strain curves for Silane-V (0.20%)- treated glass fibre composite with different scales (a) inch scale (b) centimetre scale.

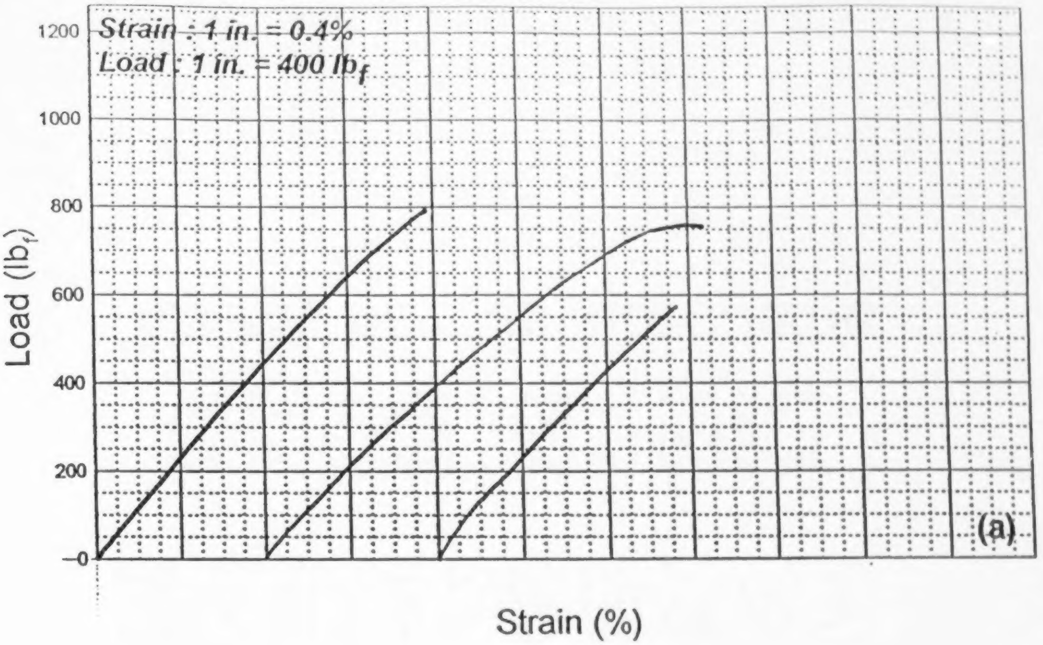

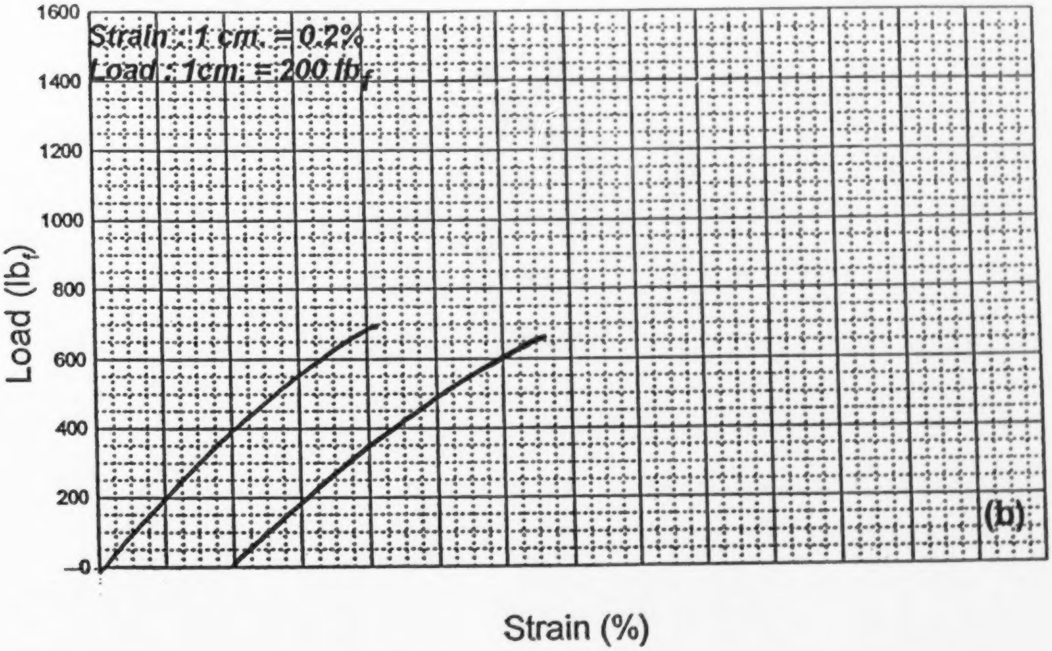

Figure 6 (a-b). Load-versus strain curves for [1]Silane-V (1.25%)-treated glass fibre composite on different scales (a) inch scale (b) centimetre scale.

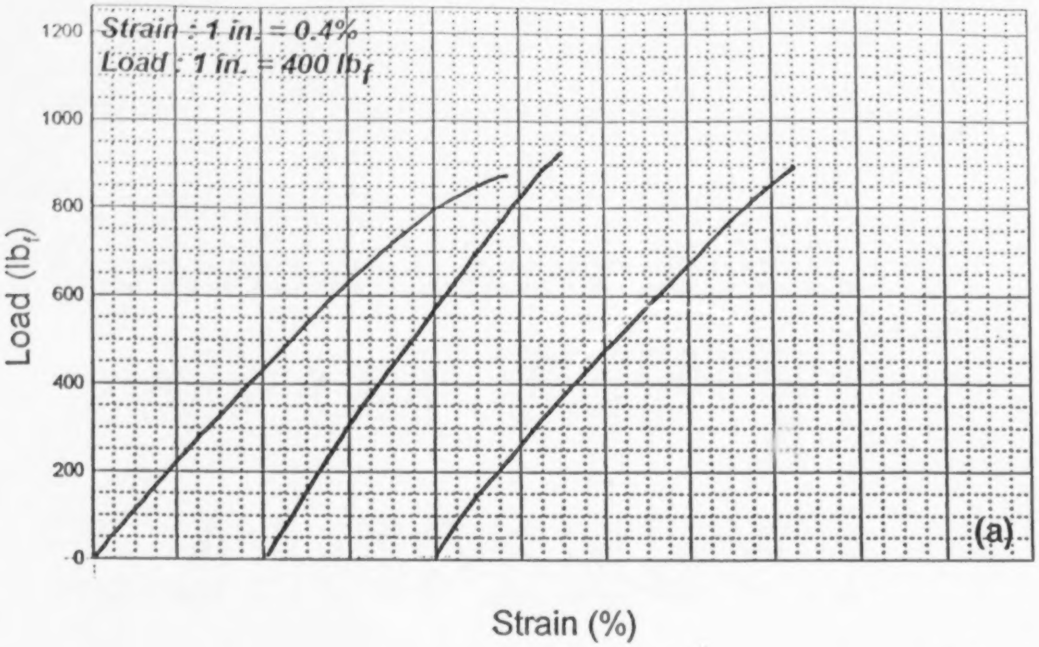

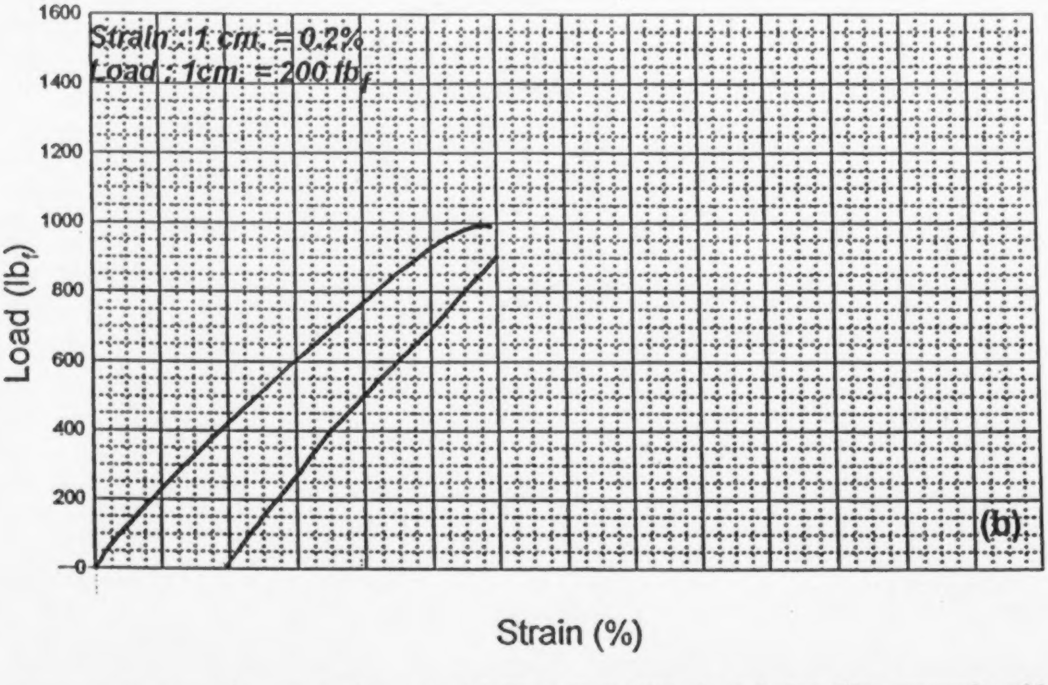

Figure 7 (a-b). Load-versus strain curves for Silane-V (2.00%)- treated glass fibre composite with different scales (a) inch scale (b) centimetre scale.

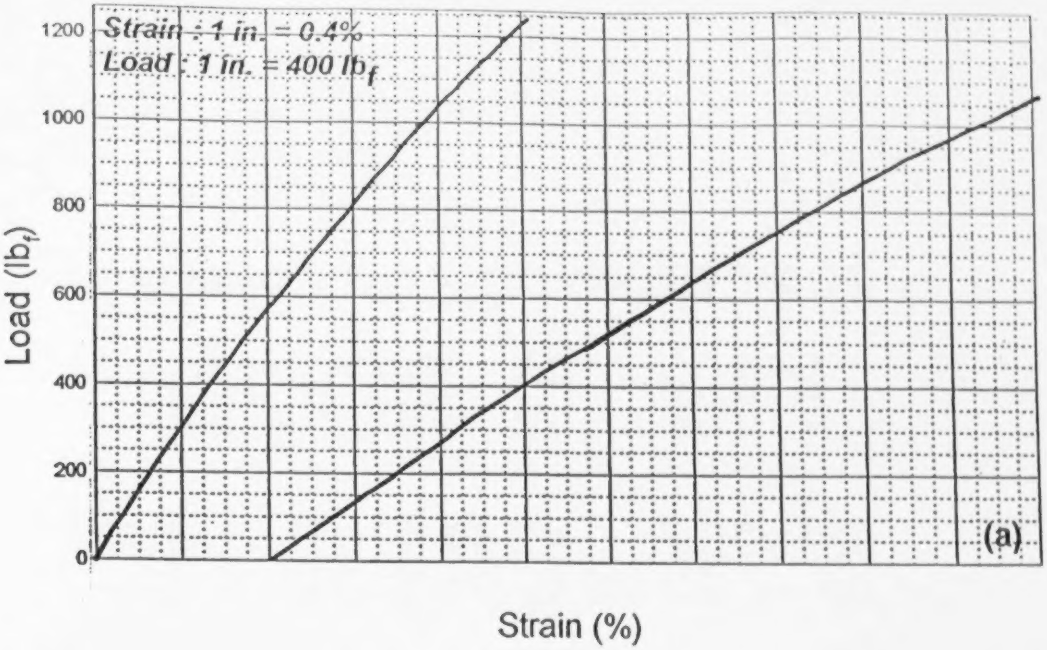

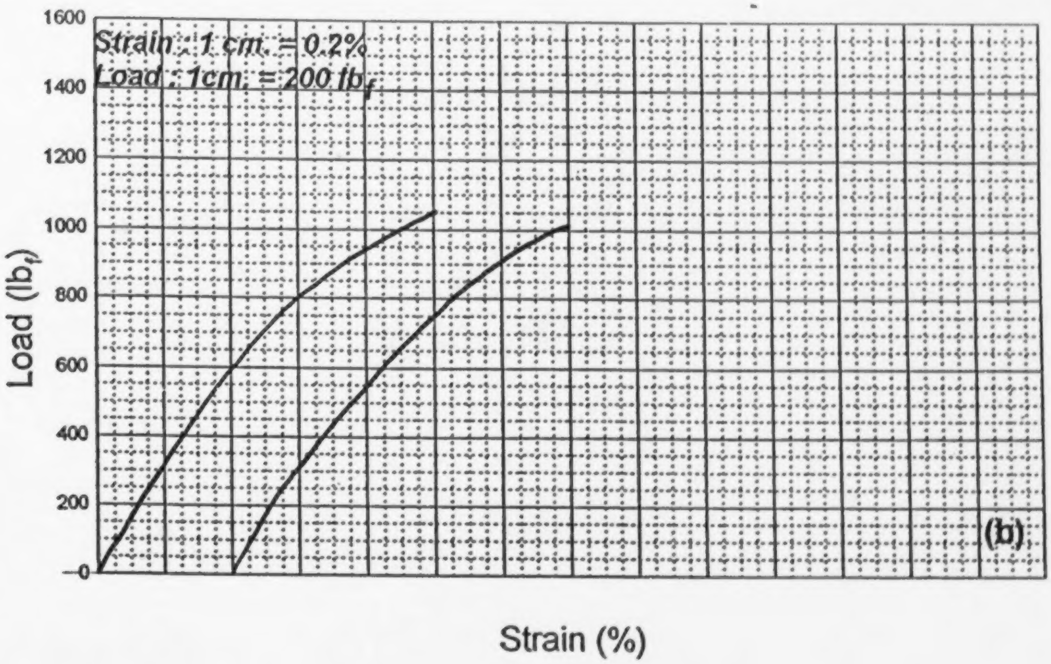

Figure 8 (a-b). Load-versus strain curves for Silane-IV (1.25% EtOH)- treated glass fibre composite with different scales (a) inch scale (b) centimetre scale.

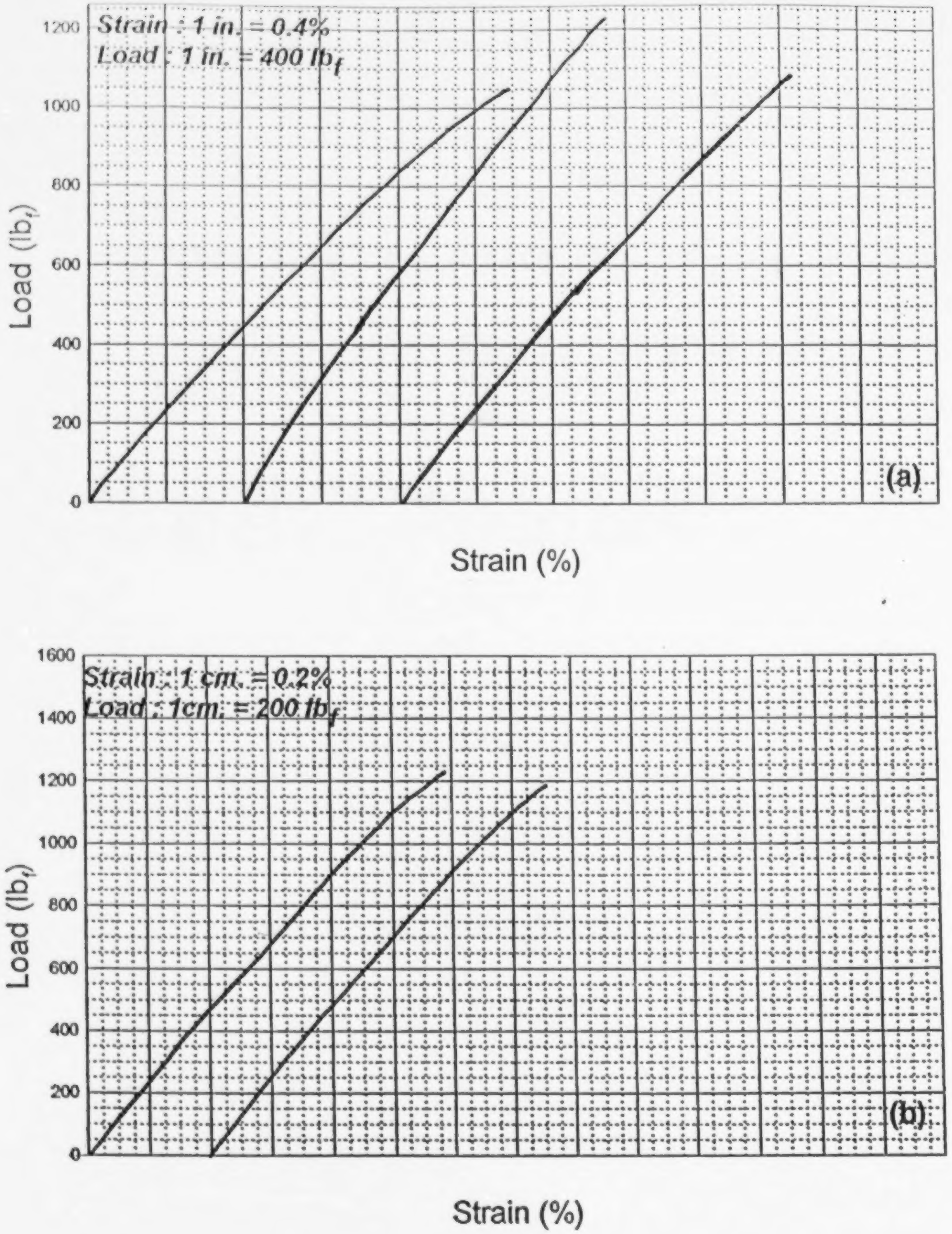

Figure 9 (a-b). Load-versus strain curves for ^{2}Silane-V (1.25%)-treated glass fibre composite with different scales (a) inch scale (b) centimetre scale.

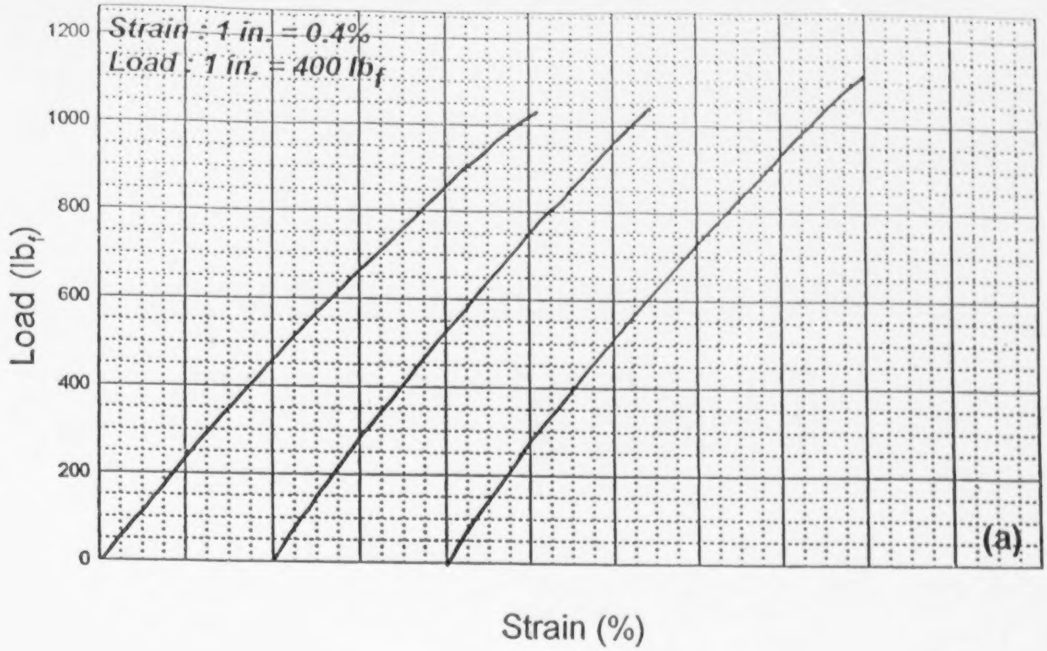

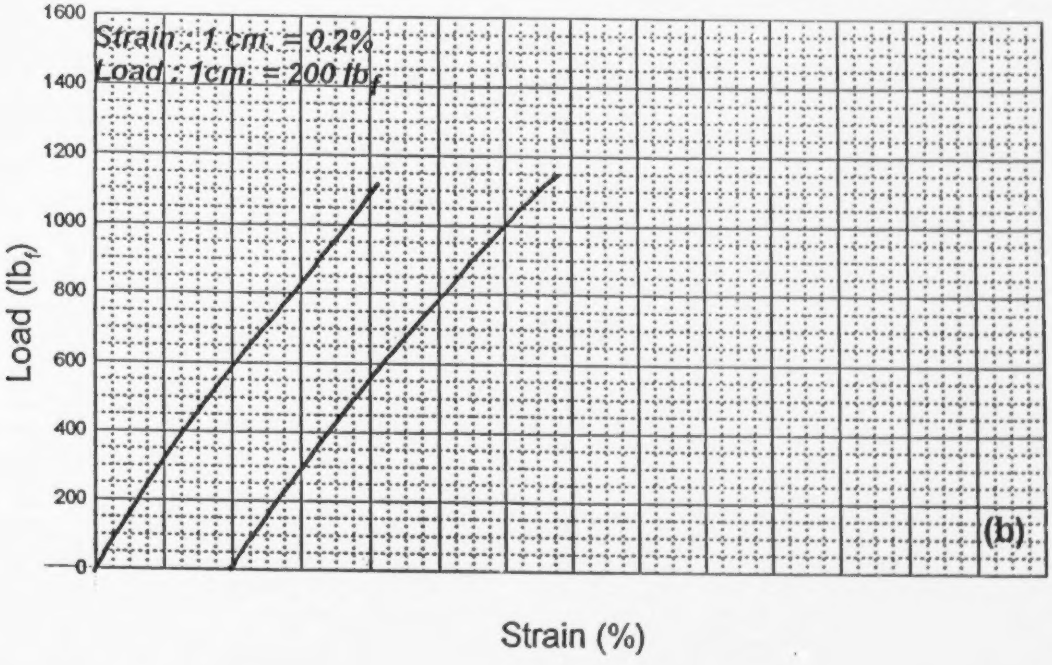

Figure 10 (a-b). Load-versus strain curves for Silane-IV (1.37% + CL)-treated glass fibre composite with different scales (a) inch scale (b) centimetre scale.

APPENDIX E

Molecular weight determination of nylon 6 using Dilute Solution Viscometry

Molecular weight of nylon 6

In addition to the factors such as void content, glass fibre volume content, glass fibre orientation; matrix properties, such as the molecular weight, morphology, etc., also play an important role in governing the mechanical properties of the resulting composite.

This work attempted to characterize the nylon that was obtained in our laboratory in terms of its molecular weight. The nylon from Allied Chemicals was also analyzed for its molecular weight, so as to be able to make comparisons between the nylon 6 synthesized in our laboratory to the commercial nylon 6.

The technique of dilute solution viscometry was employed to determine the molecular weight of nylon 6, because of its simplicity and convenience. A characteristic feature of a dilute polymer solution is that its viscosity is considerably higher than that of either the pure solvent or similarly dilute solutions of small molecules. This arises because of the large differences in size between polymer and solvent molecules. The increase in viscosity imparted by the macromolecules in solution is a direct function of the hydrodynamic volume and, hence, the molecular weight of the polymer.

The viscosities of dilute polymer solutions are most commonly measured using capillary viscometers of which there are two general classes, namely U-tube viscometers and suspended-level viscometers.

E.1. Theory in dilute solution viscometry *(Rodriguez, 1989; Young and Lovell, 1991)*

The molecular weight obtained by using a capillary viscometer is the viscosity average molecular weight, M_v. This molecular weight is less than the weight average molecular weight, M_w and more than the number average molecular weight, M_n.

Staudinger, in the early 1930s, used viscosity as a measure of the molecular weight of a polymer. He proposed the following relationship :

$$\eta_{sp} = K_s CM \qquad \text{(E.1)}$$

where, K_s is a constant for a given polymer/solvent/temperature; C the concentration; M the molecular weight; and η_{sp} the specific viscosity denoting the increase of viscosity of a polymer solution over that of the pure solvent according to the relation

$$\eta_{sp} = (\eta - \eta_0) / \eta_0 \qquad \textbf{(E.2)}$$

where η= viscosity of the polymer solution and η_0= viscosity of the solvent.

It is seen from the above equation that the specific viscosity is a function of concentration. In order to quantify a viscosity function of a polymer in a solvent, which will be independent of the concentration, the limiting value of reduced viscosity at infinite dilution is chosen and termed 'intrinsic viscosity' or 'limiting viscosity number', $[\eta]$. This term has been related to the viscosity function through the following equation by Huggins :

$$\eta_{sp} / C \;=\; [\eta] + k_g[\eta]^2C \qquad \textbf{(E.3)}$$

where k_g = Huggins constant for a given polymer/solvent/temperature system. The above equation is valid for $[\eta]C \ll 1$. The Huggins constant is essentially independent of molar mass and has values ranging from 0.2-0.3 for good polymer-solvent pairs to 0.5 for poor polymer-solvent pairs.

The intrinsic viscosity is related to the molecular weight of the polymer by the famous Mark-Houwink equation:

$$[\eta] \;=\; K.M^a \qquad \textbf{(E.4)}$$

where K and a are constants for a given polymer/solvent/temperature system. The value of a varies from 0.6 to 0.8 and is 0.5 in theta solvents. The value of a is greater than 0.7 for polymers in good solvents.

Now, let us see how intrinsic viscosity can be measured. Assume that a liquid is flowing through a capillary tube under conditions of steady laminar flow. The time required for the liquid of volume V to pass through the capillary of radius r and length l is related to its absolute viscosity by the famous Poiseuille's equation :

$$\eta = \frac{3.14 \, P \, r^4 \, t}{8Vl} \qquad (E.5)$$

where P is the pressure head under which the liquid flow takes place. The radial velocity profile corresponding to this equation is parabolic, with maximum velocity along the axis of the capillary tube and zero velocity at the wall. During the flow, P continuously decreases and is given by $P = h\rho g$, where h is the average pressure head. Therefore we can represent the equation as follows :

$$\eta = A\rho t \qquad (E.6)$$

where A is a constant for a given viscometer.

Poiseuille's equation does not take into account the energy dissipated in imparting kinetic energy to the liquid, but is satisfactory for most viscometers provided that the flow times exceed about 180 sec.

In capillary viscometry it is only necessary to determine the viscosity of a polymer solution relative to that of the pure solvent as,

$$\eta_r = \eta / \eta_0 = t / t_0 \qquad (E.7)$$

where η_r is known as the 'relative viscosity'; η_0 is the viscosity of the pure solvent. Since dilute solutions are used, it is assumed that the densities of the polymer solution and the pure solvent are the same.

E.2. Experimental setup

The viscometer used in this experiment is shown in Figure 5.11 and is called the Ubbelohde capillary viscometer. This is a simple glass capillary device. It consists of a measuring bulb, with upper and lower etched marks, which is attached directly above the capillary tube. The solution is drawn into the measuring bulb from a reservoir bulb attached at the bottom of the capillary tube, and the time required for it to flow back between the two etched marks is recorded. An additional tube is attached just below the capillary tube. This ensures that during measurement the solution is suspended in the measuring bulb and capillary tube, with atmospheric pressure acting both above and below the flowing column of liquid. Thus the pressure head depends only upon the volume of solution in and above the capillary, and so is independent of the total volume of solution contained in the viscometer. Another advantage of the Ubbelohde viscometer is that only a single solution of known concentration is required to be made to start with. Subsequent concentrations can be achieved by adding known volumes of pure solvent and mixing inside the viscometer itself. This does not require emptying, cleaning and refilling the viscometer with a fresh solution for every concentration.

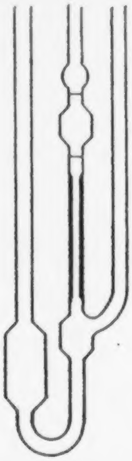

Figure E.1. Diagram of the Ubbelohde Capillary Viscometer

The viscometer was placed in a thermostatted glass walled water bath. As the viscosity is highly sensitive to temperature changes, all measurements were done at a constant temperature. A source of light was mounted behind the water bath so as to illuminate the capillary region of the viscometer.

E.3. Procedure to measure the intrinsic viscosity

Due to it's high melting point and strong intermolecular interactions between the amide linkages, nylon 6 is only soluble in highly acidic solvents such as formic and sulfuric acids or high boiling solvents such as m-cresol or fluorinated solvents such as 2,2,2-trifluoroethanol (TFE) and hexafluoroisopropanol (HFIP) *(Wang and Rivard, 1987)*. In our work, we found that the m-cresol did not dissolve the nylon at ambient temperature, so higher temperatures were required to dissolve the nylon in it. However, the high operating temperature (greater than 100°C) required in the use of m-cresol has been shown to degrade polyamides as reported by *Wang and Rivard, 1987* from Ede, 1971. In this work, we employed two different solvents to determine the molecular weight of the nylon 6. These are Formic acid (85%) and TFE.

The step-wise procedure used for determining the molecular weight of the two nylon 6 samples (our nylon and commercial nylon from Allied Chemicals) is shown below:

- A 0.1% solution (wt %) of each nylon sample was prepared in each solvent.
- From this 0.1% solution, 0.02g/dl, 0.04g/dl, 0.06g/dl and 0.08g/dl solutions of nylon were prepared by adding the required amount of solvent. The two solvents being toxic (TFE) and corrosive (Formic acid), proper precautions were taken during handling of these chemicals.
- Before use, the viscometer was thoroughly cleaned and the solvent and solutions were freed from dust by filtration.
- The water bath was heated upto 25°C and the temperature was held constant using a thermostat.
- Ethanol was added to the bath to prevent bubble formation and yield a clear solution.
- The viscometer was rinsed with the solution being used and then immersed in the bath.
- The solvent flow time (t_0) and the solution flow times (t) for the different concentrations were measured using a stop-watch.

- The 'relative viscosity' was calculated from the ratio of the two flow times i.e. t/t_0 and from this the specific viscosity η_{sp} was calculated.

- A graph of η_{sp}/C vs C was plotted and was extrapolated to C=0. The value of η_{sp}/C at C=0 was the intrinsic viscosity $[\eta]$.

- Using the Mark-Houwink constants obtained from the Polymer Handbook for the given polymer/solvent/temperature system the viscosity average molecular weight M_v was calculated.

E.4. Results and discussion

The plots of (η_{sp}/C) vs C for the two nylons with each solvent are shown in Figures E.2 (a-d) and the corresponding data is presented in Table E-1(a-d).

For nylon 6, the data for the two solvents are as follows *(Brandrup and Immergut, 1966):*

Solvent: 2,2,2-trifluoroethanol; T = 25°C

Mark-Houwink Coefficients :

a = 0.75, K = 0.0536 ml/gm
Applicable Molecular weight range: 13,000-100,000
Method of Determination : Light Scattering
Remarks : Narrow molecular weight distribution polymers ($M_w/M_n < 1.25$)

Solvent:Aqueous Formic acid (85%); T = 25°C

Mark-Houwink Coefficients :

a = 0.82, K = 0.0226 ml/gm
Applicable Molecular weight range: 7,000-120,000
Method of Determination : Light Scattering
Remarks : Narrow molecular weight distribution polymers ($M_w/M_n < 1.25$)

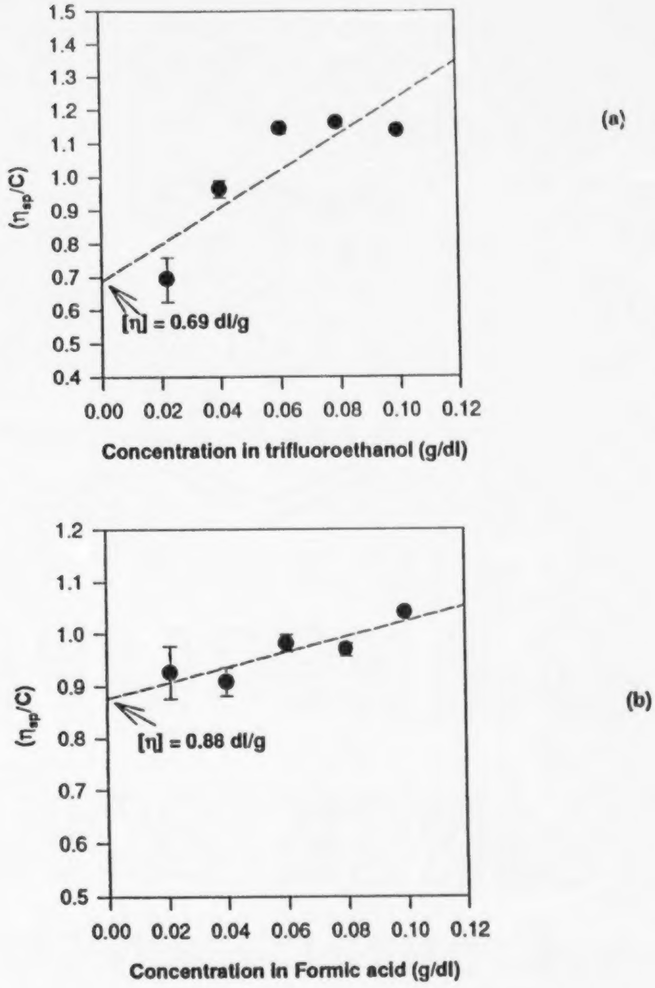

Figure E.2. Plots of (η_{sp}/C) vs (C) for laboratory nylon 6 at T=25°C using solvent (a) trifluoroethanol, (b) Aquoeus formic acid (85%)

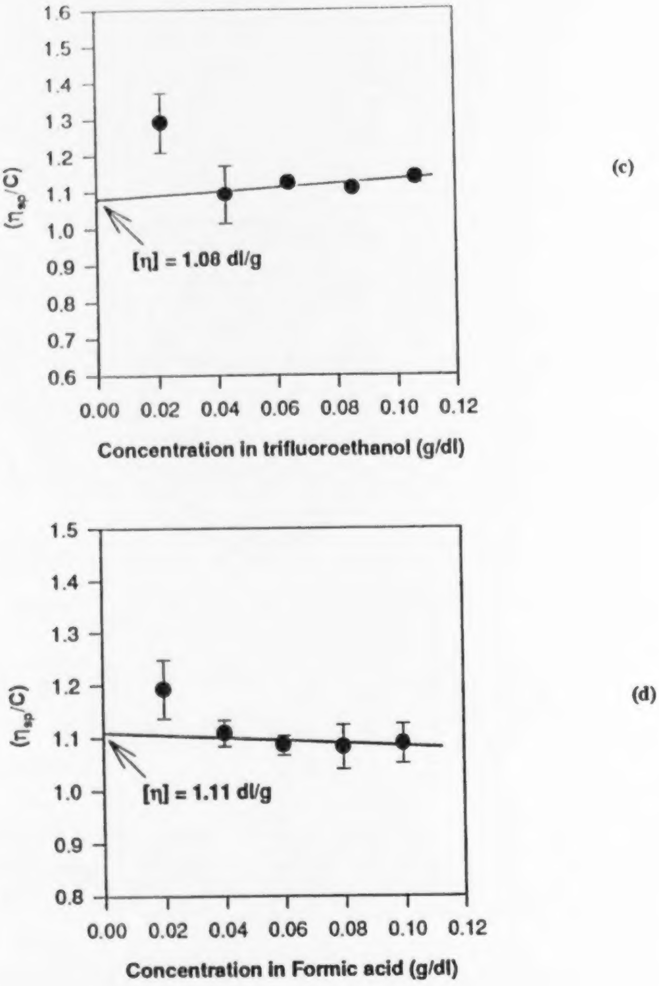

Figure E.2 (Continued). Plots of (η_{sp}/C) vs (C) for commercial nylon 6 (Allied Chemicals) at T=25°C using solvent (a) trifluoroethanol, (b) Aqueous formic acid (85%)

The molecular weights (M_v) obtained for the two samples with the two solvents were as shown below:

Sample: Laboratory nylon 6

Solvent, Trifluoroethanol: $M_v = 14{,}275$ g/gmol
Solvent, Formic acid: $M_v = 23, 575$ g/gmol

Sample: Allied Chemicals nylon 6

Solvent, Trifluoroethanol: $M_v = 25{,}300$ g/gmol
Solvent, Formic acid: $M_v = 31{,}775$ g/gmol

From Figures E.2 (a) and (b), we see that the trend obtained for the laboratory nylon with trifluoroethanol as the solvent is not linear, whereas, formic acid gave a close to perfect linear trend.The values obtained for the molecular weights from these solvents were also different. The molecular weight (M_v)obtained with trifluoroethanol (14,275 g/gmole), was lower than that obtained for formic acid (23,575g/gmole). From Figures E.2 (c) and (d), we can see that the trends obtained with the commercial nylon were also different and non-linear. However, if we take a close look at Figure E.2 (c), we find that the trend is linear if we ignore the data obtained with concentration of 0.02 g/dl. This upward deviation at concentration of 0.02g/dl may be caused due to the fact that at this extremely low concentration, even a small error can result in a very large deviation in the value of (η_{sp}/C), where the concentration term is in the denominator. So, the molecular weight (M_v) obtained by ignoring this concentration data was 25,300 g/gmol with trifluoroethanol, again lower than that obtained with formic acid (Mv = 31,775 g/gmol).

What causes the two solvents to give different molecular weights is unknown at this point. We could only comment that solvent effects are seen with nylon 6. Nylon 6 is a highly polar molecule and so are the solvents employed here, hence at such small concentrations (as 0.02 g/dl), even small complexities due to polymer-solvent interactions may have a very pronounced effect. Further, the trends obtained with both the solvents were the same.

For e.g., triflouroethanol always gave lower molecular weights than formic acid. A strong ionic effect was observed by *Wang and Rivard, 1987*, when they tried to characterize the nylon 6 using Gel Permeation Chromatography (GPC) with TFE as the solvent. They added LiBr to TFE, which helped disintegrate the nylon agglomerates through the osmotic diffusion of LiBr ions into the giant nylon molecules formed and held together by intermolecular hydrogen bonding. Polyelectrolyte effects were also reported with polyamides/formic acid systems. In fact, it has been reported that the data for the system nylon 66/formic acid does not exhibit a linear relationship on a plot of (η_{sp}/C) vs C but shows a distinct curvature *(Burke and Orofino, 1969)*, where they attributed this to the polyelectrolyte effect. Moreover, a mixed solvent system like aqueous formic acid (85%) is generally prone to errors because of the complexities arising out of the polymer-water interactions. Further, the discrepancies can also arise from experimental point of view, and the sources of experimental error might be as follows:

- The temperature was not constant throughout the experiment but tended to fluctuate. This would lead to changes in the viscosity which would be reflected as changes in the flow times.
- Since, ordinary filters were used to filter the solution, finer particles still remained inside the solution. The presence of the suspended impurities in the solutions would obstruct the free flow of solution within the capillary, leading to erroneous flow times.
- The viscometer may not have been exactly vertical. This would lead to a varying pressure head and would lead to differing flow times.

Thus, this system needs to be standardized and studied in further detail to obtain consistent molecular weight measurements. Nevertheless, a feel of the order of magnitude of the molecular weight of nylon 6 was obtained.

REFERENCES

1. Brandrup, J., and Immergut, E. H., (eds.), *Polymer Handbook*, Interscience Publishers, N.Y., **1966**.

2. Burke, J. J., and Orofino, T. A., "Nylon 66 Polymers. I. Molecular weight and Compositional Distribution", *Journal of Polymer Science*, A-2, 7, 1,**1969**.

3. Rodriguez, F., *Principles of Polymer Systems*, Hemisphere Publishing Corp., Ithaca, N.Y., **1989**.

4. Wang, P. J., and Rivard, R. J., "Characterization of Nylons by Gel Permeation Chromatography and Low Angle Laser Light Scattering in 2,2,2-Trifluoroethanol", *Journal of Liquid Chromatography*, 10(14), p. 3059-71, **1987**.

5. Young, R. J., and Lovell, P. A., *Introduction to Polymers*, Chapman & Hall, N.Y., 1991.

TABLE E-1 (a)

Sample : Laboratory nylon 6

Solvent : Triflouroethanol ; Temp = 25^0 C

Solvent time = 200.85 s

Concentration (g/dl)	Time (s)	Error	η_{sp}/C (dl/g)	% error
0.10	219.60	0.20	1.14	0.01
0.02	200.20	0.20	0.69	0.07
0.04	204.80	0.20	0.96	0.03
0.06	210.80	0.20	1.14	0.02
0.08	215.40	0.20	1.16	0.01

TABLE E-1 (b)

Sample : Laboratory nylon 6

Solvent :Formic acid ; Temp = 25^0 C

Solvent time = 203.8

Concentration (g/dl)	Time (s)	Error	η_{sp}/C (dl/g)	% error
0.10	225	0	1.04	0
0.08	219.6	0.2	0.97	0.01
0.06	215.8	0.2	0.98	0.02
0.04	211.16	0.24	0.91	0.03
0.02	207.8	0.2	0.93	0.05

TABLE E-1 (c)

Sample : Allied Chemicals nylon 6

Solvent : Triflouroethanol ; Temp = 25^0 C

Solvent time= 200.8486

Concentration (g/dl)	Time (s)	Error	η_{sp}/C (dl/g)	% error
0.0213	206.37	0.41	1.29	0.07
0.0426	210.20	0.96	1.09	0.10
0.0639	215.26	0.17	1.12	0.01
0.0852	219.80	0.17	1.11	0.01
0.1065	225.14	0.37	1.14	0.02

TABLE E-1 (d)

Sample : Allied Chemicals nylon 6

Solvent :Formic acid ; Temp = 25^0 C

Solvent time=203.3s 203.3

Concentration (g/dl)	Time (s)	Error	η_{sp}/C (dl/g)	% error
0.0199	208.12	0.32	1.19	0.07
0.0398	212.27	0.333	1.11	0.04
0.0597	216.49	0.306	1.09	0.02
0.0796	220.52	0.28	1.06	0.02
0.0995	224.60	0.2	1.05	0.01

APPENDIX F

Differential Scanning Calorimetry

Figure 1. DSC scan for nylon 6 taken from Piranha-cleaned fibre composite disk.

Figure 2. DSC scan for nylon 6 taken from HF-treated fibre composite disk.

Figure 3. DSC scan for nylon 6 taken from Silane III (0.2%)-treated fibre composite disk.

Figure 4. DSC scan for nylon 6 taken from Silane IV (1.25%)-treated fibre composite disk.

Figure 5. DSC scan for nylon 6 taken from Silane IV (1.37%+CL)-treated fibre composite disk.

Figure 6. DSC scan for nylon 6 taken from Silane V (0.2%)-treated fibre composite disk.

F.1. Differential scanning calorimeter

The differential scanning calorimeter (DSC) is an instrument used to analyze the thermal behavior of a material. It does so by recording the specific heat of the sample of the material as a function of temperature.

Two pans made of the same material (and weighing the same), one empty and the other containing the sample to be tested, are placed in the cell of the DSC on flat bases. The cell, and consequently the pans, are then heated at a certain rate (x °C/min.) and the difference between the amounts of heat absorbed by the pans is recorded as a function of temperature named "Heat Flow". This function is given by

Heat Flow = (Heat absorbed by the empty pan) - (Heat absorbed by the pan containing the sample)

Thus, a baseline in the DSC curve below the zero "Heat Flow" line indicates heating, and one above the zero "Heat Flow" line represents cooling. Similarly, a peak pointing downward denotes an endothermic transition such as melting and one pointing upward denotes an exotherm, e.g. freezing. A shift in the baseline at any point on the temperature axis indicates a change in the specific heat of the sample, which could be due to structural changes taking place in the material at that temperature, e.g. creation of additional free volume during a glass transition in polymers.

F.2. Thermal analysis of sample

The DSC standard-analysis software was used to determine the differential transitions in our material such as the glass transition temperature and the melting and crystallization transition temperatures.

Figures 1 through 6 show the results of the analyses of our composite samples. The temperatures with an "I" in parentheses adjacent to them represent glass transition temperatures of the samples and the temperatures indicated below the melting peaks represent their melting points. The heats of fusion (in J/g) of all the samples are indicated above the melting-transition peaks.

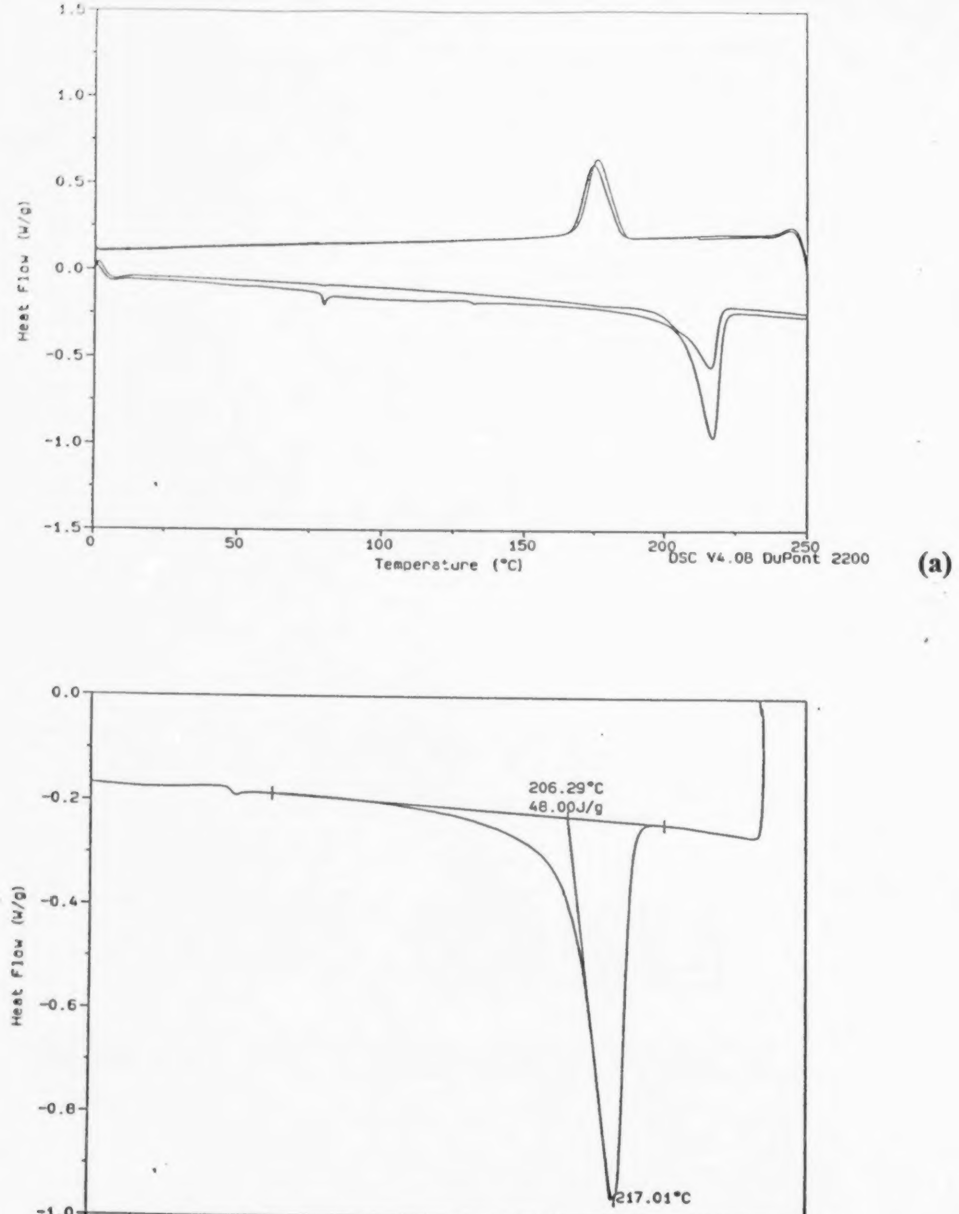

Figure 1. DSC scan for nylon 6 taken from Piranha-cleaned fibre composite disk (a) Two complete heating and cooling cycles (b) Expanded region of DSC heating trace near crystalline melting regime on the first heating scan.

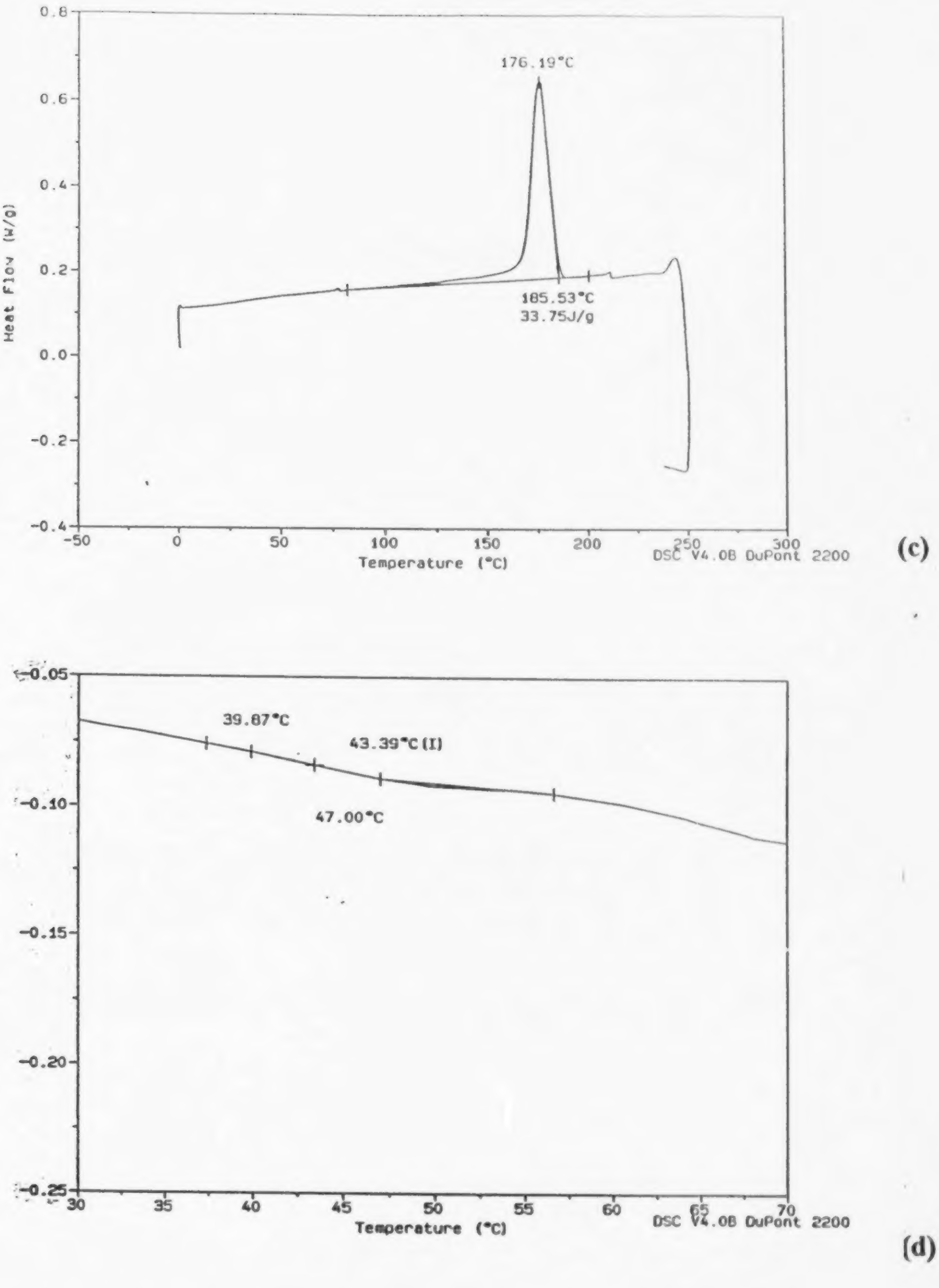

Figure 1. (Continued) (c) Expanded region of DSC cooling trace, near crystalline cooling regime following first heating scan.(d) Expanded region of DSC heating trace, near glass transition regime on first heating scan

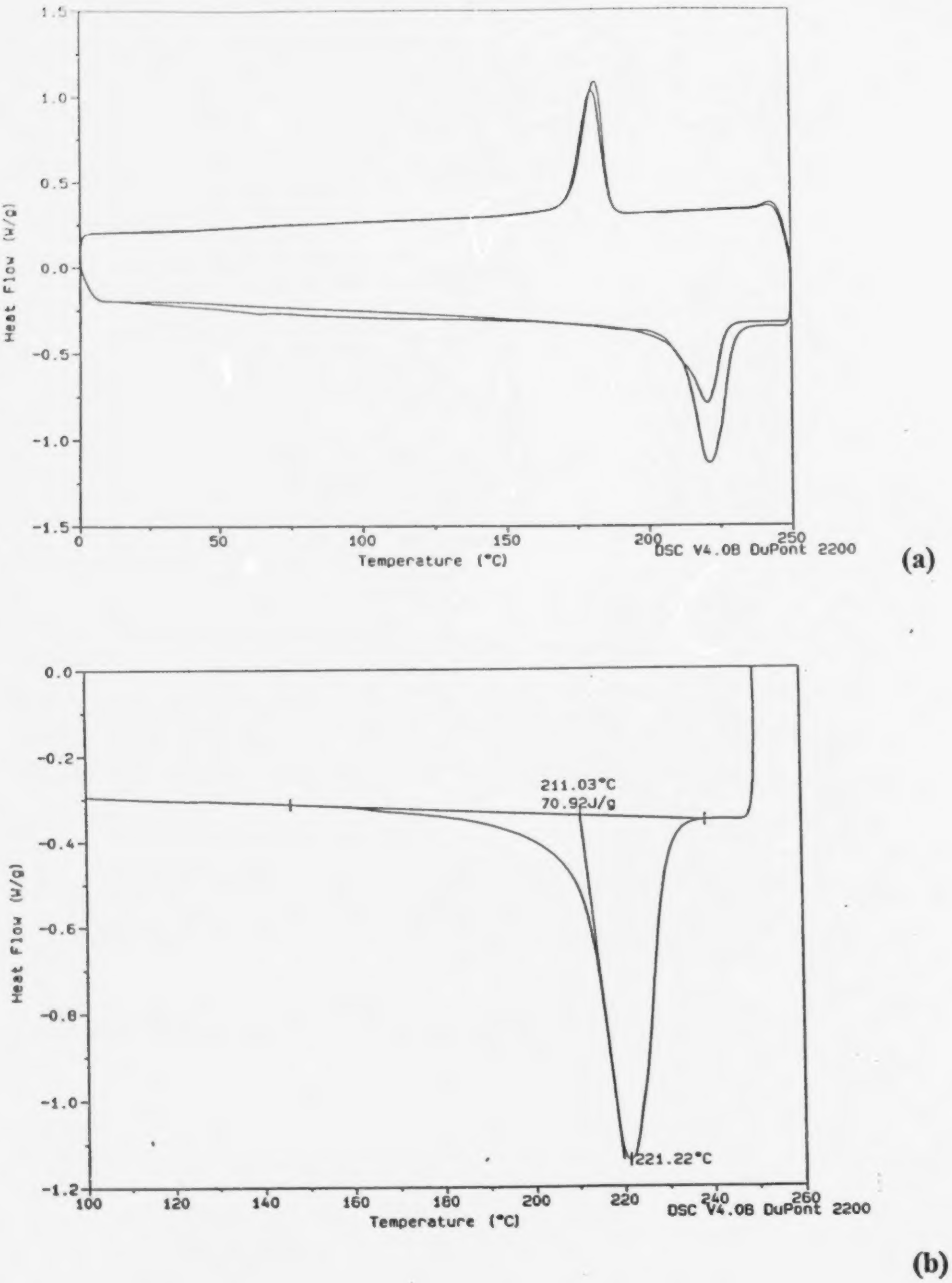

Figure 2. DSC scan for nylon 6 taken from HF-treated fibre composite disk (a) Two complete heating and cooling cycles (b) Expanded region of DSC heating trace near crystalline melting regime on the first heating scan.

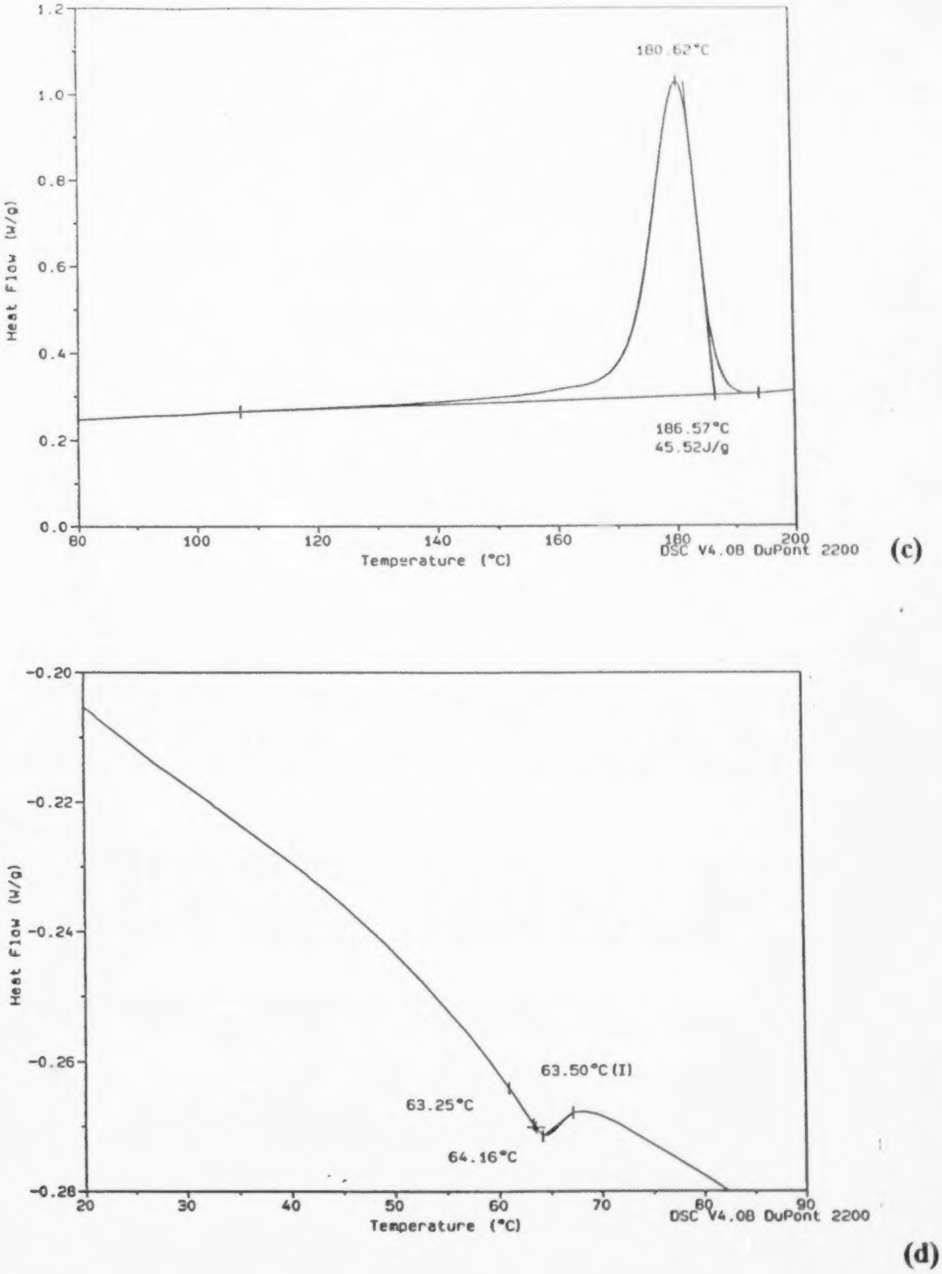

Figure 2. (Continued) (c) Expanded region of DSC cooling trace, near crystalline cooling regime following first heating scan.(d) Expanded region of DSC heating trace, near glass transition regime on first heating scan

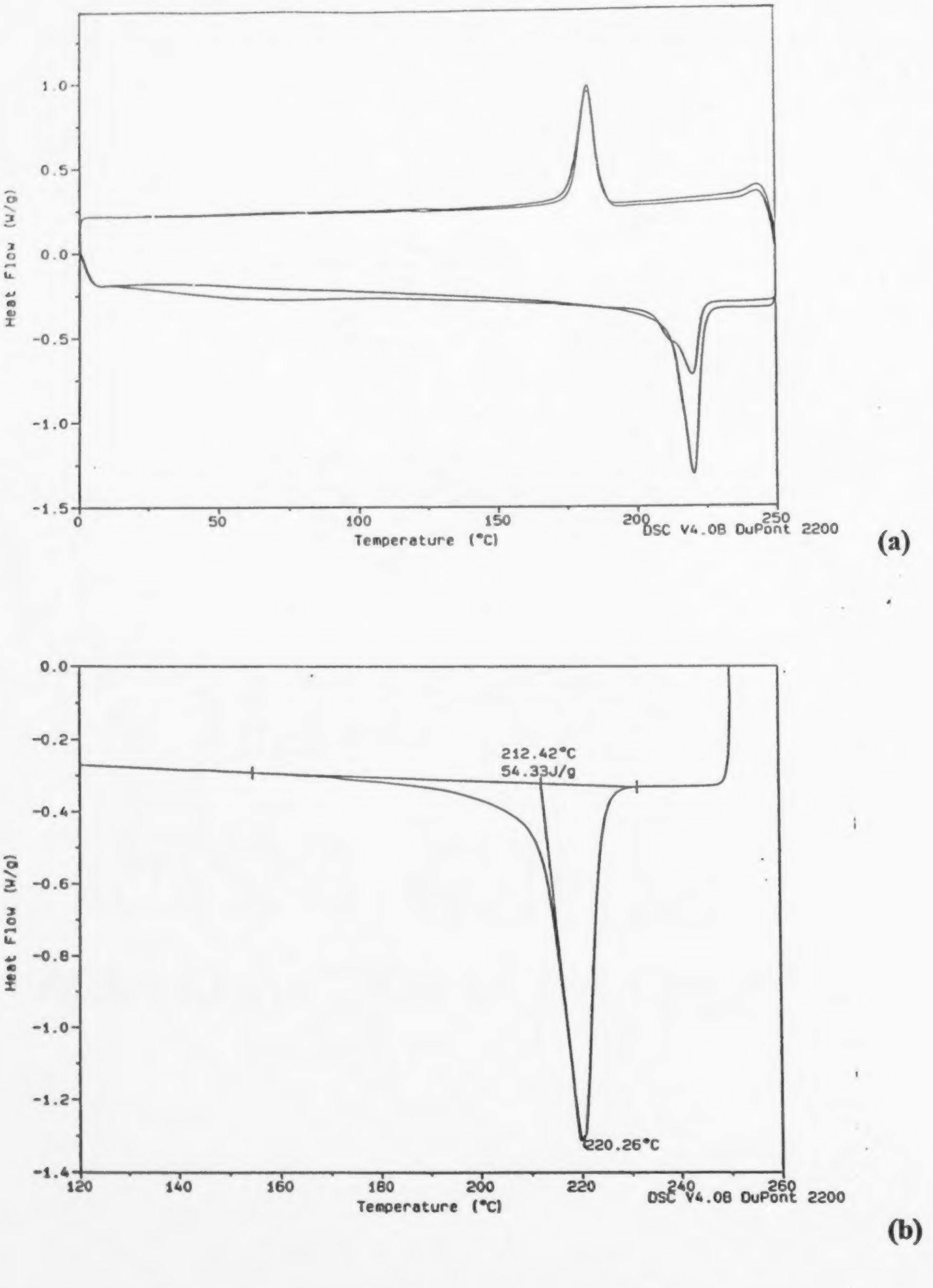

Figure 3. DSC scan for nylon 6 taken from Silane II$_L$ (0.2%)-treated fibre composite disk (a) Two complete heating and cooling cycles (b) Expanded region of DSC heating trace near crystalline melting regime on the first heating scan.

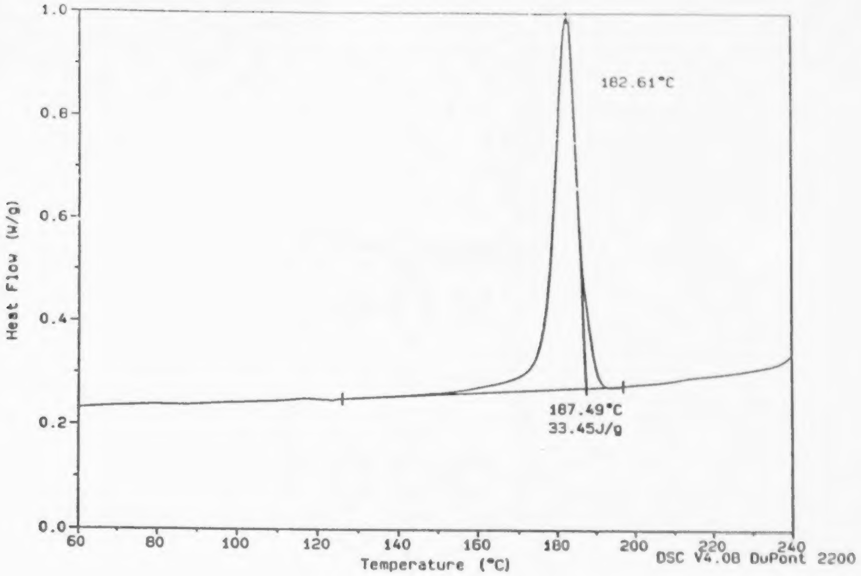

(c)

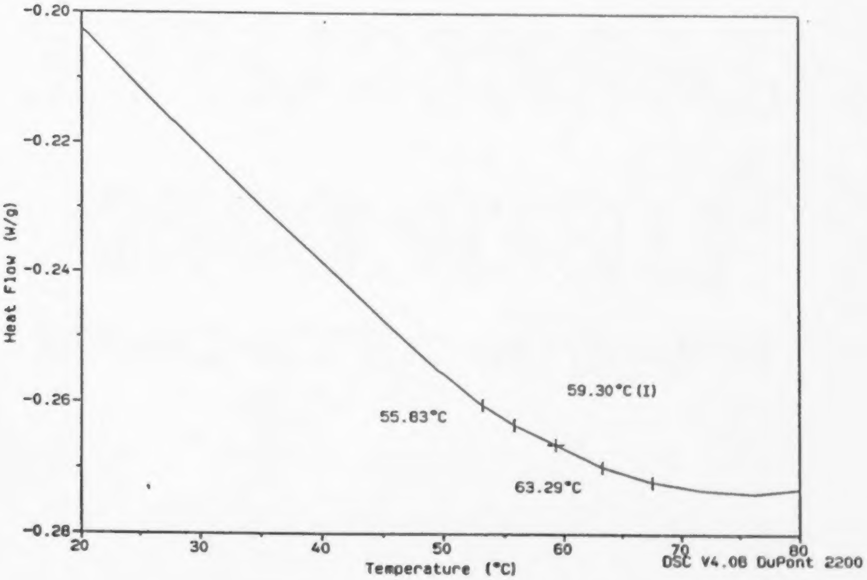

(d)

Figure 3. (Continued) (c) Expanded region of DSC cooling trace, near crystalline cooling regime following first heating scan.(d) Expanded region of DSC heating trace, near glass transition regime on first heating scan

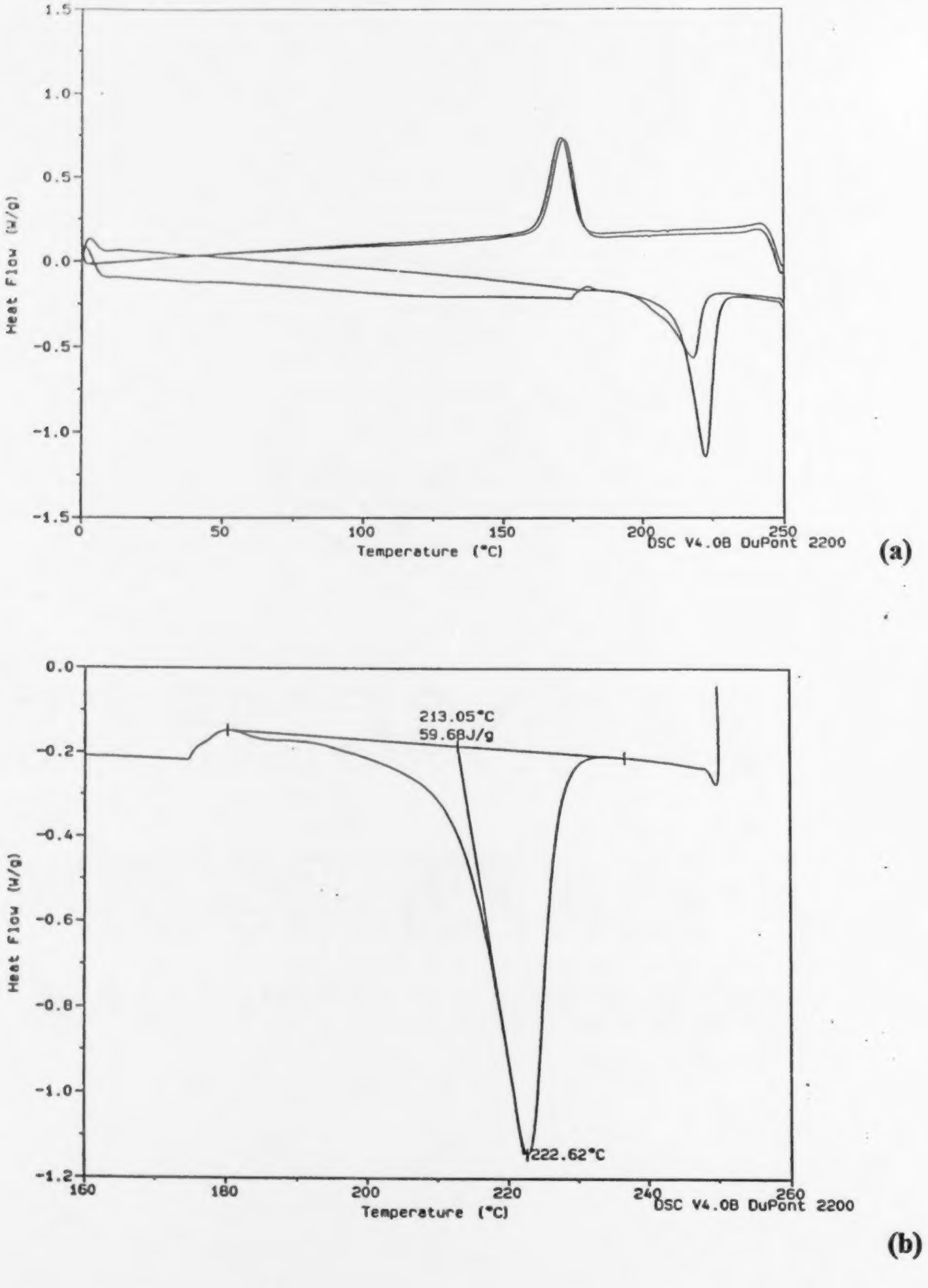

Figure 4. DSC scan for nylon 6 taken from Silane IV (1.25%)-treated fibre composite disk (a) Two complete heating and cooling cycles (b) Expanded region of DSC heating trace near crystalline melting regime on the first heating scan.

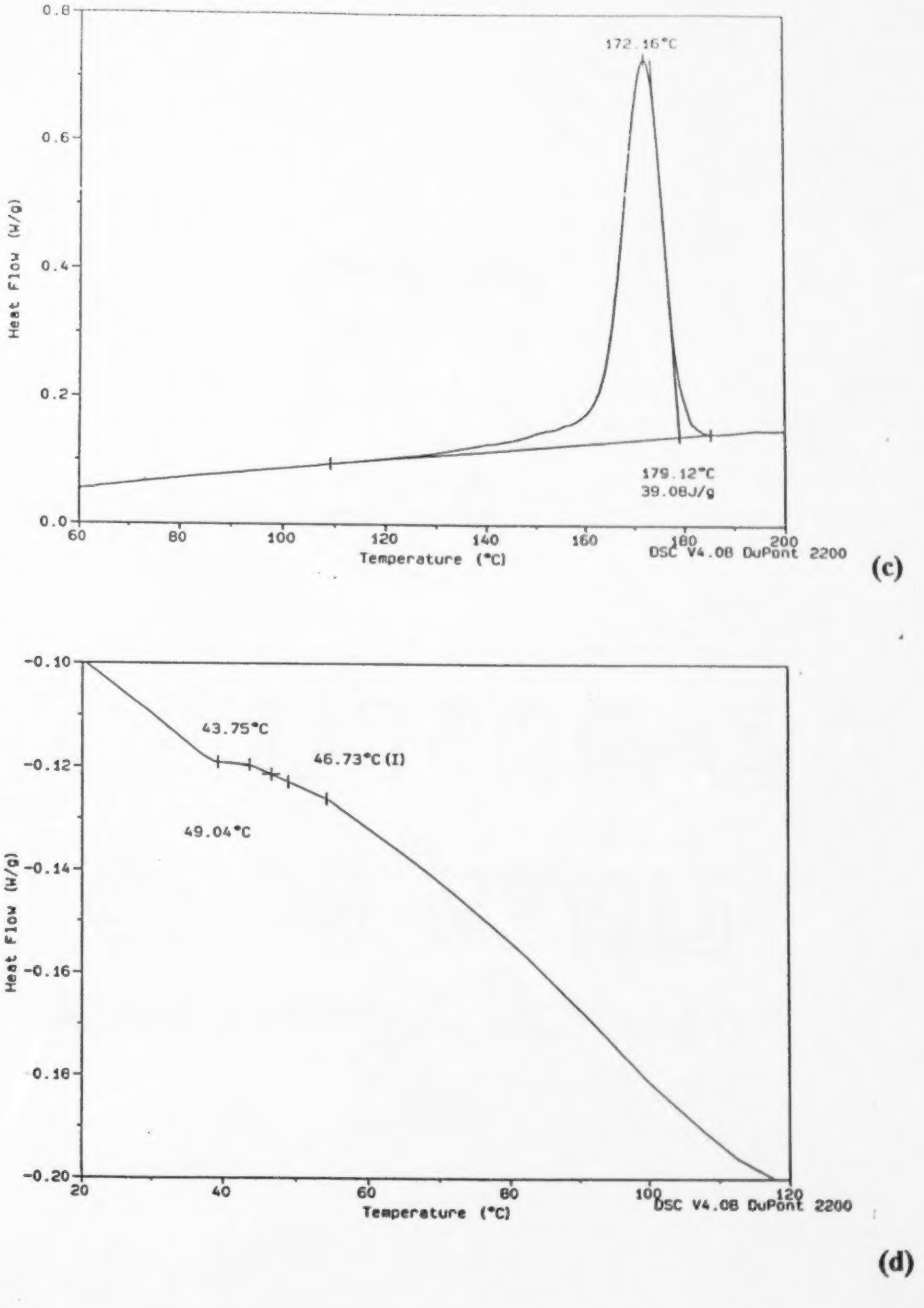

Figure 4. (Continued) (c) Expanded region of DSC cooling trace, near crystalline cooling regime following first heating scan.(d) Expanded region of DSC heating trace, near glass transition regime on first heating scan

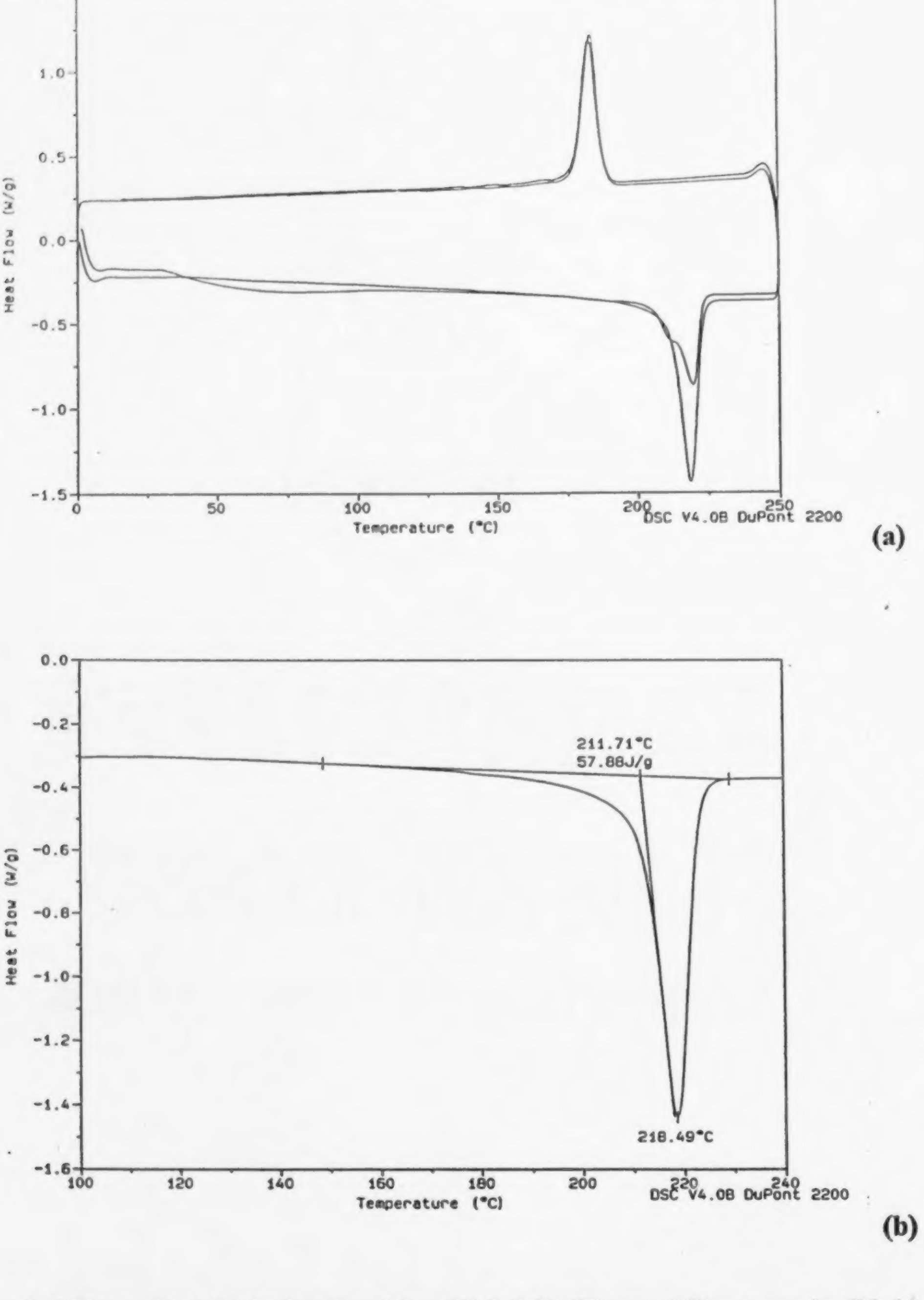

Figure 5. DSC scan for nylon 6 taken from Silane IV (1.37%+CL)-treated fibre composite disk (a) Two complete heating and cooling cycles (b) Expanded region of DSC heating trace near crystalline melting regime on the first heating scan.

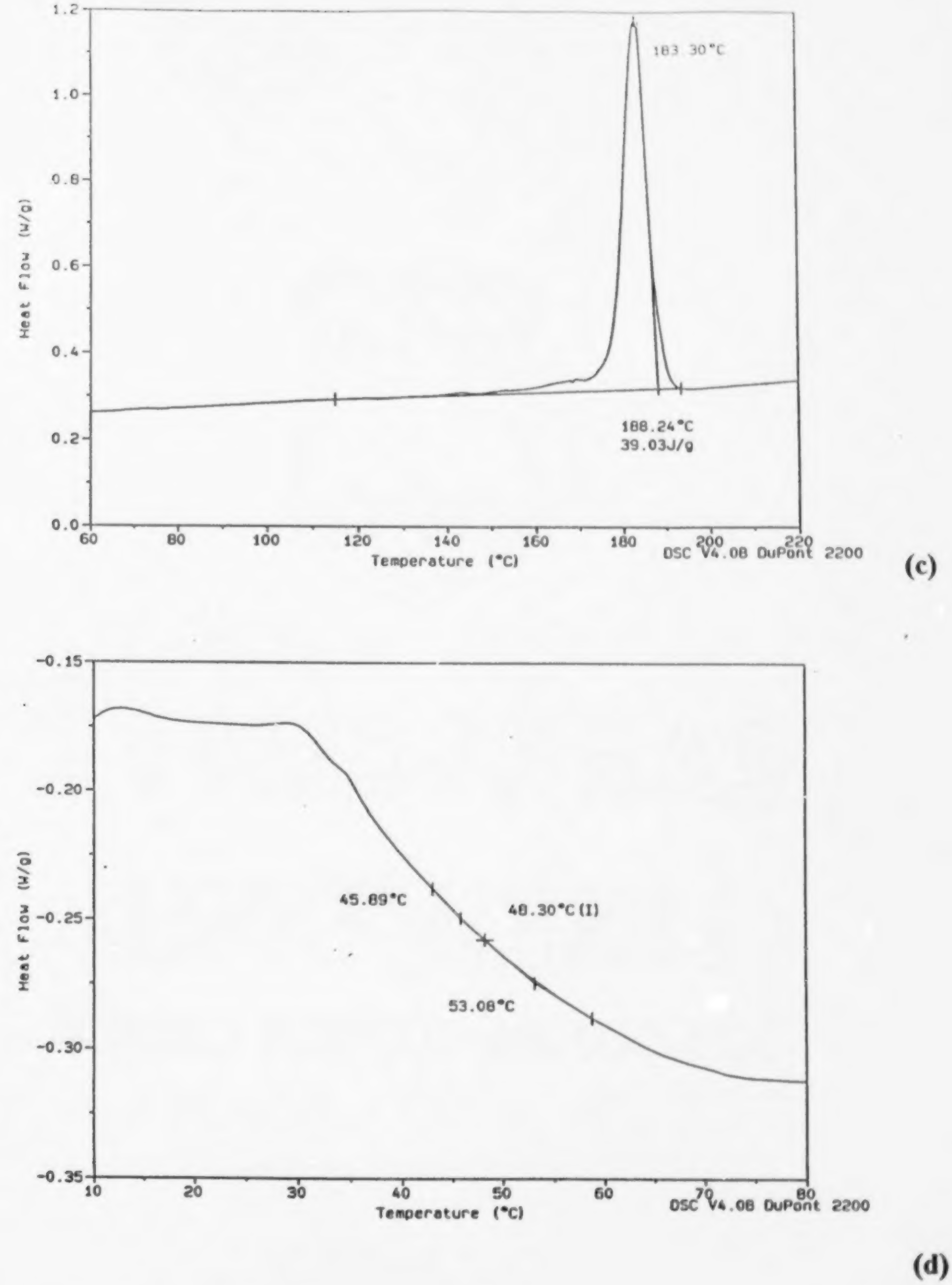

Figure 5. (Continued) (c) Expanded region of DSC cooling trace, near crystalline cooling regime following first heating scan.(d) Expanded region of DSC heating trace, near glass transition regime on first heating scan

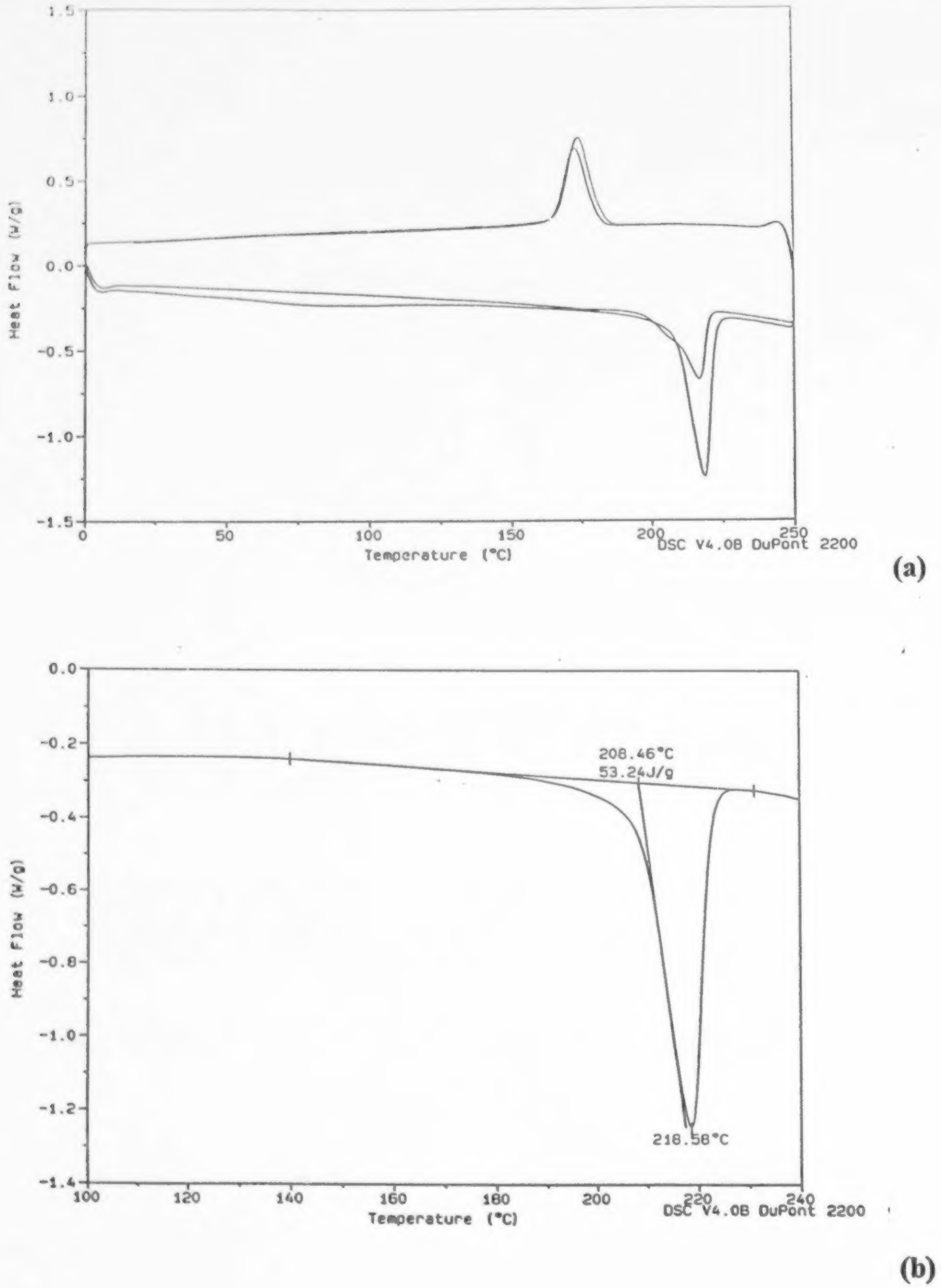

Figure 6. DSC scan for nylon 6 taken from Silane V (0.2%)-treated fibre composite disk (a) Two complete heating and cooling cycles (b) Expanded region of DSC heating trace near crystalline melting regime on the first heating scan.

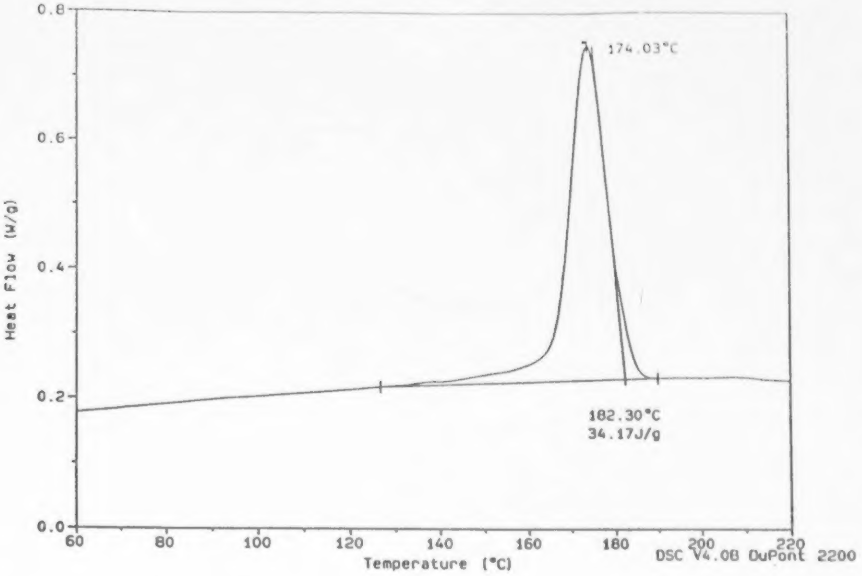

(c)

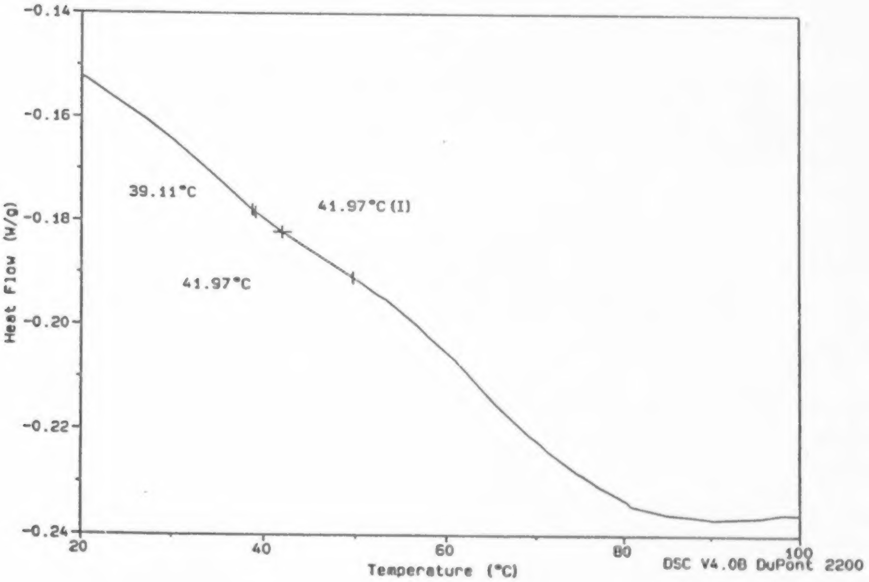

(d)

Figure 6. (Continued) (c) Expanded region of DSC cooling trace, near crystalline cooling regime following first heating scan. (d) Expanded region of DSC heating trace, near glass transition regime on first heating scan